Title
Thermodynamic Investigations of Aqueous Ternary Complexes for Am/Cm Separation

Author
Leggett, Christina Joy

Publication Date
2012

Peer reviewed|Thesis/dissertation

Thermodynamic Investigations of Aqueous Ternary Complexes for Am/Cm Separation

By

Christina Joy Leggett

A dissertation submitted in partial satisfaction of the

requirements for the degree of

Doctor of Philosophy

in

Engineering – Nuclear Engineering

in the

Graduate Division

of the

University of California, Berkeley

Committee in charge:

Professor Stanley Prussin, Chair
Professor Joonhong Ahn
Professor Heino Nitsche
Dr. Mark Jensen

Spring 2012

Abstract

Thermodynamic Investigations of Aqueous Ternary Complexes for Am/Cm Separation

By

Christina Joy Leggett

Doctor of Philosophy in Nuclear Engineering

University of California, Berkeley

Professor Stanley Prussin, Chair

The separation of americium from curium in spent nuclear fuel (SNF) has important implications for spent nuclear fuel reprocessing. Removal of curium from SNF reduces the heat load in newly refabricated fuel elements and minimizes the buildup of heavier actinides (^{252}Cf) caused by repeated recycle of curium in reactors. Unfortunately, this separation has historically been difficult to accomplish due to their similar chemistries without resorting to chromatographic or precipitation techniques. However, a size-based approach to separating these two elements has been proposed that could easily be incorporated into solvent extraction-based separations schemes like the TALSPEAK process. In this approach, the formation of aqueous-phase ternary complexes (i.e., complexes of a metal with a large primary and smaller secondary ligand) with Am(III) – but not with Cm(III) – would increase the thermodynamic stability of Am(III) relative to Cm(III), making Am(III) less extractable. As there are few reports of ternary complexes in the literature, the objective of this work was to investigate the factors that influence their formation.

Factors such as ligand size, basicity, and steric constraints influence whether or not ternary complexes form and how strong such complexes will be. Spectroscopic, calorimetric, and thermometric techniques were used to investigate how these factors affect the formation of ternary complexes containing a large polyaminocarboxylate and a smaller dicarboxylate ligand bound to americium, neodymium, samarium, holmium, terbium, or erbium. Results from investigations with diethylenetriamine-N,N,N',N',N"-pentaacetic acid (DTPA), which is the octadentate ligand used in the TALSPEAK process, and lactate as the secondary ligand indicated that inner sphere complexes were not formed under the conditions used because the DTPA ligand is too large to accommodate lactate. Outer-sphere ternary complexes may form but they were estimated to be too weak to significantly affect the TALSPEAK extraction thermodynamics.

Ternary complexes were readily formed with the septadentate DO3A (1,4,7,10-tetraazacyclododecane-1,4,7-triacetic acid) and hexadentate CDTA (*trans*-1,2-diaminocyclohexanetetraacetic acid) ligands, whose binary complexes (e.g., $Ln(CDTA)^-$) have at least one residual water of hydration that can be displaced by a small secondary ligand. The results of thermodynamic investigations of $Ln(CDTA)^-$ complexes with the secondary ligands oxalate, malonate, and iminodiacetate revealed that the strength of the ternary complexes with CDTA generally increased with decreasing ionic radius when steric hindrance was minimal, indicating that the bonding with these ligands was primarily ionic. In addition, secondary

ligands that formed five-membered ring complexes were more stable than those that formed six-membered rings, and more basic ligands formed stronger complexes. Similar ternary complexes with DO3A showed little increase in thermodynamic stability compared to analogous CDTA complexes, which is likely due to increased steric hindrance in the DO3A complexes.

Table of Contents

List of Tables

List of Figures

List of Abbreviations

UREX: Uranium Recovery by Extraction

PUREX: Plutonium-Uranium Recovery by Extraction

TALSPEAK: Trivalent Actinide-Lanthanide Separation by Phosphorus reagent Extraction from Aqueous Komplexes

PACA: Polyaminocarboxylic acid

DTPA: Diethylenetriaminepentaacetic acid

CDTA: *trans*-1,2-diaminocyclohexanetetraacetic acid

DO3A: 1,4,7,10-tetraazacyclododecane-1,4,7-triacetic acid

DO3A·tBu: tri-*tert*-butyl-1,4,7,10-tetraazacyclododecane-1,4,7-triacetate

DOTA: 1,4,7,10-tetraazacyclododecane-1,4,7,10-tetraacetic acid

EDTA: Ethylenediaminetetraacetic acid

HMES: 4-morpholineethanesulfonic acid

Ln/An: Lanthanide/Actinide

Ln(III)/An(III): Trivalent lanthanide/actinide

HOTf: Trifluoromethanesulfonic (triflic) acid

TFA: Trifluoroacetic acid

Acknowledgements

I am grateful to the many people who have directly and indirectly helped me to reach this important point in my life. I'd like to start by thanking my advisor, Professor Stanley Prussin, for accepting me into his group and allowing me to pursue a research project of my own choosing. Many thanks go to Dr. Lynne Soderholm, my group leader at Argonne National Laboratory, for allowing me to work in the Heavy Elements and Separations group for three years. I owe a large debt of thanks to Dr. Mark Jensen, my research advisor at Argonne National Lab, who taught me how to be a good experimentalist and to think critically. Professor Joonhong Ahn has also helped and supported me in many ways over the years and I really cannot thank him enough. Lisa Zemelman, the nuclear engineering department's student affairs coordinator, deserves a ton of thanks for keeping me registered and funded, providing advice, and lending an ear when I needed it. Many thanks to the Department of Energy's Office of Civilian Radioactive Waste Management and to the University of California for providing most of my financial support over the years.

I must thank my very first advisor, Professor Gregory R. Choppin, who introduced me to nuclear- and radiochemistry when I did my freshman honors research project in his lab and has been a tremendous supporter of me throughout a large part of my academic career. I learned my first bits of real organic synthesis from Dr. Thomas Haxell, someone I now consider a good friend. Professor Heino Nitsche at UC-Berkeley/LBNL allowed me work in his laboratory during the summer of my junior year of college, which influenced my decision to apply to Berkeley. Dr. Patricia Stith has directly and indirectly supported me since I was a freshman in college by making it possible for me to present my undergraduate research in a variety of venues and encouraging me to go to graduate school.

Life in Chicago and at Argonne National Laboratory would have been depressing were it not for my wonderful friends and co-workers at the lab. I enjoyed (and miss) the coffee times spent with Mark Antonio and Renato Chiarizia. Work would have been soooo much less fun without you guys around to make me laugh. The friendship, support, and advice that Renato and his wife, Dr. Kate Martin, gave me while I was at Argonne is greatly appreciated. I had the joy of interacting with three great office/lab mates – Yannick Meridiano, Baikuntha Aryal, and Gengbang Jin – during my time at Argonne. A big thank you goes to the many friends I met at the University of Chicago and at Argonne for the great times we had outside of the lab: Van Bui, Tatiana Rodriguez, Nicole Brown, Takintayo Akinbiyi, Martin (the "Jerman") Feller, Matthew Thibault, Aaron Marcus, Laura D'Amico, Maria Escudero, Francisco Javier Blas, Salil Arora, Carmen Lopez, Krishna Narayanan, Dani Torres, Marieke Heisen, and Sergio Barrera.

I am thankful that my parents have always encouraged my academic and scientific pursuits from a young age. I'm sure my mom still laughs about the numerous experiments I used to leave around the house as a kid. My sister has always been a close friend and confidant in my life and I am really thankful for that.

Lastly, but definitely not least, I give special thanks to Nathan Moore for being very patient and devoted throughout nearly all of my tenure in graduate school – even while I was away in Chicago for three years.

Chapter 1 Introduction

1.1 Nuclear Power in the United States

The successful demonstration of the world's first man-made nuclear reactor by Enrico Fermi's group on December 2, 1942[1] was a major landmark in the development of nuclear power. Besides the subsequently developed nuclear weapons deployed during World War II, the most important product of this sustained nuclear reaction is arguably the nuclear reactor. Today, nuclear reactors serve a variety of purposes, the majority of which include providing electricity, powering submarines, and producing many of the necessary radionuclides for medical imaging and treatments.

Currently, there are 104 commercial nuclear power reactors in operation in the United States. Together, they generate about 20% of all U.S. electricity and provide the largest source of emission-free electricity in the country.[2] These reactors are categorized as *light water reactors* (LWR's), meaning that they are cooled and moderated by "normal" or "light" water (H_2O) as opposed to *heavy water reactors*, which are cooled and moderated by deuterated water (D_2O). Light water reactors are further subdivided into two types: boiling water reactors (BWR) and pressurized water reactors (PWR). The majority of the reactors (69) in the United States and in the world are pressurized water reactors.

In PWRs, the coolant (water), located in the primary cooling loop, enters the reaction vessel at approximately 290°C at 15 MPa and is heated to about 325°C by flowing through the core. Because of the elevated pressures involved, the water does not boil to a significant extent inside the reactor core. Therefore, in order to generate steam, an externally-located steam generator is required. Superheated water flows out of the reactor vessel into the steam generator. Heat transfer between the superheated water in the primary loop and the colder water in the steam generator produces steam, which then passes through a turbine that drives an electrical generator. Waste steam from the turbine flows through a condenser and returns to the steam generator. Boiling water reactors, on the other hand, directly produce steam in the reactor by heating the water in the reactor core to approximately 290°C at 7 MPa pressure. After being dried by steam separators and dryers located at the top of the core, the dry steam passes out of the core to a turbine that drives the electrical generator.[3]

Nuclear fissions induced by thermal neutrons ($E_{neut} \cong 0.025$ ev) produce the majority of the heat that boils the water in PWRs and BWRs. Thermal neutrons are produced when fast (100 keV $\leq E_{neut} \leq$ 3 MeV) neutrons undergo collisions with the hydrogen in the water flowing through the core, reducing their energies. Thus, these reactors are termed *thermal* reactors, as opposed to *fast* reactors, which use fast neutrons to fission uranium nuclei. Many fast reactors are breeder reactors because they produce more than one fissile fuel atom for every fissile atom consumed. The conversion ratio, which is the average number of fissile atoms produced per fissile atom consumed, approaches three for U-238, U-235, and Pu-239 when fast neutrons are used. In contrast, when thermal neutrons are used, the conversion ratio is generally less than unity for these fissile nuclei, making breeding more difficult. Therefore, light water reactors are considered to be burner reactors.

Nuclear reactor fuels for both the PWR and BWR designs use uranium oxide fuel that is enriched up to about 5% in U-235; the remainder of the uranium is predominantly U-238. The uranium oxide fuel is comprised of powdered UO_2 that has been pressed into cylindrical pellets and sintered at high temperatures to produce a ceramic pellet. These pellets are stacked in long cylindrical tubes called *fuel rods* and are about 13 ft long in PWRs and 14.5 ft long in BWRs. The tubes themselves, often referred to as *cladding*, are generally made of stainless steel or Zircaloy, which is a zirconium alloy. The cladding provides a major barrier between the coolant and the nuclear fuel itself. Fuel rods are bundled into *fuel assemblies*; in PWRs, 264 fuel rods typically make up a fuel assembly, whereas only 63 fuel rods make up assemblies in BWRs.[4] In total, there are 150-250 fuel assemblies in a PWR and up to 750 fuel assemblies in a BWR. These assemblies comprise the core of the reactor. A PWR reactor requires 80-100 metric tons of uranium (MTU) in the core whereas the BWR requires about 140 MTU in the core.[5] Every 18 to 24 months, the reactor will discharge approximately one-third of the UO_2 fuel from the core. This discharged fuel is then considered spent nuclear fuel.

1.2 Spent Nuclear Fuel Reprocessing

1.2.1 Sources, Locations, and Composition of Spent Nuclear Fuel

Despite all of its benefits, a major drawback of nuclear reactor technologies is the spent nuclear fuel (SNF) produced as a result of reactor operation. As of 2009, the nation's total inventory of SNF from commercial nuclear reactors was approximately 63000 MTU.[6] In addition, these reactors cumulatively discharge more than 2,000 metric tons of spent nuclear fuel per year.[7] Defense-related nuclear operations have generated a combined 2,500 metric tons of spent nuclear fuel,[8] not including wastes from reprocessing. The amount of spent nuclear fuel due to research reactor operation and medical isotope production is comparatively negligible.

Spent fuel is currently stored primarily in pools of water adjacent to the reactor to allow short-lived radionuclides to decay and to allow the fuel to cool to levels that are safe for handling by nuclear workers. The spent fuel pools are designed to provide cooling and shielding and are arranged in a format that minimizes criticality risks. As the pools fill, spent fuel assemblies that have been cooled at least five years can be moved to an independent spent fuel storage facility located either on the reactor site or elsewhere. At present, there are 55 independent spent fuel storage facilities located in 33 states.[9]

It is important to know which elements are present in spent nuclear fuel in order to, at the very least, design a suitable storage facility or repository for the fuel. The most important factors that affect the composition of spent nuclear fuel are the composition of the initial fuel (e.g., enrichment levels and elemental composition), irradiation and cooling times, and the operational history (e.g., neutron flux and energies) of the reactor in which the fuel is irradiated. For example, higher-enriched uranium oxide fuel generally produces spent fuel with larger concentrations of fission products and transuranium elements than SNF generated from lower enriched fuel. Charging a reactor with uranium metal fuel would change the elemental composition of SNF relative to spent fuel generated from uranium oxide fuel. Lastly, longer

irradiation times tend to lead to higher concentrations of long-lived fission products, and increased cooling time lowers the concentration of short-lived products.[10,11]

In general, the elemental composition of SNF by volume is about 95% uranium, 3.4% fission products (including gaseous products), 1% plutonium, and 0.6% minor actinides (principally Np, Am, and Cm).[10] Figure 1 below shows a representative estimate of the yields of fission product elements present in uranium fuel that has been discharged from a 1000 MWe reactor and cooled for 150 days. The fission products can be grouped into noble gases (xenon, krypton), volatile solids (iodine), transition metals, alkali/alkaline-earth metals (primarily cesium and strontium), and lanthanide elements. The nuclear properties and chemistry of the elements in each of these groups must be considered for the design of long-term storage facilities, reprocessing systems, and fuel fabrication (after reprocessing). To elaborate, samarium and neodymium, two of the lanthanides that are produced in the greatest abundance in spent reactor fuel, have isotopes that are stable (or long-lived) and have large or very significant thermal neutron capture cross sections (e.g., 3.52×10^4 barns for Sm-149). Such elements, if included with uranium for fuel fabrication, behave as neutron poisons in power reactors. Iodine-129 ($t_{1/2} = 1.7 \times 10^7$ years) and Tc-99 ($t_{1/2} = 2.13 \times 10^5$ years) are important from an environmental perspective – technetium forms soluble pertechnetates (TcO_4^-) that are mobile in the environment and iodine forms several different soluble species (e.g., iodide), many of which are easily taken up by plants and animals.[12] These radioisotopes are also long-lived and thus are important when determining long-term health risks associated with their possible release and migration from nuclear facilities such as repositories or reprocessing plants.[13] Cs-137 ($t_{1/2} = 30$ years) and Sr-90 ($t_{1/2} = 28$ years) and their decay products are responsible for most of the heat generation for the first 60 years after SNF is discharged from the reactor.[14] The production of these and several other shorter-lived isotopes during reactor operation are the reason spent fuel requires cooling for a considerable amount of time upon discharge.

The elements present in spent nuclear fuel in the largest amount by volume are uranium (95%) followed by plutonium (1%). Typical masses of actinide isotopes and their relative isotopic compositions in uranium fuel discharged from a 1000 MWe reactor are shown in Table 1. Based on the data, the actinide isotopes present in the highest amounts are U-235, U-238, Np-237, Pu-239, Am-241, Am-243, and Cm-244.[10] Each of these isotopes has important implications for radioactive waste management and fuel recycling. For example, after approximately 100 years, 99% of the long-term decay heat and a majority of the ingestion toxicity in SNF are due to actinides – in particular, plutonium, neptunium, and americium.[10] Neptunium-237 is particularly mobile in the environment and is an important contributor to long-term (>100,000 years) radiotoxicity and activity in spent fuel.

The uranium from discharged reactor fuel can be recovered and blended with natural uranium to produce more reactor fuel that can be used in light water reactors. Also, the principal Np, Pu, Am, and Cm isotopes can in principle be destroyed in specially-designed fast reactors. Clearly, the recovery of actinides would cause a tremendous reduction in the volume of spent nuclear fuel requiring permanent disposal as well as reductions in long-term radiotoxicity, decay heat, and activity in spent fuel storage containers.

The concept of reprocessing spent nuclear fuel to recover valuable actinides is not a new one, however. Several reprocessing technologies for recovering uranium and/or plutonium have been developed over many decades beginning with the bismuth phosphate process, which was employed during World War II for plutonium recovery.

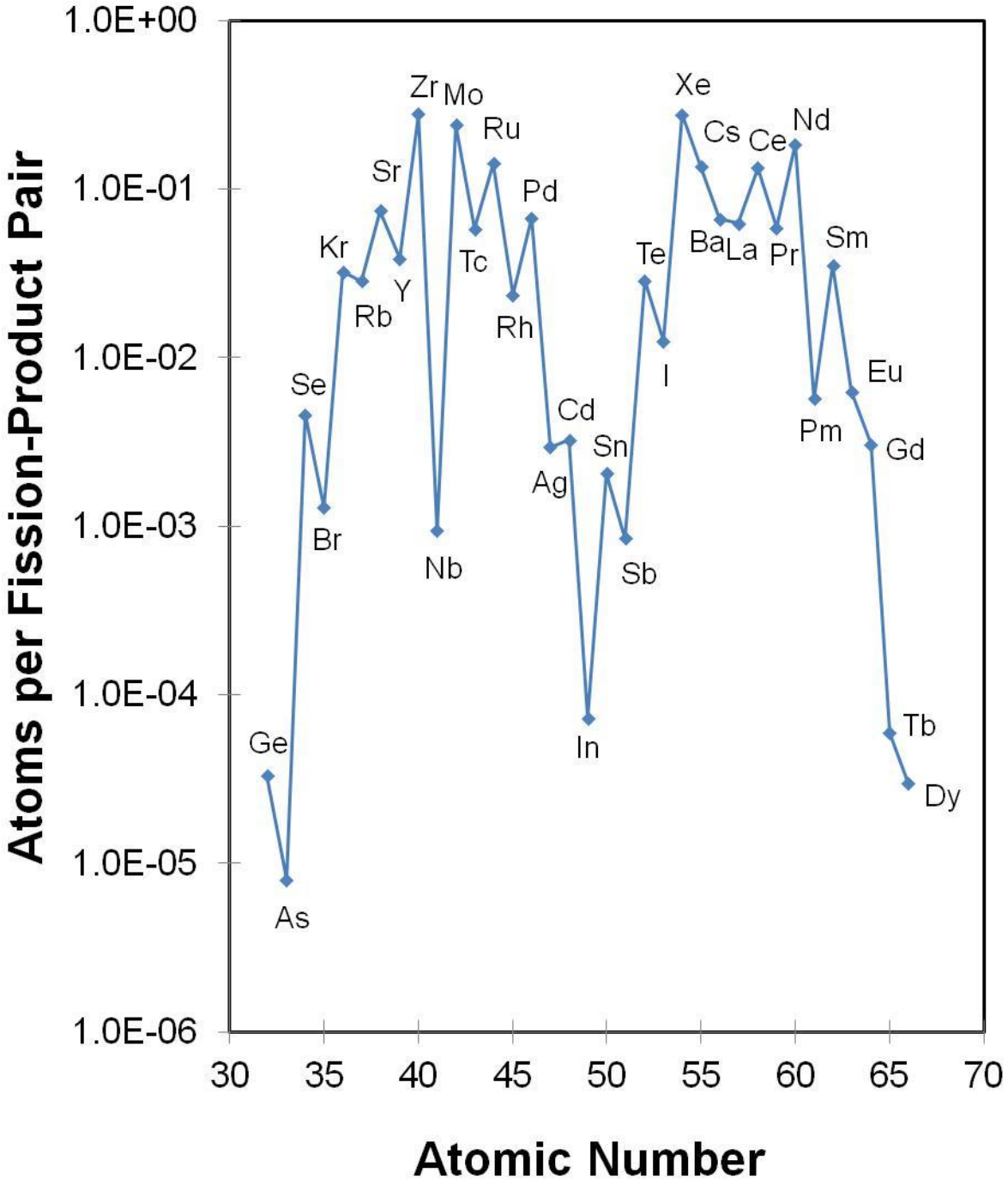

Figure 1.1 Chemical composition of fission products 150 days after discharge (uranium-fueled PWR). Generated using data obtained from reference 11. Note the logarithmic scale of the ordinate.

Table 1.1 Masses and Relative Isotopic Compositions of Spent Nuclear Fuel 150 Days after Discharge[10]

Actinide	Isotope	kg/yr in spent nuclear fuel	Relative Isotopic Composition, %
Uranium	U-234	3.1	< 0.01
	U-235	**210**	**0.8**
	U-236	110	0.4
	U-237	9.1×10^{-7}	< 0.01
	U-238	**2.6×10^{4}**	**98.8**
Neptunium	**Np-237**	**20**	**100**
	Np-239	2×10^{-6}	< 0.01
Plutonium	Pu-236	2.5×10^{-4}	< 0.01
	Pu-238	6.0	2.5
	Pu-239	**140**	**57.7**
	Pu-240	59	24.3
	Pu-241	28	11.5
	Pu-242	9.7	4.0
Americium	**Am-241**	**1.3**	**34.1**
	Am-242m	0.012	0.3
	Am-243	**2.5**	**65.6**
Curium	**Cm-242**	**0.13**	**11.8**
	Cm-243	2×10^{-3}	0.2
	Cm-244	**0.91**	**82.5**
	Cm-245	0.055	5.0
	Cm-246	6.2×10^{-3}	< 0.6

1.2.2 A Brief History of Spent Nuclear Fuel Reprocessing

1.2.2.1 Background

The development of nuclear fuel reprocessing technologies began with the discovery of plutonium two years before Enrico Fermi's demonstration of an artificially sustained nuclear reaction. From December 1940 to February 1941, Kennedy, McMillan, Seaborg, and Wahl conducted the experiments that led to the discovery of Pu-238. They bombarded natural uranium with 16 MeV deuterons at the 60-inch cyclotron located at the University of California – Berkeley and produced 2.112-day Np-238, which then decayed to Pu-238[15,16]:

$$^{238}_{92}\mathrm{U} + {}^{2}_{1}\mathrm{D} \rightarrow {}^{238}_{93}\mathrm{Np} + 2\,{}^{1}_{0}\mathrm{n}$$

$$^{238}_{93}\mathrm{Np} \rightarrow {}^{238}_{94}\mathrm{Pu} + {}^{0}_{-1}\mathrm{e}$$

Within a few months of the discovery of Pu-238 ($t_{1/2}$ = 87.7 yr), Pu-239 ($t_{1/2}$ = 2.41 x 10^4 yr) was synthesized via U-239 ($t_{1/2}$ = 23.5 min) and Np-239 ($t_{1/2}$ = 2.355 d) by bombarding uranium with neutrons at the 60-inch cyclotron[17]:

$$^{238}_{92}\mathrm{U} + {}^{1}_{0}\mathrm{n} \rightarrow {}^{239}_{92}\mathrm{U}$$

$$^{239}_{92}\mathrm{U} \rightarrow {}^{239}_{93}\mathrm{Np} + {}^{0}_{-1}\mathrm{e}$$

$$^{239}_{93}\mathrm{Np} \rightarrow {}^{239}_{94}\mathrm{Pu} + {}^{0}_{-1}\mathrm{e}$$

Although very small quantities of Pu-239 were available for study, the relatively short half-life of Pu-238 made it an excellent candidate for tracer studies of plutonium; thus, most of the early studies of the chemistry of plutonium were conducted with this isotope. The results from these studies indicated that tetravalent plutonium could be precipitated as an insoluble fluoride or iodate in the presence of a lanthanide or thorium carrier. The hexavalent state, however, was soluble under these conditions.[18] Seaborg would later apply the information obtained from these ultramicroscale experiments to the development of the first large-scale reprocessing scheme known as the bismuth phosphate process.

It was quickly discovered that Pu-239 had a thermal neutron capture cross-section that was much larger than that for U-235[19], implying that a more effective nuclear weapon could be manufactured from Pu-239. Furthermore, it could be chemically separated from uranium unlike U-235, which required repeated isotope separations. This information coupled with the success of Fermi's sustained nuclear chain reaction in 1942 prompted the government to commence the construction of nuclear reactors at the Hanford site near Richland, Washington to produce large quantities of plutonium from natural uranium. However, in order to isolate essentially pure Pu-

239 for weapons production, a large-scale separations process needed to be developed. Several separations processes were investigated, including solvent extraction, precipitation, gas centrifugation, volatility, and pyrometallurgical processes. Seaborg later stated that he decided to use the precipitation method because it "seemed to offer the greatest certainty of at least limited success in the short time interval involved."[17] The bismuth phosphate process was then developed as an outgrowth of earlier lanthanide carrier-precipitation research conducted with Pu-238 in 1941. This process represented a factor of approximately 10^9 scale-up in process design[20].

1.2.2.2 The Bismuth Phosphate Process

The bismuth phosphate process separated plutonium from uranium and all fission products in irradiated nuclear fuel by co-precipitating insoluble plutonium(IV) phosphate, $Pu_3(PO_4)_4$, with bismuth phosphate, $BiPO_4$. The process began with the dissolution of the fuel elements, which contained primarily uranium, plutonium, and fission products, in nitric acid containing a small amount of sulfuric acid. Plutonium was then reduced to Pu(IV) by the addition of sodium nitrite. The addition of a mixture of bismuth nitrate and sodium phosphate yielded insoluble $BiPO_4$ and $Pu_3(PO_4)_4$, which co-precipitated from the solution. The formation of soluble uranyl sulfate prevented uranium from also precipitating as uranyl phosphate. The $BiPO_4/Pu_3PO_4$ precipitate was then redissolved in nitric acid and plutonium was oxidized to the hexavalent state by adding sodium bismuthate or another strong oxidant. Next, $BiPO_4$ was precipitated to remove remaining fission products from the solution, thereby decontaminating the plutonium. After removal of the precipitate, the oxidized plutonium was then reduced to the tetravalent state and re-precipitated with $BiPO_4$. This decontamination cycle was done twice and was followed by a precipitation cycle in which LaF_3 was used as the carrier instead of $BiPO_4$ to further purify the plutonium. Additional steps were carried out to yield plutonium nitrate.

Although several steps were involved in the bismuth phosphate process, the overall recovery of plutonium was more than 95% and the overall decontamination factor, which is the ratio of the fraction of fission products in solution before and after fission product removal, was 10^7.[11] However, large volumes of waste were generated and the process required copious amounts of process chemicals (e.g., $BiPO_4$). Furthermore, the process was a batch operation rather than a continuous one, which slowed down plant operations. Lastly, the fact that the bismuth phosphate process did not recover uranium, a vital fuel component, was a significant problem for the process and led to the research and development of other processes like the Redox and PUREX processes after the war.

1.2.2.3 The Redox Process

After the Second World War, scientists were able to focus on developing a continuous process that could separate both plutonium and uranium from irradiated nuclear fuel for weapons production during the Cold War. Solvent extraction was most heavily researched because it was already in use on a large scale to recover uranium from ore leach liquors. The resulting Redox ("REDuction-OXidation") process was the first large scale solvent extraction process used to separate plutonium *and* uranium from irradiated fuel. The process was developed at Argonne National Laboratory in Chicago, IL and replaced the bismuth phosphate process that was used at the Hanford plant in 1951.

The Redox process used hexone (methyl isobutyl ketone) as the organic solvent and extractant. A solvating ligand, hexone forms adducts with coordinatively unsaturated compounds of trivalent, tetravalent, and hexavalent actinides[21]:

$$An^{+3}+3NO_3^-+3L(org) \Leftrightarrow An(NO_3)_3L_3(org)$$

$$An^{+4}+4NO_3^-+2L(org) \Leftrightarrow An(NO_3)_4L_2(org)$$

$$AnO_2^{+2}+2NO_3^-+2L(org) \Leftrightarrow AnO_2(NO_3)_2L_2(org)$$

where ligand L is methyl isobutyl ketone and An^{+3}, An^{+4}, and AnO_2^{+2} represent trivalent, tetravalent, and hexavalent actinides, respectively. The nitrate anion was used to balance the actinide charge because nitrates were used in the actual process at Hanford; this equation holds for other anions as well. The process was most selective for uranyl- and plutonyl-nitrate when the nitrate concentration in the aqueous phase was sufficiently high. A solution of aluminum nitrate in dilute nitric acid was selected as the aqueous phase because the aluminum nitrate is compatible with hexone; concentrated nitric acid decomposes hexone.

At the beginning of the process, plutonium was oxidized to the hexavalent state using sodium dichromate. Hexavalent plutonium and uranium were extracted into hexone, thereby removing them from the aqueous phase fission products. The hexone phase was washed with a solution of aluminum nitrate, sodium nitrate, and sodium dichromate to remove further fission product impurities prior to further processing. The plutonium in the hexone phase was then back-extracted into an aqueous solution of ferrous sulfamate and aluminum nitrate, which left the uranium and residual fission products in the hexone phase. Uranium was back-extracted into dilute nitric acid. Additional solvent extractions with each aqueous product stream were done to further purify the recovered uranium and plutonium.

Advantages of the Redox process over the bismuth phosphate process were that uranium and plutonium were recovered in good yield (99.9% and 99.8%, respectively) with decontamination factors of 10^7 for uranium and 10^8 for plutonium.[22] The process was also a continuous process rather than a batch operation. However, the necessity of a salting agent (i.e., $Al(NO_3)_3$) and large quantities of other nonvolatile reagents in the Redox process meant that high volumes of waste were generated. The volatility and flammability of hexone as well as its instability to nitric acid were also problematic for the process.

1.2.2.4 The Butex Process

British chemists working at the Chalk River Laboratories (Ontario, Canada) in the late 1940s developed the Butex extraction to preclude the need for salting agents. Indeed, the Butex process was the first large-scale process that did not use salting agents. Instead, the "salting agent" was nitric acid, which was easily recovered by evaporating the nitric acid for reuse in the cycle. This fact had the added benefit of substantially reducing the volume of waste generated.

The process consisted of two extraction cycles for plutonium recovery and purification: one cycle that used neat dibutylcarbitol ($C_4H_9OC_2H_4OC_2H_4OC_4H_9$) to extract primarily plutonium and uranium from nitric acid solutions of spent fuel and a second cycle that used 20% tributylphosphate (TBP) in kerosene for further plutonium purification. In the first extraction

cycle, the aqueous solution, which contained nitrates of Pu(IV) and Pu(VI), U(VI), and fission products was first contacted with dibutylcarbitol. The dibutylcarbitol extracts uranium, plutonium, and significant amounts of the fission product ruthenium with smaller amounts of zirconium, niobium, and cerium. Plutonium and a small amount of ruthenium were stripped from the remaining products by contacting the organic phase with an aqueous solution of ferrous sulfamate, $Fe(NH_2SO_3)_2$, which reduced plutonium to the inextractable Pu(III). The plutonium in the solution was subsequently oxidized back to the hexavalent state, extracted into dibutylcarbitol, and subsequently stripped with dilute nitric acid. At this point, the plutonium was subjected to a second extraction cycle using TBP to remove residual ruthenium, producing a relatively pure plutonium product. The uranium that remained in the organic phase after the initial plutonium stripping was stripped with dilute nitric acid. Addition of hydrazine and ferrous sulfamate converted residual plutonium and ruthenium to their inextractable forms, allowing relatively pure uranium to be extracted into dibutylcarbitol.[23]

The Butex process was successful in pilot plant tests and was employed at the Windscale plant in England to reprocess uranium irradiated to low burnup until the 1970s when an explosion occurred, terminating its use. It was replaced by the PUREX process.

1.2.2.5 The PUREX Process

The PUREX (**P**lutonium-**U**ranium **R**ecovery by **EX**traction) process was initially developed at Knolls Atomic Power Laboratory. Additional research and testing up to the pilot-plant scale were carried out at Oak Ridge National Laboratory from 1950-1952. The process was inspired by the results of research conducted by James C. Warf on solvent extractions of trivalent and tetravalent cerium nitrate with TBP. The results showed that tetravalent cerium nitrate could be extracted by tributylphosphate from trivalent rare-earths by solvent extraction; Ce(III) was unextractable by TBP. Also, thorium and hexavalent uranium were observed to be extractable by TBP.[24] It was later shown that the +1, +2, +3, +5, and +7 oxidation states of fission products were not extractable by TBP at high nitric acid concentrations.[25] The PUREX process, much like the previously discussed processes, took advantage of the extractability and inextractability of the multiple oxidation states of actinides to achieve selective separations.

The process used a solution of TBP in kerosene to extract Pu(IV) and U(VI) from nitric acid solutions of actinides and fission products. Prior to the extraction, plutonium was reduced to the tetravalent state using a suitable reductant (e.g., N_2O_4 or $NaNO_2$). Solvent extraction of this solution with 30% TBP in kerosene removed uranium and plutonium, leaving behind more than 99% of fission products and the trivalent actinides in the aqueous phase. In order to effect a separation of plutonium from uranium, the organic phase was contacted with an aqueous phase containing a suitable reductant to reduce Pu(IV) to the essentially inextractable Pu(III). Plutonium was then purified by additional solvent extraction steps and ultimately converted to PuO_2. The uranium stream was purified similarly. Major advantages of the PUREX process over Redox are that waste volumes and operating costs are lower, TBP is less volatile and flammable than hexone, and that TBP is also more stable against attack by nitric acid.

The PUREX process was eventually used at the Savannah River plutonium production facility in 1954, and in 1956, it replaced the Redox process which was being used at Hanford. Ten years later, it was used successfully for six years at the West Valley, New York reprocessing plant, which was most notable for being the only plant to reprocess privately-owned nuclear fuel in the United States. Today, the PUREX process is currently or has been used in several

countries, including France, Russia, Germany, and Japan. It is now the most popular process for recovery of pure plutonium and uranium in the world.

1.2.3 Current Status of Reprocessing in the U.S.

Although the United States has decades of reprocessing experience with defense nuclear fuel, it no longer reprocesses defense or commercial spent nuclear fuel. The decision to halt commercial reprocessing was made by President Carter in 1977 due to concerns about the possible proliferation of plutonium as a result of reprocessing with PUREX.[26] The ban on commercial reprocessing was eventually lifted by President Reagan in 1982 but no federal subsidy was or has been provided for the construction of new facilities. For the reasons described above, the United States still operates on a "once-through" or "open" fuel cycle in which uranium fuel is ultimately destined for permanent disposal after discharge from a nuclear reactor.

Government policy within the last decade has begun addressing the possibility of reprocessing in conjunction with new reactor technologies for solving "the waste problem." In 2001, the National Energy Policy Development Group (NEPDG), per the direction of President George W. Bush, published its National Energy Policy in which they recommended to the President that the United States should

> "consider technologies (in collaboration with international partners with highly developed fuel cycles and a record of close cooperation) to develop reprocessing and fuel treatment technologies that are cleaner, more efficient, less waste intensive, and more proliferation-resistant."[27]

A year later, the Department of Energy initiated the Advanced Fuel Cycle Initiative (AFCI) program, which replaced the Advanced Accelerator Applications program, in accordance with this recommendation. The primary goal of the AFCI program[28] is to develop advanced, proliferation-resistant processes to treat and destroy spent fuel. It eventually became the domestic component of the Global Nuclear Energy Partnership, proposed in 2006, with the goal of deploying reprocessing technology by 2025.

In essence, the United States was well on its way to finally realizing commercial reprocessing. However, critics believed that the relatively rapid deployment of reprocessing was commencing too quickly and still others asserted that reprocessing using currently available technology (i.e., PUREX) was too expensive. Thus, in 2009, the Obama administration cancelled the accelerated plans for commercial reprocessing and redirected the AFCI program to once again focus its efforts on researching and developing advanced, proliferation-resistant reprocessing technologies.[29] The name of the AFCI program was also changed to "Fuel Cycle Research and Development" (FCR&D) program to emphasize its new focus. The solvent extraction-based reprocessing technology that is now the most heavily studied by FCR&D-funded researchers is known as the UREX+ process.

1.2.4 The Urex+ Process

The development and successful laboratory-scale demonstration of the UREX+ process was an important product of the research efforts for the Advanced Fuel Cycle Initiative. Developed by researchers at Argonne National Laboratory, the UREX+ process is a suite of several solvent extraction steps that can be deployed to segregate the components of spent nuclear fuel into groups either for storage or for reuse in nuclear reactors. Several variants of the UREX+ process have been designed based on potential storage and/or recycling schemes as shown in Table 1.2.

Table 1.2 Variations of the UREX+ Process[30,*,†]

Process	Product #1	Product #2	Product #3	Product #4	Product #5	Product #6	Product #7
Urex+1	U	Tc	Cs/Sr	TRU/Ln	FP		
Urex+1a	U	Tc	Cs/Sr	TRU	Fp/Ln		
Urex+2	U	Tc	Cs/Sr	Pu/Np	Am/Cm/Ln	FP	
Urex+3	U	Tc	Cs/Sr	Pu/Np	Am/Cm	FP	
Urex+3a	U	Tc	Cs/Sr	U/Pu/Np	Am/Cm	FP/Ln	
Urex+4	U	Tc	Cs/Sr	Pu/Np	Am	Cm	Fp/Ln
Urex+4a	U	Tc	Cs/Sr	U/Pu/Np	Am	Cm	Fp/Ln

[*]Note that iodine is removed as an off-gas during dissolution of fuel. [†]Legend: TRU = Transuranium elements, FP = Fission products, Ln=Lanthanides

As discussed earlier, one of the primary goals of the Advanced Fuel Cycle Initiative was to develop a reprocessing scheme that is proliferation-resistant. A remarkable feature of the UREX+ suite of processes is the fact that none of its variations produces a pure plutonium product, creating enhanced proliferation resistance. In addition, each of the product streams plays an important role in the management of spent fuel as discussed in Section 1.2.1. The highly-purified uranium can be re-fabricated as LWR fuel, while the actinides in the fourth and fifth product streams can be recycled as fast reactor fuel. The removal of cesium and strontium is important for short-term decay heat management while the lanthanides, fission products, technetium, and iodine can be stabilized for long-term disposal.

1.3 Motivation for Dissertation Research Project

The UREX+4 and UREX+4a processes are unique in that they both have a separate americium and curium product stream. Although americium and curium can be burned in fast reactors to produce useful energy, the high decay heat and neutron emission due to curium isotopes creates a serious handling problem for workers. Table 1.3 below compares decay heats and neutron emissions among Pu-238, Am-241, Cm-244, and Cf-252.

Table 1.3 Decay Heats, Half-Lives, and Neutron Emission Rates for Pu, Am, Cm, and Cf Isotopes[31,32,33]

Isotope	Half-Life, yrs	Decay Heat*, W g^{-1}	Neutron Emission rate, neutrons s^{-1} g^{-1}
Pu-238	87.7	0.56	2590
Am-241	432.7	0.114	1.18
Cm-244	18.1	2.83	1.08×10^{7}
Cf-252	2.65	39	2.31×10^{12}

*Decay heat determined using data from reference 31.

Cm-244 is the most abundant curium isotope present in spent nuclear fuel and has a very high neutron capture cross section. Thus, the repeated recycle of this isotope in nuclear reactors eventually leads to californium-252 due to successive neutron capture reactions and beta minus decays (Figure 1.2). In addition to having high decay heats, the curium isotopes and Cf-252 are very strong neutron emitters – much higher than Pu-238, which is typically used in heat sources. In fact, Cf-252 neutron sources have all but supplanted traditional neutron sources, which include PuBe (plutonium-beryllium), AmBe (americium-beryllium), and CmBe (curium-beryllium) sources.[34] These two factors make curium and californium handling and storage problems as well as a health risk for radiological workers at reactors and reprocessing facilities.

In addition to the potential health hazards associated with curium and californium production, fabrication of fuel containing curium would require forced cooling and heavy shielding in fabrication facilities. Addition of extra shielding and automated cooling adversely affects the economics of reprocessing. More importantly, the presence of curium mixed with americium reduces the total amount of minor actinide (i.e., americium and curium) loading for fast reactor fuels to prevent the melting of the fuel.[35]

Thus far, only UREX+1a, UREX+2, and UREX+3a have been demonstrated on the laboratory-scale at Argonne National Laboratory.[30] The UREX+4 and UREX+4a processes have not been demonstrated because no suitable large-scale process for separating americium from curium has been developed. Therefore, FCR&D-funded research is being conducted at several national laboratories on solvent extraction processes to separate americium from curium. At Argonne National Lab, the TALSPEAK process, in which trivalent actinides are separated from trivalent lanthanides, has been a framework in which separation of americium from curium is being studied. Two possibilities exist for effecting this separation: modifying the current TALSPEAK process conditions such that americium is separated from curium *and the*

lanthanides or appending an additional step after the TALSPEAK process to separate americium from curium.

This work describes the research performed by the author on the thermodynamics of aqueous phase ternary complex formation under TALSPEAK-like conditions for the ultimate goal of separating americium from curium. Spectrophotometry, calorimetry, fluorescence, and potentiometry have been employed to measure the enthalpies, free energies, and entropies of ternary complex formation in order gain insights into the driving forces behind aqueous phase ternary complex formation.

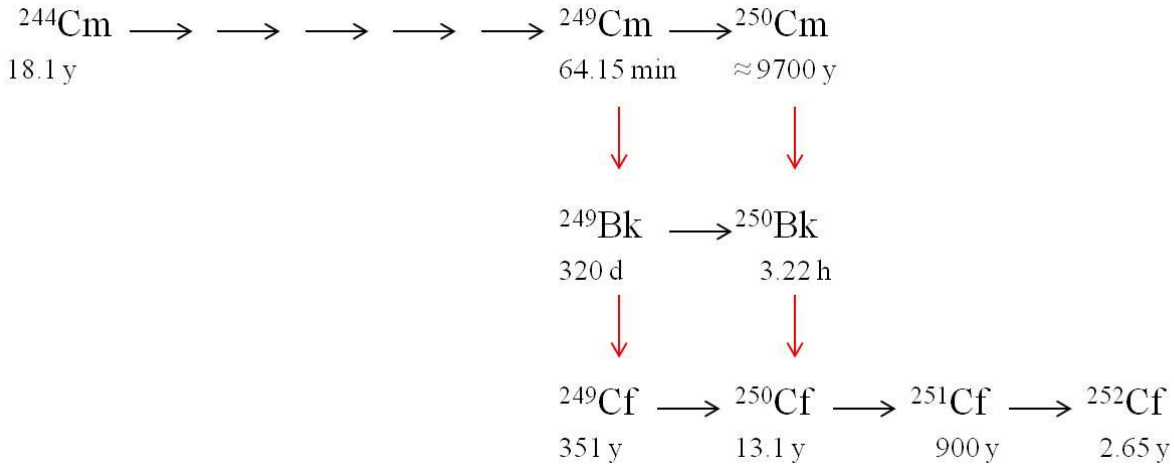

Figure 1.2 Production of ^{252}Cf adapted from reference 36. Black arrows represent capture of one neutron and red arrows represent beta minus decays. For example, according to the figure, five neutrons were captured by ^{244}Cm to produce ^{249}Cm, which then either captures another neutron or undergoes beta minus decay to form ^{249}Bk.

Chapter 2 Solution Chemistry and Thermodynamics

2.1 Metal Ions in Solution

2.1.1 Hydration of Metal Ions

Metal cations are extensively hydrated in aqueous solutions. An understanding of the nature and strength of their hydration is necessary to accurately describe the thermodynamics of their complexation reactions with a variety of ligands. The hydration state of metal cations can be understood using a model in which four structurally different zones of solvation exist around the central cation. Figure 2.1 below is an illustration of the model.

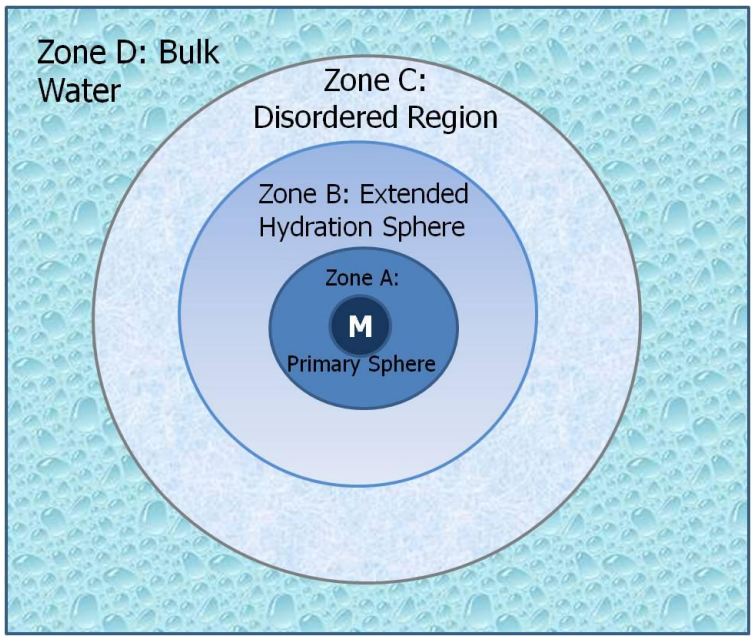

Figure 2.1 Hydration zones around a metal cation.[37]

Zone A is considered to be the primary solvation shell or primary coordination sphere. The water molecules in this region most strongly affect complexation reactions as they are directly bound to the metal cation, indicated by the letter "M" in the figure. The number of water molecules in this region defines the hydration number of the metal cation. Zone B is an extended sphere – also called the secondary coordination sphere – where additional water molecules,

though not directly bound to the metal, still experience the electric field due to the metal cation. These water molecules are likely hydrogen-bonded to water molecules in the primary coordination sphere. At this point, the total number of waters of hydration is equal to the number of water molecules in zones A and B. Beyond zone B, the third zone is a disordered region of water molecules with properties intermediate of those in the secondary coordination sphere and the bulk solvent, zone D. Of course, the water molecules in zone D have the bulk structure of water and are essentially unaffected by the presence of charged cations.

It is important to note that this model applies fully in dilute solutions and is a fairly accurate approximation in solutions with a total salt concentration of less than 0.1 M for 1:1 electrolytes (e.g., NaCl); for solutions containing polyvalent ions, the maximum concentration is lower.[38] Under these conditions, the cations and anions are sufficiently surrounded by water molecules that their mutual interactions are minimal; in more concentrated solutions, however, the effect of the anions on cation hydration must also be accounted for.

2.1.2 Classification of Metal Ions: Hard-Soft Acid-Base Theory

All metal cations are electron-pair acceptors or Lewis acids and undergo reactions with with electron-pair donors, which are Lewis bases. For brevity, a Lewis acid or Lewis base will hereafter be referred simply as an acid or a base. The types of reaction that can occur depend on the nature of the acids and bases involved and, for a long time, much effort was devoted to developing models that could predict the products of these reactions. Today, the most popular theory used to predict the products is Ralph Pearson's Hard-Soft Acid-Base (HSAB) Theory.[39] The model was first proposed in 1963 and essentially expanded on earlier models proposed by Schwarzenbach[40] and Ahrland, Chatt, and Davies[41].

In the model, Lewis acids and bases are subdivided into hard, soft, and borderline categories based on such characteristics as polarizability, electronegativity, oxidation state, electronic structure, and ionic radius. The main concept of the theory is that acids and bases in the same category generally react favorably to form a complex. That is, hard acids bind preferentially with hard bases, soft acids bind favorably with soft bases, and reactions involving acids and bases from different groups tend to proceed to a small extent. However, it must be emphasized that these are only guidelines and do not apply to all complexation reactions. Table 2.1 below summarizes the characteristics of hard and soft acids and bases.

Two main conclusions can be drawn from the information listed in the table. First, the lowest unoccupied molecular orbital (LUMO) of the hard acid is high in energy and the highest occupied molecular orbital (HOMO) of the hard ligand is low in energy, implying that very little covalent bonding is possible between hard acids and bases due to the large energy difference between the orbitals. With tightly bound atomic electrons (low polarizability), high charges, and small sizes for both hard acids and bases, it is clear that the bonding mode is predominantly ionic in nature. On the other hand, soft acids and bases have lower-energy LUMO's and high-energy HOMO's, respectively, with a smaller energy difference between them – conditions that are conducive to covalent bonding. Very little extra stability is gained from ionic interactions due to the ions' low polarizabilities and large sizes. Salts of soft acids and bases are generally much less soluble than ionic salts – i.e., those that are formed from hard acid/base reactions – in water.

Table 2.1 Summary of Hard-Soft Acid-Base Theory[42]

Property of Lewis Acid	Hard	Soft
Electropositivity	High	Low
Oxidation State/Z_{eff}	High	Low
Ionic Radius	Small	Large
Polarizability	Low	High
Molecular Orbital Description	High-energy LUMO*	Lower-energy LUMO
Property of Lewis Base	**Hard**	**Soft**
Electronegativity	High	Low
Oxidation State/Z_{eff}	High	Low
Ionic Radius	Small	Large
Polarizability	Low	High
Molecular Orbital Description	Low-energy HOMO*	Higher-energy HOMO

*Adapted from reference 42. †LUMO = Lowest Unoccupied Molecular Orbital and HOMO = Highest Occupied Molecular Orbital

Table 2.2 Examples of Hard and Soft Acids and Bases[39]

Category	Hard	Borderline	Soft
Acids	**H^+**, Li^+ - Cs^+, Be^{2+} - Sr^{2+}, VO^{2+}, Sc^{3+}, Ti^{+4}, **Fe^{+3}**, Zr^{4+}, **Co^{3+},** Cr^{3+}, Cr^{6+}, **I^{7+}, I^{5+}**, Lanthanides and Actinides	**Fe^{2+}**, **Co^{2+}**, Ni^{2+}, **Cu^{2+}**, Zn^{2+}, Pb^{2+}, Sn^{2+}, Sb^{3+}, Bi^{3+}, Rh^{3+}, Ir^{3+}, **NO^+**, SO_2	**Cu^+**, Ag^+, Au^+, Tl^+, Hg^+, Pd^{2+}, Cd^{2+},Pt^{2+}, Hg^{2+}, **I^+**, Br^+, I_2, Br_2, CH_3Hg^+
Bases	H_2O, O^{2-}, OH^-, F^-, **NO_3^-,** PO_4^{3-}, SO_4^{2-}, $CH_3CO_2^-$	N_3^-, Br^-, NO_2^-, SO_3^{2-}, $C_6H_5NH_2$, N_2, C_5H_5N	**H^-**, C_2H_4, C_6H_6, CN^-, CO, SCN^-, R_3P, $(RO)_3P$, **I^-**, CO

*The species in bold have been highlighted to provide examples of hard, soft, and borderline acids and bases of the same element whose hardness or softness differs due to differences in oxidation states (cf. $Fe^{+3}$and Fe^{+2})

Based on these criteria, the hydrogen ion and ions of alkali/alkaline earth metals, lanthanides, and actinides are all hard acids while some uni- and divalent transition metals are soft acids. Hard bases include neutral species such as water as well as ligands that bind through fluorine and oxygen atoms while soft bases include the iodide, cyanide, and hydride ions. Acids and bases on the borderline tend to have more than one oxidation state available; in this case, those in lower oxidation states tend to be softer than those in the higher oxidation states. Table 2.2 provides a partial listing of hard, soft, and borderline acids and bases.

2.2 Solution Equilibria

The stoichiometric reaction of α moles of A and β moles of B to generate ρ moles of R and σ moles of S is written as

$$\alpha A + \beta B \Leftrightarrow \rho R + \sigma S \tag{2.1}$$

where α, β, ρ,and σ are stoichiometric coefficients and indicate the *relative* amounts of compounds A and B required to produce R and S in a ρ:σ ratio. At constant temperature and pressure, the equilibrium constant, K_{eq}, for this equation is defined as

$$K_{eq} = \frac{\{R\}^{\rho}\{S\}^{\sigma}}{\{A\}^{\alpha}\{B\}^{\beta}} \tag{2.2}$$

where the curly brackets represent the *activities*, or effective concentrations, of the enclosed species. This definition of the equilibrium constant is defined similarly for reactions involving solid species; however, for reactions involving gaseous species, the effective pressures, or *fugacities*, of the gases are used instead of activities. Equation 2.2 can be generalized to apply to equilibrium systems with any number of species. Since the investigations in this work were conducted in aqueous solution (i.e., water was the solvent), the following discussions will focus on solution-phase equilibria.

For solutions containing ionic species, the activity of a species *i* is defined as the product of the concentration and the activity coefficient of that species. Hence, equation 2.2 is more explicitly written as

$$K_{eq} = \frac{\{R\}^{\rho}\{S\}^{\sigma}}{\{A\}^{\alpha}\{B\}^{\beta}} = \frac{(\gamma_R)^{\rho}(\gamma_S)^{\sigma}[R]^{\rho}[S]^{\sigma}}{(\gamma_A)^{\alpha}(\gamma_B)^{\beta}[A]^{\alpha}[B]^{\beta}} \tag{2.3}$$

where the square brackets indicate *concentrations* of the enclosed species and the values γ_i are the activity coefficients for the *i*th species. The enclosing parentheses around the γ_i terms are

shown for clarity. As it is not possible to measure activity coefficients for individual ions[43], several analytical and empirical equations have been developed to facilitate calculation of the *mean* activity coefficients. Equation 2.4 below is one such equation known as the Davies equation[44]:

$$\log \gamma_{\pm} = -0.5 z_{+} z_{-} \left(\frac{\sqrt{0.5I}}{1+1.5\sqrt{I}} - 0.3I \right) \tag{2.4}$$

where z_i is the charge on the *ith* ion and $\gamma_{\pm}$ is the mean activity coefficient of a cation-anion pair of charge ±z. This equation and all other such equations depend on the ionic strength, I, of the solution, which is a charge-weighted concentration of all ions present:

$$I = \frac{1}{2} \sum_{i} c_i z_i^2 \tag{2.5}$$

where c_i is the concentration of the *i*th species, typically in molar or molal concentration units, and z_i is the charge on the *i*th ion.

In practice, activity coefficients are difficult to determine accurately even with such equations as the Davies equation, which fails at ionic strengths greater than approximately 0.5 M. However, the ionic strength is readily calculable and, because the activity coefficients (and consequently, the equilibrium constants) depend on the ionic strength, most tabulated equilibrium constants are defined in terms of concentrations and specify the ionic strength to allow for comparison.

2.2.1 Equilibrium of Pure Water

The thermodynamic investigations described in this work were conducted in aqueous solutions (i.e., water was the solvent). Therefore, before discussing the relevant equilibria *in* water, it is necessary to discuss the equilibria *of* water. Pure water itself undergoes self-ionization to form the hydronium (H_3O^+) and hydroxide (OH^-) ions at equilibrium:

$$H_2O + H_2O \leftrightarrow H_3O^+ + OH^- \tag{2.6}$$

The above reaction is essentially an acid-base reaction in which a water molecule, acting as an acid, donates a proton to another water molecule to produce the hydronium- and hydroxide ions. For simplicity, the self-ionization reaction is usually written as the equivalent dissociation reaction:

$$H_2O \leftrightarrow H^+ + OH^- \quad (2.7)$$

with equilibrium constant

$$K_{eq} = \frac{\{H^+\}\{OH^-\}}{\{H_2O\}} \quad (2.8)$$

Based on conductivity measurements and the density of pure water[45], the concentrations of H^+ and OH^- are 1 x 10^{-7} M while that of H_2O is 55.5 M at 25°C. It is clear that the pure water is in excess of its constituent ions and its concentration will likely be unaffected by changes in $[H^+]$ and $[OH^-]$; therefore, the denominator of Equation 2.8 is typically included with K_{eq} and the expression for the autoionization of water becomes

$$K_w = \{H^+\}\{OH^-\} = \gamma_{H^+}[H^+]\gamma_{OH^-}[OH^-] \quad (2.9)$$

where K_w is called the ionization constant of water and has the value of 10^{-14} for pure water at 25°C. For nearly all reaction equilibria in aqueous systems, the tabulated equilibrium constants implicitly include the activity of water.

The above value of the ionization constant is only true for pure water or for very dilute solutions. In systems of general experimental interest, however, other cations and anions are also present in the aqueous solution at comparatively high concentrations (e.g., 0.1 M). As discussed earlier, the presence of these ions affects the activities of all ions present, including the autoionization products of water.

Taking the negative logarithm of equation 2.9 gives the potential "p" of each term in the equation – e.g., $pK_w = -\log K_w$. The potential of the hydronium ion concentration, pH, is an important quantity that strongly influences equilibrium conditions in aquatic, biological, and all other aqueous systems. The pH of a solution can be readily measured with pH meters; knowledge of this value greatly facilitates the calculation of equilibrium constants associated with ligand-dissociation- and metal complexation reactions.

2.2.2 Ligand Protonation Equilibria

An understanding of aqueous metal ion complexation equilibria is very important for the design of solvent extraction systems to selectively recover specific elements. Such reactions are extremely diverse and include reactions with organic and/or inorganic ligands, which themselves may undergo reactions in solution. Because the equilibrium constants for ligand protonation and metal complexation are tabulated in the literature as concentration equilibrium constants at a given ionic strength, equilibria throughout this and subsequent chapters will be defined in terms of concentrations, not activities.

In aqueous solution, an acidic ligand, H_nL, with *n* dissociable protons exists at equilibrium with its *n* conjugate bases. An example is shown below for an acidic ligand, H_5L:

$$H_5L \leftrightarrow H_4L^- + H^+ \quad (2.10a)$$
$$H_4L^- \leftrightarrow H_3L^{2-} + H^+ \quad (2.10b)$$
$$H_3L^{2-} \leftrightarrow H_2L^{3-} + H^+ \quad (2.10c)$$
$$H_2L^{3-} \leftrightarrow HL^{4-} + H^+ \quad (2.10d)$$
$$HL^{4-} \leftrightarrow L^{5-} + H^+ \quad (2.10e)$$

The negatively-charged species on the right side of the equation are the conjugate bases of the more acidic ligand on the left side of the equation. At very low pH, the acidic ligand may actually be further protonated to form cationic species such as H_6L^+. In general, a single dissociation reaction can therefore be written as

$$H_nL \leftrightarrow H_{n-1}L + H \quad (2.11)$$

The charges are not shown for clarity. The equilibrium constants associated with the above reactions are called acid dissociation constants. They are typically written in the form K_{an}, where K_{a1} refers to the dissociation of the first acidic proton, K_{a2} refers to the reaction in which the second proton dissociates, etc. The larger the K_{an} value, the more acidic is the ligand as evidenced by the greater degree of its dissociation. It should be noted that the above description of the acid dissociation constant applies equally well to the dissociation of inorganic acids such as sulfuric acid, H_2SO_4. Measured values of the acid dissociation constant are tabulated in the literature as pK_a's at a particular ionic strength. Potentiometry is a commonly employed technique for the determination of pKa's using a calibrated pH electrode.

2.2.3 Metal Complexation Equilibria in Aqueous Solutions

The HSAB theory described in section 2.1 provides a basis for predicting the types of metal complexation reactions that are likely to occur between a given metal and ligand. In general, the complexes formed are of two types: inner-sphere and outer-sphere complexes. Inner-sphere complexes are comprised of ligands in clearly defined sites within the primary coordination sphere of the metal. The *coordination number*, CN, of the complex is the number of ligating atoms bound to the central metal ion and depends on the metal and ligand sizes (ionic radii), charges, and, for transition metals in particular, on the geometry of their molecular orbitals. An example of an inner-sphere complex is the hexaamminenickel(II) cation, $Ni(NH_3)_6^{2+}$, which has a CN of six from the ammonia ligands directly bound to Ni^{2+}.

Outer-sphere complexes, which are also called "ion-pairs", contain ligands that are weakly associated to the inner-sphere complex (e.g., the hydrated metal ion) via hydrogen bonding or other electrostatic attractions. These complexes usually form because the ligand is

not strong enough to displace the inner-sphere water molecules necessary to form a complex. Thus, a layer of water molecules lies between the bare metal cation and the ligand. An example of an outer-sphere complex is $EuCl^{2+}$ in water.[46] Figure 2.2 illustrates the concept of inner- and outer-sphere complexes.

To account for the fact that these inner-sphere water molecules can be displaced during complexation, it is most accurate to write complexation reactions in terms of hydrated metal ions:

$$M(H_2O)_x + L \leftrightarrow M(H_2O)_{x-y}L + yH_2O \qquad (2.12)$$

where *x* is the number of water molecules coordinated to the metal and *y* is the number of molecules that have been displaced. Defining complexation reactions in this way is useful for studying chelation reactions in which several water molecules are displaced by a single chelating ligand. Techniques such as fluorescence spectroscopy can be used to determine the equilibrium constant for such reactions based on changes in the number of water molecules bound to the metal upon complexation.

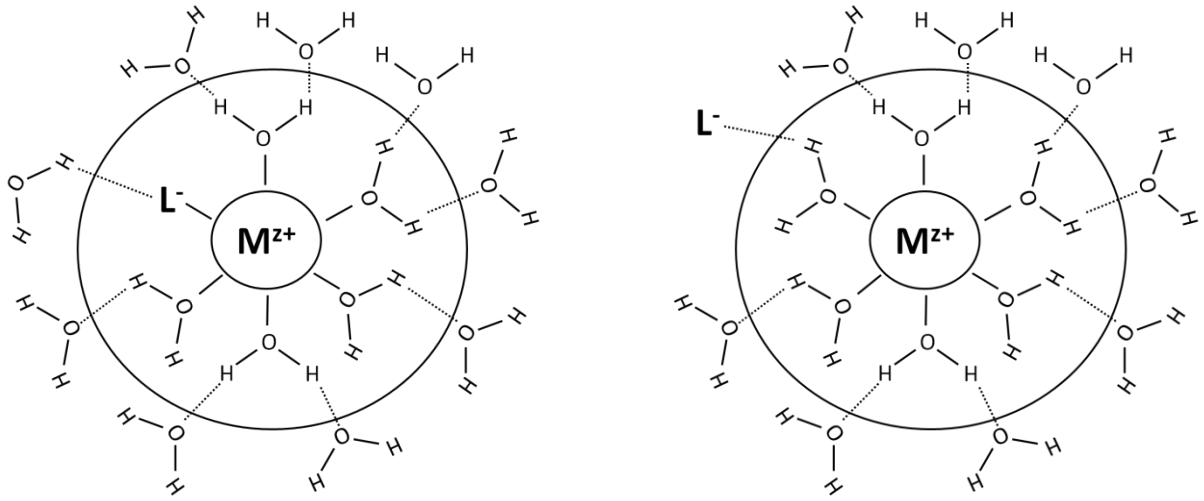

Figure 2.2 Comparison of Inner- (Left) and Outer-Sphere (Right) Complexes. The large outer circle represents the border between the inner sphere and the outer sphere, which is more accurately referred to as the secondary hydration sphere in aqueous systems. The dotted lines between hydrogen and oxygen atoms are hydrogen bonds, M^{z+} refers to any metal of charge z, and the ligand L^- represents a generic ligand that does not necessarily have a charge.

Although it is more accurate and occasionally more useful to write the equilibrium reactions in terms of hydrated metal ions, it is more common to write such equations without showing the waters of hydration:

$$M + L \leftrightarrow ML \tag{2.13a}$$

$$ML + L \leftrightarrow ML_2 \tag{2.13b}$$

$$\vdots$$

$$ML_{n-1} + L \leftrightarrow ML_n \tag{2.13c}$$

Metal cation charges, total ligand formal charge, and aquo ligands coordinated to the metal have been omitted for clarity. The equilibria for the above reactions are summarized by the stepwise equilibrium constants

$$K_{1n} = \frac{[ML_n]}{[ML_{n-1}][L]} \tag{2.14}$$

where the subscript in the constant K_{1n} refers to the formation of one metal with *n* ligands. The concentration [L] refers to the concentration of the *free* ligand, which is uncomplexed and completely deprotonated. The complexes ML_n are called *mononuclear* complexes because they are comprised of a single metal with one or more coordinated ligands. *Polynuclear* complexes, in which multiple metal ions are bound to the same ligand, can also form but are not as common as mononuclear complexes. Thus, the metal ion equilibria discussed in this section will focus exclusively on mononuclear complexes.

An alternate way of describing complexation reactions with acidic ligands that accounts for changes in the pH upon complexation is shown below for a generic ligand HL:

$$M + HL \leftrightarrow ML + H \tag{2.15}$$

with protonated stepwise equilibrium constants defined as

$$K_{1n} = \frac{[ML][H]}{[M][HL]} \tag{2.16}$$

with [M] being the free uncomplexed metal concentration. However, when the pH is low enough, part of the ligand that is not coordinated to the metal can also be protonated:

$$ML+H \leftrightarrow M(HL) \quad (2.17)$$

with equilibrium constant

$$K_{mlh} = \frac{[M(HL)]}{[ML][H]} \quad (2.18)$$

where the subscripts *m*, *l*, and *h* are the numbers of metal ions, ligands, and hydrogen ions, respectively, in the complex. Note that the H in M(HL) is bound to *L*, not *M*.

A consequence of the strong Lewis-acidity of metal cations is that the water molecules bound to the inner coordination sphere can be more acidic than pure water due to the strongly polarizing nature of the cation. Thus, hydrolysis reactions, which can predominate over other complexation reactions in the solution, can occur in solutions at near-neutral to basic pH. Hydrolysis is not restricted to basic and weakly acidic solutions, however: formation of hydroxo complexes can occur at pH values less than one for plutonium solutions.[47] A variety of complexes with different hydroxide compositions and strengths may be formed depending on the metal, oxidation state, and pH. The stepwise formation of such complexes can be written as

$$M(H_2O)_n \leftrightarrow M(OH)(H_2O)_{n-1} + H \quad (2.19)$$

The equilibrium constant for this reaction is called the hydrolysis constant:

$$K_{hyd} = \frac{[M(OH)(H_2O)_{n-1}][H]}{[M(H_2O)_n]} \quad (2.20)$$

Hydrolysis is not limited to monosubstitution; multiple substitutions can occur and, eventually, polynuclear species with very low solubilities can form. Also, for strongly binding ligands, mixed metal-hydroxo-ligand complexes may exist.

2.2.4 Overall and Apparent Stability Constants

The equilibrium constants for all of the reactions written above are *stepwise* equilibrium constants. Inspection of Equations 2.13 reveals that the summation of *n* equilibrium reactions generates a single reaction representing the *overall* complex formation:

$$M+nL \leftrightarrow ML_n \quad (2.21)$$

The corresponding equilibrium constant is called the *stability constant*:

$$\beta_{1n} = \frac{[ML_n]}{[M][L]^n} \tag{2.22}$$

It is easy to show that

$$\beta_{1n} = \prod_{i=1}^{n} K_{1i} \tag{2.23}$$

Hence, the stability constant for the formation of the complex ML_3, for example, is equal to the product $K_{11}K_{12}K_{13}$.

The magnitude of the stability constant is related to the thermodynamic favorability of a reaction, which will be explained further in the next section. Based on the definition of the stability constant, it is clear that the larger the value of the stability constant, the higher the product concentration must be at equilibrium. The magnitude of the stability constant is dependent upon several thermodynamic and statistical factors related to ligand structure and denticity as well as the strength of electrostatic interactions between the metal and ligand.[48]

Stability constants allow one to calculate the ratio $[ML_n]/[M]$ at any free ligand concentration. For example, in equation 2.22, if [L] = 0.1 M and $\beta_{11} = 10^4$, the ratio [ML]/[M] *must be* 10^3 *regardless* of the total metal concentration in the limit of constant activities. Furthermore, this ratio can be calculated for various free ligand concentrations and used to generate a speciation diagram. In this case, the speciation diagram is a plot of the percent formation of a species as a function of free ligand concentration.

For the experimental design and study of buffered biochemical and solvent extraction systems, it is useful to be able to determine the $[ML_n]/[M]$ ratio at a given pH. As written, reaction 2.21 and equation 2.22 do not explicitly give information about the corresponding pH for a particular value of $[ML_n]/[M]$. Furthermore, these equations imply that the only forms of the free metal or ligand present in the solution are L and M. However, in reality, the ligand may also be present in any of its various protonation states and/or the metal may exist as hydrolyzed species depending on the pH. In order to determine the [ML]:[M] ratio for a particular pH, Equation 2.22 can be redefined as an *apparent* stability constant:

$$\beta'_{1n} = \frac{[ML_n]}{[M'][L']^n} \tag{2.24}$$

where [M'] and [L'] are concentrations of the uncomplexed metal and ligand, respectively:

$$[M'] = [M]_{TOT} - [ML] \tag{2.25}$$

$$[L']=[L]_{TOT} - [ML] \tag{2.26}$$

For the sake of example, [M'] and [L'] will be defined below for a system in which the metal is not hydrolyzed, only one complex is formed, and the ligand is of the form H_4L:

$$[M'] = [M]_{TOT} - [ML] = [M] \tag{2.27}$$

$$[L'] = [L]_{TOT} - [ML] = [L]+ [HL]+ [H_2L] + [H_3L] + [H_4L] \tag{2.28}$$

Using the general equation for proton dissociations of an acid ligand (Equation 2.11) and the definition of the acid dissociation constant, the fraction [L'] can now be written as

$$[L']=[L]+ \frac{[L][H]}{K_{a4}}+ \frac{[L][H]^2}{K_{a4}K_{a3}} + \frac{[L][H]^3}{K_{a4}K_{a3}K_{a2}}+ \frac{[L][H]^4}{K_{a4}K_{a3}K_{a2}K_{a1}} \tag{2.29}$$

$$=[L]\left(1+ \frac{[H]}{K_{a4}}+ \frac{[H]^2}{K_{a4}K_{a3}} + \frac{[H]^3}{K_{a4}K_{a3}K_{a2}}+ \frac{[H]^4}{K_{a4}K_{a3}K_{a2}K_{a1}}\right)$$

We now define the parameter α_L as the fraction of the uncomplexed ligand that is completely deprotonated and we see that

$$\alpha_L=\frac{[L]}{[L']}= \left(1+ \frac{[H]}{K_{a4}}+ \frac{[H]^2}{K_{a4}K_{a3}} + \frac{[H]^3}{K_{a4}K_{a3}K_{a2}}+ \frac{[H]^4}{K_{a4}K_{a3}K_{a2}K_{a1}}\right)^{-1} \tag{2.30}$$

Thus, we can write

$$\beta'_{1n}= \frac{[ML_n]\alpha_L}{[M][L]^n}=\beta_{1n}\alpha_L \tag{2.31}$$

In essence, the apparent stability constant is a pH-dependent overall stability constant, meaning that it is not constant. The pH corresponding to the largest apparent stability constant is the pH at which the maximum amount of desired complex will be formed.

A wide variety of techniques that include UV-VIS spectrophotometry, potentiometry, calorimetry, solvent extraction, nuclear magnetic resonance spectroscopy, and fluorescence

spectroscopy allow the determination of overall- and/or apparent stability constants. In the literature, these measured stability constants are usually tabulated as log β_{1n} values along with the experimental temperature and ionic strength to facilitate comparison to other systems.

2.2.5 Solvent Extraction Equilibria

The previous subsections have dealt with the speciation of acidic ligands and their complexation reactions with metals in a *single* phase. Solvent extraction, on the other hand, is a two-phase liquid-liquid extraction, meaning that in addition to equilibria in the aqueous phase, equilibria between phases and within the organic phase must also be considered. In any solvent extraction system, it is possible to define a *distribution ratio* for a metal:

$$D_M = \frac{[M_{TOT}]_{org}}{[M_{TOT}]_{aq}} \tag{2.32}$$

where $[M_{TOT}]_{org}$ and $[M_{TOT}]_{aq}$ are the total analytical concentrations of the metal in the organic and aqueous phase, respectively. It includes all forms of the metal present in a given phase. Similar distribution ratios can be defined for the aqueous- and organic phase ligands.

When comparing the distribution of two metals, it is useful to define the separation factor, SF:

$$SF_{M'/M} = \frac{D_{M'}}{D_M} = \frac{[M'_{TOT}]_{org}}{[M'_{TOT}]_{aq}} \frac{[M_{TOT}]_{aq}}{[M_{TOT}]_{org}} \tag{2.33}$$

where the metal M'≠ M. Thus, the higher the separation factor, the better the separation of M' from M.

Because of the large variety of organic extractants used in solvent extraction, several types of extracted metal complexes are possible. The equilibrium constant for extractions of metals from the aqueous phase into the organic phase is called the *extraction constant*, K_D, and is defined in several ways depending on the nature of the extractant. Three of the five types of extracted complexes generally encountered in solvent extraction are discussed below.

Organic extractants that form anions in the aqueous phase can react with metals to form neutral chelate complexes of the type MA_n which then partition into the organic phase:

$$M^{z+}(aq) + nA^-(aq) \leftrightarrow MA_n(aq) \tag{2.34}$$

$$MA_n(aq) \leftrightarrow MA_n(org) \tag{2.35}$$

$$K_D = \frac{[MA_n]_{org}}{[MA_n]_{aq}} \quad (2.36)$$

Charges are included to indicate the role of the organic acid HA in charge neutralization. Lipophilic organic acids forming complexes of this type include dicarboxylic acids, dialkylphosphoric acids, and β-diketones. The charge-neutral complexes formed by these ligands may or may not be coordinatively saturated; in the case of coordinative *unsaturation*, other neutral ligands such as water bind to complete the coordination.

Other lipophilic organic ligands form adducts with metal-ligand complexes to increase their lipophilicity in the organic phase. These neutral ligands are very strong donors (hard bases) and displace the remaining inner-sphere water molecules of the metal complex. The overall reaction is written as

$$M^{z+}(aq) + zL^-(aq) + xX(org) \leftrightarrow ML_zX_x(org) \quad (2.37)$$

$$K_{ex} = \frac{[ML_zX_x]_{org}}{[M^{z+}]_{aq}[L^-]^z_{aq}[X]^x_{org}} \quad (2.38)$$

where [X] is the concentration of the adduct ligand X; L^- can be an inorganic or organic ligand. In the case where addition of a ligand X increases the distribution ratio for the metal, the phenomenon is called synergism[48]. A classic example of an adduct complex is the $UO_2(NO_3)_2 \cdot 2TBP$ complex that is extracted synergistically in the PUREX process.[49]

A third type of complex commonly encountered in solvent extraction is the ion-pair complex. In this case, the organic extractant first forms a *charged* adduct with a proton; the resulting adduct's charge is balanced by inorganic anions in solution. This ion pair can then undergo anion-exchange reactions with *anionic* metal complexes in the aqueous phase. The concept is illustrated below using a primary amine, RN, as the extractant:

$$RN(org) + H^+(aq) + X^-(aq) \leftrightarrow RNH^+X^-(org) \quad (2.39)$$

$$zRNH^+X^-(org) + ML_n^{z-}(aq) \leftrightarrow (RNH^+)_zML_n^{z-}(org) + zX^-(aq) \quad (2.40)$$

$$K_{ex} = \frac{[(RNH^+)_zML_n^{z-}]_{org}[X]^{z-}_{aq}}{[RNH^+X^-]^z_{org}[ML_n^{z-}]^z_{aq}} \quad (2.41)$$

where the ligand X^- represents any inorganic anion. The extractants that are used for this type of extraction tend to be alkylamines for practical reasons. A wide range of anionic metal complexes can be extracted using this method.

2.3 Solution Thermodynamics

2.3.1 The Gibbs Free Energy and Equilibrium

Investigations of chemical reactions are usually carried out at constant temperature and pressure. Under these conditions, it is convenient to use the Gibbs free energy, G, which depends on temperature and pressure, to describe reaction conditions. The reaction *quotient*, Q, for the generic reaction below taking place at constant temperature and pressure is defined as:

$$\alpha A + \beta B \leftrightarrow \gamma C + \delta D \tag{2.42}$$

$$Q = \frac{\{C\}^{\gamma}\{D\}^{\delta}}{\{A\}^{\alpha}\{B\}^{\beta}} \tag{2.43}$$

The change in the free energy of the above reaction with reaction quotient Q is defined as

$$\Delta G_{rxn} = \Delta G^{o}_{rxn} + RT\ln Q \tag{2.44}$$

where the constant R is the ideal gas constant, ΔG_{rxn} is the change in the reaction free energy between the products and the reactants as the reaction progresses, and ΔG^{o}_{rxn} refers to the total change in reaction free energy when the products and reactants are in their standard states (i.e., unit activity at 1 M concentration). The units of ΔG_{rxn} and ΔG^{o}_{rxn} are usually either in kcal/mole or kJ/mole. The reaction quotient Q is calculated similarly to the equilibrium constant except that it pertains to non-equilibrium conditions.

The relationships among ΔG_{rxn}, Q, ΔG^{o}_{rxn} and K can be explained by introducing the concept of the "extent of reaction". The extent of reaction determines the position from equilibrium and takes the values from zero, which corresponds to a system in which only reactants are present in their standard states, to a maximum value that corresponds to essentially having only products present in their standard states. Figure 2.3 shows a visual description of the concept. For each point ξ in the figure, a corresponding value of Q exists, and when $(\delta G/\delta\xi)_{T,P} = 0$, the total reaction free energy is at a minimum and $Q=K_{eq}$. Thus, Equation 2.44 becomes

$$\Delta G^{o}_{rxn} = -RT\ln K_{eq} \tag{2.45}$$

Since ΔG^{o}_{rxn} is the free energy of a given reaction when reactants and products are in their standard states, its relationship to K_{eq} allows direct comparison of different reactions that may or may not have been carried out under standard state conditions.

The reaction free energy is useful because it determines the direction in which a reaction that is not at equilibrium will spontaneously progress in order to reach equilibrium. To elaborate, the reaction described by the leftmost box in Figure 2.3 will *spontaneously* move from the left to the equilibrium point because $(\delta G/\delta\xi)_{T,P}$ is negative but will move spontaneously from right to left when $(\delta G/\delta\xi)_{T,P}>0$. Furthermore, since the value of ξ at equilibrium is large, implying a high concentration of products, it is clear that the equilibrium constant must be large. Also, the value of $\Delta G°$ is negative, which means that the reaction would be *spontaneous* under standard state conditions. The box on the right side represents the completely opposite situation in which the total free energy of the products is greater than that of the reactants, and the extent of reaction is small. Thus, the equilibrium constant will be small and $\Delta G°$ is positive, indicating a *nonspontaneous* reaction.

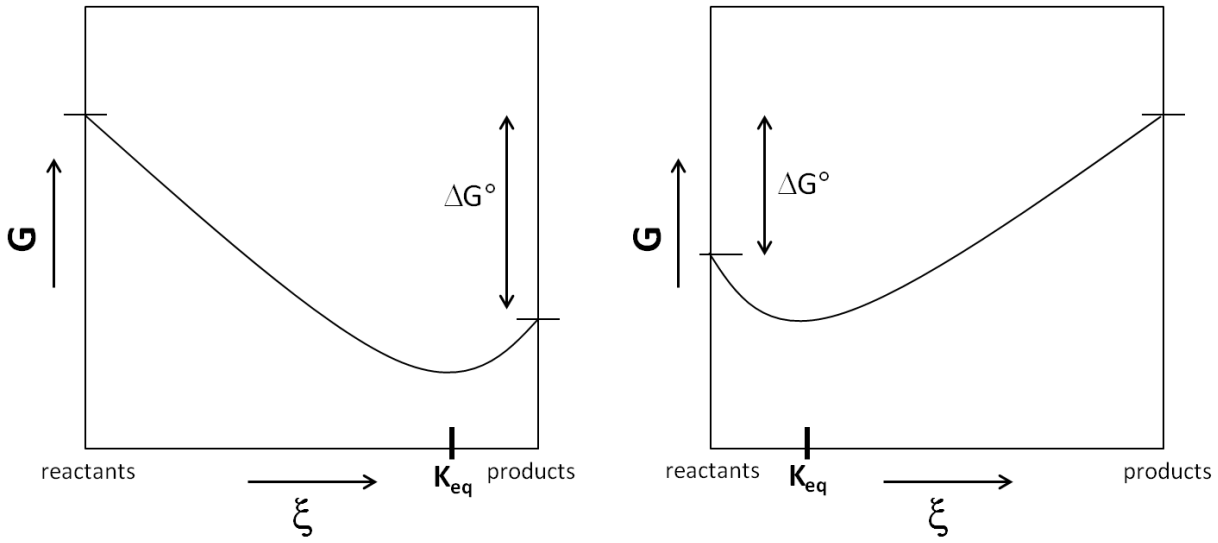

Figure 2.3 Free Energy Diagrams. The extent of reaction ξ ranges from zero, which corresponds to a system in which all reactants are in their standard states, to a reaction-dependent maximum value in which all products are in their standard states. When $(\delta G/\delta\xi)_{T,P} = 0$, the free energy of the system is at a minimum and $Q=K_{eq}$. The tick marks represent the total free energy of the reactants (left side of box) and the products (right side of box) when they are in their standard states. The difference between these values is $\Delta G°$.

2.3.2 Free Energy, Enthalpy, and Entropy

The change in reaction free energy is related to the reaction enthalpy- and entropy changes at constant temperature as follows:

$$\Delta G_{rxn} = \Delta H_{rxn} - T\Delta S_{rxn} \quad (2.46)$$

and at equilibrium, Equation 2.43 becomes

$$\Delta G^{o}_{rxn} = \Delta H^{o}_{rxn} - T\Delta S^{o}_{rxn} \quad (2.47)$$

where the H and S terms refer to enthalpy and entropy, respectively. Because the measured quantities of interest in this work are the equilibrium values ΔG^{o}_{rxn}, ΔH^{o}_{rxn}, and ΔS^{o}_{rxn}, all further discussions of thermodynamic parameters will pertain to these values. Spontaneous reactions ($\Delta G^{o}_{rxn}<0$) for which only the enthalpy term in Equation 2.47 is negative are *enthalpy-driven* while those in which the entropy term, $-T\Delta S°$, is negative are *entropy-driven*. Reactions can be both enthalpy- and entropy-driven if the enthalpy and entropy terms are negative.

The enthalpy of reaction is simply the amount of heat absorbed or released during a reaction at constant pressure and can be readily be measured from thermometric or calorimetric titrations. In conjunction with previously measured equilibrium constants, the entropy can be calculated using Equations 2.45 and 2.47. Thus, the stability constant and enthalpy of reaction are the only two thermodynamic parameters needed to obtain all of the thermodynamic data for a reaction.

2.3.3 Enthalpy-Entropy Compensation in Metal Complexation Reactions

Although the measured enthalpy and entropy values indicate the driving forces for a given reaction, the value alone provides only superficial information about the driving forces of a reaction. For example, knowing that a particular group of reactions has very exothermic enthalpies and positive entropy changes does not provide insights into *why* heat is released or *what* causes the entropies to increase during a reaction. Therefore, it is necessary to discuss the factors that affect the magnitude of the measured enthalpies and entropies for metal complexation reactions. For simplicity, binary complexes, which are complexes between a metal and only one type of ligand, will be used in the discussion.

In order to discuss the component entropy and enthalpy terms, it is necessary to rewrite the metal complexation reactions to take into account the solvation state of the metal and the ligand:

$$M(H_2O)_x + L(H_2O)_y \Leftrightarrow M(H_2O)_{i+j}L + (x+y-i-j)H_2O \quad (2.48)$$

This complexation reaction can be broken into two steps:

1. Desolvation of the metal cation and the ligand.
2. Formation of a metal-ligand bond.

Thus, the enthalpy and entropy components of the reaction free energy can be broken into four terms corresponding to the enthalpies and entropies of desolvation and complexation:

$$\Delta H^o_{rxn} = \Delta H^o_{desolv} + \Delta H^o_{comp} \quad (2.49)$$

$$\Delta S^o_{rxn} = \Delta S^o_{desolv} + \Delta S^o_{comp} \quad (2.50)$$

Here ΔH^o_{rxn} and ΔS^o_{rxn} are the respective measured enthalpy and calculated entropy. For hard acids, the enthalpy of desolvation, ΔH^o_{desolv}, is a very positive number because of the strength of the metal-aquo bond. The enthalpy of desolvation of the ligand is positive as well, though likely not as positive as the enthalpy of dehydration of the metal cation. However, the entropy of desolvation is also positive because the number of molecules in the system increases upon dehydration. For complexes between hard acids and a variety ligands, there has been shown to be a linear correlation between the enthalpy and entropy of desolvation such that they essentially offset each other – that is, $\Delta H^o_{desolv} = T\Delta S^o_{desolv}$.[50,51] This result is known as the *enthalpy-entropy compensation*.

The enthalpy of complexation (ΔH^o_{comp}) contribution from step two is negative for hard acid-hard base complexation reactions because the bonding is primarily electrostatic. The magnitude of this term is also affected by steric and electronic effects: bulkier ligands cause a reduction in the enthalpy of complexation due to steric hindrance by other ligands present, and more basic ligands form stronger complexes especially when sigma bonding or pi-backbonding is involved. The change in entropy due to bond formation is negative because the total number of molecules decreases and/or the translational entropy is lost.

An important implication of the enthalpy-entropy compensation is that the total reaction free energy is dependent primarily on the enthalpy- and entropy of complexation terms in step two. Thus, the measured free energy, enthalpy and entropy of reaction values for two different metals with the same ligand can be directly compared if their ionic radii and hydration number are similar.

Using the complexation model above, measured enthalpies and entropies can be used to predict whether the complexes formed are inner- or outer-sphere complexes. The difference between an inner- and an outer-sphere complex is that ligands capable of forming inner-sphere complexes can displace one or more coordinated water molecules, which requires energy, and bind directly to the metal. Therefore, if the measured reaction enthalpy and entropy are very positive, it is likely that the ligand displaced one or more inner-sphere water molecules prior to coordinating to the metal center. On the other hand, a less positive or even negative reaction enthalpy and entropy means that very little dehydration has occurred and that the ligand is

binding only weakly to the metal through long-range electrostatic attractions and/or hydrogen-bonding with inner-sphere water molecules. In this case, it is likely that the major contributor to both thermodynamic parameters is the complexation term.

2.3.4 Thermodynamics of the Chelate Effect

The "chelate effect" is used to explain the enhanced thermodynamic stability of five- or six-membered ring complexes formed with multidentate ligands compared to monodentate ligands of the same total denticity. To explain the chelate effect from a thermodynamic perspective, the parameters β_n, $\Delta H°$, and $\Delta S°$ for a series of copper complexation reactions with ammonia and ethylenediamine (en) are shown in Table 2.3 below.

Comparison of thermodynamic data for the reactions of the di- and tetraamminecopper(II) complex with those of the en complexes with similar denticity reveals that the stability constants of formation for the ammonia complexes are significantly lower than those of the en complexes. In addition, the enthalpy and entropy values are more favorable for the *en* complexes, with negative entropies even becoming positive. Several factors contribute to the observed differences in thermodynamic stabilities, enthalpies, and entropies. First, although both the en and ammonia ligands bind via a total of two nitrogen ligands, the two monodentate ammonia ligands each forms a single bond with the metal whereas the *en* ligand forms a complex that contains a five-membered ring, which is more stable than the linear complexes formed with monodentate ligands. Second, the *en* ligand is more basic than the ammonia ligand, meaning that the M-N bond in the *en* complex is likely stronger than the ammonia ligand. This extra stability is likely seen in the additional 2 kJ/mol more favorable enthalpy of reaction. Third, the entropy change of formation of the $Cu(NH_3)_2^{2+}$ complex is small because the total number of molecules in the reaction (three) is unchanged when the ammonia ligands displace an equivalent number of water molecules. In contrast, formation of a single $Cu(en)^{2+}$ complex displaces two water molecules, yielding a total of three product molecules, thereby increasing the entropy of the reaction system. All of these factors contribute to the increased overall stability of the $Cu(en)^{2+}$ complex. The impacts on enthalpy, entropy, and the stability constant due to the chelate effect are even greater when comparing the tetraammine complex with the di-en complex.

The thermodynamic model used to explain the chelate effect includes additional contributions to the enthalpy and entropy terms that were discussed in the previous section.[42] Three more enthalpy terms must be considered to describe chelation reactions:

- Ligand Repulsion
- Ligand Distortion
- Crystal Field Stabilization Energy

The repulsion caused by two or more ligands approaching a metal contributes an unfavorable enthalpy term. "Pre-organized" ligands, which are ligands that are structurally configured for complexation, can reduce this term; flexible chelators, on the other hand, have to reconfigure themselves in solution to minimize repulsion. For this reason, rigid ligands such as *trans*-diaminocyclohexanetetraacetic acid (CDTA) have stability constants significantly higher than the more flexible EDTA, which has the same denticity.[52] Chelates in general also contribute an unfavorable distortion term because the bond angles between the metal and ligand are distorted

from the ideal bond angles in the free ligand upon complexation. However, if the chelate contains a one or more five- or six-membered rings, this term may be minimized. Lastly, chelating ligands generate a larger crystal field splitting than monodentate ligands.[42] This third term is not as important for chelation with lanthanides and actinides for reasons discussed in the next chapter.

Table 2.3 Thermodynamic Parameters for Copper Complexation with Ethylenediamine (en) and NH_3

Complexation Reaction*	Log β_n †	$\Delta H°$, (kJ/mol) †	$\Delta S°$, J/(K-mol) †
$Cu(H_2O)_6^{+2} + 2NH_3 \Leftrightarrow Cu(H_2O)_4(NH_3)_2^{+2} + 2H_2O$	7.58	-43.5	-0.837
$Cu(H_2O)_6^{+2} + en \Leftrightarrow Cu(H_2O)_4(en)^{+2} + 2H_2O$	10.80	-55.2	+20.1
$Cu(H_2O)_6^{+2} + 4NH_3 \Leftrightarrow Cu(H_2O)_2(NH_3)_4^{+2} + 4H_2O$	12.6	-90.7	-63.5
$Cu(H_2O)_6^{+2} + 2en \Leftrightarrow Cu(H_2O)_2(en)_2^{+2} + 4H_2O$	20.3	-107	+27.2
Net Reactions			
$Cu(NH_3)_2^{+2} + en \Leftrightarrow Cu(en)^{+2} + 2NH_3$	**3.22**	**-11.7**	**+20.9**
$Cu(NH_3)_4^{+2} + 2en \Leftrightarrow Cu(en)_2^{+2} + 4NH_3$	**7.70**	**-16.3**	**+90.7**

*Waters of reaction are included for complexation reactions of the hexaaquocopper(II) ion to emphasize the fact that inner-sphere water molecules are displaced in these reactions. The thermodynamic parameters were measured at 25°C at 1 M ionic strength. †Values obtained from the Critical Stability Constant Database (ref. 52)

Some of the entropy contributions to the chelate effect can be summarized as follows:

- Translational Entropy
- Internal Entropy Factor
- Entropy of Dilution

The translational entropy is considered to be the main contributor to the entropy increase due to the chelate effect. When a multidentate ligand complexes a metal, there is a gain in translational entropy due to the increase in displaced ligands (e.g., water) upon complexation. At the same time, a loss of translational entropy is incurred because the chelating ligand no longer has the freedom of motion it possessed as a free ligand. However, the increase in translational entropy due to ligand displacement is typically greater than the loss incurred upon complexation. As the chain lengths between coordinating atoms in a chelating ligand increase, the internal entropy of the ligand increases as well. This internal entropy is lost upon chelation as the chelating ligand is now locked into a rigid position with the metal.

Using two different approaches, Schwarzenbach[53] and Adamson[54] proposed that the increased thermodynamic stability of a chelate over similar monodentate complexes increases with increasing dilution and decreasing ring size. In dilute solutions, the dilution entropy contribution to the chelate effect is higher because the effective activity (or concentration) of the chelate's donor atoms around the metal ion is higher. Using the *en* ligand as an example, in a dilute solution, once the first nitrogen atom binds to the metal, there is a higher probability of the second nitrogen binding to the metal than there would be in a more concentrated solution. Second, longer chain lengths *reduce* the extra entropy contribution to the point where it disappears altogether when the chain length becomes much greater than three or four atoms between the donor atoms. This is because the second dangling donor atom presumably occupies a space so large that its effective concentration is greatly reduced to the point where it is essentially a free, unbinding ligand. From these two points, it can be concluded that the smaller the chelate ring size, the more favorable the entropy contribution becomes because the effective concentration of the other donor group(s) of the chelating ligand prior to bonding is higher. Formation of more than one chelate ring would likely increase the entropy contribution further.

Chapter 3 Lanthanide and Actinide Solution Chemistry

3.1 The f-Elements

The lanthanide (Ln) and actinide (An) series comprise the elements of rows six and seven of the periodic table, respectively, and are collectively referred to as the "f-elements". They are also referred to as lanthanoids and actinoids to avoid confusion of the metals with anions.[55] The lanthanide series begins with the eponymous element lanthanum and, starting with cerium, the 4f-orbitals are successively filled until lutetium, which possesses a $4f^{14}$ configuration, is reached. Similarly, the actinide series begins with actinium and ends with lawrencium. The element promethium is notable for being the only lanthanide in the series that is exclusively radioactive. As Table 3.1 shows, technically, neither lanthanum, actinium, nor thorium belongs to either series since they do not possess f-electrons in the ground states of those elements, but as their chemistries tend to overlap with their respective series, these two elements are typically included. Also included with the lanthanides in chemical investigations are scandium and (especially) yttrium because they display similar physical properties and chemical behavior as the lanthanides. Evidence of these traits is the fact that these two elements are found in nature with lanthanides and thorium and/or uranium. When scandium and yttrium are included with the lanthanides, the group is called the *rare-earths*.[55]

Although the lanthanides are called rare-earths, they are in reality fairly abundant in the environment. Indeed, the term *rare-earth* previously referred to the group of elements that were historically difficult to isolate from each other in oxide minerals[56] – the element dysprosium, for example, was so-named because it was "hard to get" (from Greek, *dysprositos*). Lanthanides are found in nature in several minerals such as gadolinite, xenotime and, most importantly, monazite and bastnasite, as these two minerals are the only ones of commercial importance. Monazite is a mixed thorium- and lanthanide phosphate of the form $LnPO_4$, with the lanthanide content being composed primarily of cerium, lanthanum, neodymium, and praseodymium in that order. Bastnasite, a mixed lanthanide fluorocarbonate with the general formula $LnFCO_3$, has a similar lanthanide composition as monazite (i.e., mainly Ce, La, Nd, Pr) but is less radioactive and contains heavier lanthanides (e.g., terbium). It is the world's most important single source of lanthanides.[56]

Table 3.1 Electronic Configurations of Lanthanides and Actinides[57]

Lanthanide	Electronic Configuration (Metal)	Electronic Configuration (M^{3+})	Actinide	Electronic Configuration (Metal)	Electronic Configuration (M^{3+})
Lanthanum	$[Xe]5d^16s^2$	[Xe]	Actinium	$[Rn]6d^17s^2$	[Rn]
Cerium	$[Xe]4f^15d^16s^2$	$[Xe]4f^1$	Thorium	$[Rn]6d^27s^2$	n/a
Praseodymium	$[Xe]4f^36s^2$	$[Xe]4f^2$	Protactinium	$[Rn]5f^26d^17s^2$	$[Rn]5f^2$
Neodymium	$[Xe]4f^46s^2$	$[Xe]4f^3$	Uranium	$[Rn]5f^36d^17s^2$	$[Rn]5f^3$
Promethium	$[Xe]4f^56s^2$	$[Xe]4f^4$	Neptunium	$[Rn]5f^46d^17s^2$	$[Rn]5f^4$
Samarium	$[Xe]4f^66s^2$	$[Xe]4f^5$	Plutonium	$[Rn]5f^67s^2$	$[Rn]5f^5$
Europium	$[Xe]4f^76s^2$	$[Xe]4f^6$	Americium	$[Rn]5f^77s^2$	$[Rn]5f^6$
Gadolinium	$[Xe]4f^75d^16s^2$	$[Xe]4f^7$	Curium	$[Rn]5f^76d^17s^2$	$[Rn]5f^7$
Terbium	$[Xe]4f^96s^2$	$[Xe]4f^8$	Berkelium	$[Rn]5f^97s^2$	$[Rn]5f^8$
Dysprosium	$[Xe]4f^{10}6s^2$	$[Xe]4f^9$	Californium	$[Rn]5f^{10}7s^2$	$[Rn]5f^9$
Holmium	$[Xe]4f^{11}6s^2$	$[Xe]4f^{10}$	Einsteinium	$[Rn]5f^{11}7s^2$	$[Rn]5f^{10}$
Erbium	$[Xe]4f^{12}6s^2$	$[Xe]4f^{11}$	Fermium	$[Rn]5f^{12}7s^2$	$[Rn]5f^{11}$
Thulium	$[Xe]4f^{12}6s^2$	$[Xe]4f^{12}$	Mendelevium*	$[Rn]5f^{13}7s^2$	$[Rn]5f^{12}$
Ytterbium	$[Xe]4f^{14}6s^2$	$[Xe]4f^{13}$	Nobelium*	$[Rn]5f^{14}7s^2$	$[Rn]5f^{13}$
Lutetium	$[Xe]4f^{14}5d^16s^2$	$[Xe]4f^{14}$	Lawrencium*†	$[Rn]5f^{14}6d^17s^2$	$[Rn]5f^{14}$

*Asterisks indicate predicted electronic configurations. †The electronic configuration of lawrencium has also been written as $[Rn]5f^{14}7s^27p^1$.

The only naturally-occurring actinides found in significant abundances are thorium and uranium. Of course, most of the world's thorium comes from the mineral monazite but uranium is predominantly found in the mineral uraninite, a mixed oxide with the general formula UO_{2+x} that is often "contaminated" with lanthanides, thorium, calcium, and radiogenic lead.[20] The fine-grained version of the contaminated mineral is the ore known as *pitchblende*. Protactinium and actinium are present in small quantities in uranium and thorium ores as decay products from thorium or uranium; however, protactinium can also be produced by bombarding ^{230}Th with neutrons:

$$^{230}_{90}Th + ^{1}_{0}n \rightarrow ^{231}_{90}Th \rightarrow ^{231}_{91}Pa + ^{0}_{-1}e \quad (3.1)$$

Actinium is similarly produced by bombarding radium with neutrons:

$$^{226}_{88}Ra + ^{1}_{0}n \rightarrow ^{227}_{88}Ra \rightarrow ^{227}_{89}Ac + ^{0}_{-1}e \quad (3.2)$$

The *trans*-uranium elements – that is, the actinides beyond uranium – are produced by successive bombardment of uranium with neutrons. This process is effective until the isotope ^{257}Fm is reached; capture of another neutron produces ^{258}Fm, which solely undergoes spontaneous fission with a half-life of 0.37 ms.[31,58] Thus, elements heavier than fermium are normally produced by bombarding lighter actinides like curium with heavy ions of such elements as carbon, oxygen, and even uranium.[59,60,61]

3.2 Ionic Radii and Oxidation States

As the lanthanide and actinide series are traversed, the successive addition of electrons to the f-orbitals of lanthanides and actinides causes the ionic (and metallic) radii to progressively decrease. These phenomena, known as the *lanthanide-* and *actinide contractions*, are due to the fact that the added electrons only partly shield the electrons in the outer orbitals, causing them to contract. The overall lanthanide- and actinide contractions have been shown to be due partly to relativistic effects, with the contribution to the contraction being higher for actinides than lanthanides.[62,63] The contraction of the ionic radii is fairly smooth for the lanthanides and, in conjunction with their trivalent nature, allows intra-group lanthanide separations to be achieved. The ionic radii for trivalent actinide and lanthanides are tabulated in Table 3.2 and plotted in Figure 3.1 below. From the data, it is evident that there is considerable overlap of the ionic radii of the actinides and lanthanides.

Table 3.2 Ionic Radii* of Trivalent Actinides and Lanthanides

Lanthanide	Ln^{3+} Radius, (pm)	Actinide	An^{3+} Radius (pm)
Lanthanum	103.2	Actinium	112
Cerium	101	Thorium	n/a
Praseodymium	99.6	Protactinium	105
Neodymium	98.3	Uranium	102.8
Promethium	96.8	Neptunium	101.1
Samarium	95.8	Plutonium	99.5
Europium	94.6	Americium	98.0
Gadolinium	93.7	Curium	97.0
Terbium	92.3	Berkelium	95.5
Dysprosium	91.2	Californium	94.5
Holmium	90.0	Einsteinium	93.4
Erbium	88.9	Fermium	92.2
Thulium	87.9	Mendelevium	91.2
Ytterbium	86.9	Nobelium	90.2
Lutetium	86.3	Lawrencium	89.6

*Ionic Radii were taken from David[64] for trivalent lanthanide and actinide ions with a coordination number of six.

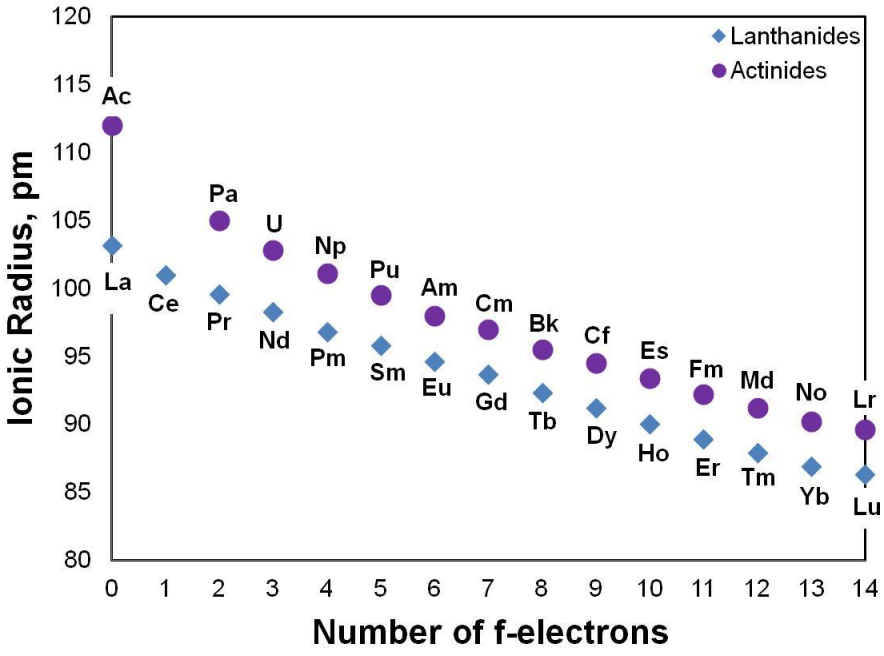

Figure 3.1 Comparison of Ionic Radii of trivalent actinides and lanthanides. *Note that thorium only exists in the tetravalent state in solution and is not shown in the figure. Values taken from David.[64]

The electrons in the 4f orbitals of the lanthanides are significantly closer to the nucleus (i.e., more *localized*) and therefore more tightly bound than the 5d and 6s orbitals. Hence, it is the electrons from the outer-lying orbitals that are generally removed first when lanthanide cations are formed.[58] All of the lanthanides form stable trivalent cations in solution as well as easily accessible cations of Yb^{2+}, Eu^{2+}, and Ce^{4+}. Sm^{2+} can also be prepared but it is unstable. Tetravalent cerium has a xenon configuration (cf Table 3.1), and divalent europium and ytterbium have half-filled ($4f^7$) and completely filled ($4f^{14}$) orbitals, respectively, which enhances their stability.[57]

In contrast to the lanthanides, the early actinides display a variety of oxidation states that are not stable for lanthanides. This is because the energies of 5f, 6d, and 7s electrons of the early actinides (Th to Pu) are nearly degenerate. In fact, the 6d atomic orbital is actually *lower* in energy than the 5f orbital for these elements.[58] However, as the 5f subshell is filled, the electrons in the subshell become more localized than the 6d and 7s electrons because of actinide contraction and become more lanthanide-like. Thus, after plutonium, the trivalent state becomes the most stable oxidation state with the exception of No^{2+}, which has a $5f^{14}$ configuration. Table 3.3 tabulates the experimentally-observed oxidation states in aqueous solution.

Because the chemistry of the trivalent lanthanides and minor actinides (principally Am, Cm) is most relevant to lanthanide/actinide separations, all further discussions of lanthanides and actinides will focus on the chemistry of their trivalent states. Fewer studies have been conducted with curium due to its high rate of neutron emission and to its limited availability but it will also be included in discussions when possible.

Table 3.3 Oxidation States of Actinides in Solution*

z	Ac	Th	Pa	U	Np	Pu	Am	Cm	Bk	Cf	Es	Fm	Md	No	Lr
+2															
+3															
+4															
+5															
+6															
+7															

*Grey boxes represent known oxidations states in solution; the dark grey boxes represent stable oxidation states in solution. For more detailed discussions of actinide oxidation states, the reader should refer to reference 20.

3.3 Ln(III)/An(III) Coordination Chemistry

3.3.1 Lanthanides and Actinides in Solution

Lanthanide- and actinide cations in the trivalent and all other oxidation states are hard acids. Furthermore, the f-electrons of the trivalent lanthanides and the trans-plutonium elements in particular are shielded from the external environment by valence electrons, giving these ions a "core-like" character. As a result, crystal field effects due to the presence of a ligand are generally very small, making the bonding predominantly ionic. Indeed, the trivalent cations behave more like alkali or alkaline-earth metals than transition metals, bonding preferentially with hard donors such as oxygen or fluorine. In addition, the bonding of hard ligands has less directional dependence than transition metals. Instead, these ligands arrange themselves around the metal center in a manner that minimizes repulsion, which leads to a variety of symmetries and high coordination numbers.

In solution, the primary hydration number for lanthanide cations is approximately nine for the early, lighter lanthanides and eight for the heaviest lanthanides due to the lanthanide contraction. X-ray absorption fine structure spectroscopy measurements have indicated that a transition region in which the primary hydration number progressively decreases from nine to eight lies between Nd(III) and Tb(III).[65] Optical absorbance and luminescence studies have shown that the primary hydration numbers for trivalent americium and curium are both around nine.[66,67]

3.3.2 Complexation with Hard Donors

Because the trivalent cations engage in predominantly ionic bonding, the coordination numbers in complexes are variable, ranging from three to twelve with the actual value depending on the steric bulk of the ligands and on electrostatic effects. Clearly, large, bulky ligands have lower coordination numbers while smaller ligands – especially ligands with small bite angles (e.g., CO_3^{2-} or NO_3^-) – tend to have higher coordination numbers.[57] Nevertheless, on the average, the coordination numbers are eight or nine, similar to the primary hydration numbers. In addition, the complexes are quite labile, with the coordinated ligands exchanging rapidly with the solvent or other ligands present. Chelating ligands, however, form more kinetically stable complexes, which is one of the properties that makes gadolinium chelates attractive as magnetic resonance imaging contrast agents.[68]

Trends in the stability constants and free energies of complexation for trivalent f-element complexes with hard anions provide additional evidence of the ionic nature of the bonds. To elaborate, the Gibbs free energies of complexation for a variety of ligands tend to *increase* with decreasing cation radii, implying that predominantly electrostatic interactions occur between the cation and anion (assuming steric effects are minimal).[69] Münze[70] demonstrated this by calculating the Gibbs free energy of formation for trivalent lanthanide and actinide acetate complexes assuming purely ionic bonding and found very good agreement between experimental and calculated free energies across the lanthanide series. A natural consequence of this is that Ln(III)'s and An(III)'s with similar ionic radii tend to have approximately the same stability constants. Moreover, the considerable overlap in the ionic radii of Ln(III)'s and An(III)'s makes

it difficult to achieve inter-group separations using hard ligands; intra-lanthanide separations are also complicated by the similarity of the ionic radii within the group.

The stability constants also tend to increase as a function of ligand basicity, which can be defined as the sum of all the pK_a's of a given ligand.[71] Furthermore, as the overall pK_a of the ligand increases, the complexes tend to become more inner-sphere in nature.[72] Complexes formed with ligands whose pK_a's are less than one tend to have predominantly outer-sphere character. Such ligands are usually the conjugate bases of strong acids (e.g., $HClO_4$, $HBrO_3$, etc.), which have pK_a's that are generally negative. On the other hand, ligands with pK_a's greater than one tend to form predominantly inner-sphere complexes. This group includes the conjugate bases of weaker inorganic acids as well as a large majority of organic acids.

3.3.3 Complexation with Soft- and Polyaminocarboxylate Ligands

Though the previous discussions have focused primarily on bonding with hard ligands, bonding with softer donor atoms such as nitrogen is also important from a separations standpoint and therefore must also be addressed. "Soft" in this case refers to ligands that are softer than oxygen (e.g., N, S, P). It is well known that in aqueous solutions where lanthanide and actinide cations are strongly hydrated, soft, nonchelating ligands are not strong competitors for inner-sphere water molecules. In fact, investigations of soft donor complexes in aqueous solutions usually require high ligand concentrations in order to accurately measure stability constants. In order for soft donor ligands to effectively compete with water, they must be chelating ligands such as the hexacoordinate TPEN [N,N,N',N'-tetrakis(2-pyridylmethyl)ethylenediamine] (Figure 3.2) ligand.[73]

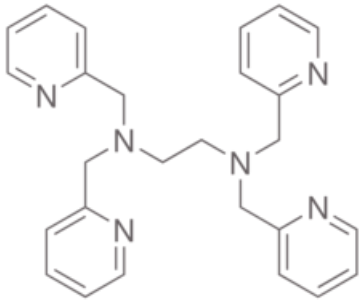

Figure 3.2 N,N,N',N'-tetrakis(2-pyridylmethyl)ethylenediamine (TPEN)

In many cases, there is a modest increase in the stability constant for an actinide complex compared to an analogous lanthanide complex when the ionic radii of the two elements are similar. The origin of the increased stability is still an active area of investigation, and theories have suggested that the source of this increased stability may be due to participation of, for example, the 5f orbitals[74], to the bonding. Evidence of increased covalence includes the measurement of shorter bond lengths[75] in crystalline soft donor complexes and more exothermic

enthalpies of reaction[76] for trivalent actinides compared to lanthanides with similar ionic radii. Exploitation of the small differences in thermodynamic stabilities of trivalent lanthanide and minor actinide soft donor complexes has been the basis of several solvent extraction-based trivalent lanthanide/actinide separation schemes.

Although chelating soft donor ligands tend to form stronger complexes with minor actinides than trivalent lanthanides, even stronger complexes can be formed with polyaminocarboxylic acids (PACAs). These ligands are comprised of hard carboxylate ligands and soft amine ligands that are linked by alkyl or aryl bridges. Examples include *trans*-1,2-diaminocyclohexanetetraacetic acid (CDTA), diethylenetriaminepentaacetic acid (DTPA), and ethylenediaminetetraacetic acid (EDTA). The stability constants for PACA complexes are often over ten orders of magnitude greater than those for soft chelates. When PACA complexes form, the hard carboxylate ligands first displace inner-sphere water molecules, allowing the soft amine ligands to bind more freely to the metal center. As with the soft chelates, PACAs form stronger complexes with trivalent actinides than lanthanides of similar ionic radius, implying that slightly more covalent bonding is involved in the actinide complexes. This additional stability has allowed the efficient separation of lanthanides from minor actinides in the solvent extraction scheme known as the TALSPEAK (Trivalent Actinide-Lanthanide Separation by Phosphorus-reagent Extraction from Aqueous Komplexes) process.

3.3.3.1 A Brief Overview of the TALSPEAK Process

The TALSPEAK process[77] takes advantage of the differences in the thermodynamic stabilities of minor actinide and trivalent lanthanide polyaminocarboxylates to effect a separation of the two groups. The initial aqueous phase consists of trivalent lanthanides, minor actinides and DTPA in an acidic medium that is buffered by lactic acid at a pH of around 3.5. The organic phase contains the acidic extractant, HDEHP (di-(2-ethylhexyl)phosphoric acid, Figure 3.3), in a suitable diluent. Though both the minor actinides and trivalent actinides form very strong binary complexes with the octadentate DTPA ligand, the An(III)-DTPA complexes are thermodynamically more stable than those of the lanthanides. The An(III)-DTPA complexes are thus held back in the aqueous solution, allowing HDEHP to preferentially extract lanthanides into the organic solution.

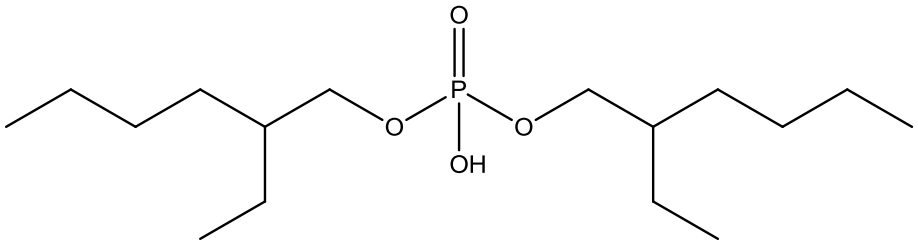

Figure 3.3 HDEHP (di-(2-ethylhexyl)phosphoric acid)

3.4 Am(III)/Cm(III) Separations

3.4.1 Current Methods of Separating Am from Cm

The chemical similarities between Am(III) and Cm(III) make the separation of these two actinides very difficult to achieve quantitatively without resorting to multi-stage methods. The separation has been accomplished using a variety of chromatographic techniques as well as those that exploit the higher oxidation states of americium. Below is a brief summary of the methods that have been used to achieve separation of Am(III) from Cm(III).

Chromatographic techniques reported to adequately separate Am(III) from Cm(III) include ion exchange, high performance liquid chromatography (HPLC), and counter-current chromatography (CCC). These techniques amplify the small thermodynamic differences in the strengths of Am(III) and Cm(III) complexes to effect their separation. Ion exchange has been used routinely in laboratories to separate Am(III) from Cm(III) (and/or the individual trivalent lanthanides) using a solution of α-hydroxyisobutryic acid (α-HIBA) as the eluant. The separation factor for adjacent elements is approximately 1.4 in this case[78]. HPLC experiments with α-HIBA have generated slightly lower separations factors (1.3).[79] On the other hand, Myasoedov and co-workers used CCC with malonamide extractants to obtain americium fractions containing up to 99.4% Am and 0.5% Cm in about 100 minutes.[80]

The reported separation factors for ion exchange and HPLC with α-HIBA are too low for commercial applications. Although Myasoedov and co-workers reported very good separations using CCC, this technique along with ion exchange and HPLC are designed for laboratory use and thus are not suitable for large-scale separations. These techniques cannot, for example, be easily employed in a streamlined multistage capacity. Furthermore, solid resins generate additional quantities of radioactive solid waste requiring permanent disposal.

Though the most stable oxidation state of americium is the trivalent state, other oxidation states ranging from the divalent to the heptavalent state have been observed in solution (cf. Table 3.3). Oxidation of Am(III) to the hexavalent state in particular have been used to effect the separation of Am(VI) from Am(VI)/Cm(III) solutions and from solutions containing Cm(III) and the trivalent lanthanides. These separations have been accomplished using precipitation and solvent extraction. For either technique, Am(III) is usually oxidized to the hexavalent state using strong oxidizing agents such as peroxydisulfate ($S_2O_8^{2-}$); trivalent lanthanides and Cm(III) are unaffected. The lanthanides and/or curium have been precipitated as fluorides[81] and as double sulfates[82] (i.e., $Ln_2(SO_4)_3{\cdot}Na_2SO_4{\cdot}2H_2O$). For example, Nash et al.[82] reported precipitation of the double sulfates of lanthanides and curium with separation factors as high as 10-11. Successful Am(VI)/Cm(III) separations have been reported via solvent extraction with HD[DIBM]P (bis-2,6-dimethyl-4-heptylphosphoric acid) as the extractant.[83,84]

Though the use of oxidized Am(VI) in precipitation and solvent extraction systems has led to good separation factors, an additional step is required to oxidize Am(III) prior to precipitation or extraction. Oxidations with peroxydisulfate are slow[84] without the use of a silver catalyst in dilute nitric acid ($[HNO_3] < 0.5$ M); peroxydisulfate itself decomposes at higher nitric acid concentrations and actually *reduces* Am(VI).[83] Moreover, Am(VI) is a strong oxidizing reagent that is difficult to keep in the hexavalent state for long times.

3.4.2 A Size-Based Approach to Separation of Am(III) from Cm(III) *and the Ln(III)'s*

A separations method based on solvent extraction without the need for oxidized americium is an ideal method of separating Am from Cm because it can more easily be incorporated into one of the solvent-extraction-based UREX+ schemes discussed in Chapter 1. TALSPEAK process conditions provide a very good framework for achieving the separation of Am(III) from Cm(III) and the trivalent lanthanides because the process is already designed to separate Am(III) and Cm(III) *from the lanthanides*. Thus, the TALSPEAK process could either be modified (e.g., change the polyaminocarboxylate or extractant) to allow selective retention of Am(III) while extracting Cm(III) with the lanthanides, or an additional solvent extraction step could be added after the TALSPEAK process to separate Am(III) from Cm(III).

Because one of the factors that determines the thermodynamic stabilities of Ln(III) and An(III) complexes is the *size* of the metal cation and the ligand, a size-based approach to separating Am(III) from Cm(III) could be used. In this approach, a large primary ligand (L^1) present in the aqueous phase nearly completely encapsulates the cations of interest, leaving residual water molecules in the inner coordination sphere. A small secondary ligand (L^2) of the right size would displace the remaining water molecules to form a *ternary complex* of the form $M(L^1)(L^2)$ that is more stable than the simple binary $M(L^1)$ complexes. Ideally, the secondary ligand would be too *big* to form a ternary complex with Cm(III) or the smaller trivalent lanthanides (or form weaker outer-sphere ternary complexes) but would fit in the remaining space around Am(III). The formation of $Am(L^1)(L^2)$ would lead to a lower extraction of Am because the extractant – HDEHP, for example – would no longer be able to compete for Am(III) as well as it could for Cm(III) and the Ln(III)'s. In other words, the difference in the stability constants (and free energies) would be *thermodynamically amplified* due to formation of more stable ternary $Am(L^1)(L^2)$ complexes. Figure 3.4 below illustrates the concept of thermodynamic amplification.

The utility of this approach is that small thermodynamic differences in the stability of the complexes can lead to significant increases in separation factors that are further amplified in a multi-stage solvent extraction system. The separation factor (Equation 2.33) between metals M_2 and M_1 can be written in terms of the difference in their respective Gibbs free energies of ternary complex formation as

$$\Delta\Delta G^\circ = RT \ln\left(S.F._{(M2/M1)}\right) \tag{3.3}$$

Using the Gibbs free energy of complexation as a measure of thermodynamic stability, a difference in the Gibbs free energy ($\Delta(\Delta G^\circ)$) of only 0.5 kJ mol^{-1} leads to a separation factor of approximately 1.2. Table 3.4 shows how small the difference in free energies of the complexes could be to achieve reasonably large separation factors. Clearly, very small thermodynamic differences translate to large separation factors. Separation factors of at least 10, corresponding to free energy differences of 5.7 kJ mol^{-1}, are desirable for large-scale separations.

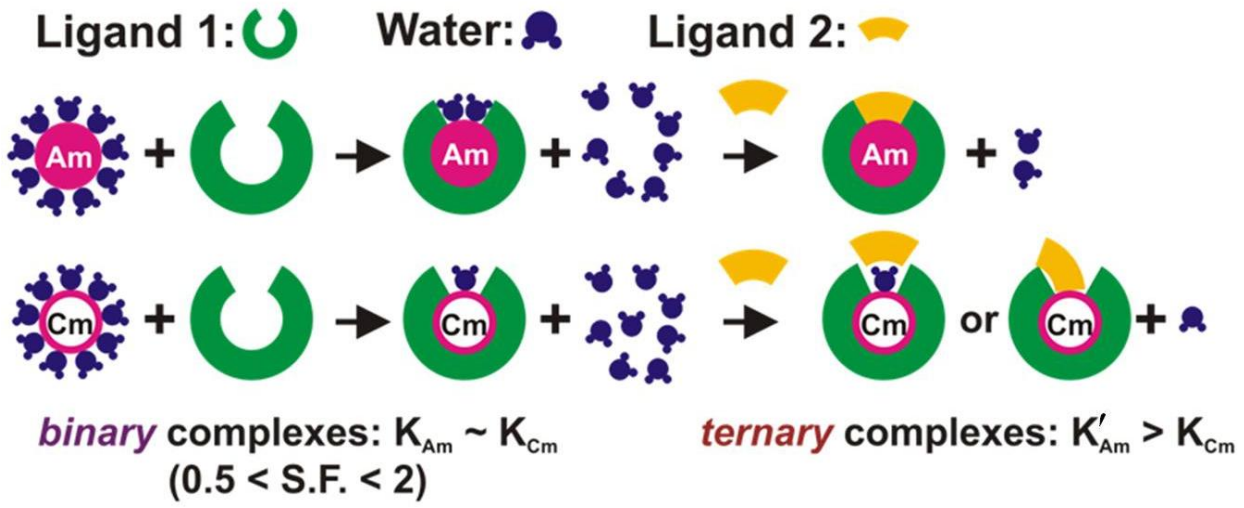

Figure 3.4 Illustration of the concept of thermodynamic amplification. The formation of the ternary complex with americium such that $K_{Am}' > K_{Cm}$ implies that the free energy difference between Am and Cm complexes has been thermodynamically amplified.

Table 3.4 Relationship Between Gibbs Free Energy Differences and Separation Factors*

Separation Factor	$\Delta(\Delta G°)$, kJ mol^{-1}
1.2	0.45
10	5.7
100	11
1000	17
10000	23

*Values of $\Delta(\Delta G°)$ were calculated using Equation 3.3 above.

3.5 Research Overview and Description of Systems Investigated

Factors such as ligand size, basicity, and steric constraints influence whether or not ternary complexes form and how strong such complexes will be. The objective of this research is to investigate these parameters from a thermodynamic perspective to provide insights into how these parameters influence ternary complex formation with dicarboxylic acids. By increasing the understanding of the thermodynamics of ternary complex formation, a rational approach to designing a size-based process that can separate americium from curium and the lanthanides can eventually be made.

3.5.1 Description of the Systems Investigated in this Work

A series of primary and secondary ligands were studied to gain thermodynamic insights into the driving forces of ternary complex formation that might be used to separate americium from curium. Ternary complexes are defined in this work to be complexes of the form $M(L^1)(L^2)$, where M represents the metal cation, L^1 is a primary polyaminocarboxylic acid (PACA), and L^2 is a secondary dicarboxylic acid or lactic acid. The primary PACAs studied in this work are shown in Figures 3.5-3.7. These ligands each form very strong, thermodynamically stable binary complexes with trivalent lanthanides and actinides, making them excellent candidates for ternary complex formation. Binary complexes formed with these ligands have a range of coordination numbers, which range from six (CDTA) to eight (DTPA), and have varying degrees of residual hydration depending on the element studied. These residual waters can be displaced by a secondary ligand to form a ternary complex.

The secondary ligands studied are a series of small dicarboxylic acids that can potentially bind in a mono-, bi-, or tridentate fashion, as shown in Figure 3.8. These ligands were chosen because they can form five- (oxalate, lactate), six- (malonate), and fused five-membered ring (IDA) complexes and may be small enough to fit in the remaining space around the binary PACA complexes. Additionally, the stability constants of these ligands are small enough that they do not displace the primary ligands under the conditions studied.

Most of the thermodynamic studies were conducted with lanthanides as they are non-radioactive and therefore simpler to work with, are easier (and cheaper) to obtain, and can be used to explore size-related trends in ternary complex formation. The lanthanides investigated were neodymium, samarium, terbium, holmium, and erbium; americium was studied when possible. Neodymium, holmium, erbium, and americium have peaks in the visible region of the electromagnetic spectrum that are sensitive to the metal coordination environment, thus making them very good candidates for studying ternary complex formation via absorption spectroscopy. Furthermore, neodymium and americium have comparable ionic radii, which means that direct comparison of their respective complexes can be made to investigate selectivity in ternary complex formation. Terbium is colorless and does not absorb in the visible region; however, fluorescence spectroscopy can be used to probe changes in the inner-sphere hydration number as the ternary complex forms. Lastly, the lanthanides studied have primary hydration numbers ranging from nine to eight due to lanthanide contraction, which can also affect whether or not ternary complex formation occurs and to what extent.

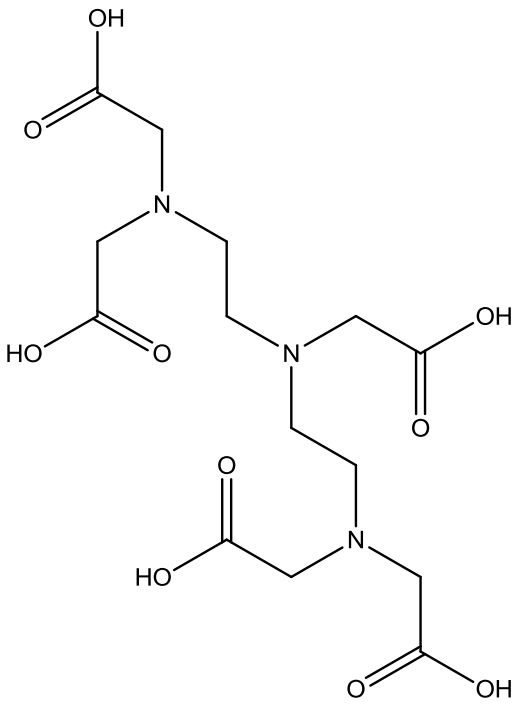

Figure 3.5 Diethylenetriaminepentaacetic Acid, DTPA. CN=8

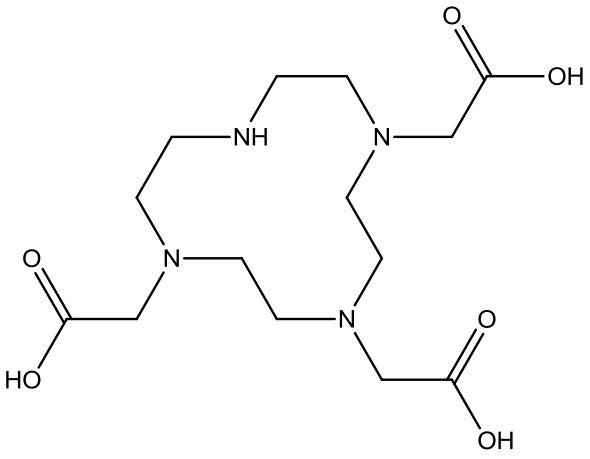

Figure 3.6 1,4,7,10-tetraazacyclododecane-1,4,7-triacetic acid, DO3A. CN=7

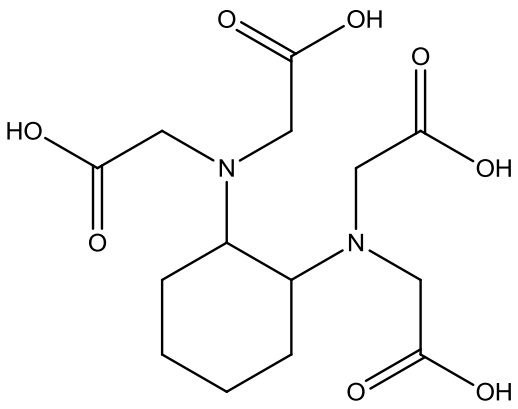

Figure 3.7 *trans*-1,2-diaminocyclohexanetetraacetic acid, CDTA. CN=6

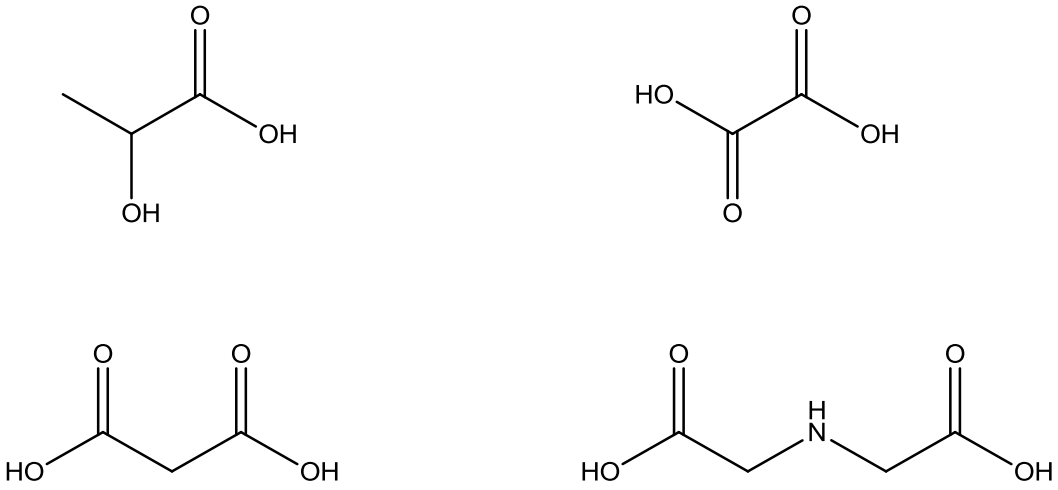

Figure 3.8 Secondary ligands investigated in this work. Row 1, left to right: Lactic acid (2-hydroxypropanoic acid) and oxalic acid (1,2-ethanedioic acid). Row 2, left to right: malonic acid (1,3-propanedioic acid) and iminodiacetic acid (IDA).

Chapter 4 Experimental

4.1 Reagents and Stock Solutions

4.1.1 Reagents

Chemicals were obtained from Sigma-Aldrich unless otherwise noted. The diethylenetriamine-N,N,N',N',N''-pentaacetic acid (H_5DTPA, >99%), trans-1,2-diaminocyclohexane-N,N,N',N'-tetraacetic acid monohydrate (H_4CDTA, 98%), sodium oxalate (Na_2Ox, Merck), lactic acid (85% w/w solution, mixture of d/l isomers), malonic acid (99%), and iminodiacetic acid (IDA, 98%) were used without further purification. The purity and water content of dichloromethane (≥99.5%), acetonitrile (≥99.5%), trifluoromethanesulfonic acid (triflic acid, HOTf), and trifluoroacetic acid (TFA, 99%) were used without any further drying or distillation. 4-morpholineethanesulfonic acid monohydrate (HMES•H_2O, 98%), its anhydrous sodium salt (NaMES, >99.5%), and $NaNO_3$ (≥99%) were also used as received.

The xylenol orange (~90%) indicator used for lanthanide-EDTA titrations was combined with sodium chloride in a 1:100 (w/w) ratio. Potassium hydrogen phthalate (>99.9%) was dried for at least two hours at 110 °C and stored in a dessicator before use.

The water used to prepare all solutions was purified to 18 MΩ•cm by a Barnsted E-pure system before use. All stock solutions with $p_cH \geq 5.5$ (see Section 4.2.1) were stored in plastic bottles under N_2 to minimize contamination by CO_2.

4.1.2 Stock Solutions

4.1.2.1 Standard Acid/Base Solutions

Sodium hydroxide solutions were prepared from an aqueous 50% (w/w) stock solution and were standardized against potassium hydrogen phthalate by titration to the phenolphthalein endpoint. Nitric acid solutions were prepared using Ultrex 70% (w/w) HNO_3 (J.T. Baker) and were standardized by titration with a standard NaOH solution to the phenolphthalein endpoint.

4.1.2.2 Metal Stock Solutions

Stock solutions of $Nd(ClO_4)_3$, $Sm(ClO_4)_3$, and $Ho(ClO_4)_3$ were obtained from Argonne National Laboratory stocks and had been prepared by dissolving the rare earth oxides (99.99%) in a slight excess of warm perchloric acid. (CAUTION!! Small quantities of organic materials present in hot concentrated perchloric acid may cause explosive compounds to be formed.) The $Nd(NO_3)_3$, $Sm(NO_3)_3$, $Tb(NO_3)_3$, $Ho(NO_3)_3$, and $Er(NO_3)_3$ stock solutions were prepared either by dissolving the rare earth nitrates in dilute nitric acid or by dissolving the appropriate amount of rare earth oxide in a slight excess of warm nitric acid. In the latter case, the solution was

filtered prior to dilution to volume. The metal concentrations in all solutions were determined by EDTA titration in pH 5 acetate buffer using xylenol orange as an indicator[85]. The pH of the resulting stock solutions ranged between 2 and 4.

The 0.04 M $Am(OTf)_3$ stock solution was obtained from Argonne National Laboratory stock. It had been chemically purified on a TRU-resin column (EIChrom), eluted with HCl, and passed through a bed of Amberlite XAD-7 resin. The resulting Am was evaporated to dryness, dissolved in 1M triflic acid, crystallized as the nonaaquo americium tris(triflate) salt[86], and redissolved in water to give the 0.04 M stock solution of Am triflate used in this study. Alpha and gamma spectroscopy indicated that the americium composition was 97.72 atom% ^{243}Am, 2.28 atom% ^{241}Am, and 0.004 atom% ^{244}Cm.

4.1.2.3 Metal-Chelate Stock Solutions

The thermodynamics of ternary complex formation was investigated via spectrophotometric and calorimetric titrations of stock solutions containing the binary metal-chelate complex with solutions containing a secondary ligand. The metal-chelate stock solutions contained a lanthanide or actinide salt, a polyaminocarboxylic acid as the chelating ligand, MES as a non-complexing buffer, and $NaNO_3$ as the background electrolyte.

Lanthanide-chelate stock solutions used in all titrations with CDTA or DTPA as the chelating ligand contained 10-40 mM $Ln(NO_3)_3$, 50 mM CDTA or DTPA, 10 mM MES, and 1 M $NaNO_3$. For the titration of $Ln(DTPA)^{2-}$ complexes with lactic acid, the lanthanide perchlorate was used instead of the nitrate. The p_cH of the solutions was adjusted to 6 for the oxalate and malonate titrations, 6.6 for the lactate titrations, and 7 for the IDA titrations. Small stock solutions of 0.8 mM $Am(OTf)_3$ /10 mM $Eu(ClO_4)_3$/50 mM DTPA/10 mM MES/1 M $NaNO_3$ were prepared by spiking a 10 mM $Eu(ClO_4)_3$/50 mM DTPA/10 mM MES/1 M $NaNO_3$ solution with a small volume of 0.04 M $Am(OTf)_3$. A 1 mM $Am(OTf)_3$/0.05 M CDTA/0.01 M MES/1 M $NaNO_3$ solution for calorimetry was prepared similarly by spiking a 50 mM CDTA/10 mM MES/1 M $NaNO_3$ solution with 0.04 M $Am(OTf)_3$ and adjusting the p_cH to 6.

Preparation of Ln(DO3A) stock solutions (DO3A = 1,4,7,10-tetraazacyclododecane-1,4,7-triaacetic acid) required a more complex procedure because it is known that Ln(DO3A) and their structurally-similar Ln(DOTA) complexes exhibit slow association kinetics and a competing dissociation reaction that are both pH-dependent.[87,88] Lanthanide/DO3A/MES/$NaNO_3$ solutions consisting of 10-15 mM $Nd(NO_3)_3$ or $Er(NO_3)_3$, 12-17 mM DO3A (a slight excess relative to the lanthanide concentration), 10 mM MES, and 1 M $NaNO_3$ were prepared by combining the required amounts of materials listed and, once the measured pH stabilized (typically after one hour), the pH was adjusted to approximately 4-5 with 50% NaOH. The pH was monitored after the addition of base. Once the pH was verified to be relatively constant (i.e., $\pm$ 0.01 pH units), an optical spectrum of the solution was taken and the entire solution was transferred to a 100 mL round bottom flask and refluxed at 60 °C for at least one week. After refluxing, the solution p_cH (section 4.2.1) was adjusted to six and diluted to volume. The density of the solution was measured as well. A visible spectrum was taken for comparison with the initial spectrum taken one week earlier. The p_cH was re-measured regularly and subsequent spectra were compared to the one-week equilibrium spectrum to verify that the complex remained stable.

4.1.2.4 Ligand and Dilution Solutions

The ligand solutions used in all experiments contained the secondary ligand (lactate, oxalate, malonate, or IDA), chelate, MES, and $NaNO_3$. The concentrations of the secondary ligand ranged from 0.5-2 M for all secondary ligands except oxalate; due to its low solubility, the maximum oxalate concentration in the titrant was 76 mM. The chelate, MES, and $NaNO_3$ concentrations were the same as in the metal-chelate stock solutions. Additionally, dilution solutions which contained 50 mM chelate, 10 mM MES, and 1 M $NaNO_3$ were prepared for use in calorimetric titrations and as diluents. All titrant and dilution solutions were prepared in an analogous fashion as the metal CDTA or DTPA solutions.

4.1.2.5 Heat of Protonation Solutions

In order to measure the heats of protonation of MES and CDTA and the pK_a of MES, four stock solutions were prepared: 1 mM CDTA/1 M $NaNO_3$, 10 mM NaMES/1 M $NaNO_3$, 10 mM HMES/1 M $NaNO_3$, and a 1 M $NaNO_3$ dilution solution.

4.2 Instrumentation

4.2.1 Conversion of pH to p_cH

The ligand protonation- and metal complex-stability constants used in this study are reported in terms of *concentrations* at a given ionic strength. Therefore, knowledge of the hydrogen ion concentration, rather than the activity, is required in order to accurately use these constants. The measured pH values can be converted to p_cH values using the equation

$$p_cH = pH + \log \gamma_H \tag{4.1}$$

where $p_cH \equiv -\log[H^+]$ (with $[H^+]$ given in units of molarity) and γ_H is the activity coefficient of the hydrogen ion at a given ionic strength.

The acidity of all solutions was measured with a ThermoOrion Ross semimicro glass pH electrode. The electrode was filled with saturated NaCl and was replenished as needed. For the initial experiments with DTPA and lactate, the electrode and pH meter were calibrated with pH 4.00 and 7.00 buffers. The conversion of pH to p_cH was accomplished by measuring the pH of a standardized 0.01 M HNO_3/1 M $NaNO_3$ solution. Using equation (4.1) above, the activity coefficient of the hydrogen ion was readily obtained and was used for subsequent p_cH calculations.

For all other experiments, the electrode was calibrated to read out in p_cH by measuring the electrode potentials during the titration of standardized solutions of 0.01 M HNO_3/1 M $NaNO_3$ with 0.1 M NaOH/0.9 M $NaNO_3$. The data obtained were subjected to a Gran analysis[89] to corroborate the expected endpoint value. By using the pK_w of water at 25 °C and the known volumes and concentrations, the hydrogen ion concentration was calculated for each addition of sodium hydroxide. The pH electrode potential readings were plotted as a function of the log of

the proton concentration yielding a straight line. The readings nearest the endpoint were removed from the line because small errors in concentrations and volumes lead to large errors in the readings in that region. Linear regression yielded a best-fit line that related electrode potential directly to p_cH.

4.2.2 Spectroscopy

4.2.2.1 Absorption Spectroscopy

Spectrophotometric titrations were executed with an upgraded On-Line Instrument Systems Cary-14 double-beam spectrophotometer. Titrations were carried out in 1 or 5 cm quartz cuvettes under nitrogen at 25 ± 1 °C and were generally performed at least thrice. The bandwidth of light passing through the sample for each point in the spectrum was less than the wavelength increments used in a given titration. The wavelength increments used in titrations were between 0.2-1 nm per point (increment), with a majority of the spectra being taken at 0.2-0.5 nm per point in order to adequately measure absorbances at the narrow peaks.

4.2.2.2 Fluorescence Spectroscopy

A Cary Eclipse (Varian) fluorimeter was used to measure the emission spectra and lifetimes of the $Tb(CDTA)^-$ complex when titrated with oxalate. Spectra were taken in a 1 cm fluorescence cuvette. An excitation wavelength of 374 nm was used for all experiments and the emission intensities were monitored at 544 and 545 nm for lifetime measurements. The instrument slits were set to yield 20 nm bandwidths for both excitation and emission and a 400 nm emission cutoff filter blocked all wavelengths less than 400 nm. The sample temperature ranged between 24 and 26 °C.

4.2.3 Calorimetry

4.2.3.1 Isoperibol Solution Calorimetry

Thermometric titrations were performed with a computer-controlled Calorimetry Sciences CSC4300 Isoperibol Solution Calorimeter. A glass Dewar cup (30 mL capacity) fitted with a corrosion-resistant stirrer, buret, and thermistor was utilized for all thermometric titrations. The temperature of the cup solution was adjusted to $24.9 \leq T_{cup} \leq 25.0$ °C prior to experiments by passing current through the thermistor at a predetermined rate. The programs ISC Collect and ISC Analyze [Calorimetry Sciences Corporation, v. 1.0] were used to extract the total heat measured in an experiment.

4.2.3.2 Isothermal Titration Calorimetry

Isothermal calorimetric titrations were executed with a computer-controlled Calorimetry Sciences CSC4200 Isothermal Titration Calorimeter (ITC). Two matching Hastelloy-C cell assemblies were used as reference and sample cells. Within the cell assemblies are a thin, flexible, corrosion-resistant stirrer and a port for a 100 μL or 250 μL syringe. An electrical calibration of the ITC was done at the outset and periodically to ensure that temperature and power measurements were correct and remained consistent.

4.3 Methods

4.3.1 Hydrolysis of DO3A, tert-butyl ester

The 1,4,7,10-tetraazacyclododecane-1,4,7-triacetic acid (DO3A) ligand was prepared by hydrolysis of the DO3A *tert*-butyl ester (DO3A·tBu, 100%, Macrocyclics). Syntheses were carried out in small batches to conserve the limited amount of DO3A·tBu available and to optimize the procedure. In general, 0.25-1 g of DO3A-tert-butyl ester was dissolved in 1-2 mL dichloromethane. The solution was transferred quantitatively using 1 mL dichloromethane to a small round-bottom flask. Trifluoroacetic acid (1-3 mL) was added in small increments over the course of one hour. The post-addition DO3A·tBu:TFA concentration ratio was 1:20 in these reactions. The solution was then stirred under argon at room temperature for 5 to 48 hours. The solution was then removed from stirring and the solvent removed via rotary evaporation (30 °C, 30 mmHg), yielding a viscous yellow- to brown-colored oil. This oil was washed with small portions of dichloromethane and re-evaporated to remove any residual trifluoroacetic acid, yielding a white to off-white solid. In cases where repeated washings were either unsuccessful or produced a *sticky* solid, a 50% CH_2Cl_2:CH_3CN solution was added (5-10 mL) with swirling and the mixture was allowed to stand. In less than an hour, a white powdery solid precipitated which was filtered and washed with dichloromethane.

All isolated solids were dried in an oven under reduced pressure at 90-100°C for at least four hours. H-1 and C-13 NMR spectra were taken of the products in deuterated water (99.9 atom % ^2H, Isotech) in an Oxford 500 MHz NMR spectrometer to verify that the hydrolysis was successful (i.e., no partially hydrolyzed species were present). Chemical shifts are indicated as ppm relative to TMS. Samples were also analyzed via mass spectrometry in methanol.

In cases where incomplete hydrolysis occurred, the partially-hydrolyzed product was re-dissolved in 10 mL of a 5% (v/v) TFA:water solution and allowed to stir overnight. The resulting mixture was concentrated via rotary evaporation slowly to a thick, nearly solid oil. A small volume of 50% CH_2Cl_2:CH_3CN was added to this oil, and after one hour, a white solid precipitate was suspended in a yellow supernatant. More CH_2Cl_2:CH_3CN was added as needed to encourage further precipitation. The supernatant was removed and the solid was washed with another small portion of the CH_2Cl_2:CH_3CN mixture. The precipitate was then filtered and washed with small portions of dichloromethane.

4.3.2 Spectroscopy

4.3.2.1 Absorption Spectroscopy

With the exception of the $Tb(CDTA)^-$ and $Am(CDTA)(Ox)^{-3}$ titrations, ternary complex formation constants were measured via spectrophotometric titrations. In experiments employing 1 cm quartz cuvettes, 2 mL of a metal-chelate stock solution was pipetted into the cuvette; experiments performed in 5 cm cells required 10 mL of the stock solution instead. To the metal-chelate stock solution, small volumes of the secondary ligand stock solution were added. In order to maintain identical experimental conditions during the titrations, after each addition, a one minute equilibration time was allotted before taking the spectrum.

Because malonate and IDA complexation were accompanied by significant changes in the solution p_cH, in titrations involving those ligands, the solution p_cH was measured (also at 25.0 °C) prior to taking each spectrum. Each spectrophotometric titration consisted of six to 14 spectra. The equilibrium constants for ternary complex formation were determined from the titration data using the program SQUAD.[90]

4.3.2.2 Fluorescence Spectroscopy

Lifetime measurements and emission spectra were taken to determine the ternary complex formation constant for the $Tb(CDTA)(Ox)^{3-}$ complex. For both sets of experiments, 2 mL of the $Tb(CDTA)^-$ stock solution was titrated with oxalate in small increments. In the lifetime experiment, after the excitation pulse was applied, the emission intensities were measured at 544 nm and 545 nm after delay times ranging from 0.1-9.1 ms had passed. This process was repeated after every addition; 17 total additions of oxalate were made.

In the second set of experiments, the emission spectrum was measured in the wavelength range 450-650 nm after each addition of oxalate. A 0.1 ms delay time was allotted prior to taking the spectrum. Nineteen total spectra were taken. In all experiments, the solution p_cH changed by < 0.005 units over the course of the titration and was thus considered constant in the calculations.

4.3.2.3 Potentiometric Titrations

Potentiometric titrations of HMES were done to measure the pK_a of the MES buffer at I = 1 M. Fifteen milliliters of a 10 mM HMES/1 M $NaNO_3$ solution were pipetted into a cup fitted with a buret and pH electrode calibrated to read out in p_cH. The solution was titrated with 0.1 M NaOH/1 M $NaNO_3$ in one hundred 20 μL increments and the potential was measured after each addition. The titration was repeated twice. The pK_a was calculated from the pcH titration data using the program PSEQUAD.[90]

4.3.2.4 Calorimetric and Thermometric Titrations

In general, two types of experiments were conducted: 1) ternary complex formation titrations in which metal-aminopolycarboxylate solutions were titrated with secondary ligand

solutions and 2) heat of protonation titrations of 10 mM MES/1 M $NaNO_3$ and 2 mM CDTA/1 M $NaNO_3$ with HNO_3. Prior to either type of experiment, heat of dilution experiments were conducted to measure the background heat evolved or absorbed due to the addition of the various titrant solutions. The measured background heats were then used to correct the observed heats obtained in the ensuing experiments.

All thermometric titrations were carried out at 25.0 °C beginning with 25 mL solution in the reaction vessel. Each titration was generally performed in triplicate. A single titration experiment consisted of a heat capacity measurement to calibrate the system, a temperature re-equilibration, one continuous addition of 1-2 mL titrant solution over the course of 4 minutes, and a post-addition temperature re-equilibration. The reaction cup temperature was monitored in 2 second intervals throughout the experiment. After the titrations, the p_cH of the cup solution was measured again. With the known stability constants, pK_a's, and pre- and post-titration p_cH values, the number of moles of each species formed was calculated. The measured heats were also corrected for ligand protonation reactions and for dilution. The molar enthalpy of complexation was then calculated by dividing the corrected heat by the number of moles of ternary complex formed.

In a standard isothermal calorimetric titration, 900 μL of a desired solution were titrated with 100 μL of the titrant solution in 2-10 μL increments. For $Am(CDTA)^-$ titrations, 800 μL Am solution was pipetted into the cup and 85 μL titrant was added in 5 μL increments. In all titrations, five minutes passed between additions. The data collected during the titration represent the rate of heat flow between the sample and reference cells. Therefore, in order to determine the amount of heat absorbed or released per addition, the program Bindworks [Calorimetry Sciences Corporation, v. 3.078] was used to integrate each peak in the thermogram. The Bindworks data were then transferred into Excel and, along with the known pK_a's, stability constants, and mass balance equations, the pertinent enthalpies of protonation or complexation were determined using the solver application.

Chapter 5 Investigation of Aqueous Ternary Complexes

5.1 General Data Treatment

5.1.1 Determination of Stability Constants

Hypersensitive peaks in trivalent Nd, Ho, and Er absorption spectra are strongly influenced by the surrounding metal environment.[91] These species' hypersensitive peaks as well as the most strongly absorbing peaks for trivalent Am and Sm are in the visible region. Therefore, UV-Visible absorption spectroscopy was employed to search for spectral evidence of inner-sphere ternary complex formation and to quantify the thermodynamic stability of those complexes that form. Fluorescence spectroscopy was used as a second means of investigating inner-sphere ternary complex formation with terbium. With this technique, both the measured lifetimes and the fluorescence intensities change as the inner-sphere hydration state of terbium changes. This fact was exploited to determine the stability constant for the formation of $Tb(CDTA)(Ox)^{3-}$.

A majority of the stability constants for ternary complex formation that were determined in this work were calculated from spectrophotometric titration data. The equilibrium for ternary complex formation that was used to calculate the stability constant is

$$M(L_1) + L_2 \leftrightarrow M(L_1)(L_2) \qquad K_{111} \equiv \frac{[M(L_1)(L_2)]}{[M(L_1)][(L_2)]} \tag{5.1}$$

where $M(L_1)$, L_2, and $M(L_1)(L_2)$ are the binary lanthanide or americium complex, secondary ligand, and ternary complex, respectively; the square brackets indicate concentrations of each species; and K_{111} is the equilibrium constant for the reaction under specific solution conditions. Charges have been omitted for clarity. During a given titration, after each addition of titrant, the measured absorbance is related to the concentrations of the species present by the Beer-Lambert Law:

$$A_{\mathbf{i,k}} = b \sum_{1}^{J} [\text{species}]_{i,j} \times \epsilon_{j,k} \tag{5.2}$$

Here $A_{i,k}$ is the absorbance at the *k*th wavelength of the *i*th spectrum, b is the pathlength, $[\text{species}]_{i,j}$ is the concentration of the *j*th species for the *i*th spectrum, and $\varepsilon_{j,k}$ is the molar

absorptivity of the *j*th species at the *k*th wavelength. Using Equation 5.1, the absorbance in Equation 5.2 can be rewritten in terms of the equilibrium constant:

$$A_{i,k}=b(\varepsilon_{M(L^1)}[M(L^1)]+\varepsilon_{L^2}[L^2]+ K_{111}\varepsilon_{M(L^1)(L^2)}[M(L^1)][L^2]) \quad (5.3)$$

The primary ligand L^1 has no significant absorbance in the region of interest; hence, the term in Equation 5.3 representing absorption due to the ligand is zero. Note that the concentrations $[M(L^1)]$ and $[L^2]$ are the *free* concentrations of the binary complex and the fully uncomplexed and deprotonated secondary ligand.

In order to calculate the equilibrium constants, mass balance equations are also necessary. The mass balance equations for the analytical concentrations of metal and secondary ligand L^2 can be written as follows:

$$C_M= [M] + \left[M(L^1)\right]+ [M(L^1)(L^2)] \quad (5.4)$$

$$C_{L^2}= [M(L^1)(L^2)] + \sum_{0}^{n_{max}} [H_n(L^2)] \quad (5.5)$$

where C_M, and C_{L^2} are the analytical concentrations of the metal, primary ligand, and secondary ligand, respectively, and the species $[H_n(L^2)]$ represent the concentration of the secondary ligand with *n* protons ranging from 0 to n_{max}. Because essentially all of the free metal was fully complexed by the primary ligand throughout the titrations, $[M]<<[M(L^1)]$ or $[M(L^1)(L^2)]$, meaning that the extent of ternary complex formation depended mainly on the total concentration of the binary complex and on the free concentration of the secondary ligand. Thus, the mass balance equation for the primary ligand was not needed and the [M] term in Equation 5.4 could be approximated as 0. The validity of this assumption was verified by HYSS speciation calculations for solutions containing a given lanthanide, polyaminocarboxylic acid, and a secondary ligand. An example is shown in Figure 5.1 at the end of this section for the Neodymium-CDTA-IDA system.

The equilibrium constants for ternary complex formation were calculated from the titration data using the program SQUAD[90]. SQUAD calculates stability constants for metal complexes by minimizing the sum of the squared residuals, U, between the measured absorbance and the SQUAD-calculated absorbance:

$$U = \sum_{k=1}^{K}\sum_{i=1}^{I}(A_{i,k}^{obs} - A_{i,k}^{calc})^2 \quad (5.6)$$

where $A_{i,k}^{obs}$ is the *measured* absorbance at the *k*th wavelength of the *i*th spectrum and $A_{i,k}^{calc}$ is the corresponding absorbance calculated by SQUAD from Equation 5.2. SQUAD first calculates the absorbance based on input analytical concentration data, mass balance equations, and estimated equilibrium constants. The sum of the squared residuals (Equation 5.6) is then calculated and is subsequently minimized by SQUAD using non-linear least squares analysis. Addition of the calculated equilibrium constant for the ternary complex to the constant for binary complex formation yields the stability constant for formation of the ternary complex:

$$M + L^1 + L^2 \leftrightarrow M(L^1)(L^2) \qquad \beta_{111} \equiv \frac{[M(L^1)(L^2)]}{[M][L^1][L^2]} \tag{5.7}$$

The SQUAD input files consisted of the absorbance spectra, the model of the expected equilibrium with estimated equilibrium constants, the analytical concentrations of metal and ligand for each spectrum taken during a titration, and any known molar absorptivities for absorbing species. Although Equation 5.1 represents the default equilibrium model used, a second model was also investigated in which the ternary complex reacts with a second ligand L^2:

$$M(L^1)(L^2) + L^2 \leftrightarrow M(L^1)(L^2)_2 \qquad K_{112} \equiv \frac{[M(L^1)(L^2)_2]}{[M(L^1)(L^2)][L^2]} \tag{5.8}$$

In general, the measured molar absorptivities of the binary complex, the free oxalate (Ox^{2-}) and malonate (Mal^{2-}) ligands, and the protonated iminodiacetate ($HIDA^-$) ligand were the absorbing species included in the input file for the relevant titration. Figure 5.2 shows the spectra of the free oxalate, malonate, and HIDA ligands that were used for titrations with $Ln(CDTA)^-$. Although the molar absorptivities of the secondary ligands were generally low (i.e., less than 0.2 $M^{-1}cm^{-1}$) throughout the wavelength range of interest, the use of high concentrations of these ligands still resulted in a significant ligand contribution to the measured absorbance. Ignoring the contribution of the uncomplexed secondary ligands typically caused an error in the calculated stability constants of about 0.02-0.2 log units and led to a poorer fit in SQUAD.

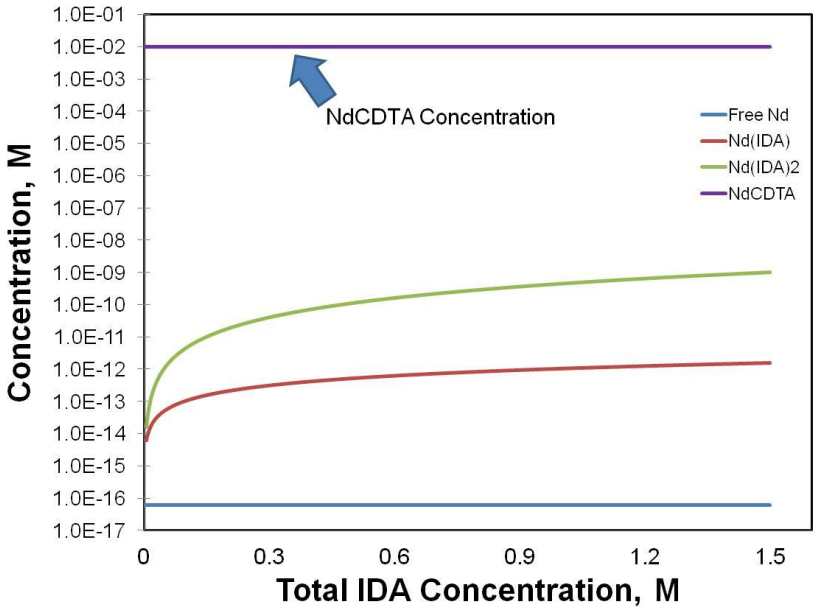

Figure 5.1 Speciation diagram for the Nd-CDTA-IDA system (no ternary complexes assumed in model) at pH 7. Analytical concentrations of the metal and ligand species are 10 mM total Nd and 50 mM total CDTA with the total IDA concentration varying from 0 to 1.5 M. Note that throughout the IDA concentration range of interest, no change in speciation of $Nd(CDTA)^-$ is noted.

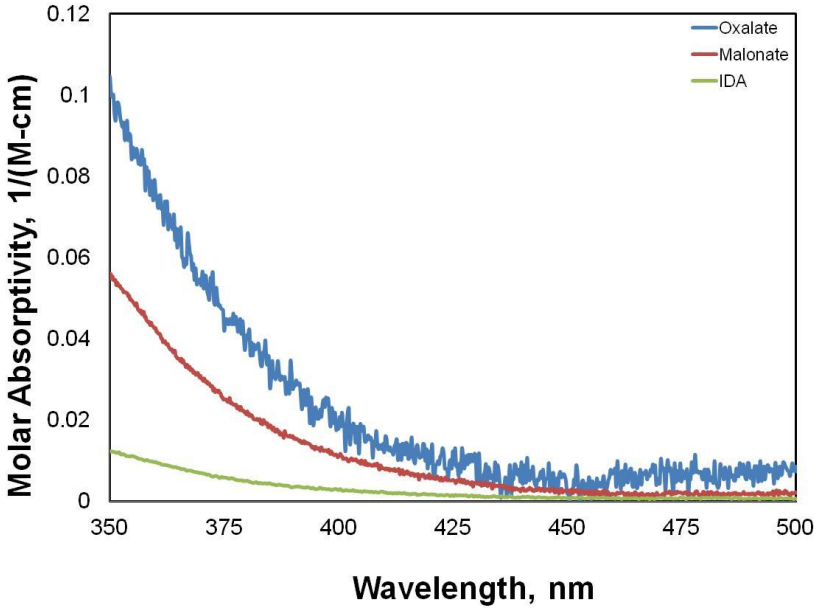

Figure 5.2 Molar absorptivities of oxalate, malonate, and iminodiacetate for the CDTA system. Concentrations of solutions used for the above spectra were 75 mM oxalate, 0.5 M Malonate, and 1.5 M IDA. Because the oxalate ligand has a low solubility at 1 M ionic strength (~ 76 mM) and a low molar absorptivity in the range of interest, low absorbances (< 0.04 au) with a poor signal-to-noise ratio were measured. This is why its spectrum is much noisier in comparison to malonate or IDA.

5.1.2 Determination of Enthalpies of Complexation

5.1.2.1 Overview

The enthalpies of ternary complex formation were calculated using data obtained from calorimetric titrations, which use the net heat absorbed or released from a reaction to determine various thermodynamic parameters (i.e., log K and/or $\Delta H°$) of the reaction. The net heat absorbed or released in these titrations were determined primarily using isoperibol solution calorimetry (ISC). With ISC, a closed dewar-type "cup" containing the desired solution is maintained at nearly isothermal conditions by being immersed in a temperature-controlled water bath. As a titration proceeds, the buret inside the cup dispenses titrant at a continuous rate and the temperature is recorded as a function of time. The total measured heat is then determined using the net temperature change and measured pre- and post-titration heat capacities. After correcting for heats not directly associated with the reaction, this measured heat can be used to determine the enthalpy of complexation. Isoperibol solution calorimetry was used for all of the titrations performed with lanthanides because the titrations were quick and copious quantities of heat were released with good reproducibility. The technique was also applied for the determination of the enthalpy of protonation of the MES buffer. However, the use of americium was not conducive to such titrations because of comparatively large volumes (25 mL) of solution used for the titration and the possibility of radioactive contamination of the large water bath required to maintain isothermal conditions. Thus, a second calorimetric technique, isothermal titration calorimetry (ITC), was used with americium. Because this technique was used to determine the enthalpy of complexation for the $Am(CDTA)(Ox)^{3-}$ complex as well as the enthalpies of protonation of H_4CDTA, further discussion of this technique will be presented in section 5.2.

5.1.2.2 Determination of the Enthalpy of Complexation Using Isoperibol Solution Calorimetry

Prior to conducting a calorimetric titration, dilution experiments were carried out for each ligand system studied to account for heat absorbed or released due solely to dilution of the ligand into the cup solution. In titrations in which there is no change in the protonation states of the ligand and complexes, the total measured heat is the dilution heat. This is also true if the initial and final p_cH values are several units above the secondary ligand's highest pK_a, as was the case for oxalate and lactate dilution experiments. However, dilution experiments with malonate and iminodiacetate were more sensitive to small p_cH changes than those with oxalate or lactate because the experiments were conducted at or near the pK_a of at least one of the ligand's protons. Because the initial p_cH of the titrant and cup solutions were not equal, the post-titration p_cH was significantly different, which resulted in changes in the ligand protonation states. Thus, the measured heats also had to be corrected for ligand protonation reactions to obtain the baseline dilution heat as follows:

$$Q_{dil} = Q_{meas} - Q_{prot} \tag{5.9}$$

Q_{dil} is the corrected dilution heat, Q_{meas} is the total heat measured during a titration, and Q_{prot} is the heat released due to protonation and deprotonation reactions. The terms in Equation 5.9 are positive for exothermic processes and negative for endothermic processes. The change in the number of moles of protonated species was calculated using the intial p_cH and concentrations of the titrant and cup solutions, the volumes of the cup solution and the added titrant, and the known pK_a values for the primary ligand, secondary ligand, and the MES buffer. The protonation heat was calculated using known protonation enthalpies with the equation

$$Q_{prot} = -\sum \Delta n_i \Delta H_i \tag{5.10}$$

where ΔH_i is the molar enthalpy of protonation of the *i*th species in solution and Δn_i is the change in the number of moles of the *i*th species. Negative enthalpy values apply to exothermic reactions and positive enthalpies apply to endothermic reactions.

Calorimetric titration data of binary metal-polyaminocarboxylate complexes with a given secondary ligand were treated similarly to dilution experiment data. In this case, the measured heats were corrected for dilution and protonation using the equation

$$Q_{complex} = Q_{meas} - Q_{prot} - Q_{dil} \tag{5.11}$$

where Q_{dil}, and Q_{meas} are the dilution- and measured heats as defined in Equations 5.9 and 5.10, and $Q_{complex}$ is the net heat of complexation. Q_{prot} in this case is the heat of protonation due to p_cH changes during a given thermometric titration, not the protonation heats from the associated dilution experiments. Using the known stability constants, pK_a's, mass balance equations, and pre- and post-titration p_cH values, the change in the number of moles of the ternary complex formed was evaluated. From these data, the molar enthalpy of complexation was calculated with the equation

$$\Delta H_{complex} = -\frac{Q_{complex}}{\Delta n_{complex}} \tag{5.12}$$

where $\Delta n_{complex}$ is the number of moles of ternary complex formed.

5.2 Thermodynamic Measurements for HMES and H_4CDTA

In order to account for protonation reactions due to pH changes during thermometric and calorimetric titrations, the relevant pK_a's and enthalpies of protonation at 1 M ionic strength were necessary. Table 5.1 is a tabulation of the thermodynamic data that was used to calculate the heat of protonation corrections. Note that the reactions are written as protonation reactions, not dissociation reactions; however, it is evident that there is an inverse relationship between log K and pK_a. A complete set of thermodynamic data was available for neither the H_4CDTA ligand nor the HMES buffer; thus, they were determined prior to calculating the enthalpies of complexation as discussed below.

The pK_a of the HMES buffer was calculated simultaneously from two sets of potentiometric titration data using the program PSEQUAD as discussed in Chapter 4. The combined dataset consisted of 185 measured potentials covering the p_cH range 4-11. The calculated pK_a, 6.194 ± 0.008, is indicative of an excellent fit, as is shown in Figure 5.3.

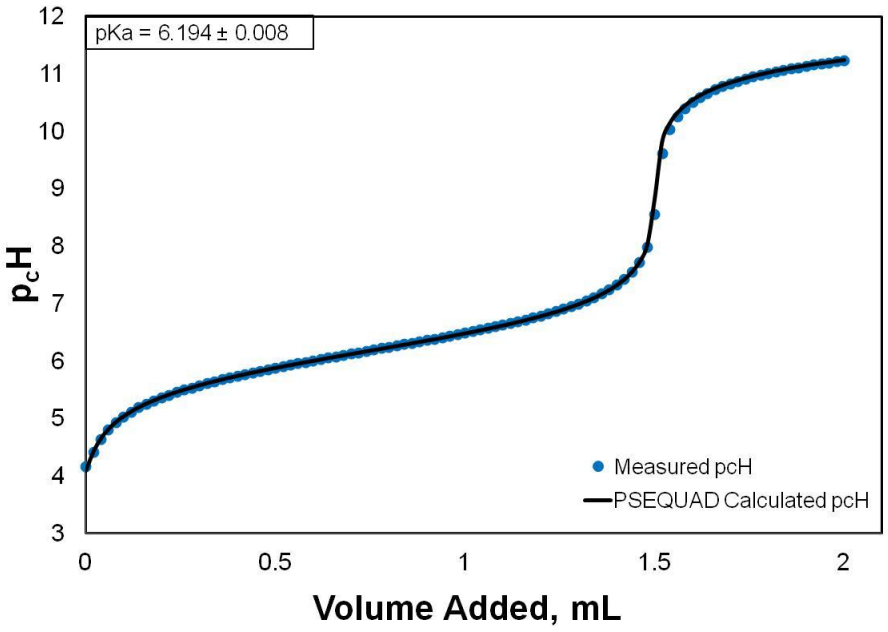

Figure 5.3 Comparison of p_cH values calculated by PSEQUAD with measured values.

Table 5.1 Thermodynamic Data for Protonation Reactions of Ligands Used in This Work

Ligand	Protonation Reaction(s)	Log K*,†	ΔH°(prot), kJ mol^{-1}
H_5DTPA	$DTPA^{5-} + H^+ \leftrightarrow HDTPA^{4-}$	9.98 ± 0.08	-33 ± 0.4‡
	$HDTPA^{4-} + H^+ \leftrightarrow H_2DTPA^{3-}$	8.29 ± 0.04	-18 ± 0.4‡
	$H_2DTPA^{3-} + H^+ \leftrightarrow H_3DTPA^{2-}$	4.15 ± 0.03	-6.3 ± 0.4‡
	$H_3DTPA^{2-} + H^+ \leftrightarrow H_4DTPA^-$	2.6 ± 0.1	-1.3 ± 0.8‡
	$H_4DTPA^- + H^+ \leftrightarrow H_5DTPA$	2.1 ± 0.2	+2.1 ± 0.8‡
HLac	$H^+ + Lac^- \leftrightarrow HLac$	3.64 ± 0.02	-1.7
H_2Ox	$Ox^{2-} + H^+ \leftrightarrow HOx^-$	3.57 ± 0.04	+3.2 ± 0.3
	$HOx^- + H^+ \leftrightarrow H_2Ox$	1.07 ± 0.07	+1.3
H_2Mal	$Mal^{2-} + H^+ \leftrightarrow HMal^-$	5.08 ± 0.06	+2.0 ± 0.04
	$HMal^- + H^+ \leftrightarrow H_2Mal$	2.58 ± 0.02	-1.5 ± 0.04
H_2IDA	$IDA^{2-} + H^+ \leftrightarrow HIDA^-$	9.26 ± 0.06	-35.6 ± 0.0
	$HIDA^- + H^+ \leftrightarrow H_2IDA$	2.60 ± 0.03	-4.2 ± 0.8
	$H_2IDA + H^+ \leftrightarrow H_3IDA^+$	1.85 ± 0.06	-4.2 ± 0.0
H_4CDTA	$CDTA^{4-} + H^+ \leftrightarrow HCDTA^{3-}$	9.22	-25.6 ± 0.3[a]
	$HCDTA^{3-} + H^+ \leftrightarrow H_2CDTA^{2-}$	5.84	-12.4 ± 0.4[a]
	$H_2CDTA^{2-} + H^+ \leftrightarrow H_3CDTA^-$	3.21 ± 0.04	-8.6 ± 2.4[a]
	$H_3CDTA^- + H^+ \leftrightarrow H_4CDTA$	2.42 ± 0.01	n/a
	$H_4CDTA + H^+ \leftrightarrow H_5CDTA^+$	1.60 ± 0.01	n/a
HMES	$MES^- + H^+ \leftrightarrow HMES$	6.194 ± 0.008[a]	-4.35 ± 0.07[b]
OH^-	$H^+ + OH^- \leftrightarrow H_2O$	13.78	-56.94 kJ/mol[c]

*All stability constants were measured in the presence of a sodium salt background electrolyte (e.g., $NaClO_4$) at 25°C and 1 M total ionic strength. Unless otherwise noted, data taken from Reference 52. †Reactions are written as stepwise protonation reactions, not dissociation reactions. ‡Enthalpy values for DTPA are for 25°C, 0.1 M total ionic strength (Na^+ electrolyte). All other enthalpy values refer to 25°C, 1 M ionic strength. [a]Enthalpy values measured in present work. [b]Value taken from Reference 92. [c]This is the enthalpy of neutralization of hydroxide.

The enthalpies of protonation of H_4CDTA at 1 M ionic strength were determined via calorimetric titrations using isothermal titration calorimetry. With this method, closed reference and sample cells containing a blank solution and the reaction solution, respectively, are suspended next to each other in a dry isothermal chamber. Prior to starting a titration, the two cells are allowed to thermally equilibrate. During a titration, each addition of titrant causes heat to be absorbed or released from the sample cell. Thermocouples located on the sample and reference cell measure the rate of heat flow between the two cells, which appears as spikes on a spectrum when plotted as a function of time. A sample spectrum is shown in Figure 5.4 below.

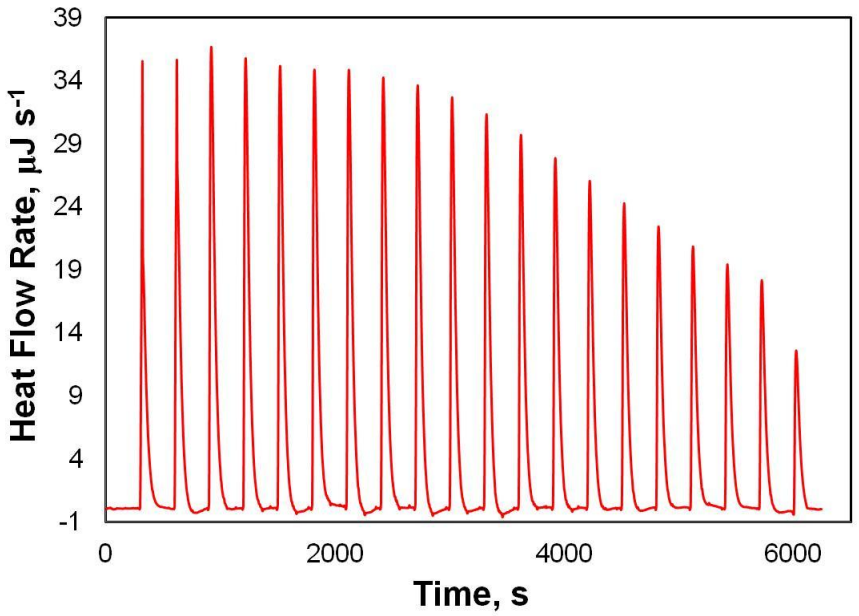

Figure 5.4 Sample spectrum from an isothermal titration calorimeter.

If a reaction is exothermic, the measured heat flow is positive whereas for endothermic titrations, the heat flow rate is negative. For a given titration, the amount of heat absorbed or released per injection was determined by integrating each peak in the spectrum using the program Bindworks. The measured heats corresponding to the first and second additions were typically not included in calculations because of the potential diffusion of titrant into the sample cell during baseline equilibration, increasing the uncertainty of those values. However, the impact on the chemical equilibrium due to those first additions was still accounted for in the subsequent additions.

In addition to the dilution correction applied to measured heats from H_4CDTA, a heat of hydroxide neutralization correction was applied to measured heats after additions in which the solution p_cH was greater than eight. At lower p_cH, this correction was negligible. An important concern when working with alkaline solutions is that diffusion of CO_2 into the solution can lead to carbonate (CO_3^{2-}) contamination. The presence of unwanted carbonates in solution lowers the apparent p_cH values due to formation of carbonic acid, leading to erroneous endpoint values in

acid-base titrations unless a correction is applied. No evidence of carbonate contamination was noted in the solutions used for the H_4CDTA titrations. Therefore, additional corrections for carbonate contamination were not necessary.

Using the literature or measured pK_a's of H_4CDTA and HMES as input parameters, a titration simulation was generated with the speciation program, HYSS. From this simulation, the changes in the moles of protonated ligand, Δn_i, were calculated and the pertinent enthalpies of protonation were determined by fitting the stepwise protonation enthalpies to the equation below:

$$Q_{cum}^{calc} = -\sum_{i} \Delta n_i \, \Delta H_i \tag{5.13}$$

Q_{cum}^{calc} is the cumulative calculated heat, ΔH_i is the cumulative molar enthalpy of protonation, and the subscript *i* refers to the number of protons in the protonated CDTA ligand or MES buffer. The best fit for each dataset was obtained by minimizing the sum of the squared residuals between measured and calculated heats via the Solver application in Excel.

A representative dataset along with a titration simulation for an H_4CDTA calorimetric titration are shown in Figure 5.5 below. In total, five datasets, each comprising about thirty measured heats in the p_cH range 3-10, were analyzed via the least squares analysis and the averages of the calculated enthalpies were taken. The Jackknife error estimation method[93] was used to estimate the uncertainties in the enthalpies. The protonation enthalpies for the addition of the first three hydrogen ions were readily calculated from the titration data and were very reproducible among datasets. The comparatively larger uncertainty in the third protonation enthalpy is due to the fact that there was a small number of usable datapoints representing solutions with a significant amount of H_3CDTA^-. According to the titration simulation, H_3CDTA^- becomes the predominant species well below p_cH 3.5, which are points near the end of the titration (i.e., $V_{titrant} \geq 0.8$ mL). At this point, H_4CDTA ($pK_a = 2.42$) also begins to form. Compounding the issue is the fact that the measured heats in the region where $p_cH < 3.5$ are at least an order of magnitude smaller than those in the higher p_cH regions. Attempts to fit this region with three (HCDTA, H_2CDTA, H_3CDTA) or four (HCDTA, H_2CDTA, H_3CDTA, H_4CDTA) species generated protonation enthalpies that were unreasonable (e.g., protonation enthalpies of -762000 kJ mol^{-1}) and had higher errors in the fit. Therefore, those points could not be included in the dataset used to determine the protonation enthalpies and, consequently, the agreement is poorer in the region where pH<3.5. A low pH titration would be necessary to more accurately measure the protonation enthalpy for H_3CDTA and to determine those for H_4CDTA and H_5CDTA. However, as the thermometric and calorimetric titrations done in this work to investigate ternary complex formation were conducted at p_cH values between six and seven, there was no need to further refine $\Delta H_{prot}(H_3CDTA)$ or to determine the protonation enthalpies for the species existing at lower p_cH.

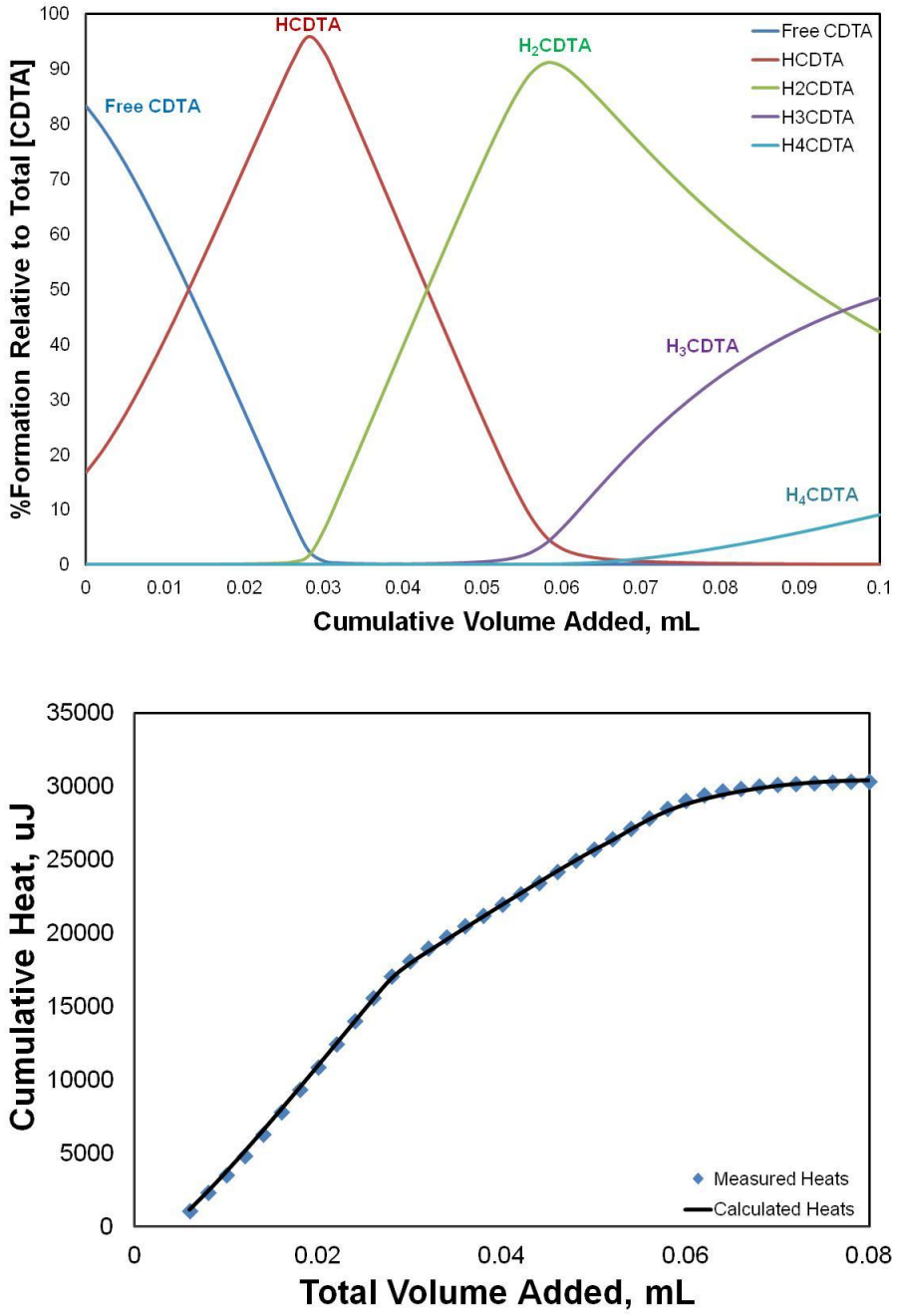

Figure 5.5 Titration simulation (top) for determination of protonation enthalpies of the CDTA ligand and a representative dataset (bottom) corresponding to the titration simulation. The fitted heats agree well with the measured heats until about 0.08 mL of titrant was added. Beyond this point, H_4CDTA begins to form but not in significant quantities to obtain an adequate fit of the data. Thus, the datasets for the analyses were cut off at 0.08 mL.

5.3 Thermodynamics of the Ln,Am-DTPA-L System

Evidence for the formation of ternary $M(DTPA)(Lac)^{3-}$ complexes of americium as well as the lanthanides neodymium, samarium, and holmium was searched for using spectrophotometric titrations. The expected equilibrium was

$$M(DTPA)^{2-} + Lac^{-} \leftrightarrow M(DTPA)(Lac)^{4-} \qquad (5.14)$$

where M represents a trivalent lanthanide or americium. In order to ensure that there was essentially complete deprotonation of lactate (pK_a = 3.64), the lanthanide experiments were conducted near p_cH=6.64, at which 99.9% of the total lactic acid is present in the free lactate form. Spectrophotometric titrations of 40 mM $Nd(DTPA)^{2-}$, $Sm(DTPA)^{2-}$, and $Ho(DTPA)^{2-}$ solutions with 2 M lactate were carried out at 25 °C in the manner discussed in Chapter 4. The results are shown in Figures 5.6-5.11. Figures 5.6, 5.8, and 5.10 show the absorbance normalized to the total lanthanide concentration and pathlength – a value which has units of molar absorptivity – as a function of wavelength. Comparison of the titration spectra for each lanthanide quickly leads to the conclusion that little to no ternary complex formation occurs with neodymium, samarium, or holmium as there is no apparent change in the spectra. It is, however, more instructive to monitor the change in molar absorptivities at peak wavelengths (especially the hypersensitive peaks) as the total lactate concentration increases. Monitoring molar absorptivities instead of absorbances is more useful because molar absorptivities take into account the contribution to the total $Ln(DTPA)^{2-}$ absorbance due to dilution that occurs during a titration. Thus, the changes in the spectra due to complex formation are more evident. Figures 5.7, 5.9, and 5.11 show these normalized absorbances as a function of $[Lac^{-}]/[Ln^{3+}]$ for the corresponding lanthanide titrations in Figures 5.6, 5.8, and 5.10. These plots indicate more clearly that ternary complexes are not observed to a significant extent under the conditions studied. If ternary complexes had formed, a change in the molar absorptivities would have occurred with increasing total lactate concentration.

Studies with americium were conducted with 1 M lactate at pH 4.1. First, a spectrum of the solution containing 0.82 mM Am, 10 mM Eu, and 50 mM DTPA was taken as reference point. The second spectrum taken was of the same solution that had been spiked with lactic acid to yield 1 M total lactate (0.75 M free lactate at pH 4.1) in solution. Comparison of these two spectra in Figure 5.12 below reveals that no significant complexation occurs even with such a large excess of lactate. Thus, the spectrophotometric titration data indicate that, at the very least, inner-sphere ternary complexes formed with lanthanides and americium with DTPA and lactate are weak at best.

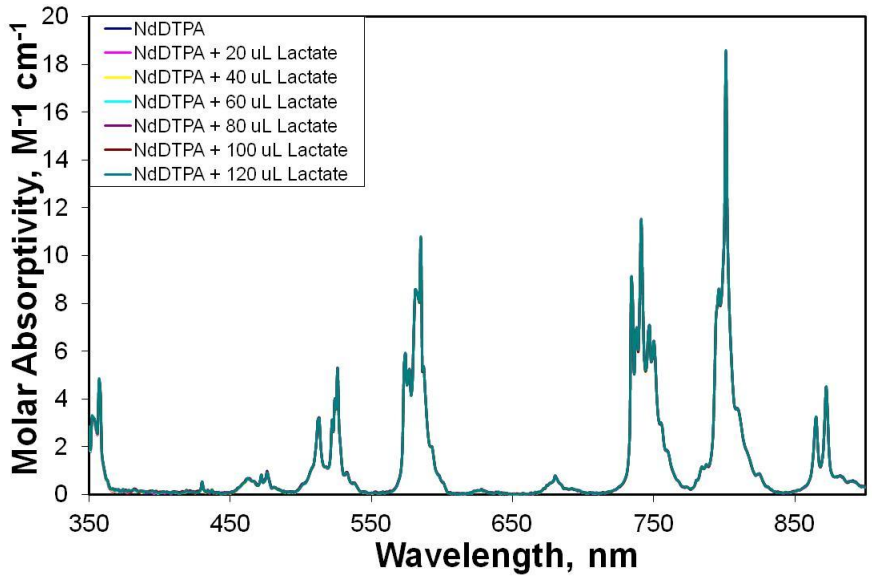

Figure 5.6 Absorption spectra for the titration of 40 mM $Nd(DTPA)^{2-}$ with 2 M lactate. Spectra have been normalized to the total analytical $Nd(DTPA)^{2-}$ concentration for each addition.

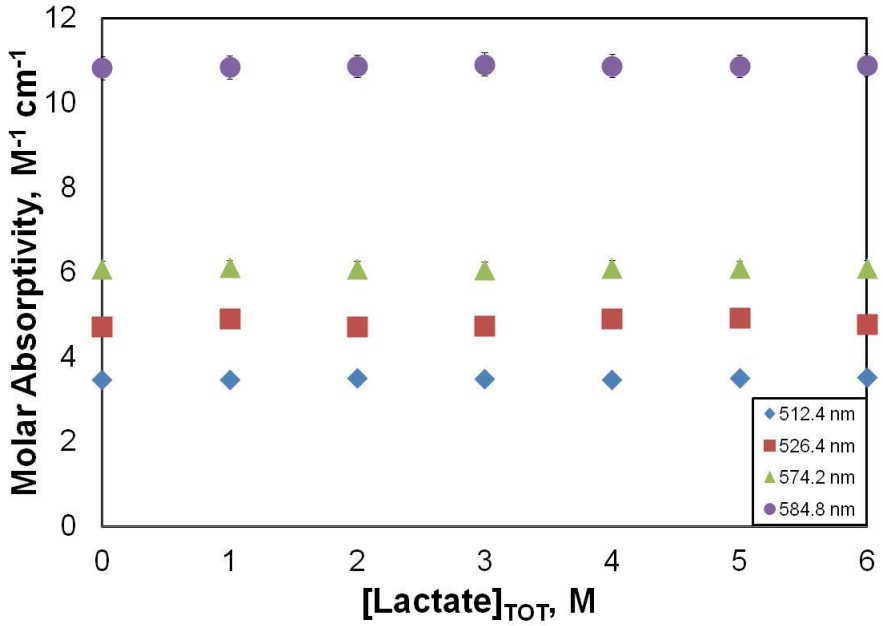

Figure 5.7 Molar absorptivities of $Nd(DTPA)^{2-}$ as a function of total lactate concentrations at peak wavelengths. The points are essentially linear, meaning that no evidence of ternary complexation is seen in this titration. Error bars may not be visible due to the size of the pictograms used to label the data points as well as the small uncertainty values.

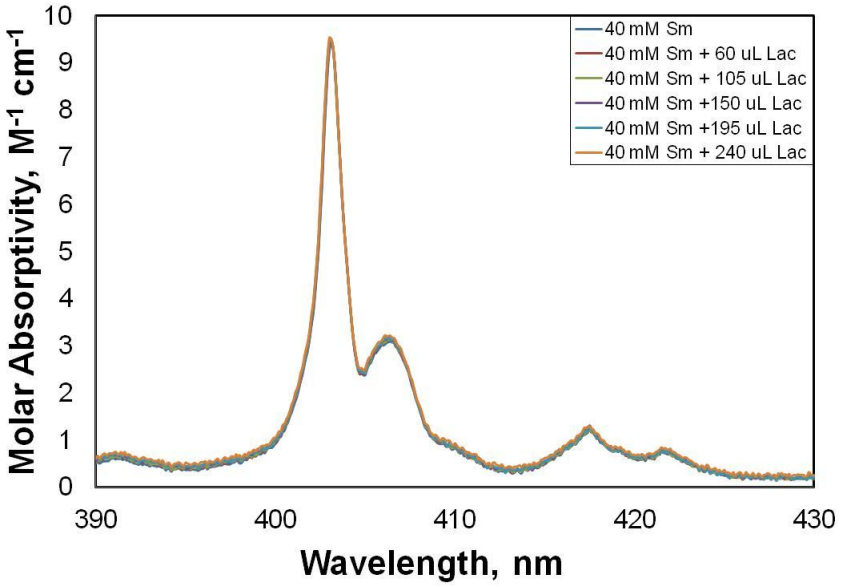

Figure 5.8 Absorption spectra for the titration of 40 mM $Sm(DTPA)^{2-}$ with 2 M lactate. Spectra have been normalized to the total analytical $Sm(DTPA)^{2-}$ concentration for each addition.

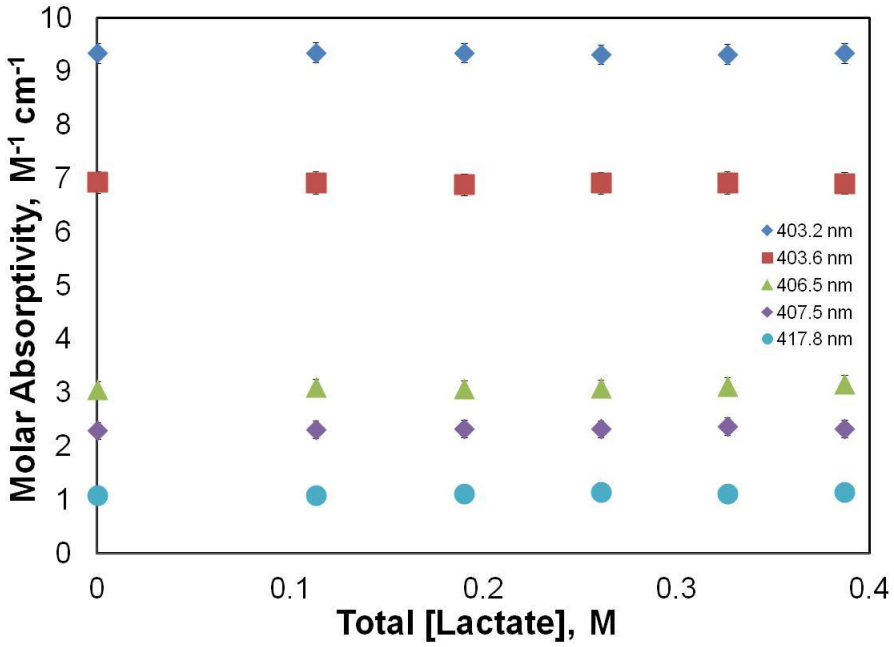

Figure 5.9 Molar absorptivities as a function of total lactate concentration at the most intense $Sm(DTPA)^{2-}$ peak, which is centered around 403 nm, along with those of smaller peaks at 407 nm and 418 nm. Error bars are shown but may not be visible due to the size of the pictograms used to label the data points.

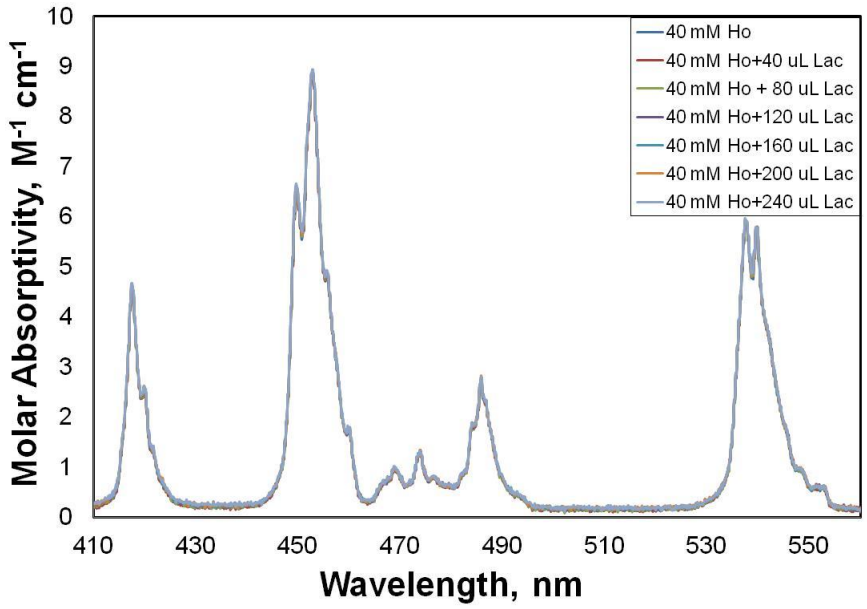

Figure 5.10 Absorption spectra for the titration of 40 mM $Ho(DTPA)^{2-}$ with 2 M lactate. Spectra have been normalized to the total analytical $Ho(DTPA)^{2-}$ concentration for each addition.

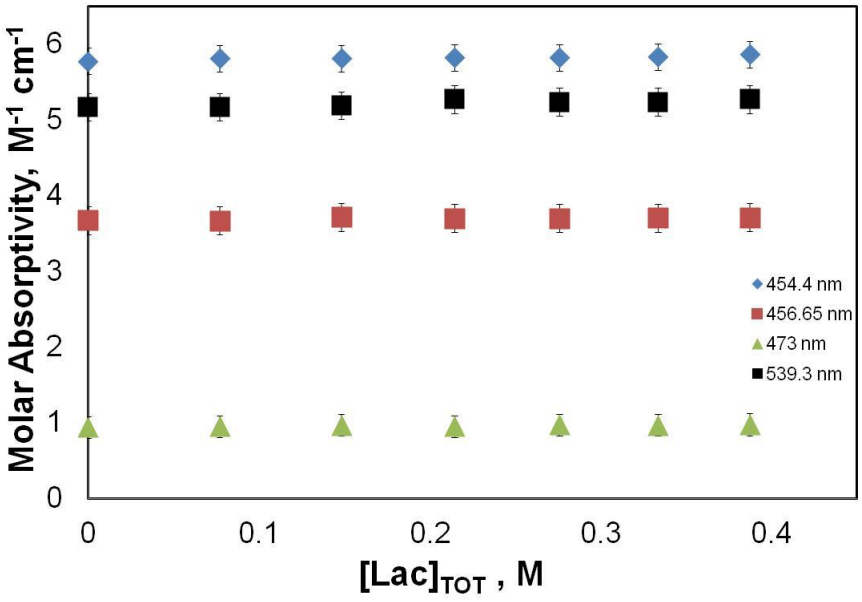

Figure 5.11 Molar absorptivity of $Ho(DTPA)^{2-}$ as a function of total lactate concentration at peak wavelengths. The point at approximately 0.4 M represents a nearly twelve-fold excess of lactate. Error bars are shown but may not be visible due to the size of the pictograms used to label the data points.

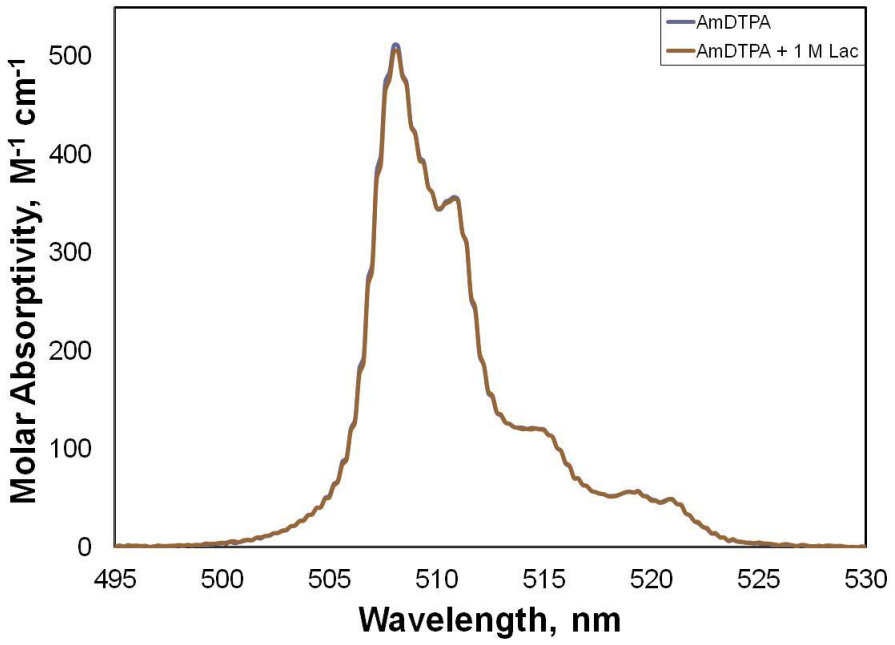

Figure 5.12 Comparison of 0.8 mM $Am(DTPA)^{2-}$ with the same solution containing 1 M total lactate.

Though inner-sphere complexes were not observed via optical spectroscopy, measurements of the heat evolved or absorbed during a titration can also indicate the formation of inner- or outer-sphere complexes. Thus, thermometric titrations with $Nd(DTPA)^{2-}$ and $Eu(DTPA)^{2-}$ were employed to search for evidence of inner- or outer-sphere ternary complex formation. The results from three titrations of 40 mM $Nd(DTPA)^{2-}$ and $Eu(DTPA)^{2-}$ solutions with 2 M lactate are tabulated in Table 5.2. From the table it is evident that, after correction for dilution and protonation reactions, the net measured heat is small and essentially negligible compared to the dilution or even protonation heats.

Table 5.2 Comparison of Thermometric Titration Data for Titrations of $Nd(DTPA)^{2-}$ and $Eu(DTPA)^{2-}$ With Lactate

Cup Solution*	Runs†	Q_{meas}, cal	Q_{dil}, cal	Q_{prot}, cal	Q_{net}, cal‡
40 mM $Nd(DTPA)^{2-}$	3	1.097 ± 0.006	0.999 ± 0.011	0.080 ± 0.001	0.018 ± 0.013
40 mM $Eu(DTPA)^{2-}$ [(a)]	3	1.037 ± 0.009	0.999 ± 0.011	0.043 ± 0.001	-0.005 ± 0.014

*The cup solution contained 24.98 mL 40 mM Ln/50 mM DTPA/10 mM MES/1 M $NaNO_3$ at p_cH = 6.6, which was titrated with 2 M lactate. †Number of replicate titrations. ‡All heats have the sign convention that negative signs refer to heat absorbed and positive signs refer to heat released. Uncertainties are tabulated as the standard error of the mean with 95% confidence. [a]Data also available in reference 92.

Similar studies were conducted with the oxalate (Ox^{2-}) ligand, which is similar in size and denticity to lactate, for comparison with the analogous CDTA and DO3A systems. More importantly, the oxalate ligand is a stronger ligand and therefore would be more likely to form a ternary complex than lactate. Spectrophotometric titrations of 10 mM $Nd(DTPA)^{2-}$, $Sm(DTPA)^{2-}$, $Ho(DTPA)^{2-}$, and $Er(DTPA)^{2-}$ solutions with 69 mM oxalate were conducted similarly to the lactate titrations. The expected equilibrium assuming ternary complex formation occurred was

$$M(DTPA)^{2-} + Ox^{2-} \leftrightarrow M(DTPA)Ox^{4-} \qquad (5.15)$$

Figure 5.13 shows the molar absorptivities as a function of wavelength for the titration of $Nd(DTPA)^{2-}$ with oxalate. The change in the spectra in the 350-450 nm range was actually due to absorption of the oxalate ligand. To verify that no additional ternary complex formation had occurred, the contribution to the total absorbance due to the free oxalate ligand was subtracted from each spectrum using the conservative assumption that none of the oxalate forms a complex with the binary $Ln(DTPA)^{2-}$ complex. As shown in Figures 5.14-5.17, these "oxalate-corrected" spectra were also identical to each other, indicating that ternary complex formation was not observed. The discrepancies in the molar absorptivities in the flat areas are due to small random fluctuations in the baseline in those regions.

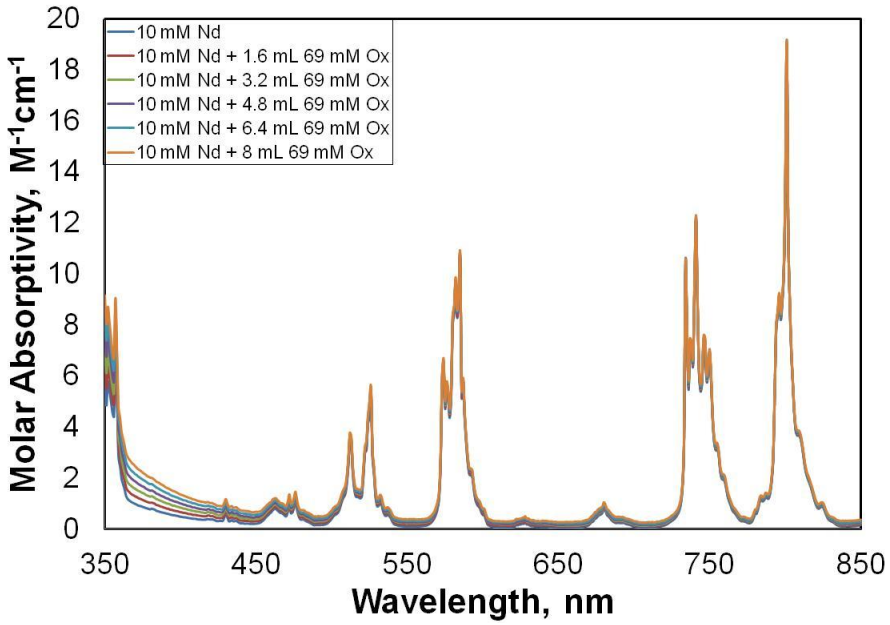

Figure 5.13 Molar absorptivities of $Nd(DTPA)^{2-}$ as a function of wavelength for the titration of 10 mL 10 mM Nd with up to 8 mL 69 mM oxalate.

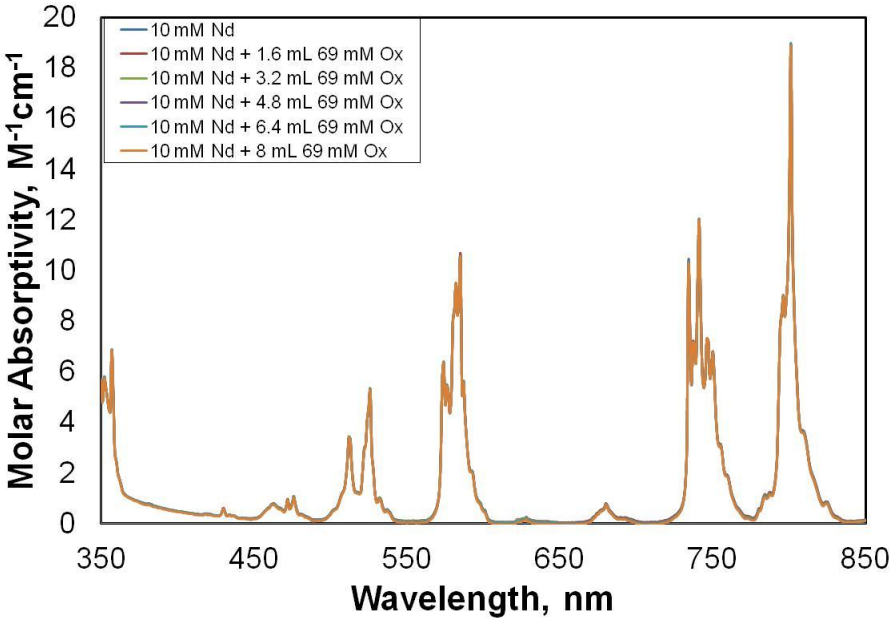

Figure 5.14 Absorption spectra from the titration of 10 mM $Nd(DTPA)^{2-}$ with 69 mM oxalate corrected for free oxalate absorption and normalized to total $Nd(DTPA)^{2-}$ concentrations.

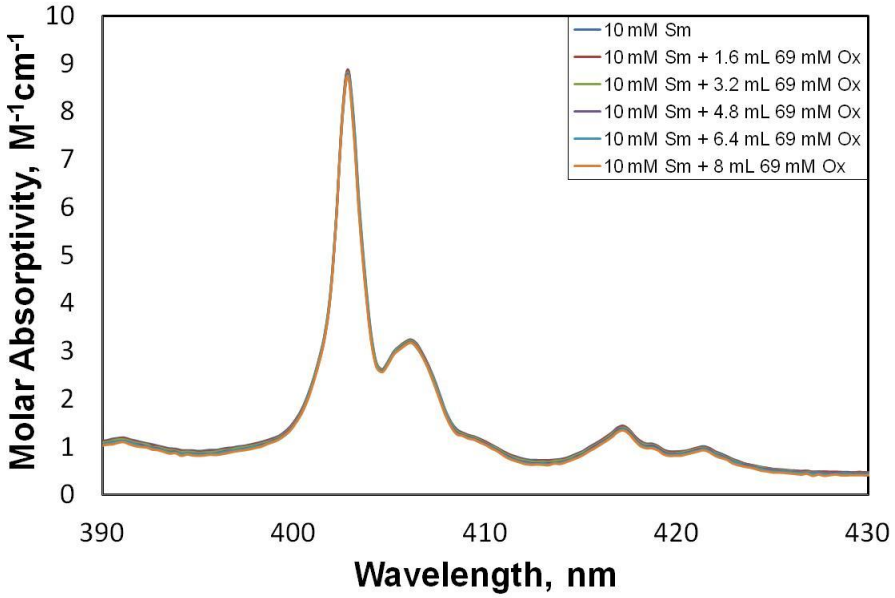

Figure 5.15 Absorption spectra from the titration of 10 mM $Sm(DTPA)^{2-}$ with 69 mM oxalate corrected for free oxalate absorption and normalized to total $Sm(DTPA)^{2-}$ concentrations.

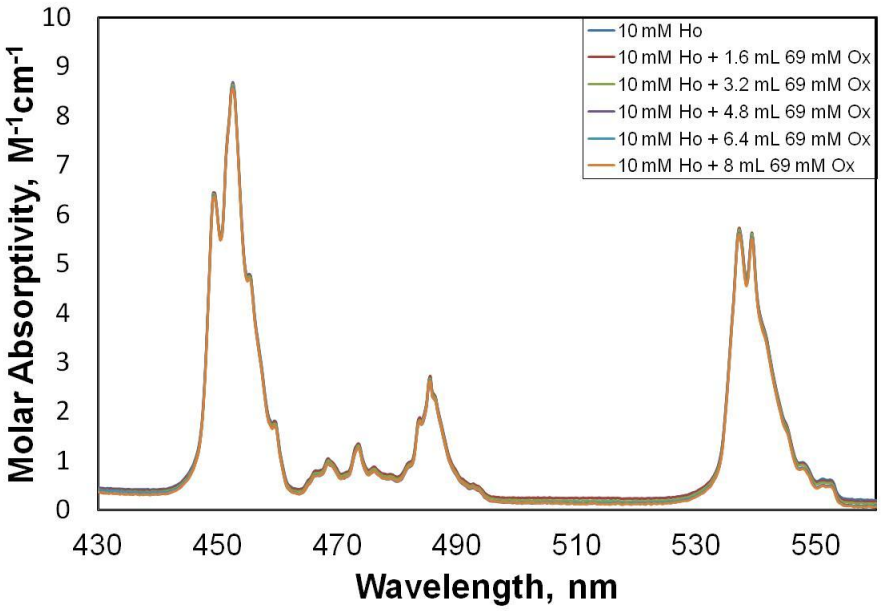

Figure 5.16 Absorption spectra from the titration of 10 mM $Ho(DTPA)^{2-}$ with 69 mM oxalate corrected for free oxalate absorption and normalized to total $Ho(DTPA)^{2-}$ concentrations.

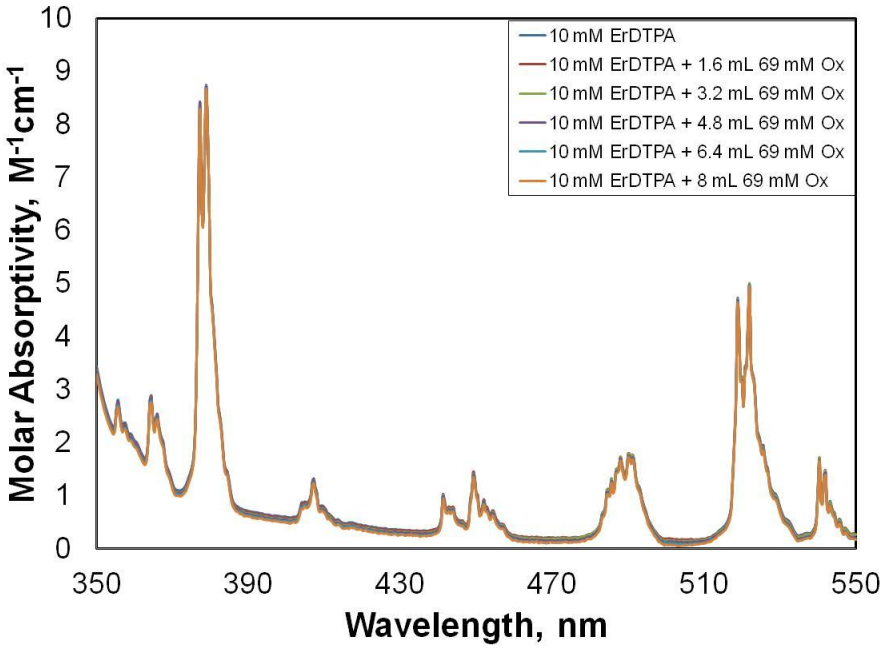

Figure 5.17 Absorption spectra from the titration of 10 mM $Er(DTPA)^{2-}$ with 69 mM oxalate corrected for free oxalate absorption and normalized to total $Er(DTPA)^{2-}$ concentrations and pathlength.

5.4 Thermodynamics of the Ln,Am-CDTA-L System

5.4.1 Ln,Am-CDTA-Oxalate System

Unlike the DTPA system, it was clear that ternary complex formation occurs with the binary CDTA complexes and oxalate. Spectrophotometric titrations of 50 mM CDTA solutions containing 10-20 mM Nd, Sm, Ho, or Er with the oxalate ligand provided visual evidence of ternary complex formation. In particular, changes in the hypersensitive peaks of neodymium, holmium, and erbium provided the most compelling evidence of ternary complexation. Figures 5.18-5.25 show how the molar absorptivities of $Nd(CDTA)^-$, $Sm(CDTA)^-$, $Ho(CDTA)^-$, and $Er(CDTA)^-$ changed as 73-75 mM oxalate was titrated into the solutions. Neodymium in particular has many narrow, relatively intense peaks – two of which are hypersensitive - in the visible region. Thus, two sets of neodymium spectra were collected with 0.2-0.3 nm bandwidths to monitor changes in the absorption spectra over the region 500-885 nm. For each set of Nd spectra, 550 data points were collected that were subsequently used for refinements. Similarly, the Sm, Ho, and Er spectra comprised at least 500 data points with 10-12 spectra collected per titration. It is noteworthy that the intensity and morphology of the major peak in the spectra for $Sm(CDTA)^-$, which has no hypersensitive peaks in the visible region, changes very little throughout the course of a typical titration. This is in stark contrast to $Nd(CDTA)^-$, whose hypersensitive peaks change greatly.

The spectra of $Ho(CDTA)^-$ and $Er(CDTA)^-$ provide the best illustrations of the sensitivity of hypersensitive peaks to the formation of ternary complexes. For these two complexes, the absorbances at their hypersensitive peaks change rapidly whereas the non-hypersensitive peaks show almost no difference in appearance or intensity during the titration.

To more clearly show the changes in the absorption spectra, the molar absorptivities of the same $Ln(CDTA)^-$ solutions as a function of oxalate concentration for selected peaks are also shown. Unlike the case with the LnDTPA-Ox spectra, noticeable changes in the titration spectra were observed when the total oxalate concentration was as low as 2 mM. When comparing the molar absorptivities at major peaks as a function of oxalate concentration, it is evident that the changes in the hypersensitive peaks (e.g., 379 nm for erbium) are much larger than those at non-hypersensitive peaks (e.g., 487 nm for erbium) as expected since these peaks are sensitive to changes in the environment around the metal cation.

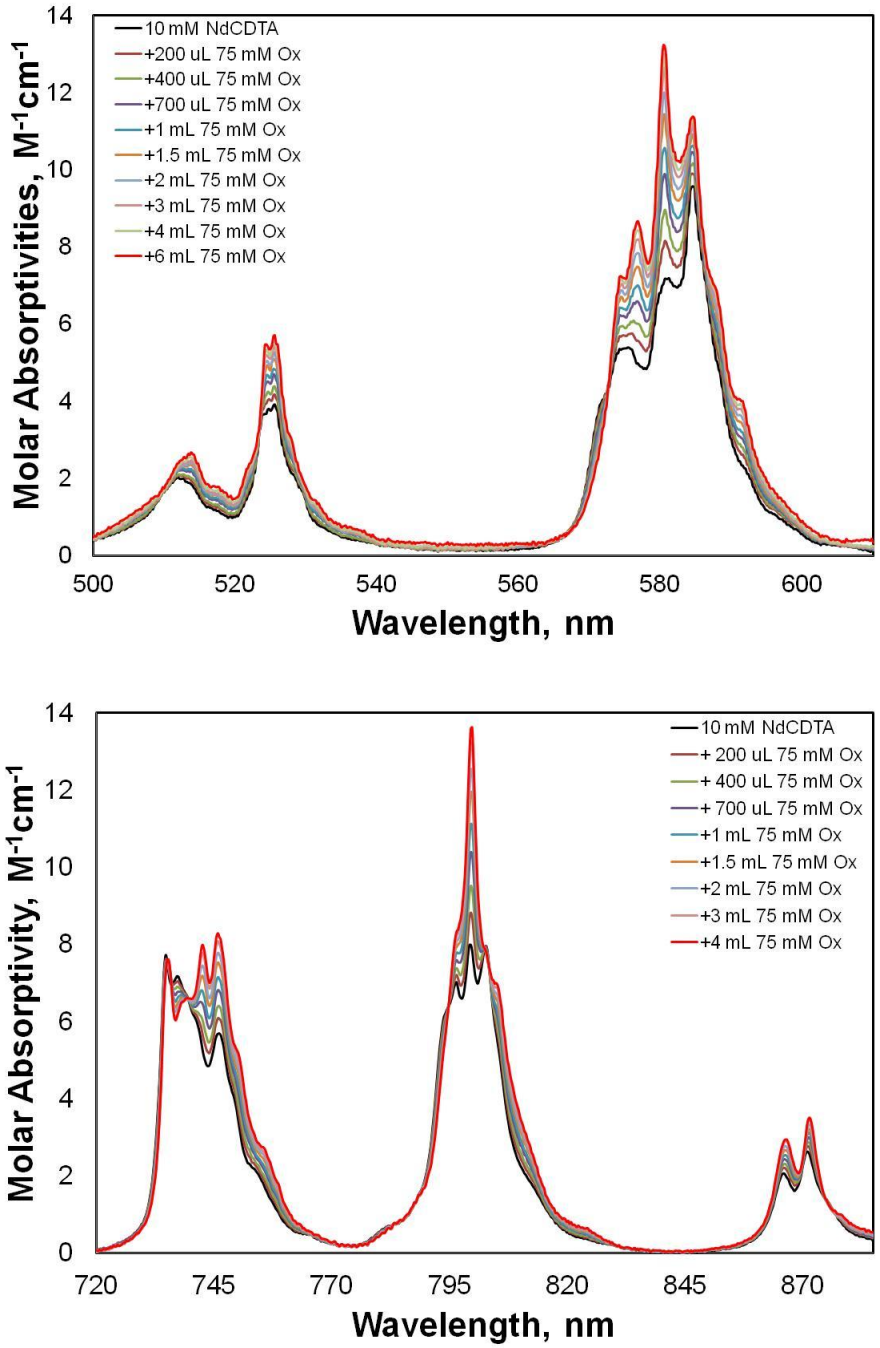

Figure 5.18 Molar absorptivities of $Nd(CDTA)^-$ as a function of wavelength. The peaks centered at 580 nm and 745 nm are the hypersensitive peaks.

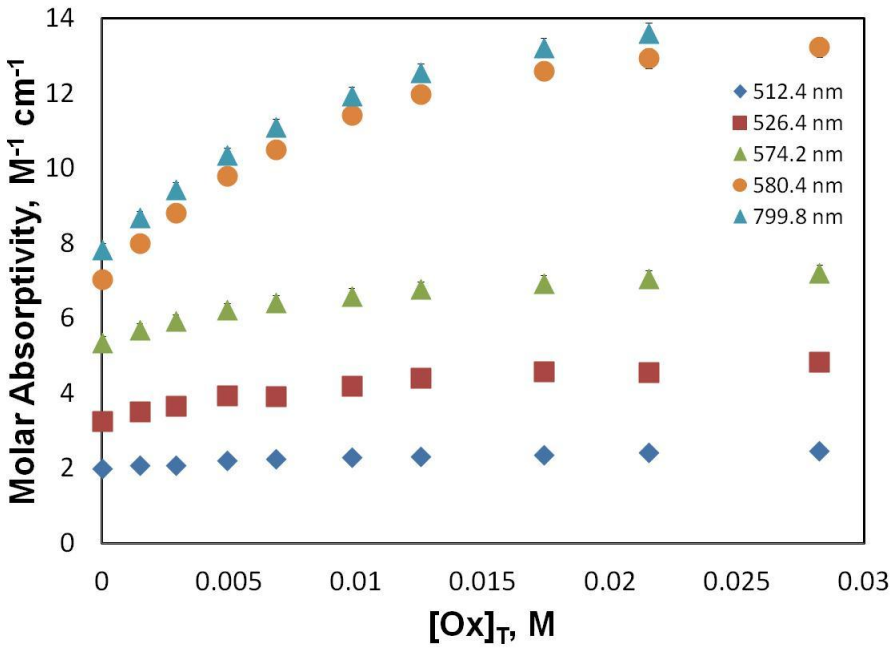

Figure 5.19 Molar absorptivities of $Nd(CDTA)^-$ as a total oxalate concentration ratio at selected wavelengths. As the hypersensitive peaks are most sensitive to the metal coordination environment, these wavelengths were chosen for display. Major peaks that are not hypersensitive are shown for comparison.

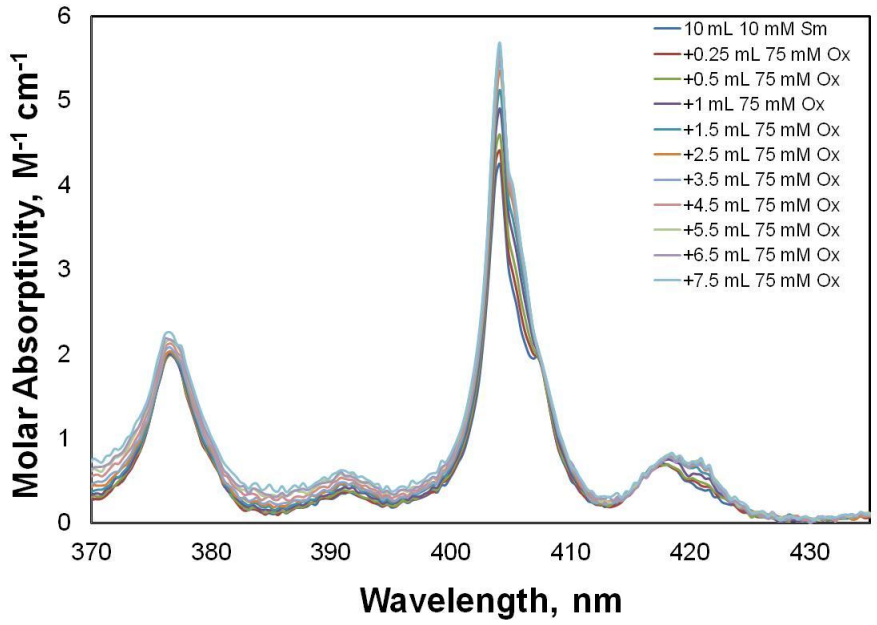

Figure 5.20 Molar absorptivities of $Sm(CDTA)^-$ as a function of wavelength. Samarium has no hypersensitive peaks in the visible region. The peak shown is the most intense peak in the visible region for $Sm(CDTA)^-$.

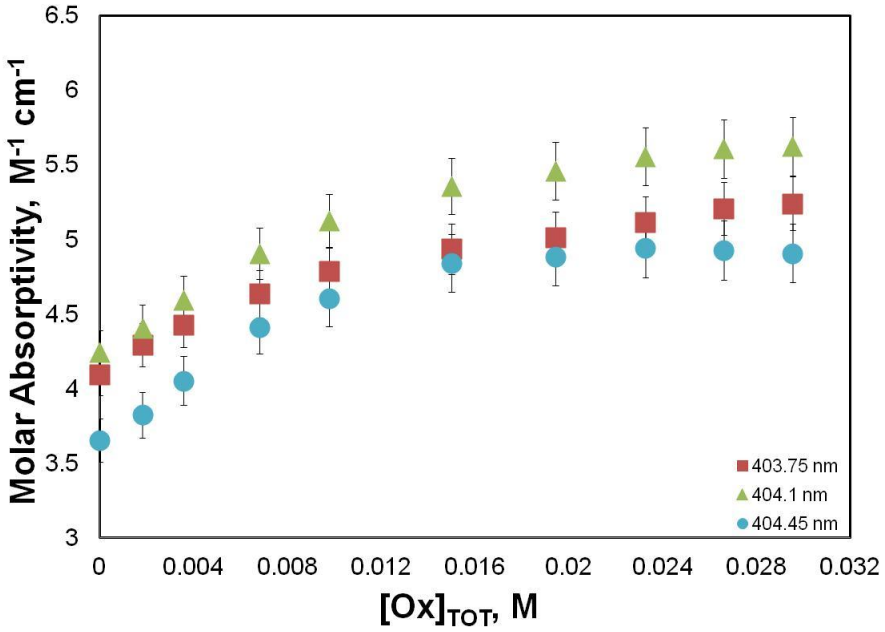

Figure 5.21 Molar absorptivities of $Sm(CDTA)^-$ as a function of total oxalate concentration at selected wavelengths at or near the most intense peak which is centered at 403 nm. Small, but noticeable changes are evident.

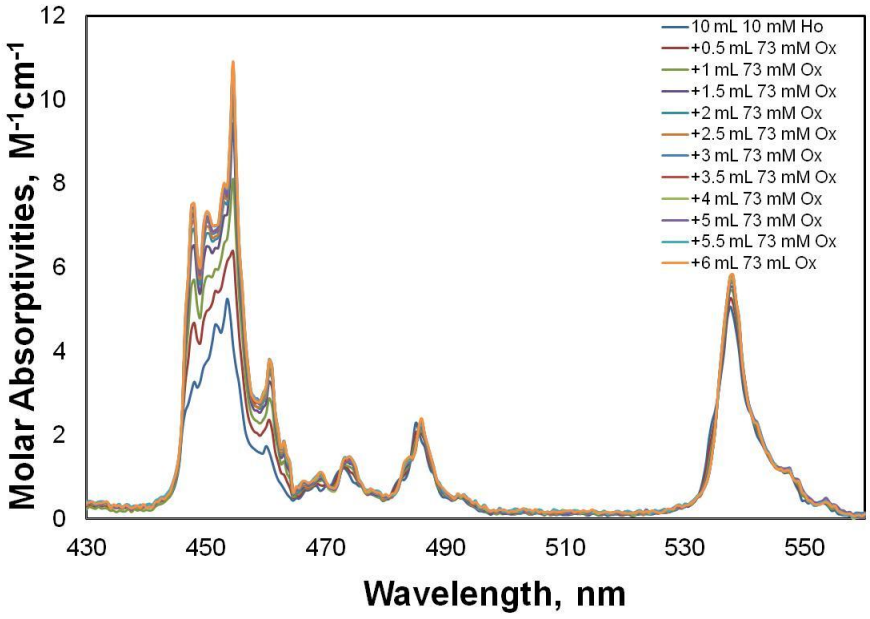

Figure 5.22 Molar absorptivities of $Ho(CDTA)^-$ as a function of wavelength. The hypersensitive peak lies in the range 440-465 nm and shows the most noticeable changes in the morphology of the spectrum. Note that the peak at 538 nm, which is not hypersensitive, shows little change in intensity or morphology.

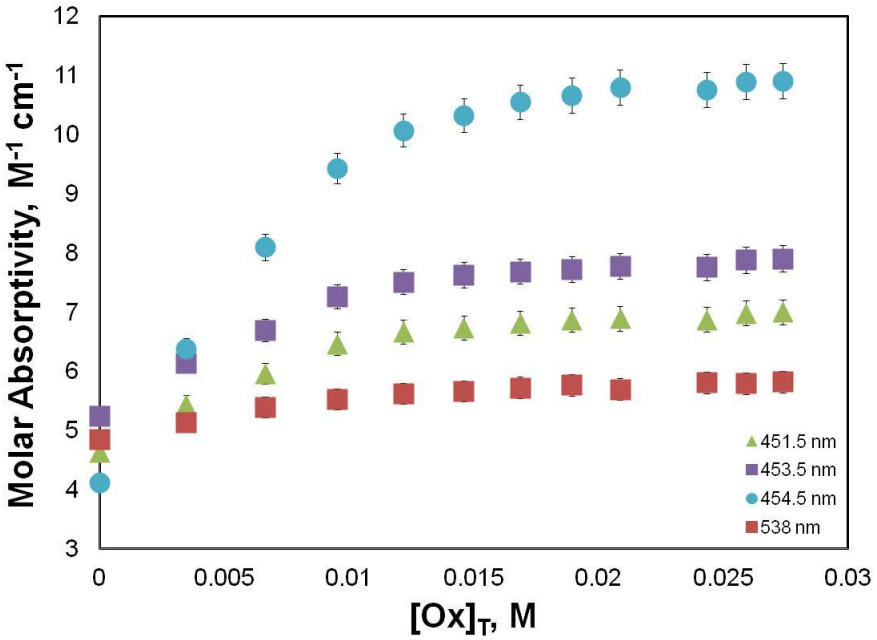

Figure 5.23 Molar absorptivities of $Ho(CDTA)^-$ as a function of total oxalate concentration. The molar absorptivities at the hypersensitive peak centered at 454 nm doubles over the range of oxalate concentrations used.

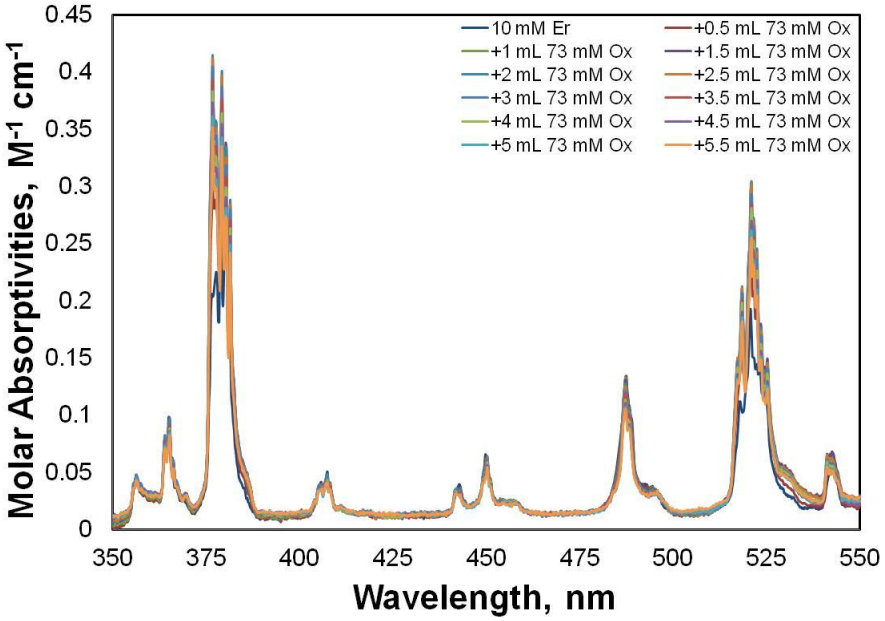

Figure 5.24 Absorption spectra of $Er(CDTA)^-$ normalized to total $Er(CDTA)^-$ concentration and pathlength. Each spectrum shown represents a cumulative addition of 73 mM oxalate as indicated in the legend. Two hypersensitive peaks are noticeable: One centered around 379 nm and the other at 521 nm.

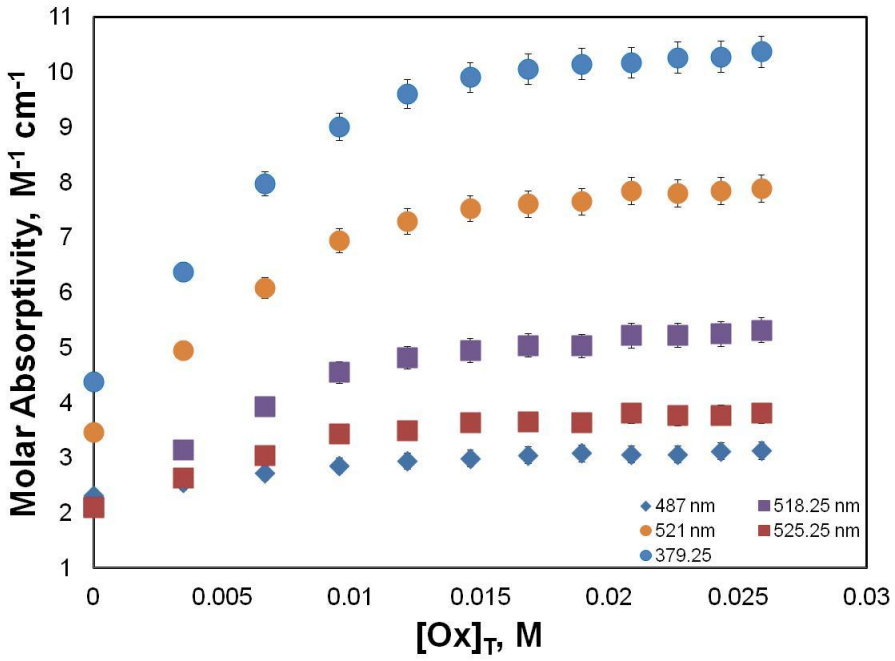

Figure 5.25 Molar absorptivities of $Er(CDTA)^-$ as a function of total oxalate concentration. The molar absorptivities at 379 nm and 521 nm are far more sensitive to complexation than the peak at 487 nm as indicated by the relatively flat slope of the 487 nm plot throughout the titration.

Because of the significant change in the measured absorbances due to complexation, SQUAD was able to calculate the equilibrium constant for the formation of $Ln(CDTA)(Ox)^{3-}$ complexes easily. Table 5.3 lists the calculated equilibrium constants for neodymium, samarium, holmium, and erbium. Although the oxalate ligand has significant absorbance, it becomes insignificant above approximately 370 nm under the experimental conditions used. Thus, there was no need to include the spectrum of the ligand in SQUAD input files except for samarium. Two chemical equilibrium models were used in SQUAD input files: one in which the equilibrium model consisted of Equations 5.7 and 5.8 and the other in which Equation 5.7 alone was used. Attempts to calculate an equilibrium constant for $Ln(CDTA)(Ox)_2^{5-}$ were either unsuccessful (i.e., no convergence) or led to a very poor fit. On the other hand, convergence was achieved using Equation 5.7 alone. Thus, the equilibrium constants listed in Table 5.3 apply to $Ln(CDTA)(Ox)^{3-}$ complexes. For the Nd and Sm titrations, the averages of the calculated equilibrium constants are tabulated in Table 5.4; for the Ho and Er datasets, the calculated equilibrium constants from simultaneous refinements of the Ho and Er datasets are given.

The absorbances based on the equilibrium constant calculated by SQUAD are compared to the measured absorbances for a representative NdCDTA-Oxalate titration in Figure 5.26. The error in the fit for the calculated equilibrium constant from this individual dataset, ±0.005, indicates that the calculated equilibrium constant for that set, 2.518, fit the data very well.

Table 5.3 Calculated Equilibrium Constants* for the Formation of $Ln(CDTA)(Ox)^{3-}$ Complexes

$Ln(CDTA)(Ox)^{3-}$	Number of Datasets	Log K_{111}‡
$Nd(CDTA)(Ox)^{3-}$	3	2.54 ± 0.03
$Sm(CDTA)(Ox)^{3-}$	3	2.67 ± 0.04
$Tb(CDTA)(Ox)^{3-}$	4	2.76 ± 0.02
$Ho(CDTA)(Ox)^{3-}$	2†	2.92 ± 0.03
$Er(CDTA)(Ox)^{3-}$	2†	2.93 ± 0.01
$Am(CDTA)(Ox)^{3-}$	3	2.78 ± 0.13

*Based on the equilibrium $Ln(CDTA)^{-} + Ox^{2-} \leftrightarrow Ln(CDTA)(Ox)^{3-}$.
†The datasets were refined together in these cases.
‡The uncertainties in the stability constants are tabulated as the standard error of the mean with 95% confidence.

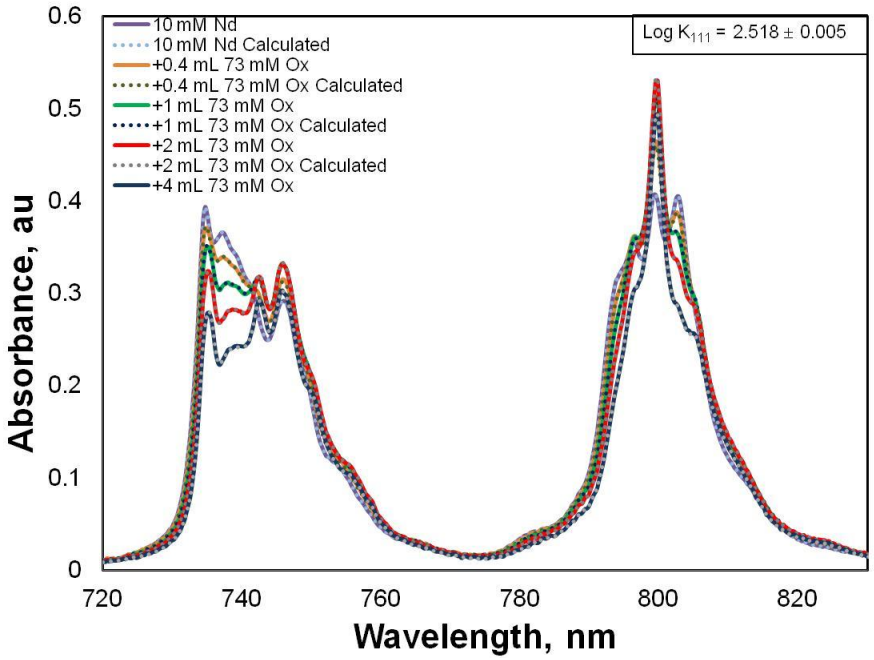

Figure 5.26 Comparison of measured spectra of $Nd(CDTA)^{-}$ and calculated spectra obtained by SQUAD. Fewer spectra and a smaller wavelength range are shown than was used in the titration for clarity.

It is entirely possible that a $Ln(CDTA)(Ox)_2^{5-}$ complex can form but simply *was not observed* in solution under the conditions studied. Therefore, "high-oxalate-containing" solutions of $Ln(CDTA)^-$ were prepared to increase the concentration of potential $Ln(CDTA)(Ox)_2^{5-}$ complexes that could be observed via UV-Visible spectroscopy. Based on previous experiments, the maximum solubility of oxalate under the experimental conditions used is about 76 mM. If a second oxalate ligand were to bind to the $Ln(CDTA)(Ox)^{3-}$ complex, the molar absorptivities of $Ln(CDTA)^-$ would likely be different at high oxalate concentrations where $Ln(CDTA)(Ox)_2^{5-}$ would dominate than those measured at lower oxalate concentrations where the $Ln(CDTA)(Ox)^{3-}$ complex dominates. Figures 5.27-5.31 show a comparison of the molar absorptivities of $Ln(CDTA)^-$ at the maximum concentration attained during the above titrations with those of 10 mM $Ln(CDTA)^-$ with approximately 69-70 mM oxalate present. Clearly, the spectra show that the $Ln(CDTA)(Ox)_2^{5-}$ complexes are not observed even with the maximum total oxalate concentration possible under the experimental conditions used, thereby validating the inability of SQUAD to calculate stability constants for any higher order complexes.

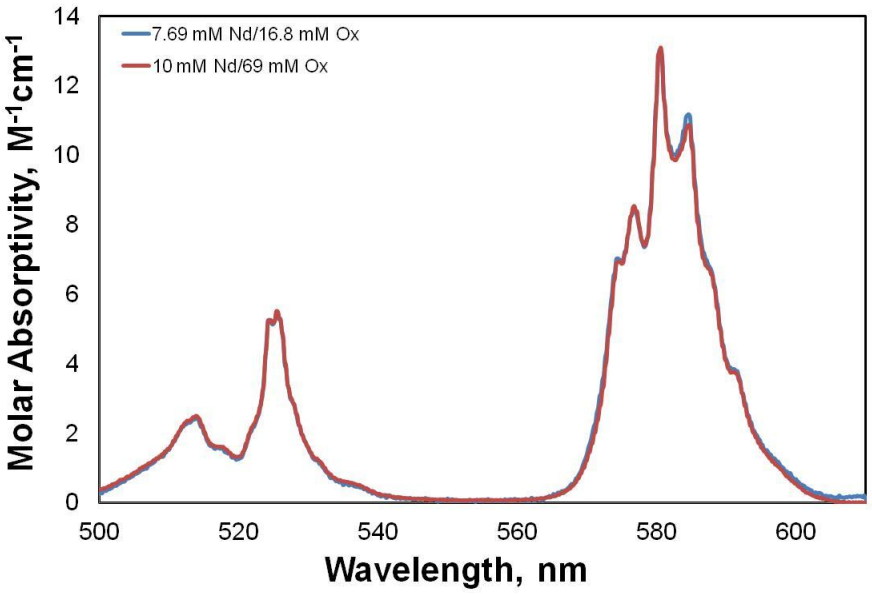

Figure 5.27 Comparison of the calculated molar absorptivities of a "low oxalate"-containing solution of $Nd(CDTA)^-$ with those of a "high-oxalate"-containing solution. Small discrepancies in the molar absorptivities are due to differences in baselines as the spectra were taken on different days.

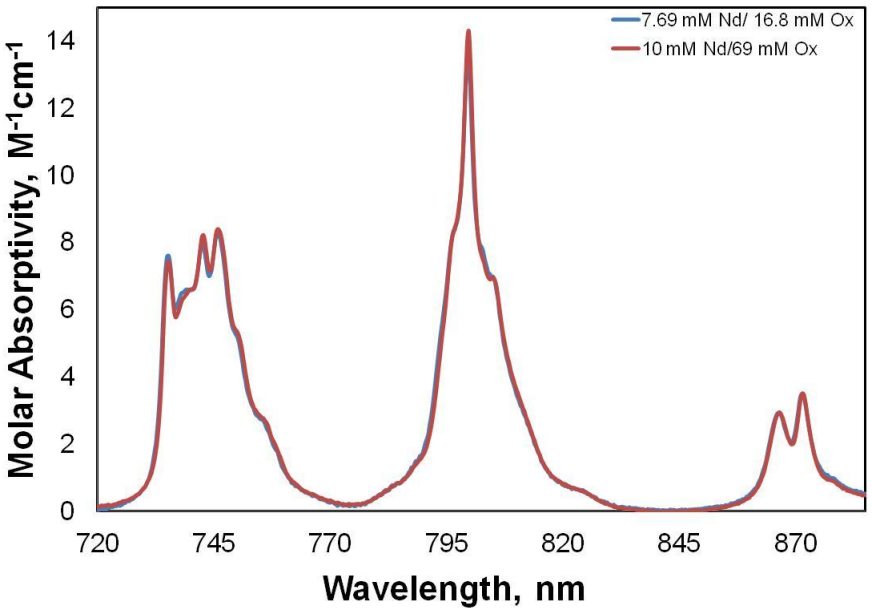

Figure 5.28 Comparison of the calculated molar absorptivities of a "low oxalate"-containing solution of $Nd(CDTA)^-$ with those of a "high-oxalate"-containing solution. This is region II of the $Nd(CDTA)^-$ spectrum.

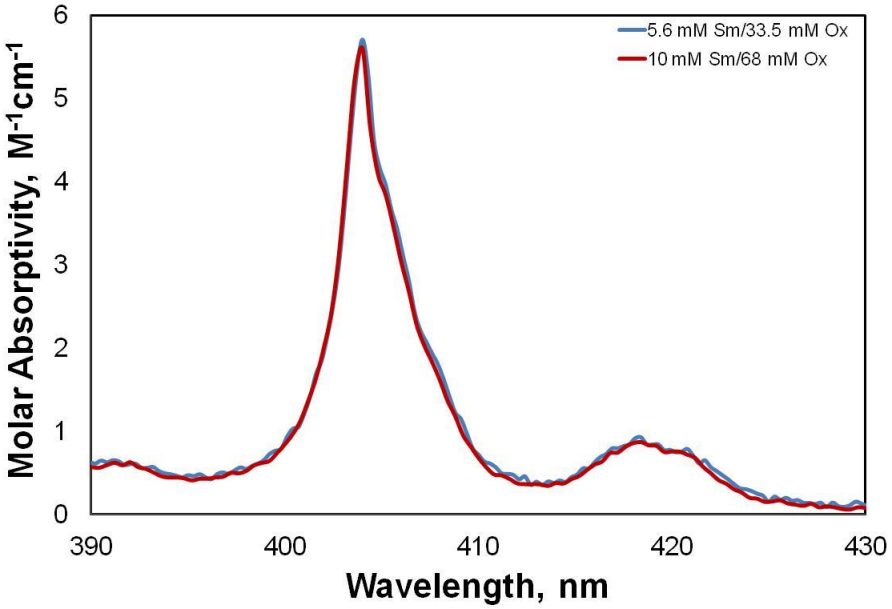

Figure 5.29 Comparison of the calculated molar absorptivities of a "low oxalate"-containing solution of $Sm(CDTA)^-$ with those of a "high-oxalate"-containing solution. Small discrepancies in the molar absorptivities are due to differences in baselines as the spectra were taken on different days. No corrections for free oxalate were needed in this region.

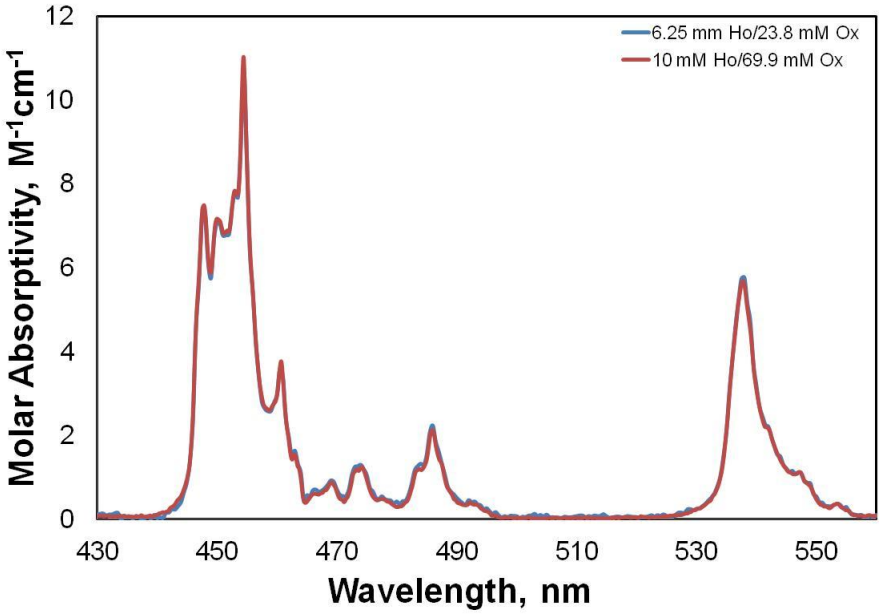

Figure 5.30 Comparison of the calculated molar absorptivities of a "low oxalate"-containing solution of $Ho(CDTA)^-$ with those of a "high-oxalate"-containing solution.

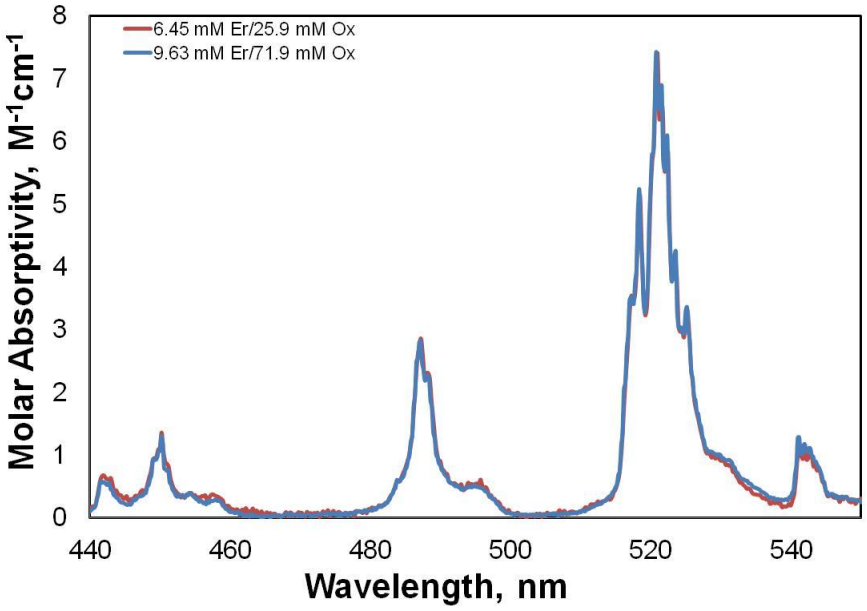

Figure 5.31 Comparison of the calculated molar absorptivities of a "low oxalate"-containing solution of $Er(CDTA)^-$ with those of a "high-oxalate"-containing solution.

The element terbium has one of the most intense lanthanide luminescence spectra after europium and is high enough to make it a good candidate for fluorescence spectroscopy. It is also approximately half-way between samarium and holmium in the lanthanides series. Thus, the determination of the equilibrium constant of the $Tb(CDTA)(Ox)^{3-}$ complex can help predict overall trends in $Ln(CDTA)(Ox)^{3-}$ complexes across the lanthanide series. The equilibrium constant for the $Tb(CDTA)(Ox)^{3-}$ complex was calculated from fluorescence measurements using two different methods.

In the first method, the measured average number of water molecules bound to $Tb(CDTA)^-$ in oxalate-containing $Tb(CDTA)^-$ solutions was used to calculate the equilibrium constant. Prior to initiating fluorimetric titrations of $Tb(CDTA)^-$ with oxalate, the lifetime and number of water molecules bound to $Tb(CDTA)^-$ were measured. Assuming that Tb^{3+} exists in solution as the octaaaquo cation[94] and that each donor atom of the ligand displaces one water molecule, coordination of the hexadentate CDTA ligand to Tb^{3+} should result in a complex with two remaining water molecules. To confirm this, emission spectra of 10 mM $Tb(CDTA)^-$ were taken in the wavelength range 542-549 nm in 1 nm increments after delay times ranging from zero to five milliseconds. For each spectrum, the measured intensities are related to the observed lifetime, τ_{obs}, by

$$I_n = I_{n0}\exp\left(-t/\tau_{obs}\right) \tag{5.16}$$

where *t* is the delay time in milliseconds, τ_{obs} is the lifetime, I_{n0} is the fluorescence intensity of the *n*th solution at zero delay time, and I_n is the measured intensity after a delay time *t*. Plotting $\ln(I_n/I_{n0})$ as a function of delay time gives a straight line whose slope is the decay constant in inverse milliseconds; taking the reciprocal of the decay constant then gives the lifetime.

The lifetime of $Tb(CDTA)^-$ is related to the number of bound water molecules by the equation

$$N_{H_2O} = (k_{H_2O} - k_{D_2O})A_{Ln} \tag{5.17}$$

where N_{H_2O} is the measured average number of residual water molecules bound to $Tb(CDTA)^-$ based on the observed lifetime values and $k_{H_2O} = \tau_{H_2O}^{-1} = \tau_{obs}^{-1}$. Equation 17 and the values of k_{D2O} and A_{Tb}, which are 0.30 and 4.2, respectively, were empirically determined by Horrocks and Sudnick[95]. Using Equation 5.16, the number of water molecules bound to the $Tb(CDTA)^-$ complex is 2.07 ± 0.5 water molecules, which is expected for octacoordinate terbium complexed with a hexadentate ligand.

In a typical fluorimetric titration, after each addition of 75 mM oxalate to the 10 mM $Tb(CDTA)^-$ solution, sets of spectra analogous to the ones described above for the initial $Tb(CDTA)^-$ solution were taken. The lifetimes measured for each solution were used to calculate the average number of water molecules, $N_{H_2O}^{obs}$, using Equation 5.17. However, since the added oxalate presumably complexes $Tb(CDTA)^-$, the measured average number of water

molecules is actually a weighted average of the number of water molecules bound to $Tb(CDTA)^-$ and $Tb(CDTA)(Ox)^{3-}$. Thus, Equation 5.17 can also be written as

$$N_{H_2O}^{calc} = N_{TbCDTA}\frac{[Tb(CDTA)^-]}{C_{Tot}^{Tb}} + N_{TbCDTA(Ox)}\frac{[Tb(CDTA)(Ox)^{3-}]}{C_{Tot}^{Tb}} \quad (5.18)$$

where N_{TbCDTA} and $N_{TbCDTAOx}$ are the numbers of waters coordinated to $Tb(CDTA)^-$ and $Tb(CDTA)(Ox)^{3-}$, respectively, and C_{Tot}^{Tb} is the total concentration of terbium in a given solution. The concentrations of the $Tb(CDTA)^-$ and $Tb(CDTA)(Ox)^{3-}$ species are related to the ternary complex equilibrium constant, K_{111}; thus, these values can be calculated easily from Equations 5.1, 5.4, and 5.5. The solver function in Excel was used to minimize the sum of the squared residuals between the observed and calculated number of water molecules by varying $N_{TbCDTAOx}$ and K_{111}:

$$U = \sum_{n=1}^{N}\left(N_{H_2O}^{obs} - N_{H_2O}^{calc}\right)_n^2 \quad (5.19)$$

N_{TbCDTA} is known from the initial measurements discussed earlier. For each titration, eighteen datapoints corresponding to successive additions of 75 mM oxalate were collected and used for fitting. Figure 5.32 shows a plot comparing the measured and calculated average numbers of water molecules as a function of total oxalate concentration for a representative titration.

In the second method, the fluorescence intensities at t=0 at wavelengths 543 and 544 nm were used to calculate the equilibrium constant. The fluorescence intensities are related to the molar absorptivities of emitting species, the fluorescence yield, pathlength, and concentration by Beer's Law as with absorption spectroscopy. Thus, for the $Tb(CDTA)^-/Tb(CDTA)(Ox)^{3-}$ solutions, the intensity is described by the equation

$$I_n^{calc} = \varepsilon_1[Tb(CDTA)^-] + \varepsilon_2[Tb(CDTA)(Ox)^{3-}] \quad (5.20)$$

which is related to the equilibrium constant by

$$I_n^{calc} = \varepsilon_1[Tb(CDTA)^-] + \varepsilon_2[Tb(CDTA)^-][Ox^{2-}]K_{111} \quad (5.21)$$

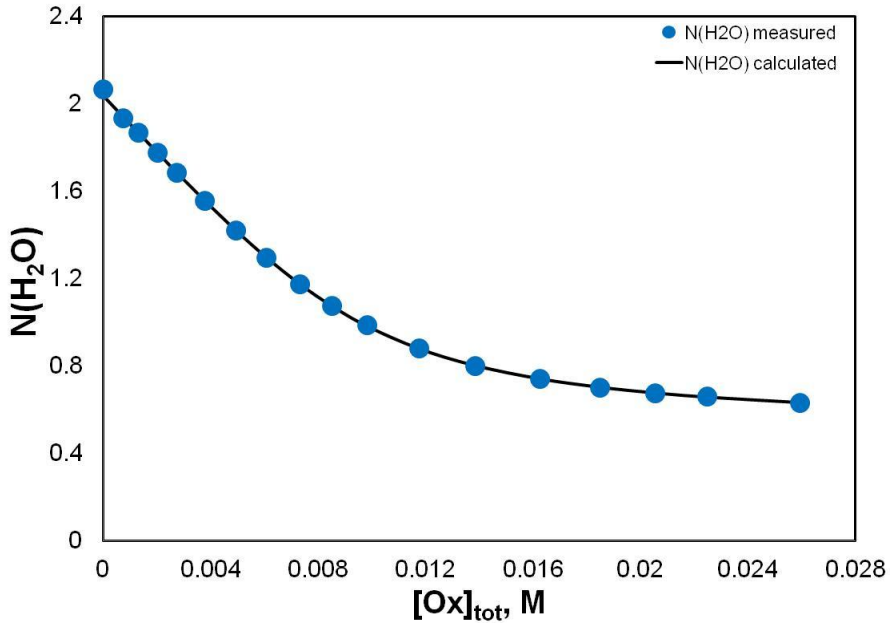

Figure 5.32 Comparison of the measured number of water molecules based on lifetime measurements with the calculated average number of water molecules obtained by fitting the number of water molecules of $Tb(CDTA)(Ox)^{3-}$ to the data. Titration conditions: 2 mL 10 mM $Tb(CDTA)^{-}$ titrated with 75 mM oxalate.

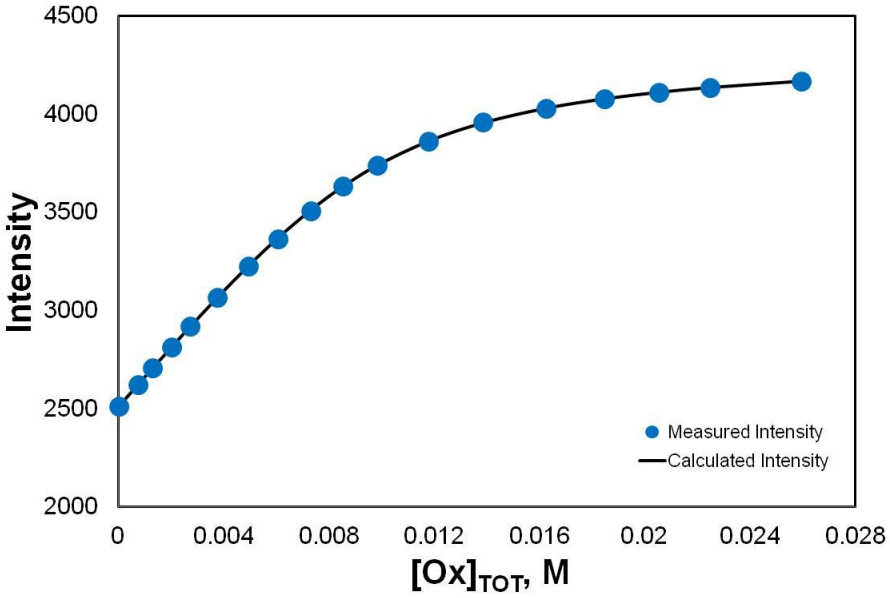

Figure 5.33 Comparison of measured intensities with calculated intensities obtained by fitting the molar absorptivity of $Tb(CDTA)(Ox)^{3-}$ at 544nm. (The molar absorptivity of $Tb(CDTA)^{-}$ was known at the outset.)

where I_n^{calc} is the calculated fluorescence intensities and the constants ε_1 and ε_2 are the molar fluorescence intensities of $Tb(CDTA)^-$ and $Tb(CDTA)(Ox)^{3-}$. In order to calculate the equilibrium constant, the sum of the squared residuals between the measured and calculated fluorescence intensities was minimized by varying ε_2 and K_{111}. The molar fluorescence intensity of $Tb(CDTA)^-$ was determined previously from the $Tb(CDTA)^-$ solution. Datasets from this method contained 18-19 datapoints for each wavelength monitored; a representative dataset fitted with K_{111} is shown in Figure 5.33. The equilibrium constants and the uncertainties in the fitted parameters for both methods were estimated using the jackknife error method. The calculated equilibrium constant obtained from the average of four stability constants was 2.76 ± 0.02, fitting nicely between Sm and Ho in the $Ln(CDTA)(Ox)^{3-}$ series.

The equilibrium constant and enthalpy of complexation for the $Am(CDTA)(Ox)^{3-}$ complex were determined simultaneously from calorimetric titrations using an isothermal titration calorimeter. Three titrations of 0.8 mL 1.14 mM $Am(CDTA)^-$ with 85 uL 76 mM oxalate, each comprising a total of 18 datapoints, were used to determine these two values. A spectrum of the initial $Am(CDTA)^-$ solution is compared with the solution after addition of 85 uL 76 mM oxalate in Figure 5.34 below. Similar to the titrations with $Ln(CDTA)^-$, a noticeable changes in the molar absorptivities were observed, indicating that ternary complex formation also occurs with the $Am(CDTA)^-$ complex.

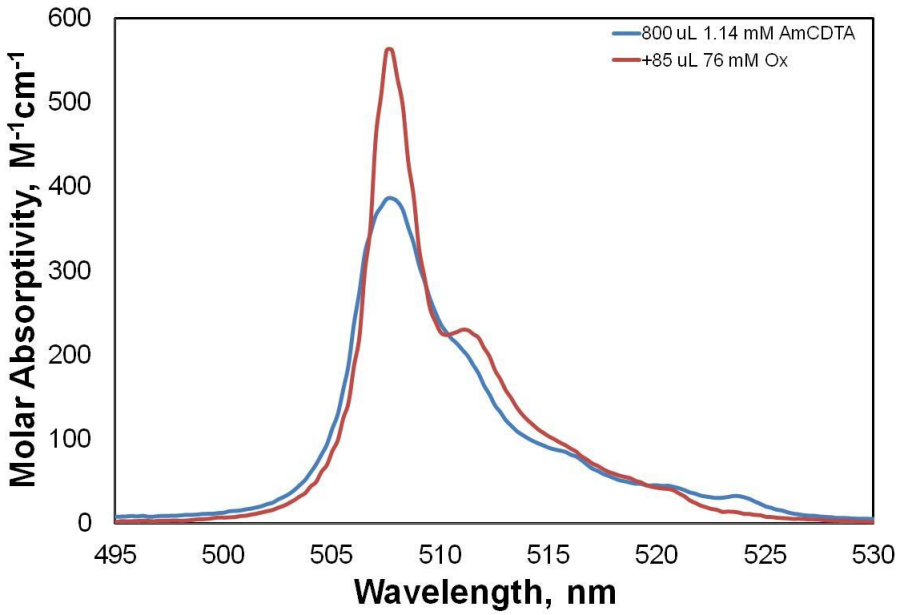

Figure 5.34 Comparison of $AmCDTA^-$ spectrum before and after addition of 85 uL 76 mM oxalate.

The equilibrium constants and enthalpy of complexation were determined simultaneously by developing a relationship among the equilibrium constant, calculated heat, and the molar enthalpy of complexation. Using the mass balance equations, known analytical concentrations, expected equilibria, and pK_a's, a quadratic equation (Equation 5.22) was derived to calculate the concentration of the $Am(CDTA)(Ox)^{3-}$ complex after each addition:

$$-K_{111}\left[Am(CDTA)(Ox)^{3-}\right]^2+\left(R+K_{111}(C_{Am}+C_{Ox})\right)\left[Am(CDTA)(Ox)^{3-}\right]-K_{111}C_{Am}C_{Ox}=0 \quad (5.22)$$

where $R = 1 + \frac{[H^+]}{K_{a1}} + \frac{[H^+]^2}{K_{a1}K_{a2}}$, C_{Am} and C_{Ox} are the respective total concentrations of $Am(CDTA)^-$ and oxalate, and the constants K_{an} are the acid dissociation constants for the dissociation of the *n*th proton from H_2Ox.

For each titration, the net heat evolved after each addition of a calorimetric titration was corrected for dilution. Since the p_cH does not change significantly (< 0.01 units) during a titration, the contribution to the total heat evolved due to protonation reactions was considered to be negligible. The calculated concentration of $Am(CDTA)(Ox)^{3-}$ was then converted to the cumulative number of moles formed and, with the approximation that the dilution-corrected measured heat was due entirely to the formation of the ternary complex, the calculated cumulative heats were determined using Equation 5.13 using a reasonable initial guess for ΔH_{111}. The Solver application in Excel was used to fit K_{111} and ΔH_{111} to Equations 5.13 and 5.22 by minimizing the sum of the squared residuals between the measured and calculated heats. A representative dataset is shown in Figure 5.35 below. The equilibrium constant based on the simultaneous refinement of three datasets is 2.78 ± 0.13 with a corresponding enthalpy of complexation of -8.46 ± 0.84 kJ/mol. The uncertainties in the parameters were determined using the jackknife error estimation method.

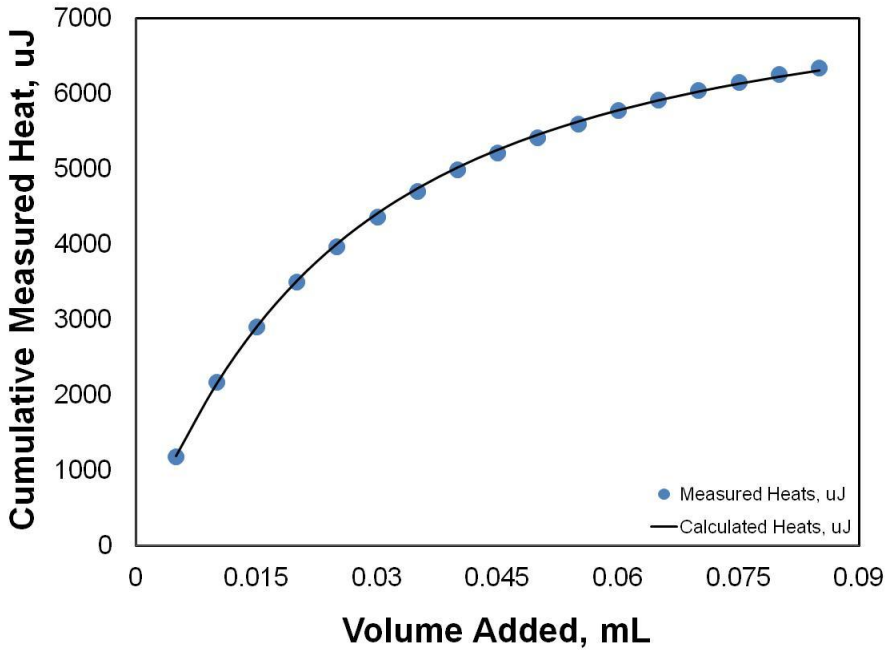

Figure 5.35 Comparison of measured and calculated heats generating for a representative titration of 800 µL 1.14 mM $Am(CDTA)^-$ with 85 µL 76 mM oxalate.

Calorimetric titration data and calculated enthalpies of complexation are shown in Tables 5.4 and 5.5. Unlike the case with the DTPA system, a majority of the measured heat was due to complexation reactions. At least three replicate titrations were conducted for each $Ln(CDTA)^-$ system studied and, as the uncertainties indicate, the measured heats were very reproducible. All titrations were conducted near $p_cH=6$ where more than 99% of the oxalate ligand exists in the Ox^{2-} form. Since the p_cH values of the cup solution changed less than 0.01 p_cH units during a titration, contributions to protonation heats were nearly negligible. Most of the uncertainty in the overall error was due to the uncertainty in the dilution heats, which were clustered in a group near 0 mcal and one at -35 mcal. Because neither group of dilution heats could be ruled out as erroneous, the average of all the dilution heats was used.

Table 5.4 Tabulation of Calorimetric Titration Data for Titration of $Ln(CDTA)^-$ with Ox^{2-}

$Ln(CDTA)^-$	Runs[a]	$[Ln(CDTA)^-]/M$[b]	$[Ox]/M$[b]	p_cH_{final}	Q_{meas} / cal	Q_{dil} / cal	Q_{prot} / cal	Q_{corr} / cal
$Nd(CDTA)^-$	4	0.0100	0.0733	6.003	0.188 ± 0.004	-0.017 ± 0.018	0.003 ± 0.001	0.202 ± 0.018
$Sm(CDTA)^-$	3	0.0100	0.0733	6.034	0.178 ± 0.001	-0.017 ± 0.018	0.001 ± 0.001	0.194 ± 0.018
$Tb(CDTA)^-$	4	0.0100	0.0753	6.003	0.294 ± 0.008	-0.017 ± 0.018	0.002 ± 0.002	0.312 ± 0.020
$Ho(CDTA)^-$	4	0.0101	0.0733	5.991	0.262 ± 0.008	-0.017 ± 0.018	0.001 ± 0.001	0.278 ± 0.020
$Er(CDTA)^-$	4	0.0100	0.0733	5.991	0.312 ± 0.008	-0.017 ± 0.018	0.001 ± 0.001	0.328 ± 0.020

[a]Number of replicate titrations.
[b]Initial analytical concentrations of titrant and titrand solutions used in titrations.

Table 5.5 Calculated Enthalpies of Complexation for Formation of $M(CDTA)(Ox)^{3-}$ Complexes

Complexation Reaction	$\Delta H°$(reaction), kJ/mol*
$Nd(CDTA)^- + Ox^{2-} \leftrightarrow Nd(CDTA)(Ox)^{3-}$	-8.70 ± 0.21
$Sm(CDTA)^- + Ox^{2-} \leftrightarrow Sm(CDTA)(Ox)^{3-}$	-7.74 ± 0.71
$Tb(CDTA)^- + Ox^{2-} \leftrightarrow Tb(CDTA)(Ox)^{3-}$	-11.46 ± 0.75
$Ho(CDTA)^- + Ox^{2-} \leftrightarrow Ho(CDTA)(Ox)^{3-}$	-9.87 ± 0.71
$Er(CDTA)^- + Ox^{2-} \leftrightarrow Er(CDTA)(Ox)^{3-}$	-11.63 ± 0.71
$Am(CDTA)^- + Ox^{2-} \leftrightarrow Am(CDTA)(Ox)^{3-}$	-8.46 ± 0.13

*Uncertainties are tabulated as the standard error of the mean.

5.4.2 Thermodynamics of the Ln-CDTA-Malonate System

Spectrophotometric titrations were carried out with 10 mL each of 10 mM Nd-, Sm-, Ho-, or $Er(CDTA)^-$ solutions and either 0.502 M Malonate or 1.022 M Malonate. Typical results from these titrations are shown in Figures 5.36-5.43. For the malonate system, significant absorption from Mal^{2-} was present up to about 430 nm (cf. Figure 5.2), which is why the absorbances in the flat regions from 350-430 nm increase with increasing malonate concentrations. Because of this fact, the malonate ligand was included in the SQUAD input files for samarium and erbium, which have major peaks in that range. When comparing the molar absorptivities as a function of wavelength, the impact of the malonate ligand on the absorbances is more evident. For example, in Figure 5.43, it is seen that the molar absorptivities of $Er(CDTA)^-$ slowly increase with increasing malonate concentration for the peak at 379 nm but at all other peaks, the molar absorptivities plateau after about 0.14 M. It is likely that at this point, the absorbance of the free malonate ligand dominates the total absorbance, meaning that the slowly increasing molar absorptivity is due to addition of Mal^{2-}. The effect of malonate absorption is most pronounced for $Sm(CDTA)^-$, where there almost appears to be a saddle point in each of the plots in Figure 5.39 due to Mal^{2-} absorption. Such effects were not noticeable for $Nd(CDTA)^-$ or $Ho(CDTA)^-$, as their major peaks were above 450 nm where malonate does not absorb significantly.

Table 5.6 lists the calculated equilibrium constants for formation of $Ln(CDTA)(Mal)^{3-}$ complexes. In general, 10 spectra were collected for each titration with at least 500 points per spectrum. The equilibrium constants were calculated in a manner similar to that $NdCDTA^-$ and $SmCDTA^-$ with oxalate. In contrast to the oxalate system, the complexes formed with Mal^{2-} are much weaker than the corresponding oxalate complexes. However, there is a definite trend in the equilibrium constants of the malonate complexes that mirrors those of the oxalate complexes as the lanthanide series is traversed from left to right.

Because the equilibrium constants for the $Ln(CDTA)(Mal)^{3-}$ complexes are much smaller than the oxalate complexes, calorimetric titrations were conducted with 40 mM $Ln(CDTA)^-$ solutions to maximize the number of moles of complex formed and associated heat measured. Tables 5.7 and 5.8 tabulate the calorimetric titrations and the associated enthalpies of complexation for formation of the $Ln(CDTA)(Mal)^{3-}$ complexes. Unlike the oxalate system in which the free Ox^{2-} comprised greater than 99% of the total oxalate concentration, about 90% of the total malonate concentration was comprised of Mal^{2-}. Thus, the p_cH changed significantly during titrations due to deprotonation of $HMal^-$, which was another indication that complexation was occurring. The total measured heat was also dominated by the heat of dilution and protonation reactions involving $HCDTA^{3-}$, H_2CDTA^{2-}, and the MES^- buffer. However, the net heat was, with the exception of $NdCDTA(Mal)^{3-}$, comparatively small and positive relative to the oxalate complexes, leading to endothermic enthalpies of complexation.

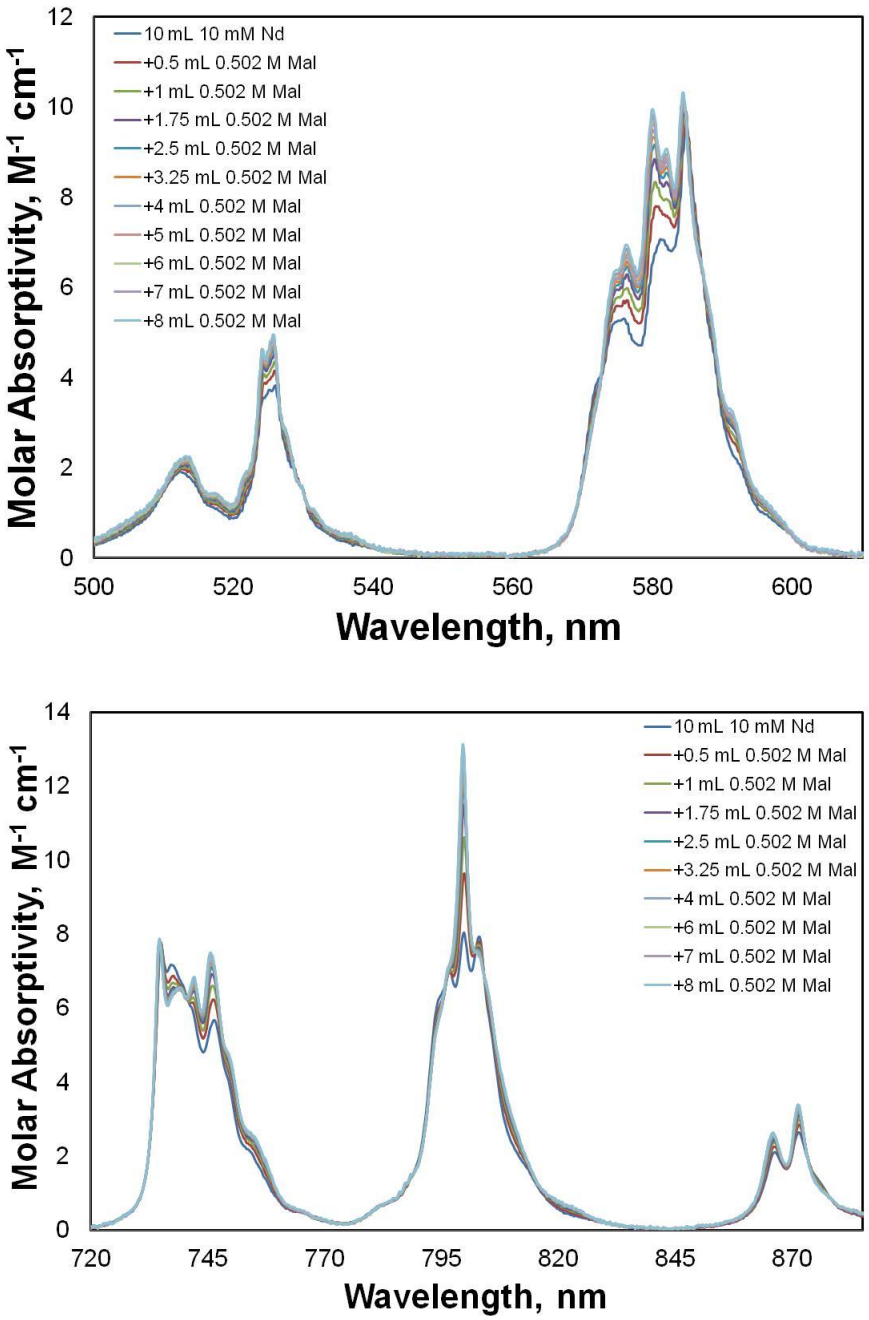

Figure 5.36 Representative titration of 10 mM $Nd(CDTA)^-$ with 0.502 M Malonate.

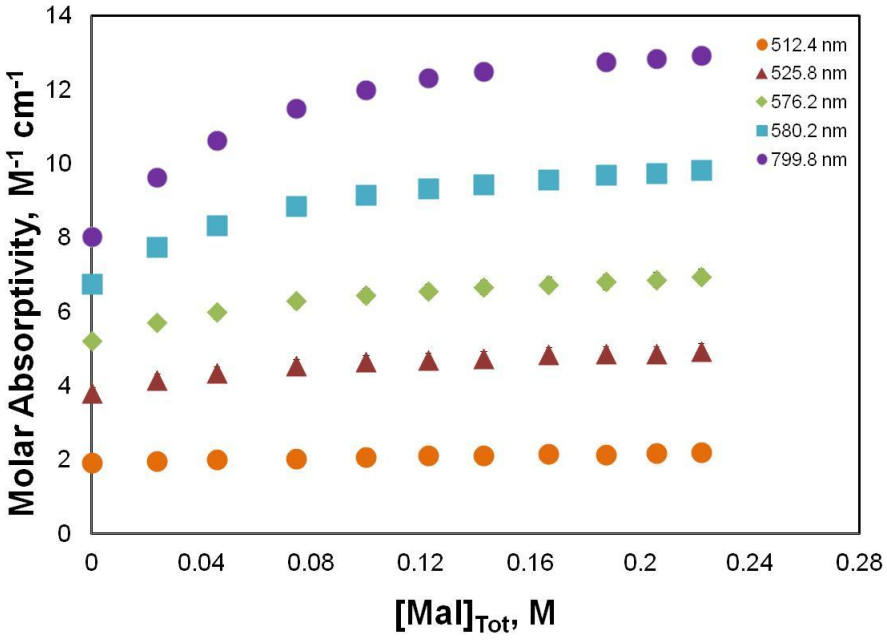

Figure 5.37 Molar absorptivities of $Nd(CDTA)^-$ as a function of total malonate concentration. Error bars are shown but they are smaller than the pictograms that represent the individual date points.

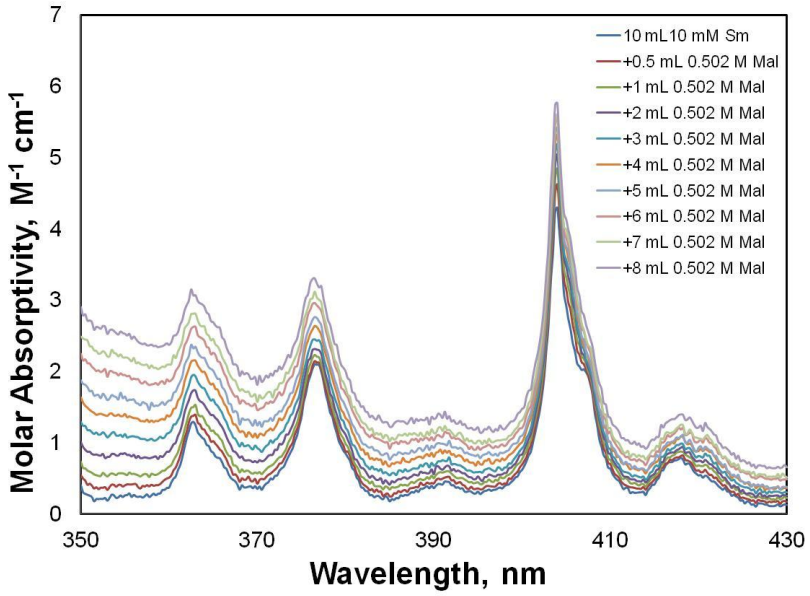

Figure 5.38 Molar absorptivities of $Sm(CDTA)^-$ as a function of total malonate concentration. The increasing absorbances throughout the region of interest are due partly to the free Mal^{2-} ligand.

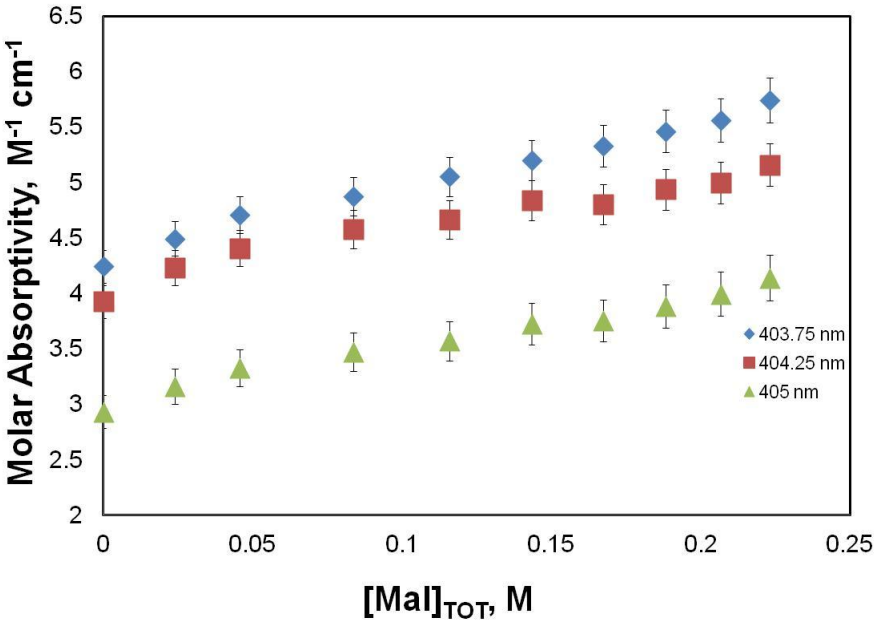

Figure 5.39 Molar absorptivities of $Sm(CDTA)^-$ as a function of total malonate concentration. The increasing molar absorptivities after approximately 0.15 M malonate are likely due to absorption by malonate.

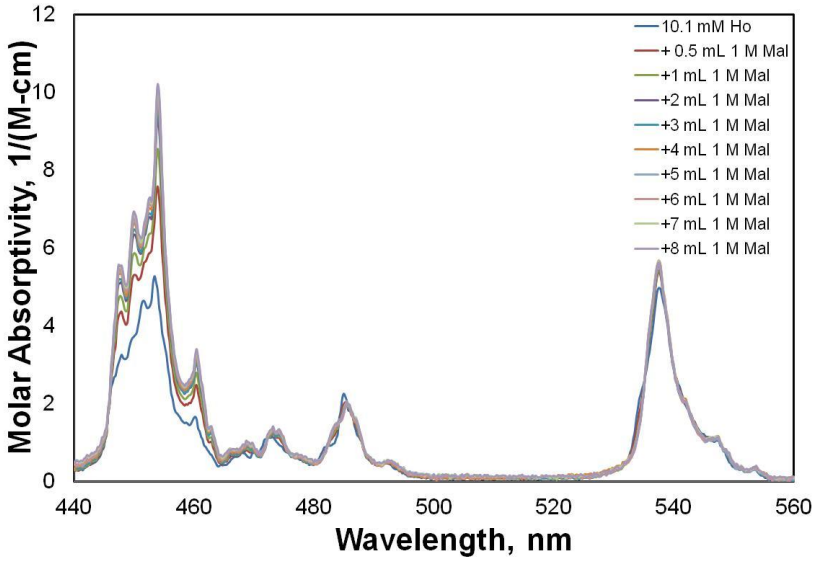

Figure 5.40 Molar absorptivities of $Ho(CDTA)^-$ as a function of wavelength for a typical titration.

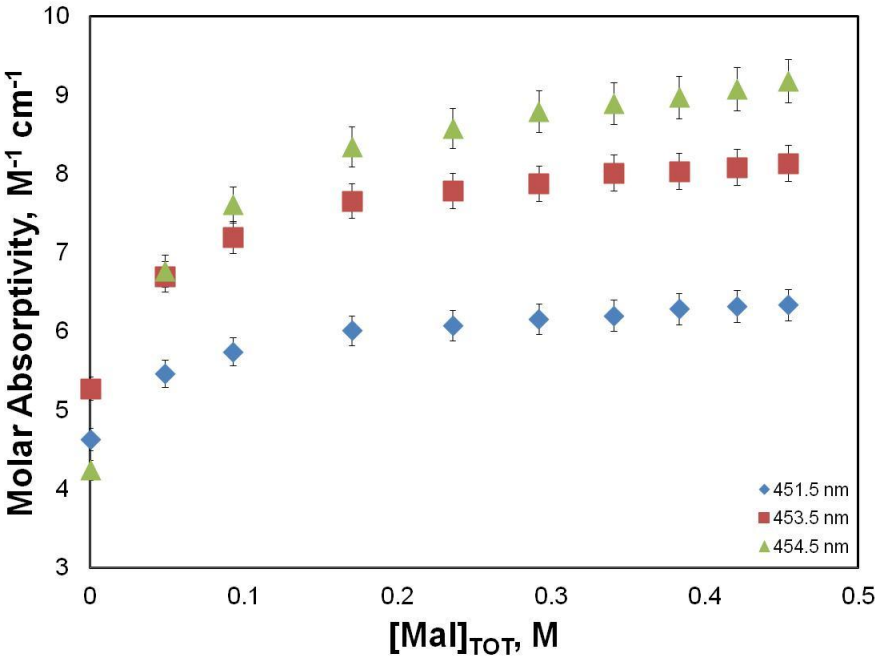

Figure 5.41 Molar absorptivities of $Ho(CDTA)^-$ as a function of total malonate concentration.

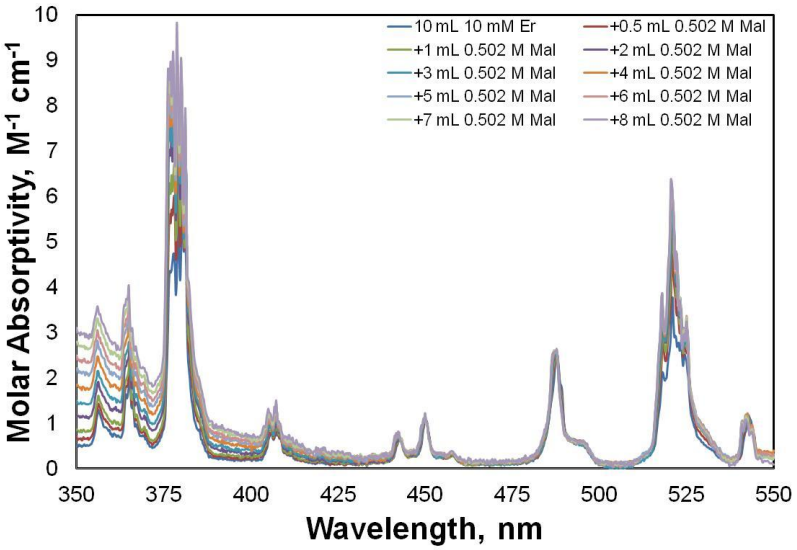

Figure 5.42 Molar absorptivities of $Er(CDTA)^-$ as a function of wavelength.

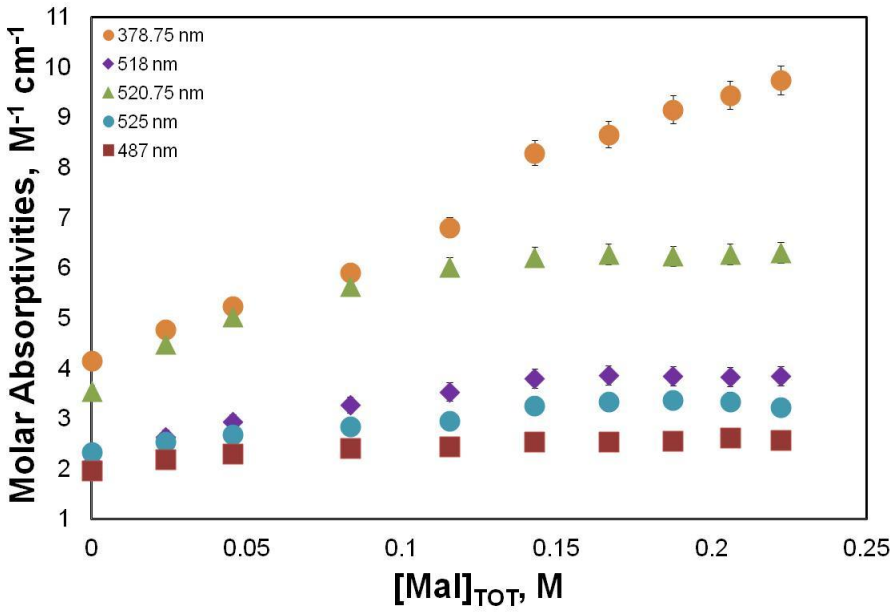

Figure 5.43 Molar absorptivities of $Er(CDTA)^-$ as a function of total malonate concentration. Note that the molar absorptivities at 378.75 nm do not plateau after about 0.12 M total malonate as it does for the other wavelengths. The observed increase is likely due to malonate absorption.

Table 5.6 Calculated Equilibrium Constants* for the Formation of $Ln(CDTA)(Mal)^{3-}$ Complexes

$Ln(CDTA)(Mal)^{3-}$	No. of Replicate Titrations	Log K_{111} †
$Nd(CDTA)(Mal)^{3-}$	5	1.19 ± 0.04
$Sm(CDTA)(Mal)^{3-}$	3	1.25 ± 0.07
$Ho(CDTA)(Mal)^{3-}$	3	1.30 ± 0.04
$Er(CDTA)(Mal)^{3-}$	3	1.31 ± 0.05

*Based on the equilibrium $Ln(CDTA)^- + Mal^{2-} \leftrightarrow Ln(CDTA)(Mal)^{3-}$.

†The uncertainties in the stability constants are tabulated as the standard error of the mean with 95% confidence.

Table 5.7 Tabulation of Calorimetric Titration Data for Titration of $Ln(CDTA)^-$ with Mal^{2-}

$Ln(CDTA)^-$	Runs[a]	$[Ln(CDTA)^-]/M^b$	$[Mal]/M^b$	p_cH_{final}	Q_{meas} / cal	Q_{dil} / cal	Q_{prot} / cal	Q_{corr} / cal
$Nd(CDTA)^-$	5	0.0402	0.502	5.965	0.035 ± 0.004	-0.107 ± 0.008	0.062 ± 0.001	0.080 ± 0.009
$Sm(CDTA)^-$	3	0.0401	0.502	5.958	-0.125 ± 0.016	-0.107 ± 0.008	0.062 ± 0.001	-0.080 ± 0.018
$Ho(CDTA)^-$	3	0.00395	1.022	5.995	-0.569 ± 0.006	-0.472 ± 0.018	0.029 ± 0.001	-0.126 ± 0.019
$Er(CDTA)^-$	4	0.0394	1.022	5.990	-0.475 ± 0.009	-0.472 ± 0.018	0.029 ± 0.001	-0.032 ± 0.020

[a]Number of replicate titrations.
[b]Initial analytical concentrations of titrant and titrand solutions used in titrations.

Table 5.8 Calculated Enthalpies of Complexation for Formation of $Ln(CDTA)(Mal)^{3-}$ Complexes

Complexation Reaction	$\Delta H°$(reaction), kJ/mol[†]
$Nd(CDTA)^- + Mal^{2-} \leftrightarrow Nd(CDTA)(Mal)^{3-}$	-1.23 ± 0.14
$Sm(CDTA)^- + Mal^{2-} \leftrightarrow Sm(CDTA)(Mal)^{3-}$	+1.14 ± 0.26
$Ho(CDTA)^- + Mal^{2-} \leftrightarrow Ho(CDTA)(Mal)^{3-}$	+1.06 ± 0.16
$Er(CDTA)^- + Mal^{2-} \leftrightarrow Er(CDTA)(Mal)^{3-}$	+0.264 ± 0.17

[†]Uncertainties are tabulated as the standard error of the mean.

5.4.3 Thermodynamics of the LnCDTA-IDA System

Spectrophotometric titrations were carried out with 10-20 mM $Ln(CDTA)^-$ stock solutions at p_cH 7. This p_cH was chosen to maximize the amount of free IDA^{2-} present (pK_{a3} = 9.26, pK_{a2} = 2.60) while remaining in a p_cH region in which the buffer capacities of $HCDTA^{3-}$ /H_2CDTA^{2-} and the MES buffer were still significant. Approximately 8-11 spectra were taken for each titration. Figures 5.44-5.51 show the normalized absorbances (molar absorptivities) of $Ln(CDTA)^-$ based on representative titrations with IDA.

The spectra of the $Ln(CDTA)^-$ complexes differ significantly from those of the analogous complexes with oxalate or malonate. In general, the change in the molar absorptivities of the major peaks is significantly smaller for the IDA spectra than for the malonate or oxalate spectra but the spectra are also noticeably different. For example, an additional shoulder at 810 nm is present in the IDA spectra for $Nd(CDTA)^-$ that is not present in the malonate or even oxalate spectra. A more pronounced blue shift to longer wavelengths is seen in the IDA spectra at 734 nm than is present for the oxalate spectrum; there is no such shift in the malonate spectrum. The shoulder in the $Sm(CDTA)^-$ spectra between 405-408 nm for the oxalate and malonate titrations disappears in the IDA spectra, becoming a smoother, rounded peak. Spectra of $Ho(CDTA)^-$ with IDA possess an additional shoulder at 541 nm that does not appear in either the oxalate or malonate spectra. The extensive peak formation that occurs between 440-460 nm upon complexation with Ox^{2-} or Mal^{2-} actually disappears in the IDA spectra.

The equilibrium constants for $Ln(CDTA)(IDA)^{3-}$ titrations are shown in Table 5.9. Complexes formed with the IDA ligand were the strongest complexes of all of the systems studied with CDTA. The absorbance of the $HIDA^-$ ligand, which was the predominant form of IDA at p_cH=7, was negligible in the regions studied so the ligand spectrum was generally not included in the SQUAD input files. Unlike the malonate and oxalate systems, in which the $Er(CDTA)^-$ ternary complexes are the most stable, for the IDA system, the stability of the complexes peaks at samarium and steadily decreases from left to right. Noteworthy is the fact that for samarium and neodymium, the increase in the stability of the IDA complexes is about one log unit larger than the stability of the corresponding oxalate complexes whereas for the smaller lanthanides holmium and erbium, the stability is reduced such that their equilibrium constants are comparable to the oxalate complexes.

In anticipation of large enthalpies of complexation based on the equilibrium constants of the $Ln(CDTA)(IDA)^{3-}$ complexes, the concentrations of $Ln(CDTA)^-$ solutions used for the calorimetric titrations were reduced to 10 mM with the exception of $Sm(CDTA)^-$, which was about 22 mM. The results of titrations of 10-20 mM $Ln(CDTA)^-$ with 1.5 M IDA are tabulated in Tables 5.10 and 5.11. Copious quantities of heat were released in the IDA titrations as opposed to the oxalate or malonate titrations. The dilution heats were by far the largest contributors to overall measured heats for all titrations except those with samarium, and a significant amount of the measured heat was also due to protonation reactions. A great majority of the IDA ligand was present as the $HIDA^-$ ligand and, as a result, the p_cH decreased by up to 0.62 units during a titration as the $HIDA^-$ was deprotonated, which substantially affected the composition of the IDA and CDTA ligands as well as the MES buffer. This explains the significant contribution to the protonation enthalpy. The data indicate that the post-titration p_cH values are correlated to the stability constant – that is, the lower the final p_cH, the higher the stability constant for experiments conducted under similar conditions. There is also a

progressive trend in the complexation enthalpies that indicates that as the lanthanide series is traversed, the enthalpy of complexation increases by -2 kJ/mol until holmium is reached, at which point the rate of increase of the enthalpy appears to decrease.

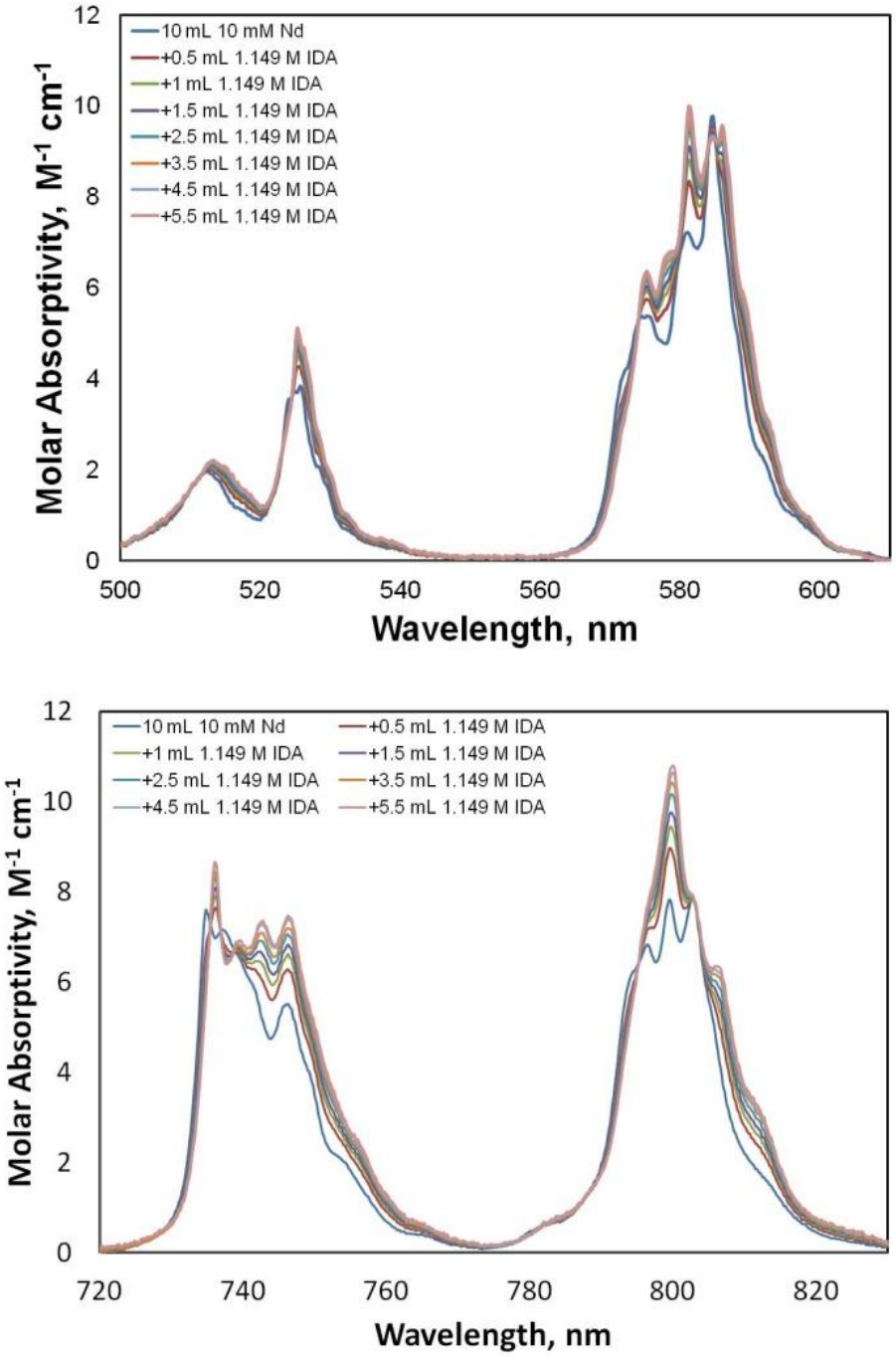

Figure 5.44 Molar absorptivities of $Nd(CDTA)^-$ based on a representative titration of 10 mM $Nd(CDTA)^-$ with 1.15 M IDA.

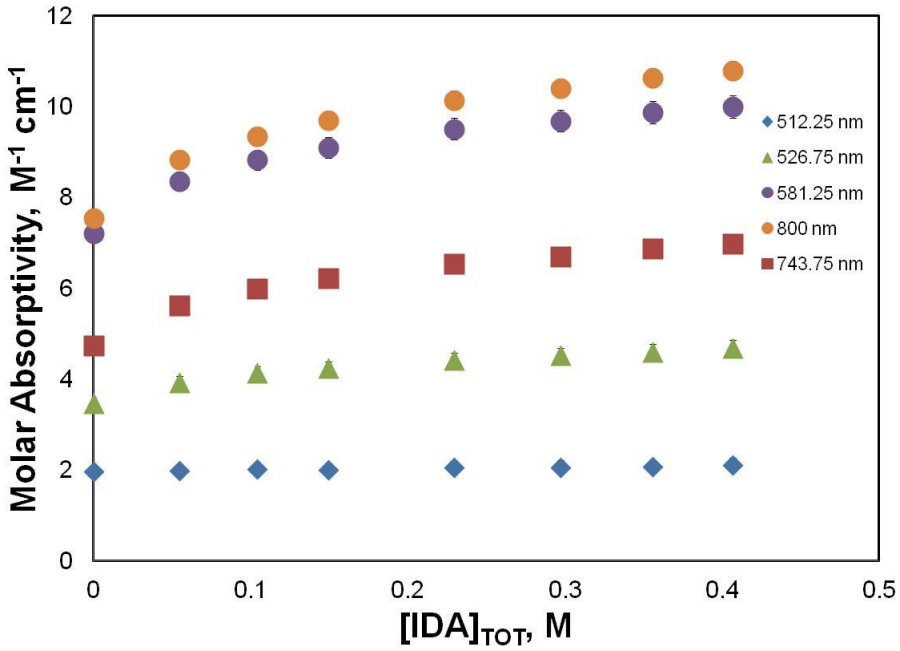

Figure 5.45 Molar absorptivities of $Nd(CDTA)^-$ as a function of total IDA concentration for selected peaks. The error bars are smaller than the pictograms used to represent the data points.

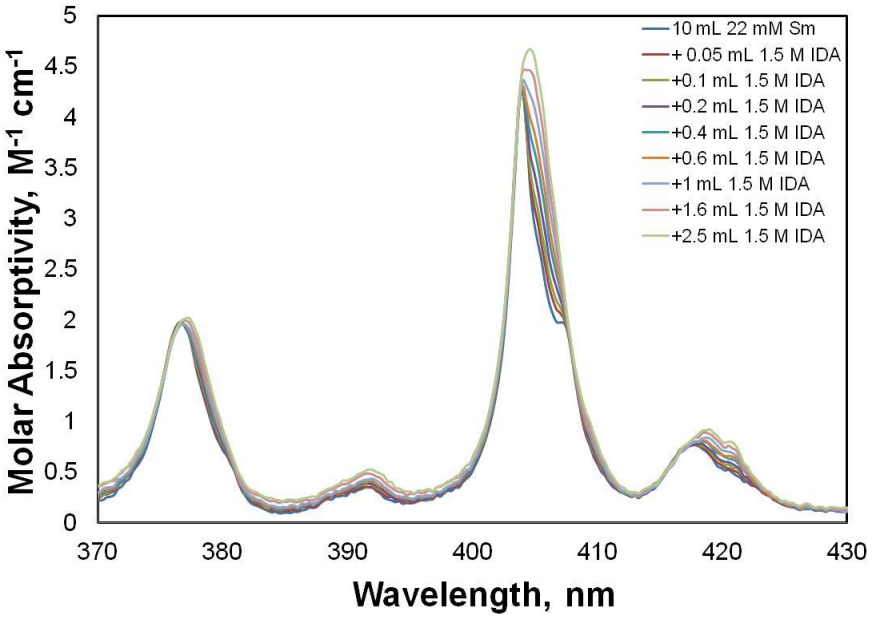

Figure 5.46 Absorption spectra of $Sm(CDTA)^-$ normalized to total $Sm(CDTA)^-$ concentration and pathlength for a representative SmCDTA-IDA titration.

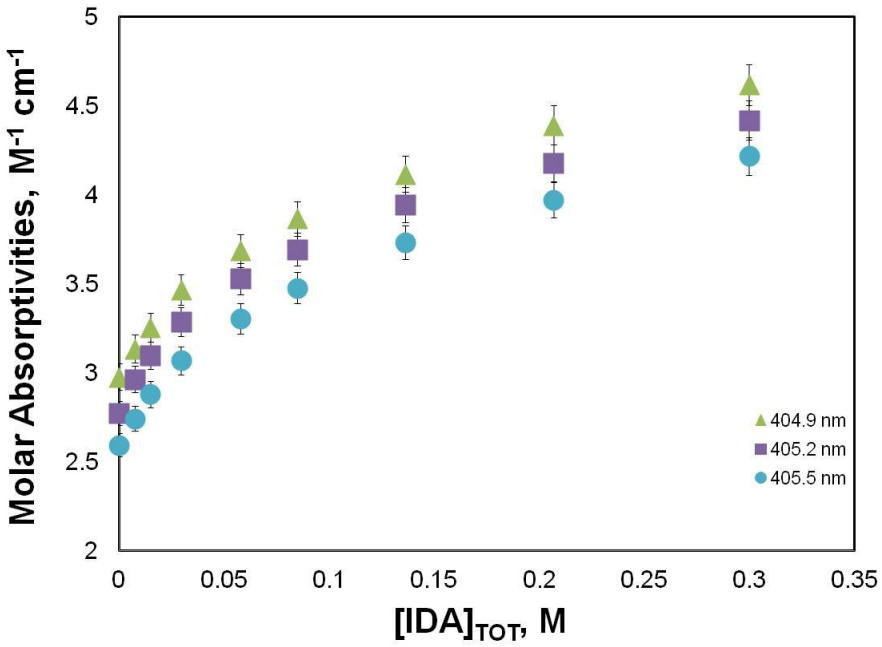

Figure 5.47 Molar absorptivities of $Sm(CDTA)^-$ as a function of total IDA concentration.

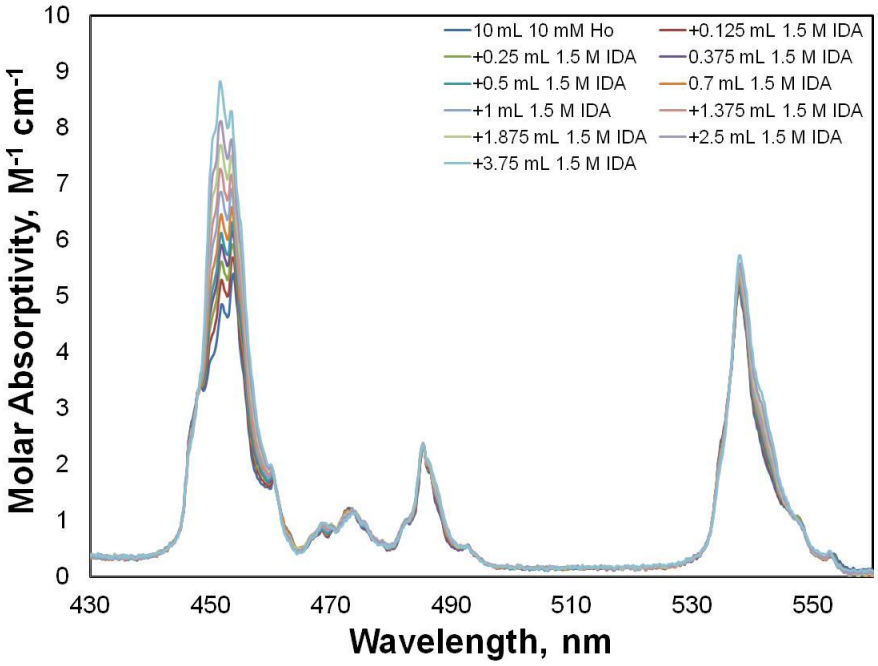

Figure 5.48 Molar Absorptivities of $Ho(CDTA)^-$ for a representative titration of 10 mM $Ho(CDTA)^-$ with 1.5 M IDA.

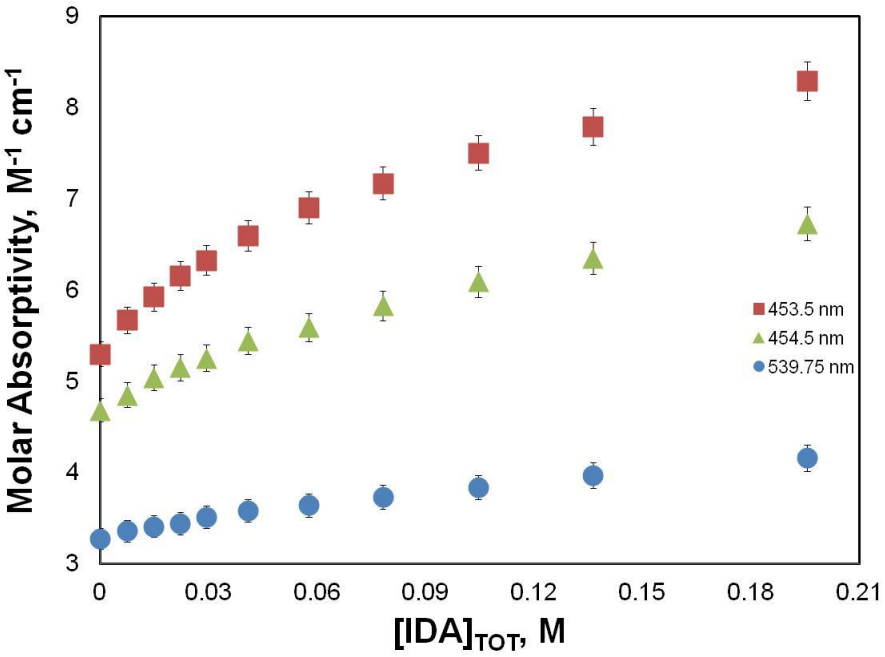

Figure 5.49 Molar Absorptivities of $Ho(CDTA)^-$ as a function of total IDA concentration at selected wavelengths.

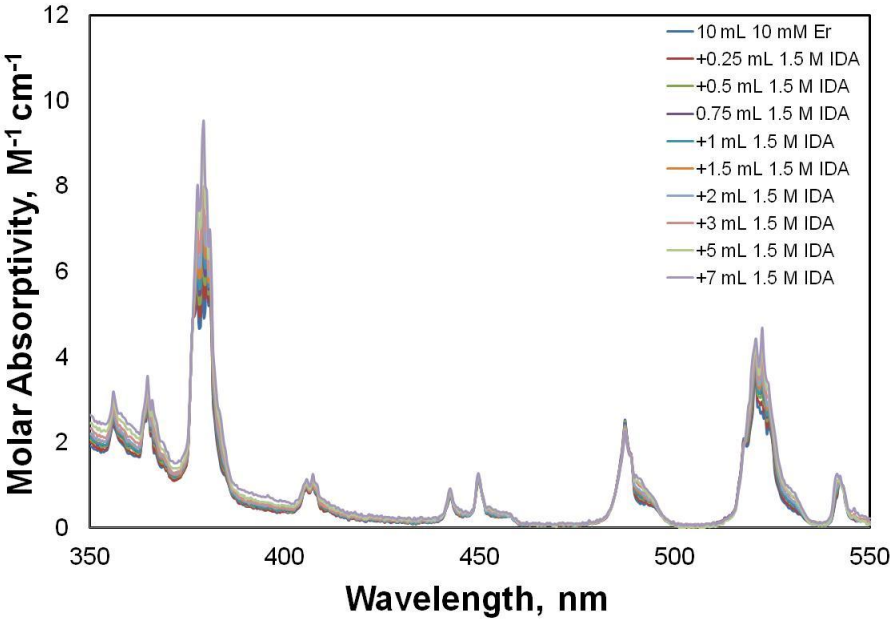

Figure 5.50 Representative titration of 10 mM $Er(CDTA)^-$ with 1.5 M IDA. Absorption spectra have been normalized to total $Er(CDTA)^-$ concentration and pathlength in the figure.

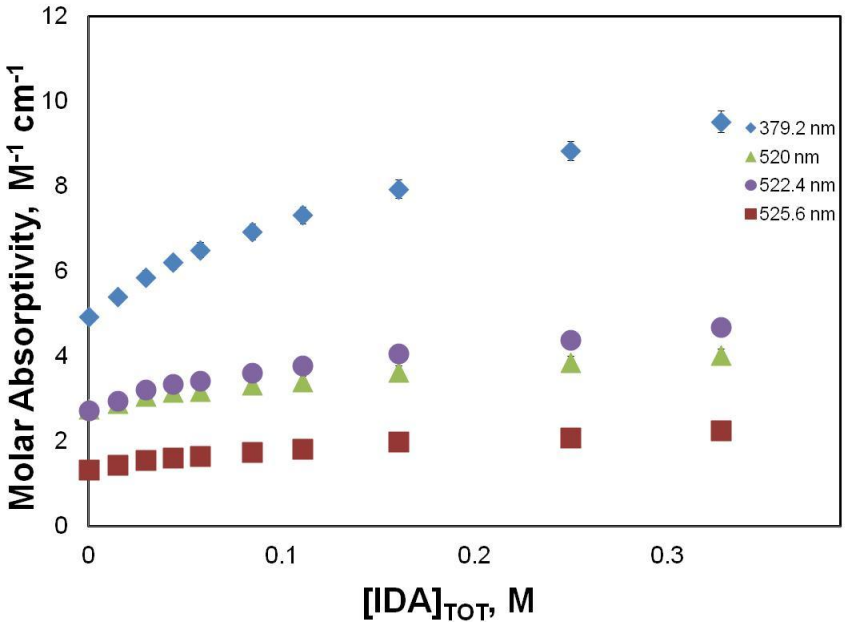

Figure 5.51 Molar absorptivities of $Er(CDTA)^-$ as a function of total IDA concentration at selected wavelengths. Most of the error bars are not visible because they are smaller than the pictograms used to display the data points.

Table 5.9 Calculated Equilibrium Constants* for the Formation of $Ln(CDTA)(IDA)^{3-}$ Complexes

$Ln(CDTA)(IDA)^{3-}$	No. of Replicate Titrations	Log K_{111} †
$Nd(CDTA)(IDA)^{3-}$	5	3.43 ± 0.05
$Sm(CDTA)(IDA)^{3-}$	3	3.72 ± 0.03
$Ho(CDTA)(IDA)^{3-}$	3	3.18 ± 0.04
$Er(CDTA)(IDA)^{3-}$	3	3.00 ± 0.08

*Based on the equilibrium $Ln(CDTA)^- + (IDA)^{2-} \leftrightarrow Ln(CDTA)(IDA)^{3-}$.
†The uncertainties in the stability constants are tabulated as the standard error of the mean with 95% confidence.

Table 5.10 Tabulation of Calorimetric Titration Data for Titration of $Ln(CDTA)^-$ with IDA^{2-}

$Ln(CDTA)^-$	Runs[a]	$[Ln(CDTA)^-]/M$[b]	$[IDA]/M$[b]	p_cH_{final}	Q_{meas} / cal	Q_{dil} / cal	Q_{prot} / cal	Q_{corr} / cal
$Nd(CDTA)^-$	3	0.0103	1.499	6.716	-1.137 ± 0.020	-0.949 ± 0.010	-0.464 ± 0.002	0.276 ± 0.022
$Sm(CDTA)^-$	4	0.0216	1.499	6.392	-0.886 ± 0.012	-0.949 ± 0.010	-1.010 ± 0.010	1.073 ± 0.016
$Ho(CDTA)^-$	3	0.0101	1.499	6.742	-0.794 ± 0.003	-0.949 ± 0.010	-0.391 ± 0.002	0.546 ± 0.011
$Er(CDTA)^-$	3	0.00999	1.499	6.802	-0.756 ± 0.003	-0.949 ± 0.010	-0.300 ± 0.002	0.493 ± 0.011

[a]Number of replicate titrations.
[b]Initial analytical concentrations of titrant and titrand solutions used in titrations.

Table 5.11Calculated Enthalpies of Complexation for Formation of $Ln(CDTA)(IDA)^{3-}$ Complexes

Complexation Reaction	$\Delta H°$(reaction), kJ/mol*
$Nd(CDTA)^- + IDA^{2-} \leftrightarrow Nd(CDTA)(IDA)^{3-}$	-10.21 ± 0.81
$Sm(CDTA)^- + IDA^{2-} \leftrightarrow Sm(CDTA)(IDA)^{3-}$	-19.78 ± 0.29
$Ho(CDTA)^- + IDA^{2-} \leftrightarrow Ho(CDTA)(IDA)^{3-}$	-27.20 ± 0.55
$Er(CDTA)^- + IDA^{2-} \leftrightarrow Er(CDTA)(IDA)^{3-}$	-30.33 ± 0.67

*Uncertainties are tabulated as the standard error of the mean.

5.5 Thermodynamics of the LnDO3A-(L^2) System

5.5.1 Deprotection of DO3A·tBu Ester

In order to prepare heptacoordinate Ln(DO3A) complexes, the DO3A·tBu ester was first deprotected to make the carboxylic acids available for complexation. More importantly, the DO3A·tBu ester is water-insoluble whereas the deprotected DO3A ligand is soluble. The carboxyl groups of the DO3A·tBu ester were deprotected using trifluoroacetic acid (TFA) in dichloromethane according to the procedure described in Chapter 4. The deprotection reaction can be written as follows:

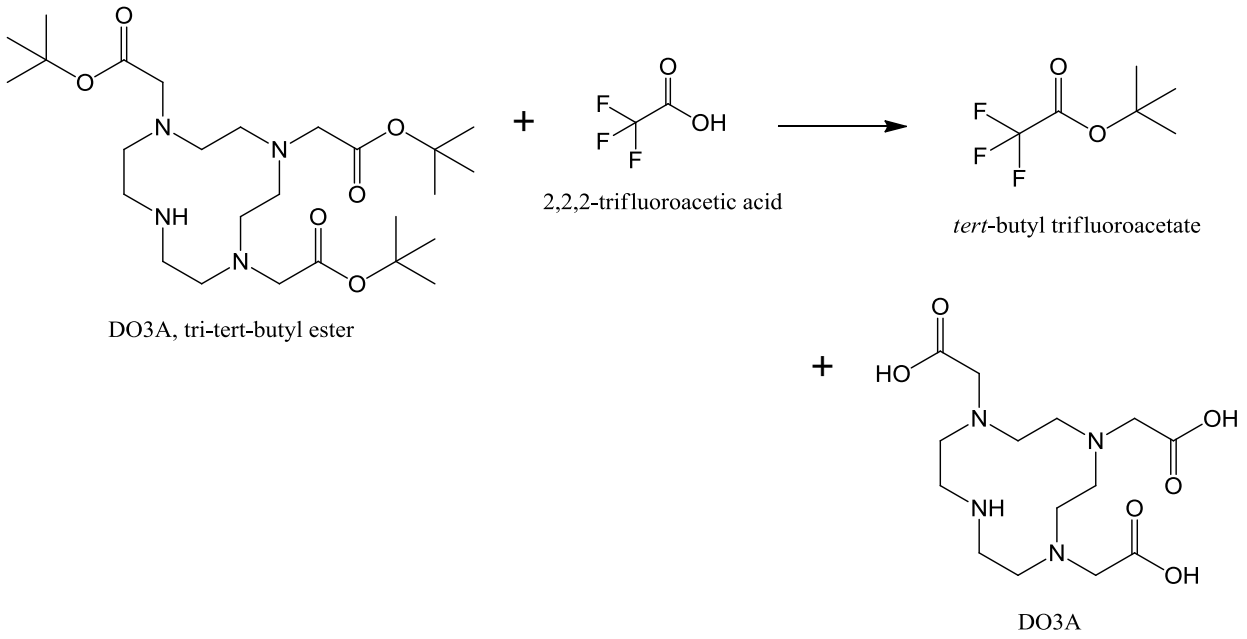

The choice of TFA as the acid catalyst was advantageous because it is soluble in dichloromethane and its low boiling point (b.p. 72°C) made it easy to remove using rotary evaporation. In addition, the side product of the reaction, tert-butyl trifluoroacetate (b.p. 83°C), is also relatively easy to remove in a vacuum oven. Proton and ^{13}C NMR were taken to confirm the successful hydrolysis. Representative spectra are shown in Figures 5.52 and 5.53.

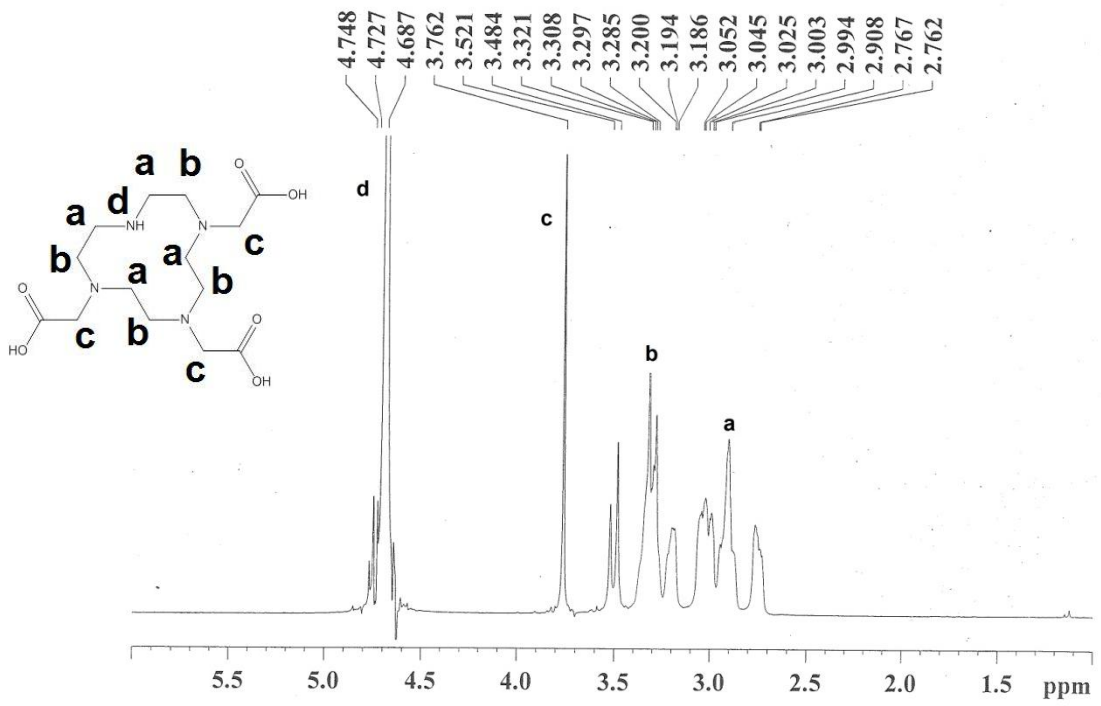

Figure 5.52 Proton NMR spectrum of hydrolyzed DO3A·tBu ester.

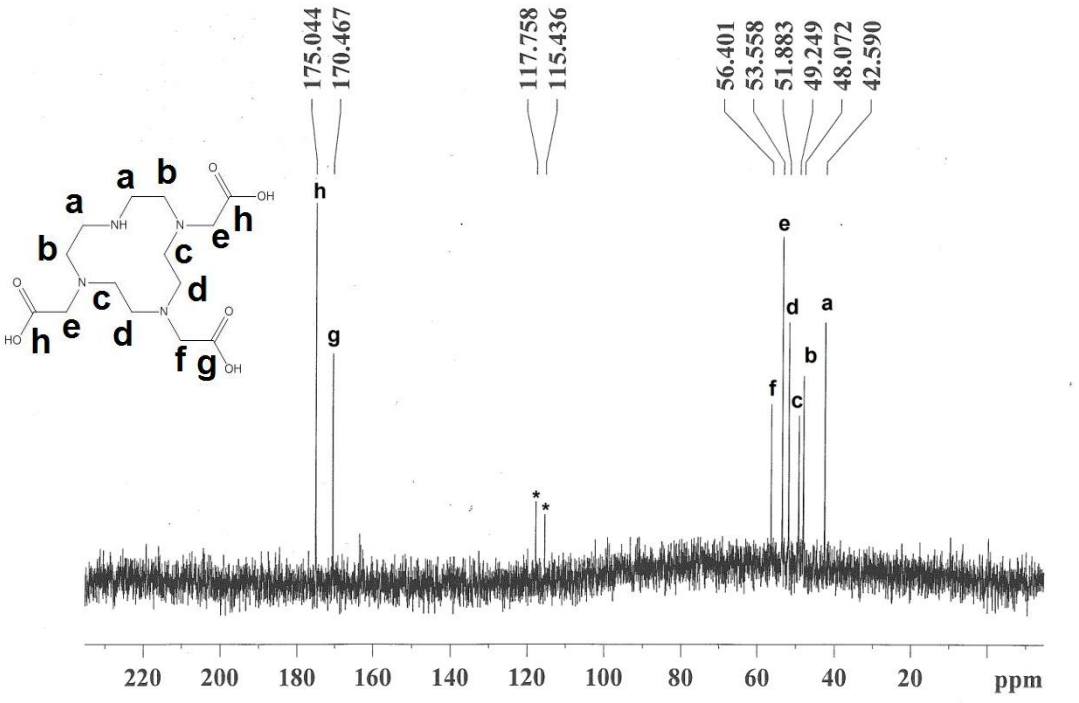

Figure 5.53 ^{13}C NMR of the hydrolyzed DO3A·tBu ester. The asterisks denote impurities in the NMR tube.

Though there were no proton NMR spectra of the DO3A or the DO3A·tBu ester available in the literature, a reasonable assignment of the peaks can still be made using NMR theory and the aid of an NMR chemical shift table. A line of symmetry bisects the molecule from the protonated amine to the nitrogen directly opposite the protonated amine, reducing the number of unique peaks in the spectrum. The protons labeled *a* and *b* are expected to be triplets based on coupling to one another. However, although there are 4 sets of protons labeled *a* and *b*, not all of these protons are *exactly* equivalent (i.e., in the same chemical environment). The protons that are on the carbons next to the secondary nitrogen atom likely split further, which may explain the additional splitting in the two triplets into distorted multiplets. Of course, the methylene protons *c*, which have no neighboring protons, should be present as a singlet. The amine proton *d* unfortunately has an overlapping resonance with the HDO residual solvent peak that appears near 4.79 ppm.[96] The HDO solvent peak is caused by exchange of the weakly acidic deuterons in the solvent D_2O with residual H_2O that is present in D_2O, forming HDO. The intensity of the HDO peak is very high; in light of this fact, the amine peak itself is likely centered at 4.73 ppm. Since the NMR spectra were taken in D_2O, rapid exchange of acidic protons for deuterons essentially quenched the signal due to the carboxylic acid protons of DO3A that would normally appear between 10-12 ppm. However, the defining feature that distinguishes DO3A from its *tert*-butyl ester is the absence of the *tert*-butyl functional group, which would appear as a sharp singlet near 1.5-2 ppm. The conspicuous absence of this peak was very good evidence that the deprotection was successful.

The chemical shifts for the ^{13}C-NMR spectrum for DO3A published by Tweedle et. al.[97] agreed well with the spectrum obtained for the hydrolyzed ester in this work, as shown in Table 5.12, with the exception of two peaks at 117 and 115 ppm. These peaks are indicative of an impurity either in the sample or in the NMR tube. Possible impurities in the sample include TFA, acetonitrile, and *tert*-butyl trifluoroacetate. Comparison of NMR spectra of these compounds indicated that none of these compounds could be responsible for the impurity. Since the NMR tubes were not new, it is probable that an unknown residue was present in the tube.

Table 5.12 Comparison of chemical shifts of DO3A measured in this work with literature values

Chemical Shifts (ppm) of DO3A, This Work*	Chemical Shifts (ppm) of DO3A, Tweedle et al.[97,*]
175.044	176.9
170.467	171.0
117.758	
115.436	
56.401	57.0
53.558	55.7
51.883	52.7
49.249	50.3
48.072	49.3
42.590	43.6

*NMR solvent was D_2O.

5.5.2 Ternary Ln(DO3A)$(L^2)^{2-}$ Complexes

Neodymium- and erbium-DO3A complexes were prepared for investigations with oxalate, malonate, and iminodiacetate. It should be noted that the kinetics of formation of Ln(DO3A) complexes is very slow, taking about a week to come to equilibrium under reflux conditions. Because of the limited amount of DO3A available, the total DO3A concentration was reduced to approximately 17 mM DO3A for erbium and 12 mM DO3A for neodymium and the experiments were conducted in 1 cm cells.

Attempts to perform spectrophotometric titrations of 10 mM Nd(DO3A) with 76 mM Ox^{2-} were unsuccessful as there was immediate precipitation of a light blue powdery solid upon addition of less than 50 μL oxalate. It is not unreasonable that the ternary $Nd(DO3A)(Ox)^{2-}$ complex is insoluble as there are reports of mixed neodymium oxalate crystals in the literature.[98,99] However, the insolubility of binary neodymium oxalate, Nd_2Ox_3, is also well known: the NIST Critical Stability Constant Database[52] reports a measured solubility product constant, K_s, of -31.11 at 25 °C and 0 M ionic strength. Therefore, it was necessary to rule out the possibility that there was incomplete reaction of Nd^{3+} with $DO3A^{3-}$. This was accomplished by comparing the spectra of Nd^{3+} with Nd(DO3A). If incomplete reaction of Nd^{3+} with $DO3A^{3-}$ had occurred, then the spectrum of the Nd(DO3A) solution should show evidence of free Nd^{3+} present. Figure 5.54 compares the spectra of free Nd^{3+} and Nd(DO3A). The spectrum of Nd(DO3A) is substantially different from that of the free neodymium cation. Several peaks and shoulders are present in the Nd^{3+} spectrum that do not appear in the Nd(DO3A) spectrum. For example, the lowest peaks in the bands centered 730 nm and 800 nm do not appear in the Nd(DO3A) spectrum. Thus, it is likely that the precipitation is not due to Nd_2Ox_3 but is possibly the $Nd(DO3A)(Ox)^{2-}$ complex balanced by the abundant sodium ions in solution.

Titrations of Nd(DO3A) with malonate and IDA were successful, however. Spectra of representative titrations are shown in Figures 5.55-5.56 below. Titrations of Er(DO3A) with oxalate and malonate did not lead to precipitation; their spectra are shown in Figures 5.57 and 5.58. At least 9 spectra were collected per titration with at least 350 points per spectrum. The titrations were carried out thrice each with Nd(DO3A) and malonate/IDA but only once for ErDO3A with oxalate and malonate. Titrations of Nd(DO3A) and Er(DO3A) differ from analogous CDTA titrations in that the changes in the molar absorptivities at major peaks are significantly smaller than those in CDTA titrations, even with large additions of 1.62 M malonate or 1.76 M IDA. Nonetheless, SQUAD was able to calculate the equilibrium constants of both sets of data with Er(DO3A) and Nd(DO3A), as indicated in Table 5.13.

It is worth pointing out that the equilibrium constants of $NdDO3A(IDA)^{2-}$ and $ErDO3A(Ox)^{2-}$ are, within error, very similar to the calculated equilibrium constants for $NdCDTA(IDA)^{3-}$ and $ErCDTA(Ox)^{3-}$, respectively. However, the weakly-binding malonate ligand actually binds more strongly to NdDO3A and ErDO3A than they do to the analogous CDTA complexes.

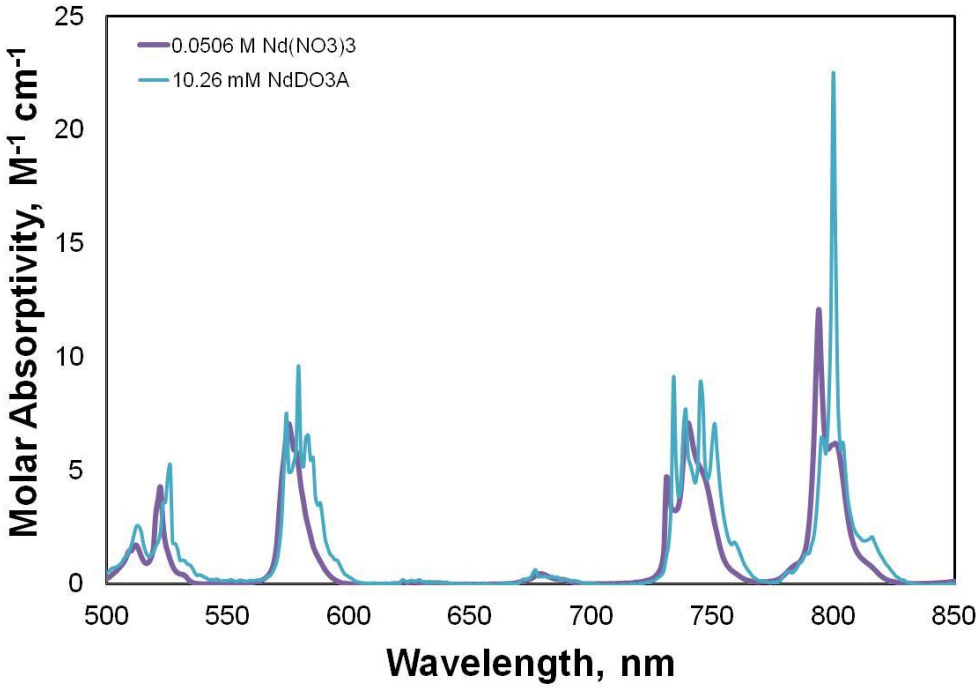

Figure 5.54 Comparison of Nd^{3+} and Nd(DO3A) spectra.

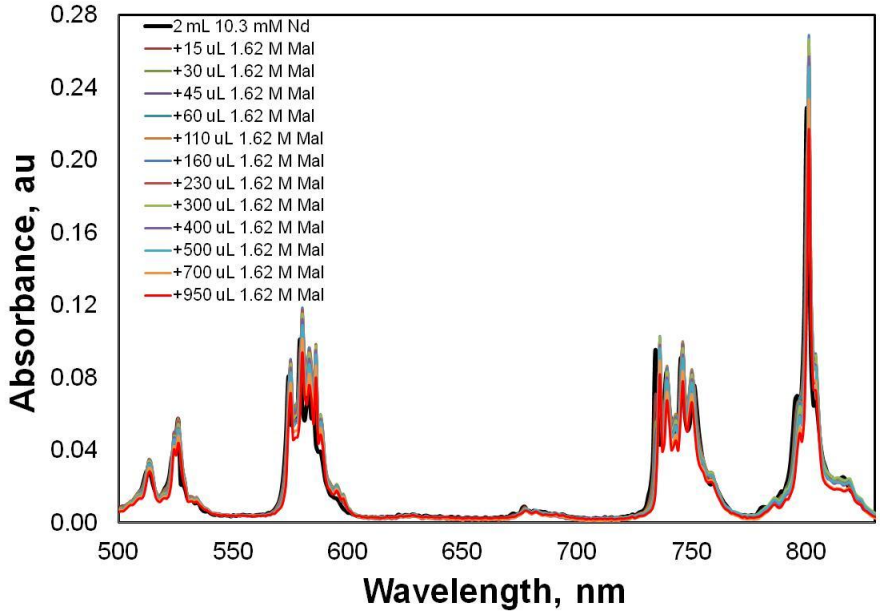

Figure 5.55 Spectrophotometric titration of 10 mM Nd with 1.62 M Malonate.

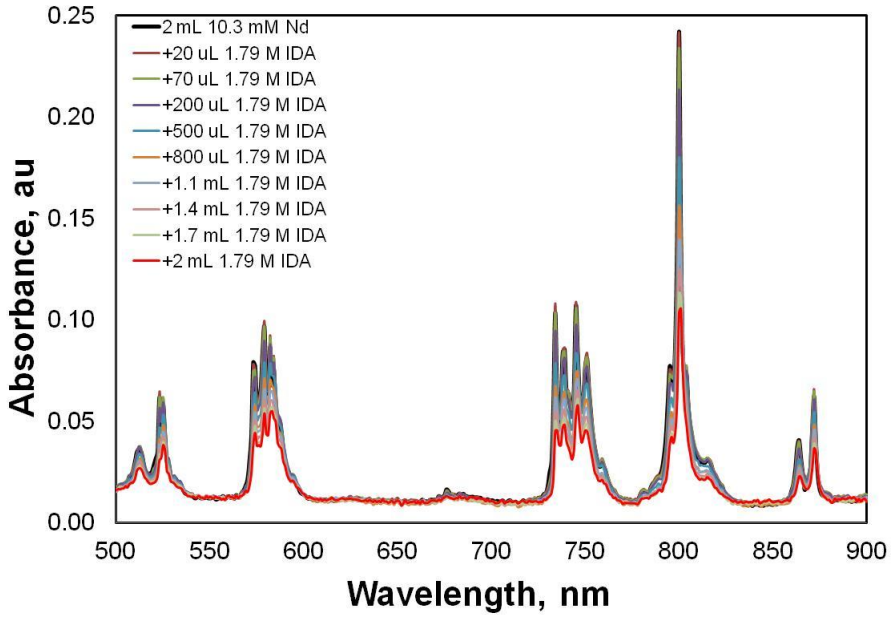

Figure 5.56 Spectrophotometric titration of 10 mM Nd(DO3A) with 1.79 M IDA.

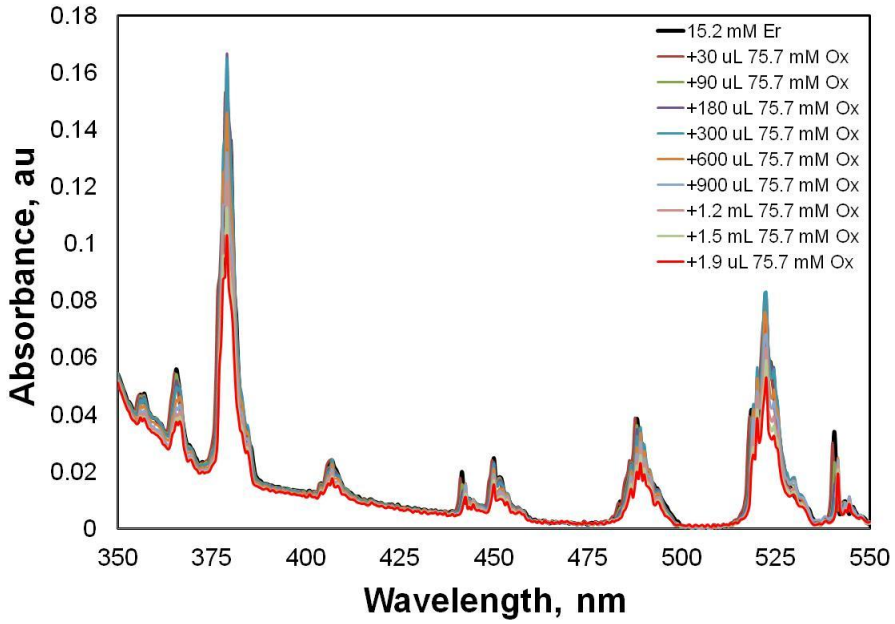

Figure 5.57 Spectrophotometric titration of 15 mM Er(DO3A) with 76 mM oxalate.

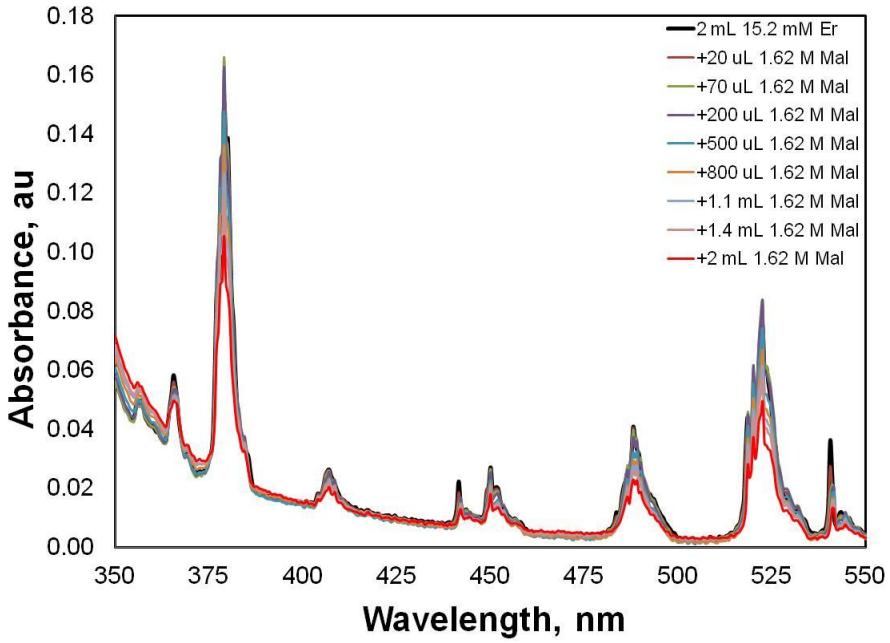

Figure 5.58 Spectrophotometric titration of 15 mM Er(DO3A) with 1.62 M malonate.

Table 5.13 Tabulated Equilibrium Constants for Ternary Ln(DO3A)(L^2)$^{2-}$ Complexes

Ligand L^2	Neodymium	Erbium
Oxalate	insoluble	2.93 ± 0.05
Malonate	1.79 ± 0.02	1.68 ± 0.02
Iminodiacetate	3.55 ± 0.05	n/a

Chapter 6 Discussion

6.1 MDTPA-(Lactate, Oxalate) Complexes

In Chapter 5 it was shown that of the three primary ligands studied, the DTPA ligand was the only ligand for which ternary complexes with the secondary ligands (i.e., lactate and oxalate) *were not observed* via spectroscopic or thermometric techniques. The most plausible reason for the lack of spectroscopic evidence of ternary complexation is that log K_{111} is very small for the formation of inner-sphere $M(DTPA)(Lac)^{3-}$ or $M(DTPA)(Ox)^{4-}$ complexes. If K_{111} were small, only a small amount of ternary complex would have formed during titrations – not enough to significantly perturb the measured spectra.

Although inner-sphere ternary complexes were not observed under the experimental conditions used, a maximum value of K_{111} can be estimated based on the highest free ligand (Lac^- or Ox^{2-}) concentrations present in the M-DTPA-Lac or M-DTPA-Ox solutions and on results from similar experiments done with DO3A and CDTA. Based on the DO3A and CDTA experiments, it was observed that a noticeable change in the absorption spectra was readily evident after approximately 10% of the total initial metal was complexed with a secondary ligand. In other words, [M(DTPA)(Lac)]/[M(DTPA)] = 0.1/0.9 = 0.11. Also, for the M-DTPA-Lac system, the maximum total concentration of lactate that showed no change in the absorption spectrum was 1 M at p_cH 4.1, which corresponds to a free lactate concentration of approximately 0.75 M. As a conservative estimate, this concentration can be assumed to be the minimum free ligand concentration that must be present in solution when 10% of the initial binary complex has reacted. Therefore, the maximum value of K_{111} for the $M(DTPA)(Lac)^{3-}$ complex is approximately

$$K_{111} \equiv \frac{[M(DTPA)(Lac)^{3-}]}{[M(DTPA)^{2-}][Lac^-]} \leq \frac{(0.1)}{(0.9)(0.75)} = 0.15 \qquad (6.1)$$

An estimate of the maximum value of K_{111} can also be made for $M(DTPA)(Ox)^{4-}$ using similar approximations. Based on the M-DTPA-lactate titration data, the maximum total concentration of oxalate present in solution at the end of a titration was 0.031 M. At p_cH 6, about 99.6% of the total oxalate concentration is the free oxalate ligand; therefore, 0.031 M can safely be used as the conservative estimate of the minimum free ligand concentration in this case. Using the same stipulation that at least 10% of the total binary complex must react with Ox^{2-} before a change in the absorption spectrum would be easily noted, an estimate of the maximum value of K_{111} can be made:

$$K_{111} = \frac{[M(DTPA)(Ox)^{4-}]}{[M(DTPA)^{2-}][Ox^{2-}]} \leq \frac{(0.1)}{(0.9)(0.031)} = 3.58 \qquad (6.2)$$

Based on the above estimate of the maximum value K_{111}, if inner-sphere $M(DTPA)(Ox)^{4-}$ complexes do form, they are still very weak in comparison to the analogous DO3A or CDTA complexes.

The spectroscopy results indicate that binary DTPA complexes do not form measurable amounts of inner-sphere ternary complexes with oxalate or lactate at 1 M ionic strength. The results of thermometric titrations appear to corroborate this conclusion. The measured heats from the titrations of Nd and Eu with lactate, -20 ± 60 mJ and 70 ± 50 mJ, respectively (Table 5.2), are very small and near zero within error. Since it is likely that all possible reactions have been accounted for, one of the two suppositions below can explain the small measured heats:

1. $\Delta H°$ for the reaction $M(DTPA)^{2-} + Lac^{-} \leftrightarrow M(DTPA)(Lac)^{4-}$ is approximately zero
2. $\Delta H°$ is non-zero but small heats are measured because K_{111} is small.

In order to investigate these two possibilities, a relationship between $\Delta H°$ and K_{111} must be developed. The equation relating the net heat with the enthalpy of complexation (Chapter 5) can be rewritten as

$$\Delta H° = -\frac{Q_{net}}{\Delta n_{M(DTPA)(Lac)}} = -\frac{Q_{net}}{V_f[M(DTPA)(Lac)^{3-}]} \tag{6.3}$$

where V_f is the total cup volume after addition of titrant. The concentration of $M(DTPA)(Lac)^{3-}$ is determined by combining the mass balance equations for total metal and lactate, which yields a quadratic equation of the form $a[M(DTPA)(Lac)^{3-}]^2 + b[M(DTPA)(Lac)^{3-}] + c = 0$, where

$$a = 1 \tag{6.4a}$$

$$b = -1\left\{C_M + C_{Lac} + \frac{1}{K_{111}}\left(\frac{[H^+]}{K_a} + 1\right)\right\} \tag{6.4b}$$

$$c = C_M C_{Lac} \tag{6.4c}$$

and C_M and C_{Lac} are the total concentrations of metal and lactate in all forms and K_a is the acid dissociation constant for lactic acid. The average heat measured from the Nd and Eu titrations with lactate is +0.026 ± 0.110 J. Using 27 mL as the final volume from a representative titration, Figure 6.1 was obtained.

To further assess the likelihood that either of the above scenarios applies to the DTPA system, the associated entropies were also calculated using the equation

$$T\Delta S° = \Delta H° + 5.709 \log K_{111} \tag{6.5}$$

A plot of the entropy term as a function of log K_{111} is shown in Figure 6.2.

The first supposition states that the measured heats are small because $\Delta H°$ is approximately zero. If $\Delta H°$ were in reality a very small value (near zero), it could only be true if log $K_{111}>1$ and $\Delta S°>0$ based on Figures 6.1 and 6.2, which would imply that an increase in disorder of the system occurs upon complexation. However, such an increase in disorder is a hallmark of inner-sphere complexation in which residual water molecules are displaced prior to complexation. Changes in the inner-sphere environment are easily detected by UV-Vis spectroscopy, but results from those studies showed no indication of inner-sphere complexation occurring. Moreover, it was shown above that the maximum value of K_{111} for inner-sphere complexation is approximately 0.15 meaning that log $K_{111}<1$, in contradiction to supposition (1). Supposition (2) states that $\Delta H°$ is non-zero but the measured heats were small because K_{111} is small. According to Figure 6.1, $\Delta H°$ is non-zero only when log $K_{111}<0$. Figure 6.2 shows that when log $K_{111}<0$, the entropy of the system should decrease, meaning that little to no dehydration of inner-sphere water molecules accompanies ternary complexation. These two facts imply that the overall enthalpy of reaction is dominated by contributions due to formation of the complex (exothermic) with almost no contribution from dehydration (endothermic). In other words:

$$\Delta H^{\circ}_{rxn} = \Delta H^{\circ}_{complex} + \Delta H^{\circ}_{dehyd} \cong \Delta H^{\circ}_{complex} \qquad (6.6)$$

Such is usually the case with formation of outer-sphere complexes.[100] It is possible that lactate could undergo hydrogen bonding with the remaining water molecule in the primary hydration sphere, which could increase order in the system. As the spectroscopic measurements are not sensitive to outer-sphere complexation, these complexes cannot be completely ruled out without additional data. Therefore, supposition (2) is the most likely scenario for the observed small heats. That is, the measured heats are small because the equilibrium constant is also small, and the complex is likely an outer-sphere complex with $K_{111}<1$.

A reasonable theory that explains why inner-sphere ternary complexes do not form to a significant extent is that DTPA is simply too big to allow an additional bidentate ligand to form an inner-sphere complex. In Chapter 3 it was pointed out that the early, larger lanthanides (and Am) have approximately nine inner-sphere water molecules whereas the smaller, heavy lanthanides have approximately eight water molecules. It can be inferred from structural studies of the $Nd(DTPA)^{2-}$ and the $Gd(DTPA)^{2-}$ complexes,[101,102] which were shown to have one residual water molecule in the inner coordination sphere, that each ligating atom in DTPA displaces one water molecule in the lighter lanthanides. If this is true across the entire lanthanide series, this means that only one water molecule remains in the $Nd(DTPA)^{2-}$ and $Sm(DTPA)^{2-}$ complexes whereas no additional molecules are present in the $Ho(DTPA)^{2-}$ and $Er(DTPA)^{2-}$ complexes. In order to form a chelate with the binary $Ln(DTPA)^{2-}$ complexes, the oxalate or lactate ligand would have to displace two water molecules for complexation to occur. Clearly, such a requirement is not met for the $LnDTPA^{2-}$ complexes. Furthermore, the lactate and (especially) oxalate ligands, regardless of whether they bind in a monodentate or bidentate (chelating) fashion, would experience significant repulsion from the doubly negative $Ln(DTPA)^{2-}$ complex, which makes it more likely that outer-sphere complexes form.

Although the lactate and oxalate ligands are too large for the binary DTPA complexes, small ligands like F^- and CO_3^{2-} have been shown to form ternary complexes with $Ln(DTPA)^{2-}$. Burai et al.[103] investigated whether binary Gd complexes with DTPA and its cyclic analogue, 1,4,7,10-tetraazacyclododecane-1,4,7,10-tetraacetic acid DOTA), form ternary complexes in vivo with biologically relevant ligands such as carbonate, citrate, and phosphate. Their results showed that DTPA and DOTA formed ternary complexes with CO_3^{2-} and PO_4^{3-} at pH>8 but none were formed with the tridentate citrate at any pH.

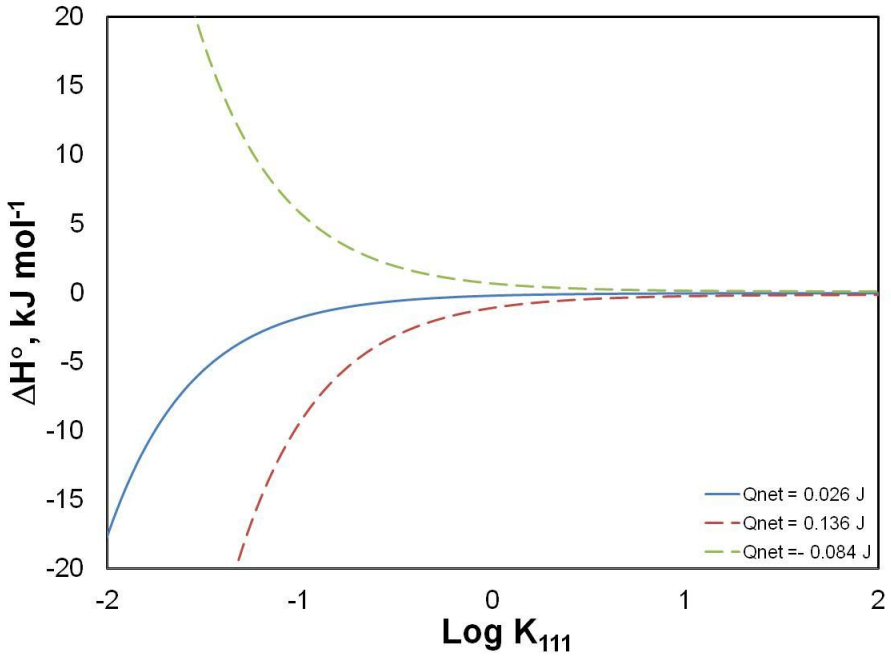

Figure 6.1 Estimated enthalpies associated with a range of Log K_{111} values. The values were calculated using the average measured heats from the Eu and Nd titrations, Q = +0.026 ± 0.110 J. The dotted lines represent the uncertainties in the calculated enthalpies accounting for the uncertainties in the measured heats at 95% confidence.

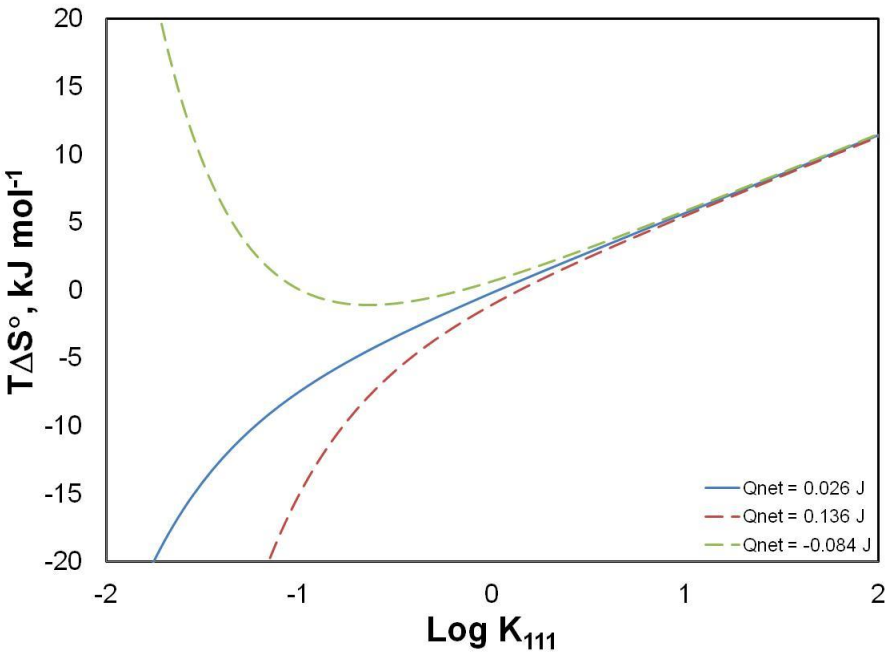

Figure 6.2 Calculated entropies determined from a range of Log K_{111} values and the associated enthalpy of complexation values.

6.1.1 Aqueous Ternary Complexes in the TALSPEAK Process

The lack of observed inner-sphere M(DTPA)(Lac)$^{3-}$ ternary complexes has important implications for the extraction thermodynamics of the TALSPEAK process. Nilsson and Nash[104] showed that Ln/Am distribution ratios calculated using currently available thermodynamic data *increase* above pH 3.5 – a trend opposite that observed for the experimental values under the same conditions. These experimental and calculated distribution ratios are shown in Figure 6.3. Based on these results, Nilsson and Nash concluded that a simple thermodynamic model using only binary complexes was incomplete. They postulated in their paper[104] that, among other possibilities, previously unidentified aqueous phase ternary complexes may be responsible for the observed decrease in the distribution ratios. Ternary M(DTPA)(Lac)$^{3-}$ complexes would compete with metal extraction by HDEHP as the pH rises because of the increasing free lactate concentration. Furthermore, these ternary complexes could explain the observed increase in Ln(III)/An(III) separation factors in the presence of lactic acid.[105] Therefore, investigation of the thermodynamics of aqueous ternary complexes under TALSPEAK-like conditions can determine whether these complexes are the culprit of the deviant distribution ratios at pH>3.5.

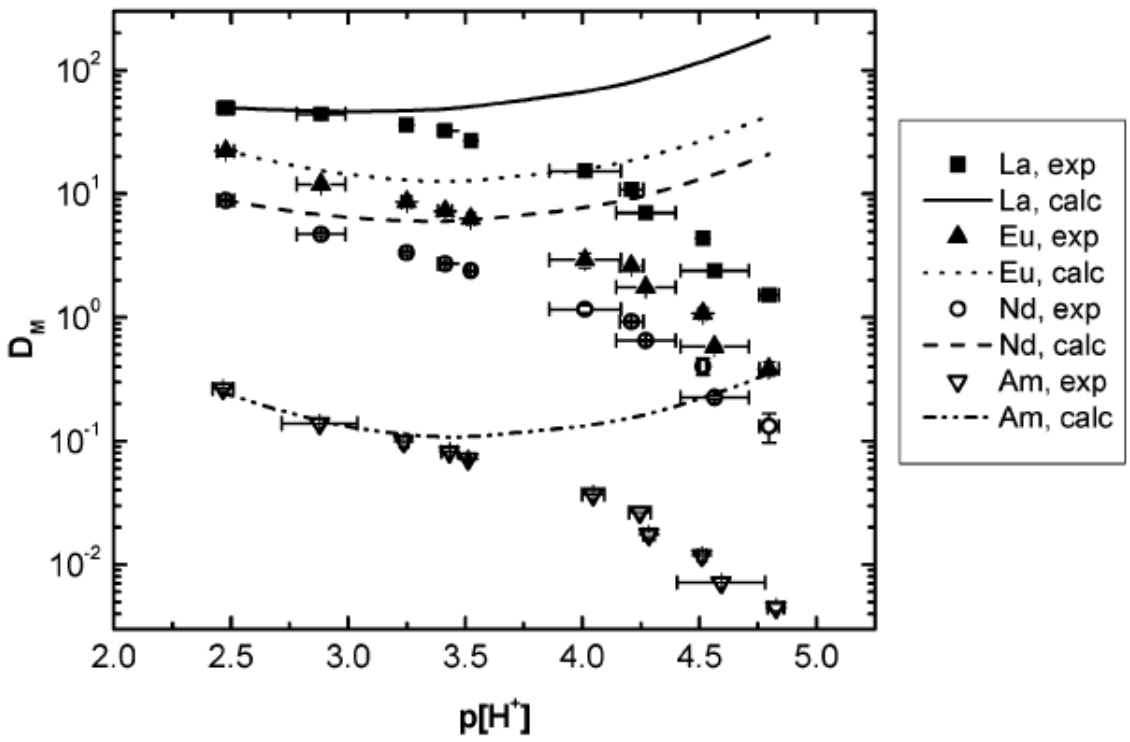

Figure 6.3 Comparison of calculated and experimentally determined distribution ratios as a function of pH as determined by Nilsson and Nash.[104] The experimental conditions they used were 1 M total lactate, 0.05 M total DTPA, 1 mM total Ln (including yttrium), 1 M total Na^+ in the aqueous phase. The organic phase contained 0.5 M HDEHP in, 1,4-diisopropylbenzene. Reprinted with permission from Taylor and Francis.

The extent to which ternary complexes affect the extraction thermodynamics of the TALSPEAK system can be gauged by calculating their effect on the theoretical distribution ratio. This can be achieved by extending the thermodynamic model used by Nilsson and Nash to account for the presence of aqueous ternary complexes. Their model consisted of aqueous phase equilibria for binary DTPA and lactate complexes with lanthanides and americium along with relevant protonation equilibria. The lanthanides and americium are present as the 1:1, 1:2, and 1:3 lactate complexes and as $M(DTPA)^{2-}$ and $M(HDTPA)^{-}$ complexes. For the case in which ternary complexes are present, the associated equilibrium is also included:

$$M^{3+} + nLac^{-} \leftrightarrow M(Lac)_n^{3-n} \qquad \beta_{1n} = \frac{[M(Lac)_n^{3-n}]}{[M^{3+}][Lac^{-}]^n} \tag{6.7}$$

$$M^{3+} + DTPA^{5-} \leftrightarrow M(DTPA)^{2-} \qquad \beta_1 = \frac{[M(DTPA)^{2-}]}{[M^{3+}][DTPA^{5-}]} \tag{6.8}$$

$$M^{3+} + DTPA^{5-} + H^{+} \leftrightarrow M(HDTPA)^{-} \qquad \beta_2 = \frac{[M(HDTPA)^{-}]}{[M^{3+}][DTPA^{5-}][H^{+}]} \qquad (6.9)$$

where *n* ranges from 1-3. DTPA is an octabasic acid while lactic acid is monobasic. The protonation equilibria is written as

$$H^{+} + Lac^{-} \leftrightarrow HLac \qquad K_{Lac} = \frac{[HLac]}{[H^{+}][Lac^{-}]} \qquad (6.10)$$

$$DTPA^{5-} + nH^{+} \leftrightarrow H_nDTPA^{n-5} \qquad \beta_{H_nDTPA} = \frac{[H_nDTPA^{n-5}]}{[DTPA^{5-}][H^{+}]^n} \qquad (6.11)$$

where *n* ranges from 1-8. In addition, the lanthanides and actinides were assumed to be extracted according to the following equilibrium:

$$M^{+3} + 3\overline{(HA)_2} \leftrightarrow \overline{M(AHA)_3} + 3H^{+} \qquad K_{ex} = \frac{[\overline{M(AHA)_3}][H^{+}]^3}{[M^{+3}][\overline{(HA)_2}]^3} \qquad (6.12)$$

where the overbars represent species in the organic phase, the species $(HA)_2$ represents the dimerized HDEHP extractant, and $M(AHA)_3$ represents the neutral extracted species $M(DEHP)_3(HDEHP)_3$; charges have been neglected for simplicity. For the system described by Equations 6.7-6.12, the distribution ratio is defined as follows:

$$D_{model} \equiv \frac{[M]_{tot,\ org}}{[M]_{tot,\ aq}} = \frac{[\overline{M(AHA)_3}]}{[M]+[M(Lac)]+[M(Lac)_2]+[M(Lac)_3]+[M(DTPA)]+[M(HDTPA)]} \qquad (6.13)$$

To include aqueous ternary $M(DTPA)(Lac)^{3-}$ complexes in the model requires that an additional term, [M(DTPA)(Lac)], be added to the denominator:

$$D_{ternary} = \frac{[\overline{M(AHA)_3}]}{[M]+[M(Lac)]+[M(Lac)_2]+[M(Lac)_3]+[M(DTPA)]+[M(HDTPA)]+[M(DTPA)(Lac)^{3-}]} \qquad (6.14)$$

Using Equations 6.7-6.12, the distribution ratios with and without ternary complexes can be rewritten in terms of free ligand concentrations, extraction constants, and equilibrium constants for complexation and protonation reactions. The resulting expression is complex and requires four additional mass balance equations to accurately determine the unknown free ligand concentrations. However, a few approximations can be made to simplify the equations:

1. The total metal concentration is sufficiently smaller than the concentrations of HDEHP and the aqueous complexants that their analytical ligand concentrations can be considered to be constant. Concentrations of the protonated ligand species are therefore governed by the aqueous phase pH.
2. The concentrations of the free metal and of the $M(Lac)_n$ species are significantly smaller than the binary DTPA complexes.
3. The major forms of DTPA present at pH 4 (TALSPEAK conditions) are H_3DTPA^{2-}, H_4DTPA^{-}, and H_5DTPA; the other forms may be neglected.

With these approximations, Equation 6.13 and 6.14 become

$$D = \frac{K_{ex}[(HA)_2]^3}{[H^+]^3} R \tag{6.15}$$

where

$$R = \left(\beta_1[DTPA^{5-}] + \beta_2[H^+][DTPA^{5-}] + \beta_1 K_{111}[Lac^-][DTPA^{5-}]\right)^{-1} \tag{6.16}$$

The third term in Equation 6.16 applies to the theoretical distribution ratio in which ternary complexes are present.

Figure 6.4 shows the effect of the $M(DTPA)(Lac)^{3-}$ complex – that is, of K_{111} – on the distribution ratios for europium that were calculated using existing thermodynamic data and Equations 6.14 and 6.15 at pH 4. The ordinate in the figure is $Log(D_{ternary}/D_{model}) = \Delta Log\ D$, which is the expected change in the theoretical distribution coefficient due to the presence of ternary lactate complexes. According to Figure 6.4, the depression of the calculated distribution ratio approaches is about 1 log unit – approximately the same depression as that noted in Figure 6.3 – when log K_{111} is approximately 1. However, in the previous section it was shown that the maximum value of the inner-sphere $M(DTPA)(Lac)^{3-}$ equilibrium constants is approximately 0.15, meaning that log $K_{111} \approx -0.82$. This value of K_{111} would only decrease the calculated distribution ratio by a factor of 0.042 log units. If the complexes formed are indeed outer-sphere complexes, the maximum value of K_{111} is 1, and the distribution ratios would decrease by 0.2 log units. It is clear that such a small decrease is not enough to substantially lower the calculated distribution ratios so that they agree with experimental values.

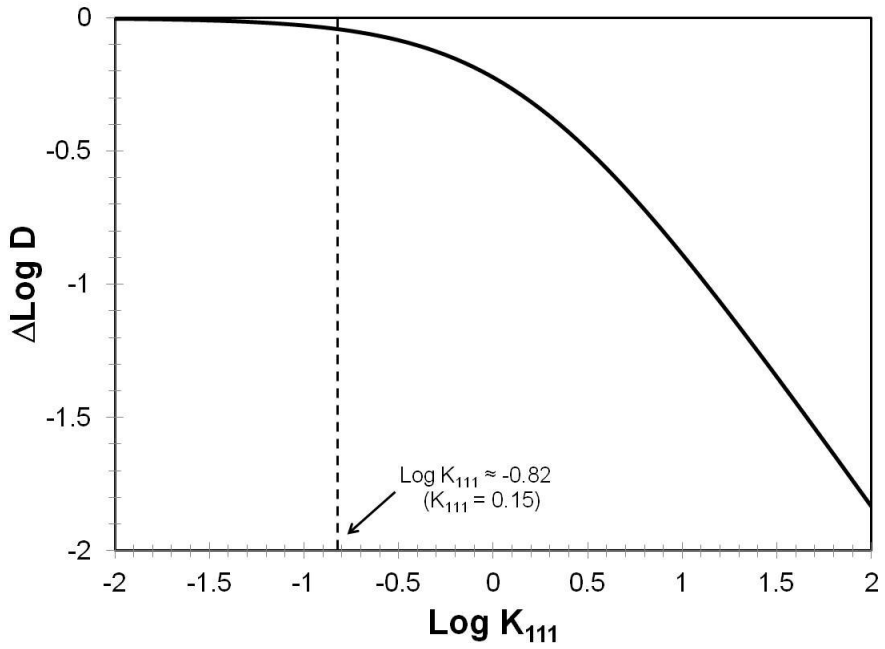

Figure 6.4 Calculated depression of distribution ratios due to formation of ternary complexes with a range of possible K_{111} values. The maximum estimated value of K_{111} based on spectroscopic experiments, K_{111} = 0.15, is highlighted on the plot. Plot was calculated for pH = 4, 1 mM total Eu, 50 mM total DTPA, 0.5 M HDEHP, and 1 M lactic acid with tabulated equilibrium constants for 25°C and 0.1 M ionic strength.

6.2 Ternary Complexes of $M(CDTA)^-$ with Oxalate, Malonate, and Iminodiacetate

Table 6.1 summarizes the equilibrium and overall stability constants for formation of M(CDTA)(L) (L=oxalate, malonate, iminodiacetate) complexes along with the literature values[55] of equilibrium constants for binary complexes formed with the primary and secondary ligands. In general, the ternary complex *stability* constants follow the same trend across the lanthanide series as the binary $M(L^1)$ complexes, increasing with decreasing ionic radius. However, this is due mainly to the fact that the differences in the equilibrium constants for $M(L^1)$ for adjacent lanthanides are larger than the difference in the equilibrium constants for adjacent $M(CDTA)(L^2)$ complexes. For example, the difference in the equilibrium constants for formation of the binary $Sm(CDTA)^-$ and $Nd(CDTA)^-$ complexes is $\Delta\log K_{110} = 0.75$ while the largest difference in the corresponding ternary complexes across the entire lanthanide series is $\Delta\log K_{111} = 0.29$ for the IDA complexes. From a practical standpoint, since most of the larger polyaminocarboxylates have similar binding constants for Am^{3+} and Cm^{3+}, it is more useful to explore the relationship between the log K_{101} and log K_{111} values rather than the relationship between log β_{111} and log K_{101}.

Table 6.1 Overall Stability Constants for Formation of Ternary Complexes

Ternary Complex	Log K_{110} *†	Log K_{101} ‡	Log K_{111}	Log β_{111}
$Nd(CDTA)(Ox)^{3-}$	17.86	Insoluble	2.54 ± 0.03	20.4 ± 0.03
$Sm(CDTA)(Ox)^{3-}$	18.61	n/a	2.67 ± 0.04	21.3 ± 0.04
$Tb(CDTA)(Ox)^{3-}$	19.22	5.45	2.76 ± 0.02	22.0 ± 0.02
$Ho(CDTA)(Ox)^{3-}$	19.80	n/a	2.92 ± 0.03	22.7 ± 0.03
$Er(CDTA)(Ox)^{3-}$	20.08	n/a	2.93 ± 0.01	23.0 ± 0.01
$Am(CDTA)(Ox)^{3-}$	18.20	4.62 ± 0.01	2.78 ± 0.13	21.0 ± 0.13
$Nd(CDTA)(Mal)^{3-}$	17.86	3.38	1.19 ± 0.04	19.1 ± 0.04
$Sm(CDTA)(Mal)^{3-}$	18.61	3.67	1.25 ± 0.07	19.9 ± 0.07
$Ho(CDTA)(Mal)^{3-}$	19.80	3.83	1.30 ± 0.04	21.1 ± 0.04
$Er(CDTA)(Mal)^{3-}$	20.08	3.83	1.31 ± 0.05	21.4 ± 0.05
$Nd(CDTA)(IDA)^{3-}$	17.86	6.50	3.43 ± 0.05	21.3 ± 0.05
$Sm(CDTA)(IDA)^{3-}$	18.61	6.64	3.72 ± 0.03	22.3 ± 0.03
$Ho(CDTA)(IDA)^{3-}$	19.80	6.97	3.18 ± 0.04	23.0 ± 0.04
$Er(CDTA)(IDA)^{3-}$	20.08	7.09	3.00 ± 0.08	23.1 ± 0.08

*T = 25°C, μ = 0.5 M, Na^+ salt as background electrolyte. Equilibrium constants obtained from the Critical Stability Constants database, reference 52. †Equilibrium and stability constants are tabulated as Log $K_{ML_1L_2}$ and as Log $\beta_{ML_1L_2}$, respectively. ‡Equilibrium constants for μ = 1 M, T = 25°C except for $Tb(Ox)^+$, which is for μ = 0.1 M, 25 °C. Data obtained from reference 52.

Three trends are immediately evident upon comparison of the log K_{101} and log K_{111} values. First, the ternary complex equilibrium constants are substantially weaker than the corresponding 1:1 binary complexes with the secondary ligands. Second, with the exception of the IDA complexes, the trend in the ternary complex equilibrium constants across the lanthanide series is similar to the trend in the stability of the respective binary complexes. Third, the order of stability of the ternary complexes is IDA > oxalate > malonate.

In order to explain the first trend, it is helpful to compare the structure of the metal ion with the secondary ligand when forming both complexes. For the sake of example, the malonate ligand will be used for the comparison. When Mal^{2-} approaches the metal center in the absence of a polyaminocarboxylate ligand, the charge on the metal-aquo cation is tripositive. Therefore, a stronger, favorable electrostatic interaction is expected to occur between Mal^{2-} and Ln^{3+}. On the other hand, the reaction of Mal^{2-} with $Ln(CDTA)^-$ involves the interaction of a dianion with a

monoanion, which is a much less favorable interaction due to repulsion of the anions. In fact, the equilibrium constant for formation of the binary complex, $Ln(Mal)_3^{3-}$, from $Ln(Mal)_2^-$ is very similar to the ternary complex equilibrium constant for formation of $Ln(CDTA)(Mal)^{3-}$ from $Ln(CDTA)^-$. Table 6.2 compares the measured ternary complex equilibrium constants with those of the $Ln(Mal)_3^{3-}$ complexes from the literature.

Table 6.2 Comparison of Binary and Ternary Equilibrium Constants

Complexation Reaction*	Log K†
$Ho(Mal)_2^- + Mal^{2-} \leftrightarrow Ho(Mal)_3^{3-}$	1.33
$Ho(CDTA)^- + Mal^{2-} \leftrightarrow Ho(CDTA)(Mal)^{3-}$	1.30 ± 0.04
$Er(Mal)_2^- + Mal^{2-} \leftrightarrow Er(Mal)_3^{3-}$	1.23
$Er(CDTA)^- + Mal^{2-} \leftrightarrow Er(CDTA)(Mal)^{3-}$	1.31 ± 0.05
$Tb(Ox)_2^- + Ox^{2-} \leftrightarrow Tb(Ox)_3^{3-}$	3.80
$Tb(CDTA)^- + Ox^{2-} \leftrightarrow Tb(CDTA)(Ox)^{3-}$	2.76
$Am(Ox)_2^- + Ox^{2-} \leftrightarrow Am(Ox)_3^{3-}$	3.73
$Am(CDTA)^- + Ox^{2-} \leftrightarrow Am(CDTA)(Ox)^{3-}$	2.78
$Ho(IDA)_2^- + IDA^{2-} \leftrightarrow Ho(IDA)_3^{3-}$	4.31
$Ho(CDTA)^- + IDA^{2-} \leftrightarrow Ho(CDTA)(IDA)^{3-}$	3.18 ± 0.04

*Binary complexation reactions shown are from available data in the NIST Critical Stability Constant Database.[52] Uncertainties in NIST data are shown where available. †T = 25°C, μ = 1 M, Na^+ salt as background electrolyte.

Similar comparisons of the stepwise equilibrium constants for formation of the $Am(Ox)_3^{3-}$, $Tb(Ox)_3^{3-}$, and the $Ho(IDA)_3^{3-}$ complexes with their respective ternary $M(CDTA)(L^2)$ complexes reveals that the ternary complexes are substantially weaker. This appears to indicate that steric effects play a more important role in the formation of $M(CDTA)(Ox)^{3-}$ and $M(CDTA)(IDA)^{3-}$ complexes.

The fact that the order of complexing strength of ternary $Ln(CDTA)(L^2)$ complexes decreases in the order IDA > oxalate > malonate – a trend that exists with the simple binary

complexes as well – is an indication that formation of ternary complexes with dicarboxylic acids is partially dependent upon the size of the rings formed. It is well known that IDA and oxalate both form five-membered rings whereas malonate only forms six-membered rings under ideal conditions. Hancock[106] used molecular mechanics to show that the bond strain in complexes is minimized when five-membered ring complexes are formed with "large" metal cations (e.g., lanthanides). Six-membered rings, however, are weaker because of the increased strain caused by shorter metal-ligand bonds and non-ideal bite angles in such a ring. Choppin, Dadgar, and Rizkalla[107] investigated the thermodynamics of binary complex formation with simple dicarboxylic acids and showed that the strength of binary polyaminocarboxylates becomes successively weaker as the ring size of the complex increases from five to nine.

6.2.1 Thermodynamics of the LnCDTA-Oxalate System

Comparison of the thermodynamic parameters for formation of ternary $Ln(CDTA)(L^2)^{3-}$ complexes can provide additional insights into the potential causes of the trends noted above. Table 6.3 tabulates the thermodynamics of the M-CDTA-oxalate systems. For visual clarity, these thermodynamic parameters are plotted as functions of the inverse ionic radius for each metal studied in Figure 6.5.

Table 6.3 Thermodynamics of the Ln-CDTA-Ox System

Ternary Complex	Log K_{111}	$-\Delta G°$, kJ mol^{-1}	$\Delta H°$, kJ mol^{-1}	$\Delta S°$, J mol^{-1} K^{-1}
$Nd(CDTA)(Ox)^{3-}$	2.54 ± 0.03	14.5 ± 0.17	-8.70 ± 0.21	19 ± 1
$Sm(CDTA)(Ox)^{3-}$	2.67 ± 0.04	15.2 ± 0.23	-7.74 ± 0.71	25 ± 3
$Tb(CDTA)(Ox)^{3-}$	2.76 ± 0.02	15.8 ± 0.11	-11.46 ± 0.75	15 ± 3
$Ho(CDTA)(Ox)^{3-}$	2.92 ± 0.03	16.67 ± 0.17	-9.87 ± 0.71	23 ± 2
$Er(CDTA)(Ox)^{3-}$	2.93 ± 0.01	16.73 ± 0.06	-11.63 ± 0.71	17 ± 2
$Am(CDTA)(Ox)^{3-}$	2.78 ± 0.13	15.9 ± 0.74	-8.46 ± 0.13	25 ± 3

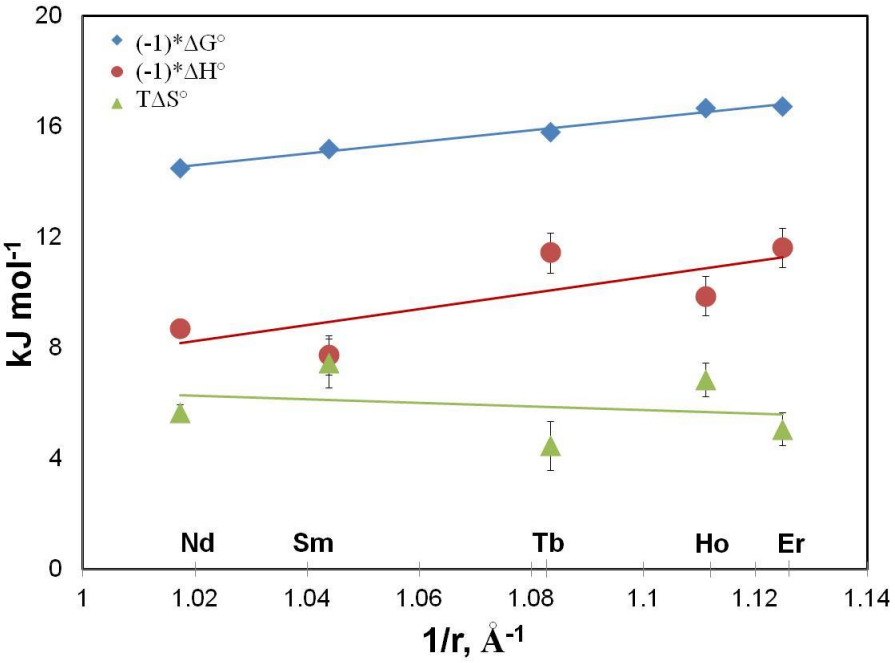

Figure 6.5 Comparison of thermodynamic parameters for the formation of $Ln(CDTA)(Ox)^{3-}$ complexes. Lines shown represent best fit lines. Error bars are shown for all data points but some are not visible due to the size of the pictograms used to label the data points.

The free energies of $Ln(CDTA)(Ox)^{3-}$ complexes indicate a slowly increasing thermodynamic stability from neodymium to erbium. As shown in Figure 6.5, as the ionic radius decreases, the Gibbs free energy of complexation increases almost linearly. This is expected since the charge density of the cation increases towards the heavier lanthanides and, assuming that the bonding is primarily electrostatic, results in stronger complexes with anionic ligands as long as steric requirements are satisfied. The formation of the complexes is favored by negative enthalpies and positive entropies. Since the enthalpies of dehydration, which are endothermic, are very similar across the lanthanide series,[108] the increase in the measured exothermic enthalpies is due mostly to increasing strengths of the ionic bonds. Assuming that the total entropy change is influenced primarily by dehydration, the fact that the entropies are fairly similar and positive appears to indicate that the same number of water molecules (two) is displaced from the inner coordination sphere upon coordination with the lanthanides. Results from fluorimetric titrations of $Tb(CDTA)^-$ with oxalate corroborate this conclusion; based on lifetime measurements, the number of water molecules decreased from 2.07 ± 0.5 water molecules in $Tb(CDTA)^-$ to 0.51 ± 0.5 water molecules in the $Tb(CDTA)(Ox)^{3-}$ complex, meaning that within error, between one and two water molecules were displaced upon complexation. The lower stability of the $Ln(CDTA)(Ox)^{3-}$ complexes compared to the $Ln(Ox)_3^{3-}$ complexes may be due to increased steric hindrance in the bulky $Ln(CDTA)^-$ complexes, which reduces the approach of the oxalate ligand. A second possibility is that, although two water molecules are presumably displaced upon complexation, the oxalate ligand is binding to the $M(CDTA)^-$ complex in a monodentate fashion.

The $Am(CDTA)(Ox)^{3-}$ complex is unexpectedly closer in stability to the $Tb(CDTA)(Ox)^{3-}$ complex than the $Nd(CDTA)(Ox)^{3-}$ complex even though the ionic radius of

Am^{3+} (98.0 pm) is closer to that of Nd^{3+} (98.3 pm). Even within error, the $Am(CDTA)(Ox)^{3-}$ complex is closer in stability to $Sm(CDTA)(Ox)^{3-}$. Enhancements in the thermodynamic stability of Am(III) complexes versus Nd(III) complexes normally have been observed with soft donor ligands and have been attributed to an increased covalent contribution to the total bonding. However, the difference between the stability constants of $Am(CDTA)(Ox)^{3-}$ and $Nd(CDTA)(Ox)^{3-}$ (approximately 0.24 log units) is small enough that it may be due to the difference in the method used to measure the americium and neodymium complex stability constants, not increased covalence in the Am-O bond.

Though ternary complexes with polyaminocarboxylates are not as well-studied as the analogous binary complexes, some literature data exists that is useful for comparison. Király and co-workers[109] measured the stability constants of $Ln(EDTA)(Ox)^{3-}$ complexes using potentiometry. The trend in the stability of $Ln(EDTA)(Ox)^{3-}$ complexes is similar to, but not as monotonic as that of the $Ln(CDTA)(Ox)^{3-}$ complexes discussed in this work. The values are tabulated in Table 6.4 below. Note that the equilibrium constants from Király et al. were measured at 0.1 M ionic strength. Since equilibrium constants tend to decrease as a function of the ionic strength (up to about 2 M), it is likely that at 1 M ionic strength, the $Ln(EDTA)(Ox)^{3-}$ complexes would be weaker than the $Ln(CDTA)(Ox)^{3-}$ complexes at the same ionic strength. This is evident for the Ho complex whose stability is higher than the $Ln(EDTA)(Ox)^{3-}$ complexes without taking into account the ionic strength discrepancies.

Choppin and coworkers[110] investigated the thermodynamics of a series of ternary complexes with hexadentate ligands (EDTA, CDTA) and smaller dicarboxylic acids (iminodiacetate, oxydiacetate, oxalate) at 0.1 M ionic strength. They also reported that the $M(CDTA)(Ox)^{3-}$ complexes were stronger than the $M(EDTA)(Ox)^{3-}$ complexes. However, their EXAFS studies with europium indicated that both $Eu(CDTA)(Ox)_2^{5-}$ and $Eu(EDTA)(Ox)_2^{5-}$ complexes formed. The results showed that in these complexes, either a nitrogen atom or a carboxylate from the primary ligand (CDTA, EDTA) was displaced by the second oxalate ligand to maintain the oxalate ligand's bidentate chelating mode. There were no thermodynamic data presented for the $Ln(L^1)(Ox)_2^{5-}$ complexes.

No evidence of an $Ln(CDTA)(Ox)_2^{5-}$ complex was observed in this work. Solutions containing up to a seven-fold excess of oxalate showed no spectroscopic evidence of $Ln(CDTA)(Ox)_2^{5-}$, which does not agree with the results presented by Choppin et al. However, the experiments conducted by Choppin et al. were solvent extraction studies using very low concentrations ($1x10^{-7}$ M or less) of Eu and CDTA or EDTA with oxalate concentrations that were 3-4 orders of magnitude higher. These conditions could not be obtained in the spectrophotometric titrations.

Table 6.4 Comparison of Equilibrium Constants of the $Ln(CDTA)(Ox)^{3-}$ and the $Ln(EDTA)(Ox)^{3-}$ Complexes

Lanthanide	Log K_{111}, $(Ln(CDTA)(Ox)^{3-})$	Log K_{111},* $(Ln(EDTA)(Ox)^{3-})$
Nd	2.54	3.00
Sm	2.67	3.25
Tb	2.76	3.07
Ho	2.92	2.80
Er	2.93	3.05

*Values obtained from reference 109 at 0.1 M ionic strength.

6.2.2 Thermodynamics of the LnCDTA-Malonate System

Table 6.5 and Figure 6.6 show the thermodynamics for formation of the $Ln(CDTA)(Mal)^{3-}$ system. The equilibrium constants for the $Ln(CDTA)(Mal)^{3-}$ complexes are weaker than the oxalate complexes and, although similar patterns of increasing stability are noted with the malonate and oxalate complexes, the increase across the series is less pronounced. Between neodymium and erbium, the equilibrium constant changes by only 0.12 log units as opposed to 0.39 log units with oxalate complexes. Therefore, the Gibbs free energy of complexation remains fairly constant across the lanthanide series. However, unlike the oxalate or IDA complexes, the reactions are *entropy-driven* and have *endothermic* enthalpies. Thus, it is likely that the contribution to the total enthalpy due to electrostatic interactions is smaller than the enthalpy of dehydration: the displacement of water molecules serves to push the reaction forward.

The entropies increase very slowly until holmium is reached, at which point they begin to decrease again. Interestingly, the same trend is noted with the binary $Ln(Mal)_3^{-3}$ complexes, as shown in Table 6.6. Furthermore, the entropies of complexation are similar to those measured for the analogous $Ln(CDTA)(Ox)^{3-}$ complexes. Since two water molecules are released during formation of $Ln(CDTA)(Ox)^{3-}$ complexes, it is reasonable to propose that two water molecules are also released upon formation of $Ln(CDTA)(Mal)^{3-}$ complexes.

Although the equilibrium constants for the $Ln(CDTA)(Mal)^{3-}$ and the $Ln(Mal)_3^{3-}$ complexes are similar (Table 6.2), the entropies of complexation for binary $Ln(Mal)_3^{3-}$ complexes are about twice that of the $Ln(CDTA)(Mal)^{3-}$ complexes and the enthalpies of complexation of the $Ln(Mal)_3^{3-}$ complexes are substantially more endothermic. In other words, the $Ln(CDTA)(Mal)^{3-}$ complex is more ordered with a more exothermic enthalpy.

Table 6.5 Thermodynamics of the Ln-CDTA-Mal System

Ternary Complex	Log K_{111}	$-\Delta G°$, kJ mol^{-1}	$\Delta H°$, kJ mol^{-1}	$\Delta S°$, J mol^{-1} K^{-1}
$Nd(CDTA)(Mal)^{3-}$	1.19 ± 0.04	6.79 ± 0.23	-1.23 ± 0.14	19 ± 1
$Sm(CDTA)(Mal)^{3-}$	1.25 ± 0.07	7.14 ± 0.40	+1.14 ± 0.26	28 ± 2
$Ho(CDTA)(Mal)^{3-}$	1.30 ± 0.04	7.42 ± 0.23	+1.06 ± 0.16	28 ± 1
$Er(CDTA)(Mal)^{3-}$	1.31 ± 0.05	7.48 ± 0.29	+0.264 ± 0.17	26 ± 1

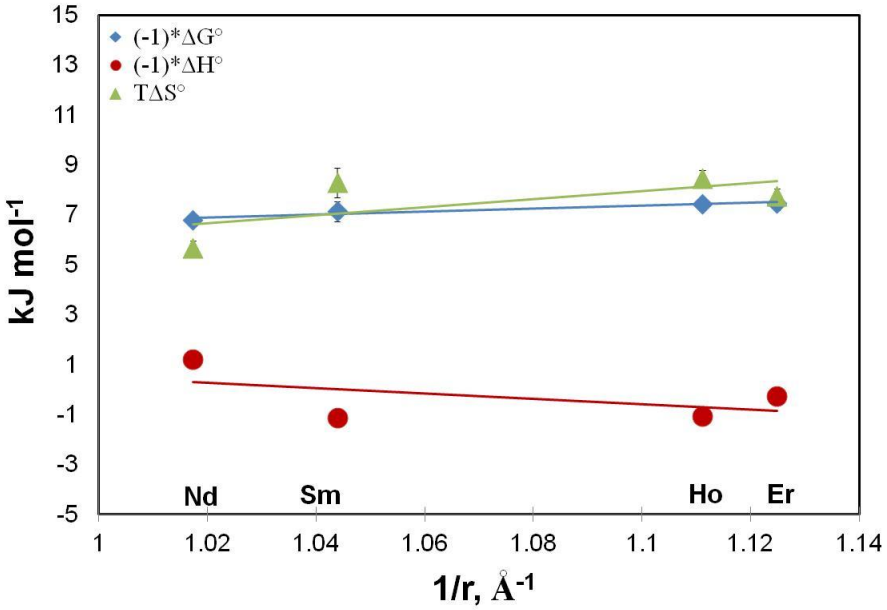

Figure 6.6 Thermodynamics of the Ln-CDTA-Mal System. Error bars are shown for all data points but some are not visible due to the size of the pictograms used to label data points.

Table 6.6 Comparison of the Enthalpy and Entropy Contributions of Binary $Ln(Mal)_2^-$ Complexes with $Ln(CDTA)^-$ Complexes

Complexation Reaction*	ΔH°, kJ mol^{-1}	ΔS°, J mol^- K^{-1}
$Ho(Mal)_2^- + Mal^{2-} \leftrightarrow Ho(Mal)_3^{3-}$	+8.0	+52
$Ho(CDTA)^- + Mal^{2-} \leftrightarrow Ho(CDTA)(Mal)^{3-}$	+1.06 ± 0.16	+28 ± 1
$Er(Mal)_2^- + Mal^{2-} \leftrightarrow Er(Mal)_3^{3-}$	+6.7	+46
$Er(CDTA)^- + Mal^{2-} \leftrightarrow Er(CDTA)(Mal)^{3-}$	+0.264 ± 0.17	+26 ± 1

6.2.3 Thermodyamics of the LnCDTA-IDA System

The complexation thermodynamics of the $Ln(CDTA)(IDA)^{3-}$ system (Table 6.7, Figure 6.7) indicate that a more delicate interplay exists between electrostatic interactions and steric requirements of these complexes. For this system, the stability constants increase from neodymium to samarium and, at some point between samarium and holmium, the stability constants begin to decrease again. By the time holmium is reached, the resulting complex formed is thermodynamically weaker than the neodymium complex. Although the enthalpies of complexation continue to increase across the lanthanide series, the initially favorable entropies decrease almost concomitantly until they become unfavorable. Clearly, the influence of steric requirements on formation of ternary complexes is more important for the IDA system than for the malonate or oxalate systems. The iminodiacetate ligand typically replaces three water molecules in order to bond through both carboxylate oxygens and nitrogen to the metal center. This is a relatively easy task to accomplish with the larger lanthanides whose binary $Ln(CDTA)^-$ complexes have three residual water molecules. However, beyond samarium, the coordination numbers of the lanthanides slowly progresses towards octacoordination, meaning that there are no longer three residual water molecules available. Therefore, in order to form a ternary complex with $Ho(CDTA)^-$ or $Er(CDTA)^-$, the IDA ligand could undergo one of three types of binding with the metal center: a.) binding of one oxygen atom from each of the two carboxylate groups upon displacement of two water molecules, b.) binding of the central nitrogen atom and an oxygen atom from one of the two carboxylates with displacement of two water molecules, or c.) formation of a bridging complex with the IDA ligand.

Table 6.7 Thermodynamics of the Ln-CDTA-IDA System

Ternary Complex	Log K_{111}	$-\Delta G°$, kJ mol^{-1}	$\Delta H°$, kJ mol^{-1}	$\Delta S°$, J mol^{-1} K^{-1}
Nd(CDTA)(IDA)$^{3-}$	3.43 ± 0.05	19.6 ± 0.29	-10.21 ± 0.81	31 ± 3
Sm(CDTA)(IDA)$^{3-}$	3.72 ± 0.03	21.2 ± 0.17	-19.78 ± 0.29	5 ± 1
Ho(CDTA)(IDA)$^{3-}$	3.18 ± 0.04	18.2 ± 0.23	-27.20 ± 0.55	-30 ± 2
Er(CDTA)(IDA)$^{3-}$	3.00 ± 0.08	17.1 ± 0.46	-30.33 ± 0.67	-44 ± 3

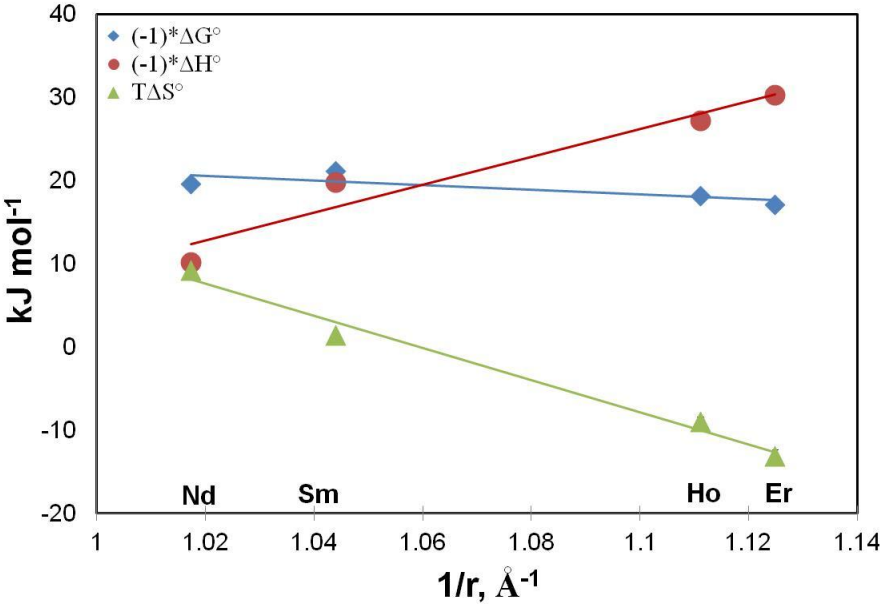

Figure 6.7 Thermodynamics of the Ln-CDTA-IDA system. Error bars are included but are not visible due to the size of the pictograms used to label the data points.

If an oxygen atom from each of the terminal carboxylates were to bind with the metal, an eight-membered ring would result. Based on the calculated stability constants for ternary malonate complexes from this work and on literature values for binary malonate complexes, it is likely that such a ring would be very weak. The equilibrium constant for pentanedioic acid (glutaric acid), which forms an eight-membered ring complex, is weaker than that for malonic acid.[52] Therefore, scenario (a) is possible, but not likely. Binding of the central nitrogen atom and a pendant carboxylate oxygen leads to a five-membered ring with a dangling acetate group. This acetate group could undergo hydrogen bonding with the surrounding water molecules, which would increase the order of the system, accounting for the decrease in entropy of the

system. Such a complex would be essentially equivalent to forming a complex with glycine (aminoacetic acid). Lastly, the iminodiacetate ligand could form a bridging complex between two $Ln(CDTA)^-$ moieties of the form [Ln(CDTA)-(IDA)-Ln(CDTA)]. Formation of this type of complex would decrease the overall entropy of the system and can be fairly strong complexes.

The enhanced stability of the $Ln(CDTA)(IDA)^{3-}$ complexes compared to the $Ln(CDTA)(Ox)^{3-}$ complexes for the lighter lanthanides (Nd, Sm) is likely due to the fact that the iminodiacetate ligand, which contains an additional nitrogen atom, is more basic than the oxalate ligand, indicating that ligand basicity is an important factor for ternary complex formation when similar steric effects are present. The influence of ligand basicity is also evident when the equilibrium constants of oxydiacetate, the oxygen analog of iminodiacetate, are compared. Replacement of the more basic nitrogen atom with an oxygen atom lowers the equilibrium constant for the associated ternary complex even though three water molecules are still released.[110]

6.2.4 Comparison of $Ln(CDTA)(L^2)^{3-}$ and $Ln(DO3A)(L^2)^{2-}$ Complexes

Although ternary complex equilibrium constants are the only thermodynamic data available for the DO3A system, some additional insights can be gained by comparing ternary complexes of DO3A and CDTA formed with neodymium or erbium and the same secondary ligand. Comparison of the oxalate, malonate, and IDA equilibrium constants with DO3A and CDTA for the same metal shows that, with the exception of the malonate complexes, the equilibrium constants for the ternary complexes are very similar for the same system. Several factors are likely responsible for the observed difference. First, neodymium and erbium represent lanthanides at the two opposite extremes of hydration states – that is, Nd has nine inner-sphere water molecules and Er has eight inner-sphere water molecules. Therefore, in complexes with heptadentate DO3A, the Nd(DO3A) complex has two residual water molecules while Er(DO3A) only has one residual water molecule. In contrast, the $Nd(CDTA)^-$ complex has three water molecules while $Er(CDTA)^-$ has two. Second, the M(DO3A) complexes are electrically neutral whereas the $M(CDTA)^-$ complexes possess a negative charge. A dianion experiences a higher repulsion from a negatively charged complex than from a neutral complex. Third, the dicarboxylates may have different coordination modes (e.g., bidentate vs tridentate) or otherwise bind differently with the M(DO3A) complexes compared to the $M(CDTA)^-$ complexes, as postulated below for the IDA and oxalate complexes. The ternary complex equilibrium constants are re-tabulated in Table 6.8 below.

Table 6.8 Equilibrium Constants for Ternary $Ln(DO3A)(L^2)^{2-}$ Complexes

Ternary Complex	Log K_{101} †	Log K_{111}
$Nd(DO3A)(Mal)^{2-}$	3.38	1.79 ± 0.02
$Nd(DO3A)(IDA)^{2-}$	6.50	3.55 ± 0.05
$Er(DO3A)(Ox)^{2-}$	n/a	2.93 ± 0.05
$Er(DO3A)(Mal)^{2-}$	3.83	1.68 ± 0.03

*T = 25°C, μ = 1 M, Na^+ salt as background electrolyte. †Equilibrium constants are tabulated as Log $K_{M(L^1)(L^2)}$ for μ = 1 M, T = 25°C. Log K_{101} values were obtained from reference 52.

As stated in the previous section, iminodiacetate normally displaces three water molecules in order to form two five-membered rings. Therefore, in the $Nd(CDTA)(IDA)^{3-}$ complex, three water molecules have likely been displaced to form the complex. On the other hand, the Nd(DO3A) complex has one fewer water molecule. In order to form the ternary complex with IDA, either an eight-membered ring is formed with an oxygen from the two terminal carboxylate groups on IDA or a five-membered ring complex is formed via participation of one carboxyl oxygen and the amine. In general, complexes involving eight-membered rings are much less stable than five-membered rings. It is therefore more likely that IDA behaves like a bidentate ligand with the Nd(DO3A) complex and as a tridentate ligand with the $Nd(CDTA)^-$ complex. The additional stability of the $Nd(DO3A)(IDA)^{2-}$ complex compared to $Nd(CDTA)(IDA)^{3-}$ likely stems from the difference in the charge of the complexes.

The $Er(CDTA)(Ox)^{3-}$ and the $Er(DO3A)(Ox)^{2-}$ complexes are of the same thermodynamic stability within error (as is $Er(CDTA)(IDA)^{3-}$). Based on the similarity of the equilibrium constants and the evidence from $Tb(CDTA)^-$ fluorescence measurements that oxalate binds in a bidentate fashion to $Ln(CDTA)^-$ complexes, it can be postulated that the oxalate ligand also binds in a bidentate fashion to Er(DO3A). However, in order to do so, either two of the pendant acetate arms of DO3A or a water molecule and a pendant acetate arm of DO3A would need to be displaced in order for oxalate to fit. It is doubtful that oxalate binds with Er(DO3A) in a monodentate fashion because the stability constant is too large.

Although there is no data for the $Er(DO3A)(IDA)^{2-}$ complex, assuming that Er(DO3A) has a single water molecule, if ternary complex formation occurs, it would likely entail displacement of at least one acetate arm from the DO3A ligand in order to fit. By comparison, the formation of the $Er(CDTA)(IDA)^{3-}$ complex was accompanied by a net *decrease* in disorder; it was discussed earlier that one way of achieving this was to displace the two water molecules and bind in a bidentate fashion. Perhaps the displacement of an acetate arm and a water molecule will similarly allow the formation of ternary $Er(DO3A)(IDA)^{2-}$ complexes.

Binary DO3A complexes have a limited number of secondary ligands with which it can bind strongly because most of the region around the metal center is occupied. Therefore, multidentate ligands may be forced to form complexes with reduced denticity and stability. However, this does not preclude the use of bulky septadentate ligands for separations processes. Although M(DO3A) complexes likely react with several types of secondary ligands, modification of the structure of the primary ligand may provide enhanced selectivity. Aime et

al.[111] used NMR relaxometry to study ternary lactate complexes with gadolinium and a series of modified DO3A ligands. These substituted ligands were of varying basicities and imparted different charges to the resulting binary complex. They showed that the binary complex with the most positive charge formed the most stable ternary complex with lactate with a binding constant nearly sixty times higher than the corresponding $Gd(DO3A)(Lac)^-$ complex. This binary complex contained a modified DO3A ligand whose acetate groups were replaced with neutral acetamide (i.e., $-CH_2C(O)NH_2$) groups. The replacement of one of the carboxylate oxygens with the more basic nitrogen atom may have also contributed to the increased stability.

6.2.5 A Size-Based Approach to Separating Americium from Curium: Can It Work?

The overall objective of this work was to investigate some of the factors that influence the formation of ternary complexes comprised of large polyaminocarboxylates and small dicarboxylic acids to determine whether a size-based approach can be used to separate americium from curium. An important result from the DTPA studies is that the TALSPEAK process cannot be modified without changing the primary ligand. The magnitude of the work that would be required to redesign the TALSPEAK process to separate americium from curium *and the lanthanides* using a different polyaminocarboxylate and dicarboxylic acid makes such a task prohibitive. Therefore, the size-based approach to separating americium and curium would need to be carried out in a separate solvent extraction step.

The factors that affect the trends in the thermodynamic stabilities of ternary complexes are very difficult to control for two ligands. For example, in section 6.2, it was pointed out that the trend in the stability constants for the $Ln(CDTA)(L^2)$ complexes was governed primarily by the strength and rigidity of the primary ligand while the influence of the secondary ligands on overall complex stability was comparatively small. Even though patterns of increasing or decreasing stability were observed for the secondary ligands, the total stability was governed more by the stability and rigidity of the primary ligand. A possible option would be to use stronger secondary ligands but it is difficult to choose a secondary ligand that does not compete with the primary aminopolycarboxylate and at the same time is of the correct size and basicity. Therefore, separation of Am from Cm using the aminopolycarboxylate-dicarboxylate combination is not likely to work.

A potentially easier task may be to design a single rigid ligand that incorporates soft ligating atoms to achieve the An(III)/Ln(III) selectivity that is also the right size to discriminate against curium. Another approach is to use ternary complexes in the *organic* phase to selectively extract americium. Geist et al.[112] have already conducted a laboratory-scale solvent extraction demonstration using a synergistic mixture of a soft donor ligand and a hard ligand to recover Am(III), Cm(III), and Cf(III) from an acidic solution containing trivalent lanthanides, americium, curium, and californium. Subsequent steps led to recovery of 99.8% of the total Am(III), which only had 0.47% Cm(III) contamination. Thus, modification of the organic phase may represent a useful application of ternary complexes to separate americium from curium.

Chapter 7 Conclusions

Spectroscopic, thermometric, and calorimetric techniques were used to search for evidence of ternary complexation and to quantify the thermodynamics of those complexes that form. Several important thermodynamic insights were gained from the investigations of binary DTPA, DO3A, and CDTA complexes with the smaller lactate, oxalate, malonate, and iminodiacetate ligands. Investigations with DTPA revealed that octadentate ligands are too big to form significant concentrations of inner-sphere ternary complexes with the lactate and oxalate ligands at 1 M ionic strength. Although evidence of inner-sphere ternary $M(DTPA)(Lac)^{3-}$ or $M(DTPA)(Ox)^{3-}$ complexes was not observed in this work, the spectrophotometric titration data were used to calculate a maximum value of K_{111} for the inner-sphere $M(DTPA)(Lac)^{3-}$ complex ($K_{111} \leq 0.15$) and for the $M(DTPA)(Ox)^{3-}$ complex ($K_{111} \leq 3.58$). Furthermore, results from thermometric titrations with lactate were used to show that $M(DTPA)(Lac)^{3-}$ complexes likely have a non-zero, exothermic enthalpy of formation and a negative entropy of formation, which is indicative of the formation of an outer-sphere complex. If such an outer-sphere complex formed, the only way that it can have an exothermic enthalpy and negative entropy of formation is if the equilibrium constant for formation of the complex is less than one. The techniques used in this work were not able to rule out the possibility of outer-sphere complexes.

Another important consequence of this result is that the concentrations of the proposed outer-sphere $M(DTPA)(Lac)^{3-}$ complexes that may be present in the existing TALSPEAK process are not high enough to significantly reduce the calculated distribution coefficients at pH>3.5 such that they agree with experimentally-determined values. Nevertheless, the understanding of the roles that lactic acid plays in the TALSPEAK process is far from complete. For example, the high concentrations of lactic acid used could be responsible for the formation of ternary *organic* phase lactate complexes.[113] Such complexes have been postulated but not experimentally confirmed. Changes in activity coefficients and ionic strengths due to extraction of lactate by HDEHP could affect the resulting distribution ratios. These and other possibilities should be explored further to enhance the understanding of TALSPEAK extraction thermodynamics.

The results from this work corroborate literature results for binary complexes of DTPA and its cyclic analogue, DOTA, which showed that ternary complexes do not form with ligands larger than carbonate or phosphate. Thus, for separation of Am from Cm, the use of ternary complexes with octadentate ligands would be ineffective using the current TALSPEAK system.

Reducing the size of the primary ligand facilitated the formation of ternary complexes. Ternary $M(CDTA)(L^2)^{3-}$ and $M(DO3A)(L^2)^{2-}$ complexes were formed with oxalate, malonate, and iminodiacetate. Steric requirements were more important for the bulky, rigid heptadentate complexes because of the smaller amount of space available in the complexes. Also, the overall charge of the binary complex ion appears to be an important factor in determining the relative stability of ternary complexes. In general, the $M(DO3A)(Ox)^{2-}$ and $M(DO3A)(IDA)^{2-}$ complexes were found to have similar equilibrium constants as the corresponding $M(CDTA)(Ox)^{3-}$ and $M(CDTA)(IDA)^{3-}$ complexes even though the DO3A ligand is larger than the CDTA ligand. This seems to imply that any additional stability due to using a neutral M(DO3A) complex was offset by an increase in steric repulsion gained by using the larger, bulkier DO3A. However, the lack of additional thermodynamic data prevents any further

postulation about the driving forces for formation of $M(DO3A)(L^2)^{2-}$ complexes and should be investigated further.

Steric requirements were generally less important for ternary CDTA complexes because ample space was available for the secondary ligand, which made it possible to explore the effects of chelate ring size and ligand basicity. The trend in the equilibrium constants for oxalate and malonate complexes followed the trend in their associated binary complexes, increasing with increasing charge density of the metal cation. The fact that malonate, which has a higher pK_a than oxalate, formed a weaker ternary complex than the oxalate ligand indicates that ring size may be a more important contributor to the equilibrium constants than the overall pK_a for dicarboxylic acids under similar steric constraints. Iminodiacetate and oxalate both formed stronger ternary complexes than the malonate ligand, with IDA forming the strongest complexes for the lighter lanthanides (Nd, Sm). For these lanthanides, the IDA ligand appeared able to displace three water molecules and bind in a tridentate manner, forming up to *two* five-membered rings. This fact and the presence of the more basic nitrogen atom in the IDA ligand contributed to the increased stability of the ternary $Ln(CDTA)(IDA)^{3-}$ complexes for light lanthanides compared to $Ln(CDTA)(Ox)^{3-}$.

The equilibrium constants for the heavier $Ln(CDTA)(IDA)^{3-}$ complexes were actually *lower* than the constants for Nd and Sm. For these complexes, the steric requirements of the $Ln(CDTA)^-$ complexes were more important because of their comparatively smaller size. In fact, the equilibrium constants for the heavy $Ln(CDTA)(IDA)^{3-}$ complexes were only slightly stronger than their $Ln(CDTA)(Ox)^{3-}$ counterparts. Formation of the heavy $Ln(CDTA)(IDA)^{3-}$ complexes was accompanied by a decrease in the disorder of the system, indicating that the IDA ligand could be acting as a bridging ligand between two $Ln(CDTA)^-$ moieties or binding in a bidentate manner.

Fluorescence studies of $TbCDTA^-$ with oxalate indicated that approximately two water molecules were released upon complexation with oxalate. Because at least two water molecules are bound to $Ln(CDTA)^-$ complexes across the lanthanide series, it can be reasonably assumed that two water molecules were released also from the other $Ln(CDTA)^-$ complexes upon complexation assuming steric requirements are met. Furthermore, the entropies for both the $Ln(CDTA)(Ox)^{3-}$ and the $Ln(CDTA)(Mal)^{3-}$ complexes were similar to the entropies for $Tb(CDTA)(Ox)^{3-}$, implying that the same number of water molecules is released in those complexes.

No evidence of competition of the secondary ligand with the primary ligand was noticed because the equilibrium constant for binary $M(L^1)$ complexes were generally at least 5-10 log units greater than the stability constant for the strongest ML_3 complex. Also, the total secondary ligand concentration in solution was never more than a factor of ten greater than the total primary ligand concentration. Competition with the ternary complex has been reported with analogous EDTA complexes with nitrilotriacetic acid, a tetradentate ligand that forms very strong binary complexes.

Although changing the secondary ligands showed some size-based selectivity across the lanthanide series, the larger difference in stabilities of the binary complexes with the primary ligands dominated the overall trend in ternary complex stability. Furthermore, the rigidity of the primary ligand influenced the overall stability constants. Ternary complexes containing the rigid CDTA molecule were thermodynamically more stable than complexes containing their flexible homolog, EDTA. Choosing a secondary ligand that would amplify the thermodynamic difference between the americium complexes and those of curium and the lanthanides is a

complicated approach. Results from this work have shown that many factors affect the relative stabilities of the ternary complexes with only a small enhancement in the selectivity. Furthermore, the secondary ligands would have to form relatively weak complexes with the binary complex to avoid competition of the secondary ligand with the primary ligand. Therefore, size-based selectivity may best be achieved by modification of the size, rigidity, and basicity of the primary ligand (e.g., substitution of oxygen donors with sulfur or nitrogen, introducing aryl groups, etc.).

Ternary complexation could still be used to separate americium from curium, however. Instead of focusing on the aqueous phase, for example, organic phase complexants could be used synergistically with hard donor ligands. Promising results have already been reported in the literature about the use of synergistic extractants for Am/Cm separation; investigations of these ternary organic phase extractants represent an interesting avenue to take in the future.

References

1. Fermi, E. *P. Am. Philos. Soc.* **1946,** *90* (1), 20-24.
2. Nuclear Energy Institute: U.S. Nuclear Power Plants. http://www.nei.org/resourcesandstats/nuclear_statistics/usnuclearpowerplants (Accessed August 18, 2011).
3. Lamarsh, John R. and Baratta, Anthony J. Chapter 4, *Introduction to Nuclear Engineering*, Third Edition. Prentiss-Hall: Upper Saddle River, NJ, 2001; pp.136-147.
4. Nuclear Energy Institute: Nuclear Power Plant Fuel. http://www.nei.org/howitworks/nuclearpowerplantfuel (accessed August 18, 2011).
5. World Nuclear Association: Nuclear Power Reactors. http://www.world-nuclear.org/info/inf32.html (accessed August 31, 2011).
6. Nuclear Regulatory Commission: Storage of Spent Nuclear Fuel. http://www.nrc.gov/waste/spent-fuel-storage.html (accessed July 12, 2011).
7. Andrews, A. *Spent Nuclear Fuel Storage Locations and Inventory*. CRS Report for Congress, available at http://www.cnie.org/nle/crsreports/04dec/RS22001.pdf (accessed August 24, 2011).
8. Idaho National Laboratory: Spent Nuclear Fuel and High Level Waste Data. https://inlportal.inl.gov/portal/server.pt/community/national_spent_nuclear_fuel/389/national_spent_nuclear_fuel_-_snf_data (accessed August 24, 2011).
9. Nuclear Regulatory Commission: Fact Sheet: Dry Cask Storage of Spent Nuclear Fuel. http://www.nrc.gov/reading-rm/doc-collections/fact-sheets/dry-cask-storage.pdf (accessed August 24, 2011).
10. Baisden, P.A. and Atkins-Duffin, C.E. Radioactive Waste Management. In *Handbook of Nuclear Chemistry*, Second Edition; Vértes, A., Nagy, S., Klencsár, Z., Lovas, R. G., Rösch, F., Eds.; Springer: Dordrecht, the Netherlands, 2011; Vol. 6, pp 2808-2809.
11. Benedict, M.; Pigford, T.H.; Levi, H.W. *Nuclear Chemical Engineering*, Second Edition. McGraw Hill: New York, 1981.
12. Hou, X.; Hansen, V.; Aldahan, A.; Possnert, G.; Lind, O.L.; Lujaniene, G. *Anal. Chim. Acta* **2009**, *632*, pp 181-196.
13. Hu, Q.H.; Weng, J.-Q.; Wang, J.-S. *J. Environ. Radioactiv.* **2010**, *101*, pp 426-437.
14. Wigeland, R.; Bauer, T.H.; Fanning, T.H.; Morris, E.E.; *Nucl. Technol.* **2006**, *154*, pp 95-106.
15. Seaborg, G.T.; McMillan, E.M.; Kennedy, J.W.; Wahl, A.C. *Phys. Rev.* **1946**, *69*, Nos. 7&8, pp 366-367.
16. Seaborg, G.T.; Wahl, A.C.; Kennedy, J.W. *Phys. Rev.* **1946**, *69*, Nos. 7&8, p 367.
17. Seaborg, G.T. *The First Nuclear Reactor, the Production of Plutonium, and its Chemical Extraction*. Atomic Energy Commission. pp 15-17. Can be accessed at http://www.iaea.org/Publications/Magazines/Bulletin/Bull040su/04004701517su.pdf.
18. Seaborg, G.T.; Wahl, A.C. *J. Am. Chem. Soc.* **1948**, *70*, pp. 1128-1134.
19. Kennedy, J.W.; Seaborg, G.T.; Segré, E.; Wahl, A.C. *Phys. Rev.* **1941**, *70*, pp.555-556.
20. *The Chemistry of the Actinide and Transactinide Elements*, Fourth Edition; Morss, L.R., Edelstein, N.M., Fuger, J., Eds; Springer: Dordrecht, Netherlands, 2010; Vols. 1-6.

21. Choppin, G.R.; Liljenzin, J.-O.; Rydberg, J. The Nuclear Fuel Cycle. *Radiochemistry and Nuclear Chemistry*, Third Edition; Butterworth-Heinemann: Boston, MA, 2002; pp 608-610.
22. Paviet-Hartmann, P.; Benedict, B.; Lineberry, M.J. Nuclear Fuel Reprocessing. In *Nuclear Engineering Handbook*; Kok, K.D., Ed. CRC Press: Boca Raton, FL, 2009; pp 321-326.
23. Wick, O.J., Ed. *Plutonium Handbook: A Guide to the Technology*; American Nuclear Society: La Grange, IL, 1980.
24. Warf, J.C. *J. Am. Chem. Soc.* **1949**, *71*, pp 3257-3258.
25. Bernström, B.; Rydberg, J. *Acta Chem Scand.* **1957**, 11, pp 1173-1182.
26. Andrews, A. *Nuclear Fuel Reprocessing: U.S. Policy Development*. CRS Report for Congress, available at http://www.fas.org/sgp/crs/nuke/RS22542.pdf (accessed August 18, 2011).
27. National Energy Policy Development Group. *National Energy Policy*; Government Printing Office: Washington, D.C., 2001; p 5-17.
28. U.S. Department of Energy, Office of Nuclear Energy, Science, and Technology. *Report to Congress: Advanced Fuel Cycle Initiative: Objectives, Approach, and Technology Summary*. http://www.fas.org/programs/ssp/_docs/afciConglRprtMay05.pdf.
29. *Fed Regist.* **2009**, *74*, No.123, pp 31017-31018.
30. Pereira, Candido. UREX+ Process Overview. Presented at the Topical Seminar Series on Nuclear Fuel Separation Processes. March 25-26, 2008. http://www.ne.doe.gov/pdfFiles/DOENRCUREXSeminar.pdf
31. W. M. Haynes, Ed., *CRC Handbook of Chemistry and Physics*, 92nd Edition (Internet Version 2012), CRC Press/Taylor and Francis, Boca Raton, FL.
32. Martin, R.C.; Knaver, J.B.; Palo, P.A. *Production, Distribution, and Applications of Californium-252 Neutron Sources.* Presented at the Industrial Radiation and Radioisotope Measurement Applications Conference, Raleigh, North Carolina October 3-7, 1999.
33. Phillips, J.R.; Bosler, G.E.; Halbig, J.K.; Klosterbuer, S.F.; Lee, D.M.; Menlove, H.O. *Neutron Measurement Techniques for the Non-Destructive Analysis of Irradiated Fuel Assemblies.* Report # LA-9002-MS. Los Alamos National Laboratory, Los Alamos, NM, 1981.
34. Karelin, Y.A.; Gordeev, Y.N.; Karasev, V.I.; Radchenko, V.M.; Schimbarev, Y.V.; Kuznetsov, R.A. *Appl. Radiat. Isotopes* **1997**, *48* (10-12), pp 1563-1566.
35. Pillon, S.; Somers, J.; Grandjean, S.; Lacquement, J. *J. Nucl. Mater.* **2003**, *320*, pp 36-43.
36. Nagame, Y.; Hirata, M.; Nakahara, H. Production and Chemistry of Transuranium Elements. In *Handbook of Nuclear Chemistry*, Second Edition; Vértes, A., Nagy, S., Klencsár, Z., Lovas, R. G., Rösch, F., Eds.; Springer: Dordrecht, the Netherlands, 2011; Vol. 2, pp 820-821.
37. Rizkalla, E.N., Choppin, G.R. Chapter 127: Lanthanides and Actinides Hydration and Hydrolysis. In *Handbook on the Physics and Chemistry of Rare Earths*; Gschneider, K.A.,Jr., Eyring, L., Choppin, G.R., Lander, G.H., Eds.; Elsevier B.V., 1994; Vol. 18, pp 529-531.
38. Burgess, J. *Metal Ions in Solution*; Halsted Press: New York, 1978.
39. Pearson, R.G. *J. Am. Chem. Soc.* **1963**, *85* (22), pp 3533-3539.
40. Schwarzenbach, G. *Adv. Inorg. Chem. Radiochem.* **1961**, *3*, p 257.
41. Ahrland, S.; Chatt, J.; Davies, N.R.Q. *Rev. Chem. Soc.* **1958**, p 12.

42. Hartley, F.R.; Burgess, C.; Alcock, R.M. *Solution Equilibria*; Halsted Press: New York, 1980; pp 256-267.
43. Malatesta, Francesco. *J. Solution Chem.* **2000**, *29* (9), pp 771-779.
44. Davies, C.W. *Ion Association*; Butterworths, London, 1962.
45. Light, T.S.; Licht, S.; Bevilacqua, A.C. *Electrochem. Solid St.* **2005**, *8* (1), pp E16-E19.
46. Choppin, G.R., Unrein, P.J. *J. Inorg. Nucl. Chem.* **1963**, *25*, pp 387-393.
47. Yun, J.-I.; Cho, H.-R.; Neck, V.; Altmaier, A.S.; Marquardt, C.M.; Walther, C.; Fanghänel, T. *Radiochem. Acta* **2007**, *95*, pp 89-95.
48. Rydberg, J., Musikas, C., Choppin, G.R., Eds.; *Principles and Practices of Solvent Extraction*; Marcel Dekker: New York, 1992, pp 98-100.
49. Irving, H., Edgington, D.N., *J. Inorg. Nucl. Chem.* **1960**, *15*, pp 158-170.
50. Choppin, G.R.; Schneider, J.. *J. Inorg. Nucl. Chem.* **1970**, *32*, pp 3283-3288.
51. Choppin, G.R. *J. Less-Common Met.* **1983**, *93*, pp 323-330.
52. Smith, R.M.; Martell, A.E.; Motekaitis, R.J. *NIST Critically Selected Stability Constants of Metal Complexes Database*; Standard Reference Data Program, NIST: Gaithersburg, MD, 2004.
53. Schwarzenbach, G. *Helv. Chim. Acta* **1952**, *35*, pp 2344-2359.
54. Adamson, A.W. *J. Am. Chem. Soc.* **1954**, *76*, pp 1578-1579.
55. *Nomenclature of Inorganic Chemistry: IUPAC Recommendations 2005*; The Royal Society of Chemistry: Cambridge, UK, 2005.
56. Greenwood, N.N., Earnshaw, A. *Chemistry of the Elements*; Elsevier: Amsterdam, 2005.
57. Aspinall, H.G. Chapter 1: Introduction, *Chemistry of the f-Block Elements*; Gordon & Breach Science Publishers: Amsterdam, 2001; p 20.
58. Cotton, S. Chapter 3, *Lanthanides and Actinides*; Oxford University Press: New York, 1991, pp 85-88.
59. Fields, P.R.; Friedman, A.M.. *Phys Rev* **1958**, *107*, pp 1460-1462.
60. Silva, R.J.; Dittner, P.F.; Mallory, M.L.; Keller, O.L.; Eskola, K.; Eskola, P.; Nurmia, M.; Ghiorso, A. *Nucl. Phys. A* **1973**, *216*, pp 97-108.
61. Schädel, M.; Brüchel, W.; Gäggeler, H; Kratz, J.V.; Sümmerer, K.; Wirth, G.; Herrmann, G.; Stakemann, R.; Tittel, G.; Trautmann, N.; Nitschke, J.M.; Hulet, E.K.; Lougheed, R.W.; Hahn, R.L.; Ferguson, R.L. *Phys. Rev. Lett.* **1982**, *48* (13), pp 852-855.
62. Laerdahl, J.K.; Fægri, K., Jr.; Visscher, L.; Saue, T. *J. Chem. Phys.* **1998**, *109* (24), pp 10806-10817.
63. Küchle, W.; Dolg, M.; Stoll, H. *J. Chem. Phys. A* **1997**, *101*, 7128-7133.
64. David, F. *J. Less-Common Met.* **1986**, *121*, pp 27-42.
65. Yamaguchi, T.; Nomura, M.; Wakita, H.; Ohtaki, H. *J. Chem. Phys.* **1988**, *89* (8), pp 5153-5159.
66. Carnall, W.T. *J. Less-Common Met.* **1989**, *156*, pp 221-235.
67. Kimura, T.; Choppin, G.R. *J. Alloys Compd* **1994**, *213/214*, pp 313-317.
68. Caravan, P.; Ellison, J. J.; McMurry, T.J.; Lauffer, R.B. *Chem. Rev.* **1999**, *99*, pp 2293-2352.
69. Choppin, G.R. *J. Less-Common Met.* **1983**, *93*, pp 323-330.
70. Münze, R. *J. Inorg. Nucl. Chem.* **1972**, *34*, pp 661-668.
71. Choppin, G.R. *J. Alloys Compd* **1997**, *249*, pp 1-8.
72. Choppin, G.R.; Bertha, S.L. *J. Inorg. Nucl. Chem.* **1973**, *35*, pp 1309-1312.

73. Jensen, M.P.; Morss, L.R.; Beitz, J.V.; Ensor, D. D. *J. Alloys Compd* **2000**, *303/304*, pp 137-141.
74. Diamond, R.M.; Street, K., Jr.; Seaborg, G.T. *J. Am. Chem. Soc.* **1954**, *76* (6), pp 1461-1469.
75. Mazzanti, M.; Wietzke, R.; Pécaut, J.; Latour, J.M.; Maldivi, P.; Remy, M. *Inorg Chem* **2002**, *41*, pp 2389-2399.
76. Miguirditchian, M.; Guillaneux, D.; Guillaumont, D.; Moisy, P.; Madic, C.; Jensen, M.P.; Nash, K.L. *Inorg Chem* **2005**, *44*, pp 1404-1412.
77. Weaver, B.; Kappelman, F.A. *TALSPEAK: A New Method of Separating Americium and Curium from the Lanthanides by Extraction from an Aqueous Solution of an Aminopolyacetic Acid Complex with a Monoacidic Organophosphate or Phosphonate*; ORNL-3559; Oak Ridge National Laboratory, Oak Ridge, TN, 1964.
78. Choppin, G.R.; Silva, R.J. *J. Inorg. Nucl. Chem.* **1956**, *3*, p 248.
79. Billon, A. *J. Radioanal. Chem.* **1979**, *51* (2), pp 297-305.
80. Myasoedov, B.F.; Maryutina, T.A.; Litvina, M.N.; Malikov, D.A.; Kulyako, Y. M.; Spivakov, B.Y.; C. Hill, C.; Adnet, J.-M.; Lecomte; M.; Madic, C. *Radiochim. Acta* **2005**, *93*, 9-15.
81. Stephanou, S.E.; Penneman, R.A. *J. Am. Chem. Soc.* **1952**, *74*, pp 3701-3702.
82. Shehee, T.; Martin, L.R.; Zalupski, P.R.; Nash, K.L. *Separ. Sci. Technol.* **2010**, *45*, 1743-1752.
83. Mason, G.W.; Bollmeier, A.F.; Peppard, D.F. *J. Inorg. Nucl. Chem.* **1970**, *32*, 1011-1022.
84. Musikas, C.; Germain, M.; Bathellier, A.; *Actinide Separations;* ACS Symposium Series 117; American Chemical Society: Washington, DC, 1980.
85. Lyle, S.J.; Rahman, Md. M. *Talanta* **1963**, *10*, pp 1177-1182.
86. Matonic, J.H.; Scott, B.L.; Neu, M.P. *Inorg. Chem.* **2001**, *40*, pp 2638-2639.
87. Kumar, K.; Chang, C.A.; Tweedle, M.F. *Inorg. Chem.* **1993**, *32*, pp 587-593.
88. Wang, X.; Jin, T.; Comblin, V.; Lopez-Mut, A.; Merany, E.; Desreux, J.F. *Inorg Chem* **1992**, *31*, pp 1095-1099.
89. Rossotti, F.J.C.; Rossotti, H. *J. Chem. Educ.* **1965**, *42* (7), 375-378.
90. Leggett, David J. *Computational Methods for the Determination of Formation Constants*; Plenum Press: New York, 1985.
91. Carnall, W.T. *The Absorption and Fluorescence Spectra of Rare Earth Ions in Solution*. In *Handbook on the Physics and Chemistry of the Rare Earths*; Gschneider, K.A.,Jr., Eyring, L., Eds.; North Holland Publishing Company, 1979, Vol. 1, pp 172-208.
92. Leggett, C.J., Liu, G.; Jensen, M.P. *Solvent Extr. Ion Exc.* **2010**, *28* (3), pp 313-314.
93. Caceci, M.S. *Anal. Chem.* **1989**, *61* (20), pp 2324-2327.
94. Habenschuss, A.; Spedding, F.H. *J. Chem. Phys.* **1979**, *70*, 2797-2806.
95. Horrocks, W.D., Jr.; Sudnick, D.R. *Accounts Chem. Res.* **1981**, *14*, pp 384-392.
96. Gottlieb, H.E.; Kotlyar, V.; Nudelman, A. *J. Org. Chem.* **1997**, *62*, pp 7512-7515.
97. Dischino, D.D.; Delaney, E.J.; Emswiler, J.E.; Gaughan, G.T.; Prasad, J.S.; Srivastava, S.K.; Tweedle, M.F. *Inorg Chem* **1991**, *30*, pp 1265-1269.
98. Trombe, J.C.; Jaud, J. *J. Chem. Crystallogr.* **2003**, *33* (1), pp 19-26.
99. Roméro, S.; Trombe, J.C. *Polyhedron* **1999**, *18*, pp 1653-1659.
100. Khalili, F.I.; Choppin, G.R.; Rizkalla, E.N. *Inorg. Chim. Acta* **1988**, *143*, pp 131-135.
101. Stezowski, J.J.; Hoard, J.L. *Isr. J. Chem.* **1984**, *24*, pp 323-334.

102. Gries, H.; Miklautz, H. *Physiol. Chem. Phys. Med. NMR* **1984**, *16*, pp 105.
103. Burai, L.; Hietapelto, V.; Király, R.; Tóth, É.; Brücher, E. *Mag. Res. Med.* **1997**, *38*, pp 146-150.
104. Nilsson, M.; Nash, K.L. *Solvent Extr. Ion Exc.* **2009**, *27* (3), pp 354-377.
105. Weaver, B.; Kappelmann, F.A. *Journal Inorg. Nucl. Chem.* **1968**, *30*, pp 263-272.
106. Hancock, R.D. *Acc. Chem. Res.* **1990**, *23*, pp 253-257
107. Choppin, G.R.; Dadgar, A.; Rizkalla, E.N. *Inorg. Chem.* **1986**, *25*, 3581-3584.
108. Smith, D.W. *J. Chem. Educ.* **1977**, *54* (9), pp 540-542.
109. Király, R.; Tóth, I.; Zékány, L.; Brücher, E. *Acta Chim. Hung.* **1988**, *125* (3), pp 519-526.
110. Thakur, P.; Conca, J.L.; Van de Burgt, L.J.; Choppin, G.R. *J. Coord. Chem.* **2009**, *62* (23), pp 3719-3737.
111. Terreno, E.; Botta, M.; Boniforte, P.; Bracco, C.; Milone, L.; Mondino, B.; Uggeri, F.; Aime, S. *Chem. Eur. J.* **2005**, *11*, pp 5531-5537.
112. Modolo, G.; Kluxen, P.; Geist, A. *Radiochim. Acta* **2010**, *98*, pp 193-201.
113. Grimes, T.S.; Nilsson, M.A.; Nash, K.L. *Sep. Sci. Technol.* **2010**, *45* (12/13), 1725-1732.

Appendix

A.1 Sample SQUAD Input File

The SQUAD (**S**tability **Qu**otients from **A**bsorbance **D**ata) program was used to calculate the stability constants for all complexes investigated in this work with the exception of the $Am(CDTA)(Ox)^{3-}$ and the $Tb(CDTA)(Ox)^{3-}$ complexes. One of two regression methods can be used to calculate the stability constants in SQUAD: non-negative least squares (NNLS) or multiple regression (MR) analysis; the method of choice is indicated in the input file. The input file below is a representative SQUAD input file that was used to analyze spectrophotometric titration data. For a complete description of each section of the file, the reader should refer to the book, *Computational Methods for the Determination of Formation Constants* by David J. Leggett. However, the important features of the input file are highlighted below, with a sample input file following the description.

In the input file, the ligands, metals, and protons (if applicable) are defined in the "DICTIONARY" section. The next section, "SPECIES", contains the assumed equilibrium model, which is comprised of relevant ligand protonation and metal complexation reactions along with their associated stability constants. These stability constants are either fixed ("FB") or varied ("VB") in SQUAD; similarly, their associated molar absorptivities can be fixed ("FE") or varied ("VE"). The "DATA" section lists the range of wavelengths used and the increments between wavelengths. Including the command "NNLS" or "MR" dictates the refinement method that SQUAD will use to minimize the sum of the squared residuals between the experimental and calculated absorbances. Any known molar absorptivities are included in the section called "MOL. ABS". Lastly, the spectra taken during a spectrophotometric titration are listed under the section "SPECTRA"; the first row of each set of absorbance data lists the ligand and metal concentrations, the pH of the solution (if applicable), and the pathlength of the cuvette containing the solution. A sample input file is included below.

```
Spectrophotometric Titration of 10 mL 10.26 mM Nd with 1.499 M IDA, pcH = 7
Nd-IDA, I ~ 1 M
DICTIONARY:
LIG1=IDA;MTL1=ND;PROT=H:
END:
SPECIES:
H(1)IDA(1);9.300;FB;FE:
H(2)IDA(1);11.8;FB;FE:
H(3)IDA(1);13.74;FB;FE:
ND(1)IDA(1);2.500;VB;VE:
ND(1)IDA(2);3.500;VB;VE:
END:
DATA:
720.00    885.00    0.30
LOGB
```

PRIN
NOCD
NNLS
NOPL
CRT
100
1.0
MOL.ABS.:
ND:
END:
0.1532
0.1318
0.1571
0.1746
0.1746
0.2019
0.2039
0.2097
0.2097
0.2351
0.2448
0.2429
0.2565
0.2702
0.3033
0.2896
0.3306
0.3637
0.3813
0.4105
0.4397
0.4456
0.4709
0.4865
0.5216
0.5392
0.5548
0.5937
0.6093
0.6776
0.7185
0.7867
0.8452
0.9095
1.0187
1.1415

1.2585
1.4241
1.6464
1.9232
2.2487
2.6659
3.1707
3.7497
4.4319
5.2078
6.1688
7.0655
7.6698
7.7770
7.5996
7.3969
7.2409
7.1805
7.2487
7.3130
7.3618
7.3969
7.2994
7.1863
7.0538
6.9895
6.8881
6.8335
6.7555
6.6659
6.5626
6.4300
6.3228
6.2312
6.1571
6.0596
5.9329
5.7224
5.5060
5.3130
5.1395
5.0089
4.8978
4.8413
4.8842
4.9680

5.1240
5.2877
5.4202
5.5158
5.5645
5.5801
5.4963
5.3910
5.2097
4.9719
4.7165
4.5548
4.4047
4.2565
4.1142
4.0031
3.8179
3.6171
3.3579
3.1103
2.8959
2.7029
2.5723
2.4495
2.3676
2.3169
2.2409
2.2214
2.1883
2.1337
2.1220
2.0791
2.0382
1.9583
1.8861
1.8160
1.7438
1.6815
1.5918
1.5236
1.4300
1.3384
1.2877
1.2234
1.1629
1.0928

0.9856
0.9719
0.9212
0.8588
0.8355
0.7516
0.7263
0.6678
0.6366
0.6191
0.6054
0.5703
0.5275
0.5099
0.5080
0.5158
0.4943
0.4787
0.5021
0.5119
0.4807
0.4807
0.4573
0.4436
0.4612
0.4417
0.4300
0.4027
0.3481
0.3150
0.3130
0.3072
0.3111
0.3013
0.2799
0.2468
0.2507
0.2448
0.2390
0.2390
0.2273
0.2370
0.2292
0.2039
0.1961
0.1785

0.1766
0.1688
0.1805
0.1941
0.1824
0.1707
0.1902
0.1766
0.1941
0.2117
0.2097
0.2195
0.2136
0.2214
0.2585
0.2799
0.2721
0.2935
0.3442
0.3696
0.3774
0.4319
0.4495
0.4709
0.4924
0.5314
0.5742
0.5762
0.6054
0.6347
0.6698
0.6834
0.6698
0.7126
0.7224
0.7360
0.7672
0.7555
0.7809
0.8004
0.7809
0.8101
0.8627
0.8569
0.9154
0.9446

0.9914
1.0148
1.0752
1.1493
1.2292
1.3013
1.3696
1.4183
1.4904
1.5898
1.6854
1.7594
1.9037
2.0577
2.2331
2.4534
2.7243
3.0382
3.3969
3.8043
4.2468
4.6776
5.1279
5.5080
5.8218
6.0479
6.2039
6.2935
6.3988
6.4475
6.5197
6.6074
6.7497
6.9076
6.9446
6.9290
6.7692
6.5898
6.5742
6.5879
6.7536
7.0128
7.3501
7.7204
7.9368
7.8939

7.6795
7.3852
7.1142
6.9895
7.0401
7.1395
7.3520
7.6113
7.8277
7.9602
7.9232
7.6522
7.2273
6.8277
6.4241
6.1064
5.8686
5.6639
5.3832
5.1610
4.8472
4.5294
4.2429
3.9154
3.6600
3.4300
3.1785
3.0323
2.8764
2.7321
2.6210
2.5080
2.4105
2.3052
2.2331
2.1629
2.1064
2.0577
1.9953
1.9407
1.8881
1.8355
1.8004
1.7010
1.6756
1.5879

1.5197
1.5060
1.3871
1.3228
1.2779
1.2117
1.1434
1.0733
1.0323
0.9700
0.9427
0.8920
0.8510
0.8043
0.7887
0.7165
0.6815
0.6756
0.6483
0.6093
0.5879
0.5548
0.5353
0.5099
0.4807
0.4709
0.4729
0.4553
0.4475
0.4164
0.4319
0.3988
0.3969
0.3930
0.3871
0.3813
0.3442
0.3676
0.3247
0.3247
0.3228
0.3013
0.3072
0.2857
0.2760
0.2663

0.2682
0.2818
0.2526
0.2448
0.2663
0.2390
0.2292
0.2136
0.2097
0.1980
0.2136
0.1844
0.2000
0.1688
0.1688
0.1727
0.1454
0.1473
0.1240
0.1201
0.1103
0.1103
0.1025
0.0850
0.0811
0.0752
0.0869
0.0772
0.0791
0.0674
0.0733
0.0440
0.0577
0.0674
0.0499
0.0635
0.0401
0.0499
0.0440
0.0655
0.0460
0.0440
0.0440
0.0499
0.0206
0.0284

0.0245
0.0206
0.0362
0.0284
0.0323
0.0070
0.0109
0.0206
0.0148
0.0245
0.0148
0.0226
0.0323
0.0323
0.0245
0.0382
0.0187
0.0265
0.0460
0.0557
0.0382
0.0479
0.0362
0.0401
0.0596
0.0518
0.0382
0.0655
0.0635
0.0733
0.0616
0.0713
0.0947
0.0830
0.0811
0.1084
0.0967
0.0986
0.1025
0.1103
0.1103
0.1356
0.1434
0.1259
0.1473
0.1532

0.1649
0.1727
0.1785
0.1922
0.2078
0.2136
0.2175
0.2331
0.2546
0.2604
0.2896
0.3091
0.3267
0.3423
0.3774
0.3891
0.4202
0.4807
0.4729
0.5353
0.5898
0.6093
0.6737
0.7380
0.8179
0.9095
1.0109
1.0947
1.2156
1.3559
1.4885
1.6444
1.7926
1.9349
2.0148
2.0908
2.1240
2.1084
2.0538
1.9700
1.9134
1.8316
1.7789
1.7146
1.6854
1.7068

1.7692
1.8257
1.9524
2.1220
2.2857
2.4553
2.5762
2.6074
2.5937
2.5099
2.4008
2.2682
2.1454
2.0362
1.9056
1.8238
1.7321
1.6893
1.6054
1.5509
1.5216
1.4475
1.4105
1.3442
1.2916
1.2039
1.1395
1.0733
1.0167
0.9563
0.9193
0.8413
0.8082
0.7575
0.7204
0.7126
0.6834
0.6444
0.6249
0.5918
0.5859
0.5859
0.5275
0.5255
0.5158
0.5021

0.5119
0.4826
0.4787
0.4904
0.4534
0.4690
0.4125
0.4280
0.4202
SPECTRA:
1.0260E-02 0.0000E+00 1.0000E-16 0.0000E+00 6.997 5.00
0.0079 0.0068 0.0081 0.0090 0.0090 0.0104 0.0105 0.0108
0.0108 0.0121 0.0126 0.0125 0.0132 0.0139 0.0156 0.0149
0.0170 0.0187 0.0196 0.0211 0.0226 0.0229 0.0242 0.0250
0.0268 0.0277 0.0285 0.0305 0.0313 0.0348 0.0369 0.0404
0.0434 0.0467 0.0523 0.0586 0.0646 0.0731 0.0845 0.0987
0.1154 0.1368 0.1627 0.1924 0.2274 0.2672 0.3165 0.3625
0.3935 0.3990 0.3899 0.3795 0.3715 0.3684 0.3719 0.3752
0.3777 0.3795 0.3745 0.3687 0.3619 0.3586 0.3534 0.3506
0.3466 0.3420 0.3367 0.3299 0.3244 0.3197 0.3159 0.3109
0.3044 0.2936 0.2825 0.2726 0.2637 0.2570 0.2513 0.2484
0.2506 0.2549 0.2629 0.2713 0.2781 0.2830 0.2855 0.2863
0.2820 0.2766 0.2673 0.2551 0.2420 0.2337 0.2260 0.2184
0.2111 0.2054 0.1959 0.1856 0.1723 0.1596 0.1486 0.1387
0.1320 0.1257 0.1215 0.1189 0.1150 0.1140 0.1123 0.1095
0.1089 0.1067 0.1046 0.1005 0.0968 0.0932 0.0895 0.0863
0.0817 0.0782 0.0734 0.0687 0.0661 0.0628 0.0597 0.0561
0.0506 0.0499 0.0473 0.0441 0.0429 0.0386 0.0373 0.0343
0.0327 0.0318 0.0311 0.0293 0.0271 0.0262 0.0261 0.0265
0.0254 0.0246 0.0258 0.0263 0.0247 0.0247 0.0235 0.0228
0.0237 0.0227 0.0221 0.0207 0.0179 0.0162 0.0161 0.0158
0.0160 0.0155 0.0144 0.0127 0.0129 0.0126 0.0123 0.0123
0.0117 0.0122 0.0118 0.0105 0.0101 0.0092 0.0091 0.0087
0.0093 0.0100 0.0094 0.0088 0.0098 0.0091 0.0100 0.0109
0.0108 0.0113 0.0110 0.0114 0.0133 0.0144 0.0140 0.0151
0.0177 0.0190 0.0194 0.0222 0.0231 0.0242 0.0253 0.0273
0.0295 0.0296 0.0311 0.0326 0.0344 0.0351 0.0344 0.0366
0.0371 0.0378 0.0394 0.0388 0.0401 0.0411 0.0401 0.0416
0.0443 0.0440 0.0470 0.0485 0.0509 0.0521 0.0552 0.0590
0.0631 0.0668 0.0703 0.0728 0.0765 0.0816 0.0865 0.0903
0.0977 0.1056 0.1146 0.1259 0.1398 0.1559 0.1743 0.1952
0.2179 0.2400 0.2631 0.2826 0.2987 0.3103 0.3183 0.3229
0.3283 0.3308 0.3345 0.3390 0.3463 0.3544 0.3563 0.3555
0.3473 0.3381 0.3373 0.3380 0.3465 0.3598 0.3771 0.3961
0.4072 0.4050 0.3940 0.3789 0.3650 0.3586 0.3612 0.3663
0.3772 0.3905 0.4016 0.4084 0.4065 0.3926 0.3708 0.3503

0.3296 0.3133 0.3011 0.2906 0.2762 0.2648 0.2487 0.2324
0.2177 0.2009 0.1878 0.1760 0.1631 0.1556 0.1476 0.1402
0.1345 0.1287 0.1237 0.1183 0.1146 0.1110 0.1081 0.1056
0.1024 0.0996 0.0969 0.0942 0.0924 0.0873 0.0860 0.0815
0.0780 0.0773 0.0712 0.0679 0.0656 0.0622 0.0587 0.0551
0.0530 0.0498 0.0484 0.0458 0.0437 0.0413 0.0405 0.0368
0.0350 0.0347 0.0333 0.0313 0.0302 0.0285 0.0275 0.0262
0.0247 0.0242 0.0243 0.0234 0.0230 0.0214 0.0222 0.0205
0.0204 0.0202 0.0199 0.0196 0.0177 0.0189 0.0167 0.0167
0.0166 0.0155 0.0158 0.0147 0.0142 0.0137 0.0138 0.0145
0.0130 0.0126 0.0137 0.0123 0.0118 0.0110 0.0108 0.0102
0.0110 0.0095 0.0103 0.0087 0.0087 0.0089 0.0075 0.0076
0.0064 0.0062 0.0057 0.0057 0.0053 0.0044 0.0042 0.0039
0.0045 0.0040 0.0041 0.0035 0.0038 0.0023 0.0030 0.0035
0.0026 0.0033 0.0021 0.0026 0.0023 0.0034 0.0024 0.0023
0.0023 0.0026 0.0011 0.0015 0.0013 0.0011 0.0019 0.0015
0.0017 0.0004 0.0006 0.0011 0.0008 0.0013 0.0008 0.0012
0.0017 0.0017 0.0013 0.0020 0.0010 0.0014 0.0024 0.0029
0.0020 0.0025 0.0019 0.0021 0.0031 0.0027 0.0020 0.0034
0.0033 0.0038 0.0032 0.0037 0.0049 0.0043 0.0042 0.0056
0.0050 0.0051 0.0053 0.0057 0.0057 0.0070 0.0074 0.0065
0.0076 0.0079 0.0085 0.0089 0.0092 0.0099 0.0107 0.0110
0.0112 0.0120 0.0131 0.0134 0.0149 0.0159 0.0168 0.0176
0.0194 0.0200 0.0216 0.0247 0.0243 0.0275 0.0303 0.0313
0.0346 0.0379 0.0420 0.0467 0.0519 0.0562 0.0624 0.0696
0.0764 0.0844 0.0920 0.0993 0.1034 0.1073 0.1090 0.1082
0.1054 0.1011 0.0982 0.0940 0.0913 0.0880 0.0865 0.0876
0.0908 0.0937 0.1002 0.1089 0.1173 0.1260 0.1322 0.1338
0.1331 0.1288 0.1232 0.1164 0.1101 0.1045 0.0978 0.0936
0.0889 0.0867 0.0824 0.0796 0.0781 0.0743 0.0724 0.0690
0.0663 0.0618 0.0585 0.0551 0.0522 0.0491 0.0472 0.0432
0.0415 0.0389 0.0370 0.0366 0.0351 0.0331 0.0321 0.0304
0.0301 0.0301 0.0271 0.0270 0.0265 0.0258 0.0263 0.0248
0.0246 0.0252 0.0233 0.0241 0.0212 0.0220 0.0216
1.0010E-02 0.0000E+00 3.6561E-02 0.0000E+00 6.809 5.00
0.0040 0.0030 0.0047 0.0046 0.0056 0.0060 0.0060 0.0071
0.0068 0.0084 0.0082 0.0082 0.0088 0.0096 0.0107 0.0114
0.0122 0.0138 0.0149 0.0167 0.0171 0.0179 0.0178 0.0202
0.0211 0.0226 0.0230 0.0246 0.0258 0.0278 0.0312 0.0338
0.0367 0.0398 0.0437 0.0499 0.0554 0.0632 0.0718 0.0856
0.1008 0.1189 0.1414 0.1671 0.1973 0.2339 0.2770 0.3176
0.3485 0.3622 0.3669 0.3712 0.3753 0.3767 0.3742 0.3662
0.3590 0.3553 0.3496 0.3453 0.3419 0.3402 0.3401 0.3385
0.3378 0.3339 0.3284 0.3220 0.3189 0.3163 0.3140 0.3115
0.3094 0.3039 0.2980 0.2920 0.2845 0.2782 0.2730 0.2689
0.2697 0.2725 0.2797 0.2877 0.2937 0.2995 0.3019 0.3026

0.2998 0.2940 0.2858 0.2726 0.2597 0.2494 0.2400 0.2327
0.2258 0.2178 0.2099 0.1999 0.1886 0.1758 0.1662 0.1564
0.1490 0.1437 0.1390 0.1348 0.1315 0.1286 0.1250 0.1212
0.1192 0.1158 0.1128 0.1095 0.1055 0.1027 0.0981 0.0945
0.0915 0.0874 0.0820 0.0793 0.0737 0.0706 0.0668 0.0631
0.0582 0.0560 0.0529 0.0506 0.0499 0.0437 0.0422 0.0398
0.0372 0.0358 0.0350 0.0325 0.0324 0.0301 0.0297 0.0290
0.0280 0.0273 0.0270 0.0273 0.0270 0.0262 0.0249 0.0244
0.0245 0.0237 0.0230 0.0216 0.0193 0.0179 0.0171 0.0158
0.0167 0.0155 0.0152 0.0134 0.0132 0.0142 0.0125 0.0131
0.0123 0.0124 0.0121 0.0113 0.0105 0.0100 0.0087 0.0088
0.0102 0.0103 0.0089 0.0077 0.0098 0.0092 0.0096 0.0091
0.0098 0.0108 0.0103 0.0106 0.0126 0.0136 0.0122 0.0141
0.0162 0.0176 0.0181 0.0196 0.0206 0.0221 0.0229 0.0244
0.0279 0.0273 0.0291 0.0306 0.0326 0.0341 0.0336 0.0336
0.0362 0.0367 0.0381 0.0374 0.0392 0.0401 0.0387 0.0394
0.0428 0.0431 0.0449 0.0465 0.0496 0.0513 0.0537 0.0566
0.0601 0.0650 0.0680 0.0701 0.0736 0.0778 0.0826 0.0855
0.0924 0.0998 0.1073 0.1175 0.1297 0.1444 0.1596 0.1785
0.1993 0.2185 0.2389 0.2574 0.2727 0.2848 0.2951 0.3030
0.3097 0.3179 0.3250 0.3329 0.3411 0.3525 0.3567 0.3589
0.3555 0.3520 0.3548 0.3593 0.3716 0.3866 0.4016 0.4216
0.4326 0.4330 0.4264 0.4130 0.3988 0.3856 0.3786 0.3772
0.3797 0.3875 0.3945 0.3982 0.3956 0.3825 0.3635 0.3441
0.3261 0.3095 0.2995 0.2919 0.2809 0.2736 0.2624 0.2494
0.2400 0.2258 0.2143 0.2025 0.1890 0.1793 0.1705 0.1604
0.1542 0.1474 0.1403 0.1362 0.1316 0.1271 0.1247 0.1209
0.1182 0.1155 0.1132 0.1095 0.1068 0.1014 0.0990 0.0943
0.0897 0.0861 0.0800 0.0755 0.0720 0.0669 0.0648 0.0595
0.0565 0.0529 0.0507 0.0473 0.0460 0.0435 0.0409 0.0391
0.0364 0.0363 0.0345 0.0326 0.0311 0.0293 0.0291 0.0276
0.0261 0.0268 0.0255 0.0250 0.0235 0.0232 0.0231 0.0218
0.0226 0.0221 0.0211 0.0212 0.0187 0.0199 0.0189 0.0178
0.0179 0.0163 0.0172 0.0159 0.0163 0.0157 0.0149 0.0143
0.0153 0.0143 0.0142 0.0133 0.0121 0.0115 0.0121 0.0102
0.0116 0.0096 0.0102 0.0091 0.0095 0.0091 0.0073 0.0077
0.0059 0.0061 0.0052 0.0055 0.0048 0.0053 0.0040 0.0046
0.0037 0.0035 0.0044 0.0037 0.0031 0.0034 0.0025 0.0032
0.0021 0.0032 0.0030 0.0023 0.0018 0.0029 0.0014 0.0022
0.0022 0.0025 0.0019 0.0022 0.0007 0.0014 0.0020 0.0021
0.0014 0.0011 0.0013 0.0011 0.0015 0.0007 0.0012 0.0013
0.0008 0.0010 0.0007 0.0014 0.0015 0.0009 0.0024 0.0027
0.0012 0.0019 0.0022 0.0021 0.0024 0.0024 0.0023 0.0034
0.0033 0.0037 0.0034 0.0037 0.0042 0.0036 0.0042 0.0050
0.0048 0.0046 0.0046 0.0049 0.0049 0.0063 0.0069 0.0058
0.0054 0.0068 0.0080 0.0075 0.0094 0.0095 0.0095 0.0100

0.0098 0.0118 0.0129 0.0131 0.0141 0.0150 0.0151 0.0165
0.0185 0.0181 0.0199 0.0231 0.0233 0.0248 0.0279 0.0297
0.0321 0.0352 0.0394 0.0428 0.0482 0.0527 0.0582 0.0649
0.0715 0.0777 0.0859 0.0927 0.0974 0.1022 0.1056 0.1059
0.1049 0.1045 0.1037 0.1022 0.1016 0.1014 0.1001 0.1008
0.1046 0.1061 0.1110 0.1171 0.1248 0.1328 0.1388 0.1423
0.1416 0.1407 0.1356 0.1287 0.1234 0.1157 0.1084 0.1013
0.0963 0.0904 0.0859 0.0809 0.0790 0.0745 0.0726 0.0687
0.0663 0.0619 0.0594 0.0566 0.0532 0.0493 0.0480 0.0458
0.0434 0.0413 0.0401 0.0387 0.0371 0.0353 0.0340 0.0332
0.0336 0.0318 0.0303 0.0296 0.0290 0.0285 0.0287 0.0272
0.0266 0.0271 0.0252 0.0270 0.0240 0.0241 0.0237
9.7714E-03 0.0000E+00 7.1381E-02 0.0000E+00 6.746 5.00
0.0031 0.0015 0.0025 0.0039 0.0042 0.0051 0.0063 0.0061
0.0064 0.0065 0.0080 0.0073 0.0080 0.0079 0.0096 0.0106
0.0119 0.0127 0.0142 0.0145 0.0153 0.0163 0.0171 0.0181
0.0193 0.0207 0.0215 0.0233 0.0240 0.0264 0.0288 0.0312
0.0343 0.0374 0.0415 0.0462 0.0511 0.0582 0.0677 0.0797
0.0936 0.1107 0.1306 0.1548 0.1817 0.2158 0.2562 0.2948
0.3247 0.3421 0.3513 0.3638 0.3744 0.3777 0.3713 0.3589
0.3473 0.3409 0.3357 0.3319 0.3292 0.3297 0.3306 0.3304
0.3304 0.3278 0.3232 0.3179 0.3144 0.3128 0.3117 0.3111
0.3103 0.3072 0.3038 0.3000 0.2935 0.2876 0.2814 0.2768
0.2771 0.2797 0.2849 0.2924 0.2982 0.3047 0.3076 0.3091
0.3062 0.3005 0.2903 0.2775 0.2655 0.2556 0.2450 0.2380
0.2300 0.2232 0.2147 0.2050 0.1933 0.1816 0.1719 0.1626
0.1545 0.1498 0.1450 0.1409 0.1369 0.1343 0.1283 0.1248
0.1218 0.1176 0.1150 0.1112 0.1067 0.1050 0.1001 0.0981
0.0939 0.0903 0.0853 0.0820 0.0768 0.0724 0.0699 0.0654
0.0598 0.0580 0.0546 0.0526 0.0518 0.0471 0.0444 0.0414
0.0386 0.0370 0.0361 0.0345 0.0328 0.0321 0.0301 0.0290
0.0279 0.0278 0.0284 0.0281 0.0266 0.0269 0.0254 0.0236
0.0239 0.0234 0.0234 0.0212 0.0196 0.0174 0.0162 0.0161
0.0167 0.0161 0.0156 0.0138 0.0137 0.0133 0.0125 0.0120
0.0119 0.0123 0.0112 0.0107 0.0100 0.0098 0.0092 0.0086
0.0099 0.0092 0.0087 0.0084 0.0101 0.0088 0.0087 0.0085
0.0091 0.0105 0.0096 0.0097 0.0110 0.0123 0.0117 0.0123
0.0146 0.0156 0.0158 0.0177 0.0196 0.0200 0.0206 0.0226
0.0259 0.0266 0.0271 0.0283 0.0313 0.0317 0.0316 0.0326
0.0335 0.0353 0.0359 0.0356 0.0385 0.0392 0.0384 0.0389
0.0405 0.0416 0.0429 0.0445 0.0474 0.0494 0.0522 0.0547
0.0585 0.0625 0.0659 0.0672 0.0711 0.0758 0.0790 0.0814
0.0879 0.0955 0.1017 0.1111 0.1228 0.1371 0.1501 0.1674
0.1874 0.2049 0.2242 0.2422 0.2576 0.2699 0.2803 0.2892
0.2975 0.3069 0.3164 0.3253 0.3362 0.3477 0.3529 0.3568
0.3553 0.3534 0.3599 0.3662 0.3803 0.3948 0.4100 0.4279

0.4396 0.4411 0.4368 0.4267 0.4098 0.3945 0.3840 0.3762
0.3751 0.3817 0.3847 0.3880 0.3852 0.3737 0.3550 0.3374
0.3196 0.3066 0.2962 0.2892 0.2803 0.2737 0.2653 0.2563
0.2473 0.2357 0.2244 0.2129 0.1988 0.1877 0.1781 0.1691
0.1611 0.1537 0.1476 0.1419 0.1377 0.1323 0.1304 0.1278
0.1243 0.1221 0.1193 0.1155 0.1122 0.1065 0.1037 0.0986
0.0925 0.0903 0.0823 0.0787 0.0748 0.0697 0.0662 0.0601
0.0579 0.0542 0.0516 0.0489 0.0456 0.0441 0.0418 0.0402
0.0372 0.0364 0.0345 0.0322 0.0326 0.0309 0.0294 0.0285
0.0261 0.0271 0.0261 0.0261 0.0245 0.0235 0.0235 0.0224
0.0231 0.0218 0.0213 0.0219 0.0192 0.0202 0.0186 0.0187
0.0183 0.0171 0.0165 0.0163 0.0155 0.0152 0.0152 0.0156
0.0148 0.0142 0.0143 0.0132 0.0121 0.0114 0.0128 0.0098
0.0107 0.0093 0.0098 0.0096 0.0081 0.0087 0.0077 0.0074
0.0049 0.0062 0.0052 0.0057 0.0059 0.0042 0.0039 0.0043
0.0035 0.0030 0.0041 0.0035 0.0033 0.0025 0.0019 0.0027
0.0026 0.0032 0.0020 0.0020 0.0023 0.0025 0.0024 0.0026
0.0019 0.0025 0.0012 0.0019 0.0006 0.0009 0.0019 0.0013
0.0014 0.0009 0.0014 0.0011 0.0013 0.0018 0.0005 0.0014
0.0011 0.0011 0.0009 0.0024 0.0008 0.0015 0.0025 0.0022
0.0020 0.0027 0.0030 0.0029 0.0031 0.0036 0.0026 0.0032
0.0031 0.0034 0.0039 0.0046 0.0050 0.0048 0.0048 0.0058
0.0056 0.0055 0.0054 0.0054 0.0068 0.0069 0.0072 0.0065
0.0069 0.0082 0.0086 0.0088 0.0098 0.0090 0.0099 0.0108
0.0109 0.0122 0.0139 0.0143 0.0155 0.0155 0.0162 0.0175
0.0194 0.0192 0.0219 0.0239 0.0247 0.0266 0.0287 0.0303
0.0327 0.0354 0.0400 0.0431 0.0474 0.0513 0.0565 0.0627
0.0690 0.0748 0.0829 0.0895 0.0945 0.0992 0.1025 0.1044
0.1053 0.1053 0.1061 0.1051 0.1062 0.1050 0.1058 0.1057
0.1087 0.1097 0.1132 0.1174 0.1248 0.1329 0.1379 0.1420
0.1429 0.1426 0.1379 0.1315 0.1255 0.1181 0.1100 0.1037
0.0965 0.0905 0.0856 0.0803 0.0769 0.0721 0.0703 0.0665
0.0637 0.0595 0.0579 0.0552 0.0524 0.0485 0.0476 0.0439
0.0420 0.0402 0.0379 0.0365 0.0365 0.0341 0.0331 0.0313
0.0307 0.0303 0.0288 0.0280 0.0286 0.0276 0.0269 0.0245
0.0246 0.0255 0.0241 0.0244 0.0233 0.0226 0.0219
9.3273E-03 0.0000E+00 1.3627E-01 0.0000E+00 6.694 5.00
0.0039 0.0031 0.0035 0.0035 0.0046 0.0061 0.0057 0.0069
0.0066 0.0065 0.0079 0.0072 0.0073 0.0082 0.0086 0.0100
0.0099 0.0114 0.0125 0.0138 0.0140 0.0144 0.0157 0.0169
0.0173 0.0190 0.0190 0.0214 0.0224 0.0243 0.0268 0.0282
0.0313 0.0339 0.0378 0.0427 0.0467 0.0525 0.0614 0.0714
0.0833 0.0983 0.1163 0.1373 0.1616 0.1923 0.2276 0.2606
0.2915 0.3126 0.3313 0.3508 0.3681 0.3738 0.3629 0.3426
0.3265 0.3195 0.3127 0.3115 0.3097 0.3114 0.3145 0.3150
0.3165 0.3148 0.3113 0.3064 0.3031 0.3022 0.3022 0.3031

0.3052 0.3053 0.3037 0.3027 0.2976 0.2912 0.2851 0.2810
0.2794 0.2806 0.2853 0.2915 0.2973 0.3039 0.3068 0.3091
0.3065 0.3011 0.2920 0.2798 0.2659 0.2550 0.2448 0.2374
0.2305 0.2230 0.2150 0.2071 0.1956 0.1853 0.1763 0.1668
0.1597 0.1549 0.1500 0.1447 0.1409 0.1373 0.1315 0.1253
0.1226 0.1191 0.1162 0.1133 0.1086 0.1055 0.1018 0.0993
0.0968 0.0920 0.0888 0.0846 0.0787 0.0741 0.0711 0.0669
0.0618 0.0598 0.0564 0.0544 0.0534 0.0491 0.0459 0.0426
0.0406 0.0382 0.0371 0.0348 0.0342 0.0324 0.0312 0.0302
0.0292 0.0276 0.0280 0.0278 0.0277 0.0264 0.0248 0.0238
0.0230 0.0232 0.0232 0.0222 0.0194 0.0171 0.0167 0.0155
0.0158 0.0154 0.0154 0.0133 0.0130 0.0132 0.0119 0.0121
0.0115 0.0120 0.0107 0.0106 0.0096 0.0101 0.0081 0.0074
0.0077 0.0093 0.0082 0.0063 0.0079 0.0083 0.0077 0.0076
0.0084 0.0096 0.0100 0.0088 0.0106 0.0110 0.0112 0.0118
0.0125 0.0150 0.0142 0.0168 0.0173 0.0178 0.0188 0.0203
0.0236 0.0242 0.0246 0.0263 0.0282 0.0303 0.0295 0.0303
0.0315 0.0332 0.0341 0.0336 0.0358 0.0370 0.0364 0.0373
0.0391 0.0398 0.0415 0.0429 0.0448 0.0469 0.0503 0.0525
0.0564 0.0587 0.0634 0.0639 0.0665 0.0708 0.0747 0.0768
0.0814 0.0893 0.0955 0.1024 0.1141 0.1256 0.1375 0.1526
0.1705 0.1868 0.2042 0.2205 0.2358 0.2472 0.2590 0.2687
0.2780 0.2889 0.3000 0.3109 0.3231 0.3346 0.3417 0.3470
0.3502 0.3505 0.3593 0.3674 0.3803 0.3974 0.4116 0.4270
0.4386 0.4440 0.4413 0.4343 0.4175 0.3986 0.3814 0.3706
0.3661 0.3676 0.3696 0.3718 0.3676 0.3578 0.3402 0.3252
0.3090 0.2957 0.2879 0.2828 0.2749 0.2713 0.2658 0.2581
0.2531 0.2437 0.2324 0.2226 0.2073 0.1957 0.1855 0.1759
0.1679 0.1606 0.1538 0.1478 0.1439 0.1396 0.1368 0.1343
0.1298 0.1282 0.1252 0.1209 0.1183 0.1123 0.1087 0.1040
0.0974 0.0936 0.0870 0.0817 0.0770 0.0717 0.0674 0.0621
0.0594 0.0550 0.0536 0.0488 0.0466 0.0447 0.0420 0.0397
0.0369 0.0367 0.0358 0.0334 0.0328 0.0307 0.0300 0.0290
0.0275 0.0278 0.0274 0.0261 0.0259 0.0243 0.0255 0.0239
0.0240 0.0236 0.0220 0.0237 0.0207 0.0212 0.0205 0.0198
0.0202 0.0190 0.0183 0.0188 0.0174 0.0177 0.0160 0.0173
0.0170 0.0153 0.0160 0.0146 0.0131 0.0121 0.0129 0.0108
0.0123 0.0105 0.0102 0.0102 0.0088 0.0095 0.0079 0.0079
0.0060 0.0069 0.0064 0.0068 0.0059 0.0051 0.0041 0.0036
0.0035 0.0037 0.0038 0.0029 0.0032 0.0036 0.0035 0.0035
0.0027 0.0030 0.0022 0.0017 0.0022 0.0031 0.0030 0.0021
0.0027 0.0026 0.0024 0.0022 0.0019 0.0012 0.0017 0.0018
0.0012 0.0015 0.0020 0.0013 0.0023 0.0011 0.0011 0.0008
0.0015 0.0011 0.0007 0.0005 0.0015 0.0004 0.0013 0.0021
0.0020 0.0013 0.0018 0.0021 0.0018 0.0020 0.0016 0.0028
0.0035 0.0030 0.0026 0.0027 0.0043 0.0030 0.0035 0.0045

0.0039 0.0046 0.0042 0.0051 0.0049 0.0059 0.0065 0.0049
0.0059 0.0067 0.0069 0.0068 0.0089 0.0087 0.0087 0.0096
0.0096 0.0105 0.0112 0.0126 0.0126 0.0147 0.0140 0.0149
0.0169 0.0172 0.0183 0.0201 0.0210 0.0230 0.0250 0.0265
0.0286 0.0311 0.0341 0.0375 0.0410 0.0453 0.0496 0.0558
0.0617 0.0672 0.0746 0.0808 0.0868 0.0905 0.0957 0.0985
0.1006 0.1018 0.1044 0.1047 0.1068 0.1072 0.1072 0.1089
0.1115 0.1120 0.1136 0.1173 0.1226 0.1295 0.1354 0.1405
0.1434 0.1424 0.1390 0.1331 0.1273 0.1195 0.1108 0.1038
0.0965 0.0895 0.0835 0.0784 0.0749 0.0705 0.0685 0.0646
0.0623 0.0580 0.0571 0.0545 0.0515 0.0503 0.0490 0.0464
0.0450 0.0426 0.0421 0.0403 0.0393 0.0380 0.0365 0.0353
0.0356 0.0336 0.0331 0.0318 0.0322 0.0311 0.0302 0.0292
0.0290 0.0304 0.0280 0.0285 0.0263 0.0271 0.0260
8.7319E-03 0.0000E+00 2.2326E-01 0.0000E+00 6.671 5.00
0.0076 0.0071 0.0076 0.0079 0.0087 0.0098 0.0100 0.0107
0.0109 0.0117 0.0110 0.0114 0.0118 0.0114 0.0130 0.0123
0.0137 0.0151 0.0161 0.0177 0.0176 0.0182 0.0198 0.0200
0.0216 0.0215 0.0231 0.0234 0.0246 0.0269 0.0277 0.0303
0.0330 0.0358 0.0395 0.0431 0.0463 0.0527 0.0587 0.0680
0.0779 0.0911 0.1064 0.1247 0.1476 0.1727 0.2029 0.2334
0.2614 0.2869 0.3090 0.3354 0.3563 0.3622 0.3489 0.3230
0.3048 0.2954 0.2900 0.2872 0.2887 0.2911 0.2946 0.2974
0.2985 0.2984 0.2945 0.2906 0.2886 0.2879 0.2887 0.2911
0.2944 0.2955 0.2973 0.2957 0.2925 0.2877 0.2811 0.2760
0.2748 0.2752 0.2786 0.2834 0.2894 0.2957 0.2993 0.3010
0.2999 0.2953 0.2864 0.2751 0.2622 0.2511 0.2405 0.2325
0.2256 0.2186 0.2119 0.2034 0.1950 0.1838 0.1758 0.1667
0.1606 0.1553 0.1500 0.1465 0.1416 0.1375 0.1308 0.1255
0.1219 0.1169 0.1145 0.1120 0.1079 0.1051 0.1014 0.0991
0.0958 0.0919 0.0885 0.0849 0.0797 0.0753 0.0712 0.0678
0.0625 0.0604 0.0564 0.0554 0.0547 0.0500 0.0476 0.0434
0.0405 0.0396 0.0379 0.0354 0.0335 0.0324 0.0311 0.0303
0.0287 0.0281 0.0279 0.0275 0.0269 0.0262 0.0245 0.0235
0.0238 0.0227 0.0223 0.0216 0.0181 0.0183 0.0160 0.0169
0.0161 0.0157 0.0153 0.0129 0.0136 0.0137 0.0117 0.0125
0.0118 0.0122 0.0113 0.0104 0.0098 0.0097 0.0092 0.0074
0.0087 0.0101 0.0084 0.0076 0.0083 0.0081 0.0090 0.0078
0.0086 0.0095 0.0093 0.0086 0.0112 0.0116 0.0109 0.0107
0.0132 0.0142 0.0131 0.0147 0.0164 0.0174 0.0175 0.0191
0.0221 0.0231 0.0243 0.0252 0.0269 0.0292 0.0289 0.0294
0.0306 0.0323 0.0334 0.0328 0.0349 0.0357 0.0348 0.0360
0.0389 0.0388 0.0403 0.0408 0.0437 0.0453 0.0480 0.0506
0.0527 0.0565 0.0608 0.0613 0.0632 0.0674 0.0713 0.0732
0.0770 0.0842 0.0891 0.0956 0.1042 0.1157 0.1256 0.1391
0.1554 0.1702 0.1853 0.2006 0.2142 0.2270 0.2377 0.2491

0.2596 0.2703 0.2830 0.2936 0.3070 0.3194 0.3258 0.3336
0.3391 0.3407 0.3492 0.3590 0.3739 0.3888 0.4014 0.4165
0.4285 0.4340 0.4355 0.4286 0.4127 0.3908 0.3723 0.3579
0.3483 0.3476 0.3482 0.3481 0.3451 0.3359 0.3209 0.3062
0.2927 0.2799 0.2726 0.2702 0.2635 0.2630 0.2594 0.2540
0.2510 0.2419 0.2326 0.2224 0.2088 0.1967 0.1870 0.1758
0.1684 0.1600 0.1545 0.1488 0.1435 0.1398 0.1372 0.1349
0.1302 0.1293 0.1253 0.1214 0.1190 0.1127 0.1089 0.1041
0.0972 0.0938 0.0854 0.0812 0.0773 0.0706 0.0680 0.0622
0.0590 0.0548 0.0521 0.0492 0.0467 0.0445 0.0417 0.0394
0.0375 0.0367 0.0350 0.0331 0.0332 0.0313 0.0302 0.0296
0.0282 0.0280 0.0270 0.0263 0.0254 0.0249 0.0251 0.0241
0.0236 0.0237 0.0214 0.0229 0.0205 0.0211 0.0200 0.0187
0.0202 0.0184 0.0176 0.0174 0.0163 0.0161 0.0153 0.0155
0.0157 0.0151 0.0155 0.0135 0.0131 0.0112 0.0114 0.0099
0.0108 0.0100 0.0097 0.0096 0.0088 0.0088 0.0066 0.0069
0.0052 0.0065 0.0053 0.0053 0.0060 0.0043 0.0042 0.0039
0.0035 0.0042 0.0038 0.0034 0.0042 0.0030 0.0032 0.0032
0.0022 0.0029 0.0025 0.0020 0.0021 0.0021 0.0016 0.0017
0.0013 0.0016 0.0021 0.0019 0.0012 0.0010 0.0016 0.0017
0.0023 0.0012 0.0017 0.0011 0.0012 0.0020 0.0008 0.0011
0.0022 0.0015 0.0007 0.0020 0.0015 0.0007 0.0027 0.0023
0.0015 0.0023 0.0019 0.0025 0.0031 0.0016 0.0023 0.0030
0.0025 0.0038 0.0029 0.0036 0.0039 0.0039 0.0046 0.0051
0.0044 0.0041 0.0052 0.0056 0.0053 0.0056 0.0069 0.0050
0.0057 0.0067 0.0076 0.0073 0.0078 0.0080 0.0088 0.0091
0.0087 0.0101 0.0110 0.0125 0.0120 0.0123 0.0129 0.0145
0.0149 0.0157 0.0166 0.0188 0.0190 0.0208 0.0236 0.0237
0.0263 0.0278 0.0314 0.0345 0.0380 0.0421 0.0456 0.0517
0.0569 0.0608 0.0684 0.0743 0.0788 0.0847 0.0894 0.0935
0.0969 0.0995 0.1019 0.1043 0.1070 0.1085 0.1080 0.1093
0.1117 0.1109 0.1125 0.1149 0.1185 0.1259 0.1316 0.1373
0.1405 0.1411 0.1376 0.1324 0.1264 0.1192 0.1096 0.1031
0.0947 0.0882 0.0823 0.0759 0.0729 0.0670 0.0653 0.0614
0.0595 0.0557 0.0545 0.0517 0.0495 0.0465 0.0462 0.0438
0.0413 0.0397 0.0377 0.0368 0.0357 0.0337 0.0335 0.0319
0.0313 0.0305 0.0294 0.0288 0.0290 0.0279 0.0273 0.0259
0.0262 0.0264 0.0249 0.0256 0.0227 0.0230 0.0232
8.0471E-03 0.0000E+00 3.2331E-01 0.0000E+00 6.675 5.00
0.0044 0.0027 0.0038 0.0044 0.0044 0.0049 0.0056 0.0063
0.0061 0.0067 0.0071 0.0069 0.0071 0.0074 0.0083 0.0085
0.0094 0.0107 0.0115 0.0121 0.0132 0.0134 0.0154 0.0149
0.0151 0.0166 0.0174 0.0191 0.0190 0.0211 0.0235 0.0242
0.0270 0.0279 0.0317 0.0359 0.0397 0.0435 0.0491 0.0578
0.0660 0.0773 0.0910 0.1073 0.1262 0.1481 0.1743 0.2011
0.2283 0.2543 0.2801 0.3094 0.3338 0.3408 0.3257 0.2995

0.2786 0.2696 0.2639 0.2622 0.2652 0.2679 0.2730 0.2761
0.2768 0.2761 0.2743 0.2706 0.2685 0.2674 0.2703 0.2725
0.2775 0.2799 0.2827 0.2842 0.2807 0.2754 0.2698 0.2634
0.2623 0.2614 0.2646 0.2692 0.2739 0.2809 0.2837 0.2861
0.2850 0.2810 0.2731 0.2606 0.2487 0.2382 0.2283 0.2209
0.2137 0.2065 0.2013 0.1937 0.1855 0.1773 0.1685 0.1619
0.1549 0.1503 0.1447 0.1403 0.1360 0.1323 0.1260 0.1204
0.1162 0.1117 0.1083 0.1067 0.1032 0.1011 0.0978 0.0951
0.0920 0.0895 0.0856 0.0826 0.0762 0.0720 0.0693 0.0653
0.0602 0.0582 0.0546 0.0537 0.0532 0.0488 0.0450 0.0427
0.0394 0.0373 0.0370 0.0343 0.0333 0.0317 0.0297 0.0293
0.0275 0.0269 0.0267 0.0271 0.0262 0.0260 0.0236 0.0230
0.0220 0.0220 0.0218 0.0204 0.0182 0.0162 0.0155 0.0159
0.0159 0.0154 0.0141 0.0132 0.0122 0.0133 0.0120 0.0125
0.0109 0.0114 0.0098 0.0095 0.0092 0.0094 0.0081 0.0074
0.0071 0.0090 0.0082 0.0070 0.0074 0.0080 0.0077 0.0076
0.0079 0.0092 0.0087 0.0073 0.0100 0.0101 0.0084 0.0093
0.0119 0.0126 0.0111 0.0137 0.0154 0.0153 0.0153 0.0175
0.0195 0.0205 0.0216 0.0211 0.0236 0.0258 0.0256 0.0265
0.0273 0.0294 0.0315 0.0293 0.0312 0.0330 0.0326 0.0326
0.0346 0.0347 0.0373 0.0375 0.0392 0.0417 0.0437 0.0454
0.0475 0.0517 0.0551 0.0551 0.0571 0.0614 0.0641 0.0650
0.0692 0.0747 0.0801 0.0850 0.0935 0.1032 0.1109 0.1224
0.1375 0.1495 0.1639 0.1778 0.1915 0.2024 0.2138 0.2251
0.2354 0.2478 0.2597 0.2710 0.2829 0.2966 0.3034 0.3110
0.3175 0.3206 0.3314 0.3412 0.3546 0.3708 0.3802 0.3945
0.4066 0.4137 0.4162 0.4108 0.3936 0.3717 0.3524 0.3349
0.3251 0.3228 0.3211 0.3199 0.3175 0.3094 0.2957 0.2830
0.2708 0.2599 0.2540 0.2516 0.2468 0.2469 0.2460 0.2428
0.2407 0.2342 0.2251 0.2155 0.2021 0.1909 0.1816 0.1706
0.1637 0.1563 0.1493 0.1442 0.1398 0.1358 0.1327 0.1303
0.1272 0.1261 0.1231 0.1186 0.1165 0.1099 0.1065 0.1012
0.0942 0.0909 0.0835 0.0792 0.0745 0.0697 0.0651 0.0596
0.0577 0.0543 0.0508 0.0474 0.0450 0.0426 0.0407 0.0387
0.0364 0.0357 0.0347 0.0330 0.0330 0.0309 0.0303 0.0290
0.0276 0.0286 0.0277 0.0273 0.0267 0.0243 0.0263 0.0238
0.0247 0.0239 0.0227 0.0238 0.0213 0.0221 0.0210 0.0203
0.0206 0.0192 0.0186 0.0185 0.0183 0.0178 0.0166 0.0164
0.0167 0.0149 0.0161 0.0140 0.0133 0.0122 0.0125 0.0108
0.0118 0.0102 0.0103 0.0093 0.0083 0.0090 0.0075 0.0073
0.0052 0.0064 0.0057 0.0053 0.0045 0.0044 0.0042 0.0035
0.0035 0.0032 0.0034 0.0036 0.0037 0.0024 0.0034 0.0033
0.0023 0.0025 0.0020 0.0025 0.0008 0.0024 0.0020 0.0016
0.0016 0.0015 0.0009 0.0017 0.0010 0.0006 0.0017 0.0013
0.0007 0.0014 0.0011 0.0014 0.0019 0.0014 0.0007 0.0011
0.0023 0.0016 0.0005 0.0021 0.0021 0.0018 0.0030 0.0037

0.0022 0.0024 0.0030 0.0033 0.0027 0.0030 0.0024 0.0041
0.0036 0.0038 0.0036 0.0040 0.0047 0.0041 0.0045 0.0053
0.0049 0.0051 0.0049 0.0055 0.0059 0.0063 0.0070 0.0060
0.0056 0.0068 0.0072 0.0071 0.0078 0.0084 0.0089 0.0091
0.0094 0.0098 0.0098 0.0117 0.0117 0.0130 0.0126 0.0132
0.0143 0.0149 0.0162 0.0178 0.0175 0.0192 0.0205 0.0219
0.0234 0.0258 0.0290 0.0301 0.0343 0.0374 0.0408 0.0455
0.0500 0.0551 0.0607 0.0660 0.0715 0.0764 0.0820 0.0864
0.0897 0.0929 0.0967 0.0993 0.1022 0.1045 0.1054 0.1054
0.1070 0.1052 0.1055 0.1082 0.1117 0.1177 0.1240 0.1294
0.1332 0.1343 0.1316 0.1262 0.1211 0.1137 0.1044 0.0967
0.0886 0.0824 0.0756 0.0707 0.0665 0.0617 0.0593 0.0567
0.0542 0.0505 0.0501 0.0474 0.0451 0.0432 0.0423 0.0401
0.0388 0.0375 0.0359 0.0353 0.0342 0.0320 0.0315 0.0302
0.0303 0.0281 0.0276 0.0269 0.0275 0.0261 0.0258 0.0243
0.0239 0.0250 0.0236 0.0241 0.0217 0.0223 0.0220
7.4618E-03 0.0000E+00 4.0882E-01 0.0000E+00 6.690 5.00
0.0053 0.0049 0.0056 0.0057 0.0056 0.0070 0.0069 0.0070
0.0071 0.0080 0.0080 0.0077 0.0084 0.0078 0.0093 0.0090
0.0105 0.0106 0.0122 0.0121 0.0139 0.0140 0.0136 0.0149
0.0149 0.0165 0.0177 0.0178 0.0187 0.0198 0.0222 0.0238
0.0259 0.0266 0.0305 0.0330 0.0361 0.0402 0.0458 0.0523
0.0602 0.0707 0.0826 0.0967 0.1131 0.1328 0.1568 0.1809
0.2057 0.2324 0.2590 0.2895 0.3146 0.3221 0.3058 0.2786
0.2587 0.2496 0.2430 0.2415 0.2449 0.2501 0.2542 0.2563
0.2592 0.2595 0.2567 0.2524 0.2518 0.2518 0.2537 0.2554
0.2611 0.2647 0.2685 0.2697 0.2685 0.2630 0.2570 0.2525
0.2495 0.2490 0.2513 0.2554 0.2600 0.2658 0.2690 0.2713
0.2704 0.2672 0.2600 0.2484 0.2371 0.2266 0.2183 0.2098
0.2032 0.1966 0.1914 0.1853 0.1781 0.1701 0.1618 0.1552
0.1491 0.1440 0.1402 0.1359 0.1305 0.1266 0.1215 0.1160
0.1120 0.1073 0.1045 0.1015 0.0996 0.0975 0.0936 0.0920
0.0890 0.0859 0.0832 0.0802 0.0740 0.0702 0.0675 0.0634
0.0588 0.0572 0.0535 0.0526 0.0521 0.0481 0.0453 0.0426
0.0391 0.0383 0.0369 0.0348 0.0342 0.0318 0.0301 0.0289
0.0282 0.0278 0.0271 0.0272 0.0266 0.0263 0.0237 0.0225
0.0226 0.0217 0.0218 0.0211 0.0181 0.0170 0.0164 0.0160
0.0164 0.0158 0.0149 0.0137 0.0134 0.0132 0.0125 0.0127
0.0121 0.0124 0.0107 0.0112 0.0106 0.0106 0.0088 0.0085
0.0087 0.0104 0.0091 0.0069 0.0094 0.0088 0.0096 0.0082
0.0091 0.0100 0.0100 0.0082 0.0099 0.0106 0.0091 0.0100
0.0118 0.0130 0.0115 0.0140 0.0144 0.0157 0.0162 0.0166
0.0193 0.0199 0.0211 0.0215 0.0241 0.0267 0.0256 0.0260
0.0268 0.0286 0.0300 0.0299 0.0315 0.0322 0.0315 0.0324
0.0332 0.0337 0.0358 0.0367 0.0383 0.0391 0.0417 0.0433
0.0451 0.0483 0.0519 0.0524 0.0540 0.0572 0.0604 0.0612

0.0643 0.0700 0.0744 0.0786 0.0859 0.0950 0.1025 0.1123
0.1258 0.1371 0.1495 0.1623 0.1747 0.1856 0.1959 0.2074
0.2174 0.2301 0.2415 0.2534 0.2641 0.2775 0.2844 0.2922
0.2993 0.3034 0.3148 0.3239 0.3372 0.3514 0.3614 0.3748
0.3851 0.3920 0.3954 0.3907 0.3748 0.3531 0.3332 0.3147
0.3046 0.3005 0.2983 0.2971 0.2949 0.2888 0.2749 0.2641
0.2532 0.2431 0.2382 0.2369 0.2318 0.2338 0.2325 0.2306
0.2300 0.2237 0.2156 0.2079 0.1942 0.1835 0.1738 0.1645
0.1568 0.1499 0.1432 0.1378 0.1342 0.1300 0.1277 0.1253
0.1227 0.1212 0.1184 0.1134 0.1115 0.1054 0.1021 0.0962
0.0902 0.0871 0.0803 0.0754 0.0706 0.0655 0.0611 0.0559
0.0536 0.0504 0.0482 0.0446 0.0427 0.0411 0.0375 0.0367
0.0356 0.0333 0.0333 0.0307 0.0309 0.0289 0.0283 0.0277
0.0262 0.0261 0.0264 0.0254 0.0249 0.0233 0.0245 0.0218
0.0225 0.0227 0.0210 0.0219 0.0198 0.0210 0.0195 0.0186
0.0187 0.0188 0.0178 0.0171 0.0171 0.0164 0.0150 0.0164
0.0153 0.0148 0.0150 0.0134 0.0127 0.0106 0.0113 0.0088
0.0099 0.0093 0.0092 0.0087 0.0075 0.0087 0.0070 0.0067
0.0048 0.0055 0.0052 0.0049 0.0055 0.0043 0.0044 0.0029
0.0037 0.0034 0.0041 0.0038 0.0035 0.0031 0.0028 0.0041
0.0023 0.0026 0.0023 0.0021 0.0021 0.0023 0.0019 0.0027
0.0025 0.0010 0.0015 0.0008 0.0016 0.0011 0.0021 0.0014
0.0011 0.0011 0.0018 0.0008 0.0013 0.0017 0.0009 0.0022
0.0020 0.0016 0.0005 0.0011 0.0023 0.0018 0.0027 0.0025
0.0012 0.0021 0.0020 0.0024 0.0022 0.0021 0.0023 0.0033
0.0024 0.0031 0.0028 0.0034 0.0044 0.0037 0.0039 0.0042
0.0033 0.0039 0.0039 0.0041 0.0049 0.0054 0.0060 0.0050
0.0052 0.0059 0.0068 0.0065 0.0065 0.0067 0.0073 0.0073
0.0080 0.0085 0.0095 0.0100 0.0101 0.0105 0.0113 0.0116
0.0134 0.0122 0.0140 0.0172 0.0156 0.0172 0.0193 0.0207
0.0219 0.0240 0.0266 0.0281 0.0307 0.0336 0.0368 0.0416
0.0456 0.0488 0.0564 0.0605 0.0662 0.0706 0.0759 0.0801
0.0850 0.0876 0.0917 0.0951 0.0981 0.1003 0.1004 0.1015
0.1035 0.1020 0.1020 0.1032 0.1063 0.1105 0.1172 0.1237
0.1276 0.1277 0.1257 0.1216 0.1156 0.1092 0.1004 0.0929
0.0856 0.0783 0.0731 0.0674 0.0636 0.0587 0.0560 0.0535
0.0514 0.0486 0.0480 0.0449 0.0436 0.0411 0.0408 0.0382
0.0370 0.0362 0.0345 0.0341 0.0330 0.0311 0.0308 0.0297
0.0288 0.0290 0.0269 0.0273 0.0270 0.0263 0.0256 0.0244
0.0248 0.0247 0.0241 0.0243 0.0225 0.0226 0.0222
6.9559E-03 0.0000E+00 4.8273E-01 0.0000E+00 6.706 5.00
0.0041 0.0035 0.0045 0.0047 0.0053 0.0062 0.0059 0.0052
0.0060 0.0064 0.0072 0.0066 0.0069 0.0073 0.0077 0.0081
0.0088 0.0093 0.0111 0.0117 0.0122 0.0126 0.0135 0.0144
0.0142 0.0149 0.0156 0.0161 0.0170 0.0184 0.0211 0.0226
0.0234 0.0246 0.0273 0.0310 0.0338 0.0372 0.0410 0.0481

0.0545 0.0646 0.0746 0.0873 0.1030 0.1208 0.1421 0.1636
0.1862 0.2132 0.2403 0.2704 0.2960 0.3029 0.2864 0.2596
0.2398 0.2306 0.2254 0.2252 0.2273 0.2323 0.2362 0.2390
0.2419 0.2417 0.2395 0.2364 0.2355 0.2348 0.2382 0.2391
0.2445 0.2499 0.2526 0.2561 0.2531 0.2485 0.2443 0.2382
0.2362 0.2340 0.2374 0.2411 0.2442 0.2500 0.2534 0.2562
0.2545 0.2513 0.2445 0.2341 0.2232 0.2141 0.2047 0.1983
0.1910 0.1852 0.1804 0.1749 0.1679 0.1598 0.1534 0.1470
0.1415 0.1358 0.1321 0.1287 0.1240 0.1205 0.1145 0.1087
0.1043 0.1008 0.0981 0.0952 0.0928 0.0906 0.0878 0.0862
0.0841 0.0811 0.0774 0.0738 0.0698 0.0657 0.0626 0.0597
0.0545 0.0533 0.0499 0.0490 0.0495 0.0451 0.0426 0.0394
0.0369 0.0345 0.0339 0.0322 0.0306 0.0297 0.0274 0.0271
0.0257 0.0246 0.0248 0.0244 0.0237 0.0230 0.0213 0.0192
0.0200 0.0190 0.0197 0.0187 0.0169 0.0152 0.0140 0.0143
0.0137 0.0147 0.0131 0.0107 0.0112 0.0119 0.0110 0.0108
0.0109 0.0106 0.0089 0.0093 0.0080 0.0080 0.0067 0.0061
0.0067 0.0074 0.0068 0.0059 0.0068 0.0075 0.0062 0.0063
0.0066 0.0074 0.0078 0.0064 0.0079 0.0096 0.0076 0.0087
0.0105 0.0110 0.0104 0.0115 0.0132 0.0134 0.0136 0.0146
0.0172 0.0185 0.0188 0.0198 0.0208 0.0225 0.0231 0.0233
0.0247 0.0258 0.0274 0.0265 0.0284 0.0295 0.0286 0.0285
0.0301 0.0313 0.0326 0.0331 0.0346 0.0363 0.0385 0.0393
0.0423 0.0447 0.0477 0.0477 0.0497 0.0531 0.0557 0.0558
0.0592 0.0642 0.0690 0.0719 0.0784 0.0870 0.0932 0.1025
0.1143 0.1252 0.1373 0.1486 0.1606 0.1703 0.1813 0.1911
0.2018 0.2125 0.2255 0.2362 0.2478 0.2604 0.2656 0.2740
0.2808 0.2862 0.2968 0.3055 0.3185 0.3325 0.3404 0.3525
0.3630 0.3695 0.3731 0.3701 0.3550 0.3337 0.3129 0.2972
0.2857 0.2797 0.2783 0.2766 0.2742 0.2684 0.2560 0.2461
0.2361 0.2259 0.2229 0.2213 0.2177 0.2202 0.2201 0.2177
0.2183 0.2127 0.2055 0.1979 0.1849 0.1753 0.1668 0.1563
0.1497 0.1426 0.1363 0.1312 0.1282 0.1240 0.1213 0.1194
0.1170 0.1150 0.1125 0.1092 0.1072 0.1006 0.0967 0.0909
0.0861 0.0832 0.0760 0.0715 0.0681 0.0623 0.0592 0.0536
0.0519 0.0484 0.0458 0.0426 0.0401 0.0389 0.0352 0.0340
0.0319 0.0317 0.0301 0.0291 0.0285 0.0279 0.0265 0.0255
0.0241 0.0256 0.0249 0.0237 0.0230 0.0213 0.0228 0.0203
0.0207 0.0209 0.0193 0.0199 0.0183 0.0179 0.0174 0.0165
0.0172 0.0152 0.0151 0.0156 0.0150 0.0139 0.0138 0.0142
0.0127 0.0120 0.0134 0.0109 0.0105 0.0085 0.0098 0.0077
0.0086 0.0086 0.0079 0.0072 0.0070 0.0077 0.0061 0.0060
0.0041 0.0050 0.0045 0.0048 0.0039 0.0036 0.0033 0.0029
0.0032 0.0036 0.0043 0.0034 0.0038 0.0028 0.0031 0.0034
0.0028 0.0035 0.0022 0.0023 0.0025 0.0026 0.0023 0.0023
0.0020 0.0020 0.0010 0.0015 0.0004 0.0003 0.0011 0.0016

0.0009 0.0000 0.0014 0.0006 0.0007 0.0023 0.0008 0.0004
0.0008 0.0006 0.0002 0.0022 0.0018 0.0011 0.0027 0.0032
0.0026 0.0033 0.0034 0.0043 0.0042 0.0037 0.0045 0.0045
0.0049 0.0044 0.0043 0.0056 0.0063 0.0056 0.0054 0.0068
0.0055 0.0056 0.0063 0.0064 0.0058 0.0060 0.0073 0.0056
0.0060 0.0068 0.0070 0.0067 0.0075 0.0074 0.0080 0.0076
0.0077 0.0076 0.0077 0.0094 0.0099 0.0104 0.0107 0.0112
0.0122 0.0110 0.0118 0.0141 0.0140 0.0152 0.0169 0.0174
0.0189 0.0209 0.0237 0.0249 0.0278 0.0303 0.0331 0.0371
0.0409 0.0450 0.0499 0.0551 0.0595 0.0640 0.0697 0.0742
0.0777 0.0811 0.0856 0.0883 0.0924 0.0945 0.0953 0.0957
0.0976 0.0955 0.0956 0.0961 0.0977 0.1040 0.1096 0.1154
0.1187 0.1199 0.1186 0.1140 0.1092 0.1012 0.0935 0.0864
0.0790 0.0731 0.0662 0.0614 0.0583 0.0530 0.0507 0.0482
0.0462 0.0431 0.0425 0.0406 0.0387 0.0361 0.0363 0.0339
0.0323 0.0316 0.0309 0.0299 0.0284 0.0273 0.0270 0.0254
0.0251 0.0242 0.0232 0.0228 0.0224 0.0220 0.0214 0.0202
0.0209 0.0208 0.0196 0.0201 0.0175 0.0179 0.0173
-1